THEORETICAL ANALYSES OF ROLL- AND PITCH-COUPLED HYDRO-PNEUMATIC STRUT SUSPENSIONS

Dongpu Cao

A Thesis

in

The Department

of

Mechanical and Industrial Engineering

Presented in Partial Fulfillment of the Requirements
for the Degree of Doctor of Philosophy (Mechanical Engineering) at
Concordia University
Montreal, Quebec, Canada

March 2008

Your file Votre référence
ISBN: 978-0-494-37763-5
Our file Notre référence
ISBN: 978-0-494-37763-5

ABSTRACT

Dongpu Cao, Ph.D.
Concordia University, 2008

Vehicle suspension design and dynamics analysis play a key role in enhancement of automotive system performance. Despite extensive developments in actively-controlled suspensions, their commercial applications have been limited due to the associated high cost and weight. Alternative designs in either passive or semi-active suspensions are highly desirable to achieve competitive vehicle performance with relatively lower cost and greater reliability. This dissertation research proposes two hydro-pneumatic suspension strut designs, including a twin-gas-chamber strut, and systematically investigates various concepts in roll- and pitch-coupled suspensions employing hydraulic, pneumatic and hybrid fluidic interconnections between the wheel struts. The proposed strut designs, including single- and twin-gas-chamber struts, offer larger working area and thus lower operating pressure, and integrate damping valves. Nonlinear mathematical models of the strut forces due to various interconnected and unconnected suspension configurations are formulated incorporating fluid compressibility, floating piston dynamics, and variable symmetric and asymmetric damping valves, which clearly show the feedback damping effects of the interconnections between different wheel struts.

The properties and dynamic responses of the proposed concepts in roll- and pitch-coupled suspension struts are evaluated in conjunction with in-plane and three-dimensional nonlinear vehicle models. The validity of the vehicle models is demonstrated

by comparing their responses with the available measured data. The analyses of the proposed coupled suspensions are performed to derive their bounce-mode, anti-roll, anti-pitch and warp-mode properties, and vehicle dynamic responses to external excitations. These include road roughness, steering and braking, and crosswinds. The results suggest that the fluidically-coupled passive suspension could yield considerable benefits in enhancing vehicle ride and handing performance. Furthermore these offer superior design flexibility.

The suspension struts offer a large number of coupling possibilities in the three-dimensions, some of which however would not be feasible, particularly for commercial vehicles where suspension loads may vary considerably. A generalized analytical model for a range of interconnected suspensions is thus developed, and a performance criterion is formulated to assess the feasibility of a particular interconnection in a highly efficient manner. The handling and directional responses of a three-dimensional vehicle model employing X-coupled hydro-pneumatic suspension are evaluated under split-μ straight-line braking and braking-in-a-turn maneuvers. The results clearly show that the X-coupled suspension offers enhanced anti-roll and anti-pitch properties while retaining the soft vertical ride and warp properties. Fundamental pitch and vertical dynamics of a road vehicle are also considered to derive a set of essential design rules for suspension design and tuning for realizing desirable pitch performance.

ACKNOWLEDGEMENTS

The author is sincerely grateful to his supervisors, Dr. S. Rakheja and Dr. C.–Y. Su, for their initiation of the research project and their guidance and efforts throughout the thesis work.

The author also wishes to acknowledge Quebec Government, Concordia University and CONCAVE Center for their financial support: International Tuition Fee Remission, Graduate Fellowship and Research Assistantship, respectively.

The author also thanks the colleagues, faculty and staff at the Department of Mechanical and Industrial Engineering, and CONCAVE Center, for their contributions to this thesis work.

Finally, the author would like to express his special thanks to his wife and members of his family, for their encouragement and supports. The author would like to dedicate this thesis to his wife, Jing Lang.

TABLE OF CONTENTS

LIST OF FIGURES

LIST OF TABLES

NOMENCLATURE

SYMBOL	DESCRIPTION
a_{12i}	Total area of damping orifices between chambers 1 and 2 of strut *i*
a_{13i}	Orifice area between chamber 1 and 3 of strut *i*
a_y	Effective lateral acceleration
A_{ji}	Effective piston area reflected on the chamber *j* side of strut *i*
A_{3j}	Annular piston area of a strut
b_i	Parameters that determine the variations in the braking torque
c_l, k_l	lateral damping and stiffness of the tire
c_t, k_t	Vertical damping and stiffness of the tire
C_d	Discharge coefficient
D , L	Diameter and length of the interconnecting pipes
E	Bulk modulus of hydraulic fluid
ESIS	Equivalent static interconnected suspension
f_{xf}, f_{xr}	Braking efforts developed by the front- and rear-axle tires
f_{yi}, M_i	Cornering force and aligning moment developed by tire *i*
f_{zf}, f_{zr}	Normal forces applied to the road surface
F_y	Centrifugal force acting on the sprung mass
F_{di}	Dissipative force developed by strut *i*
g	Acceleration due to gravity
h, h_1	C.g. heights of the sprung and unsprung masses from the ground
h_2	Vertical distance between the RC_1 and the sprung mass c.g.
I_{xxs}	Roll mass moment of inertia of the sprung mass
I_{xxu}	Roll mass moment of inertia of the unsprung mass
I_{xz}	Pitch-plane cross moment
I_{yys}	Pitch mass moment of inertia of the sprung mass
I_{wi}	Polar mass moment of inertia of wheel
I_z	Yaw mass moment of inertia of the vehicle
k_v	Suspension rate

k_P	Pitch stiffness
k_R	Roll stiffness
l_s, l_t	Half suspension-spacing and half track-width
l_f, l_r	Longitudinal distances between sprung mass c.g. & front/rear axles
LTR	Lateral load transfer ratio
m_s	Sprung mass of the vehicle
m_u	The unsprung mass of vehicle
m_{uf}, m_{ur}	Front and rear unsprung masses
M_R	Restoring roll moment developed due to restoring forces
M_P	Restoring pitch moment developed due to restoring forces
MESIS	Minimum Equivalent Static Interconnected Suspension
n	Polytropic exponent of gas
OMESIS	Order of minimum equivalent static interconnected suspension
p	Roll velocity of the sprung mass
P_0	Static gas pressure in a strut
P_{1l3r}, P_{1r3l}	Pressure drops across the connecting chambers 1 and 3
P_{4l3r}, P_{4r3l}	Pressure drops across the connecting chambers 4 and 3
P_a	Atmosphere pressure
P_{ji}	Pressure of fluid in chamber j of strut i
q	Pitch velocity of the sprung mass
Q_{1l}	Rate of change of fluid volume in chamber 1 of strut l
Q_{12l}, Q_{1l3r}	Flow rate across the damping orifices and interconnecting pipes
Q_{13i}	Flow rates between chambers 1 and 3
r_i	Effective radius of tire i
RSAF	Roll stiffness amplification factor
RSI	Roll stiffness index
RSR	Roll displacement ratio
ss_i	Longitudinal slip ratio
SAR	Vertical shock acceleration ratio
T_{bi}	Applied braking torque

u	Longitudinal velocity of the sprung mass
v	Lateral velocity of the sprung mass
VPI	Vehicle property index
w	Bounce velocity of the sprung mass
w_i	Static load supported by the strut i
x_{4i}	Relative displacement between the floating piston and main piston
x_{j0i}	Initial length of chamber j of strut i
$x_\ell; x_r$	Relative displacements of the left and right struts
x_v	Longitudinal motion of the vehicle
$\dot{x}_\ell; \dot{x}_r$	Relative velocities across the left and right struts
y_u	Lateral displacement of the unsprung mass
z_s, z_u	Vertical displacements of the sprung mass and unsprung mass
z_{uf}, z_{ur}	Vertical motions of the front and rear unsprung masses
z_{0l}, z_{0r}	Road elevations at the left and right tire-road interfaces
α_i	Slip angle
θ	Relative roll deflection
θ_s, θ_u	Roll angles of the sprung mass and unsprung mass
φ_s	Pitch motion of the sprung mass
ρ	Mass density of the fluid
σ	Parameter describing the slope of lateral acceleration
ω_f, ω_r	Angular velocities of the front and rear wheels

CHAPTER 1

INTRODUCTION AND LITERATURE REVIEW

1.1 Introduction

Heavy vehicles, with considerably higher location of center of gravity (c.g.) and larger load variations, exhibit roll and directional control performance characteristics that are considerably different from those of the light vehicles [1-3]. Constrained by the regulations on vehicle track width, heavy vehicles generally yield significantly larger lateral load transfers during cornering, and thus exhibit lower roll stability [1, 2]. The braking/acceleration is known to induce vehicle pitch motions and substantial longitudinal load transfers, particularly in vehicles with floating cargoes, as in the case of partly-filled tank trucks [4-6]. The dynamic load variations cause significant changes in normal loads on tires, which directly affect longitudinal and cornering forces developed by the tires during cornering and/or braking, and thus the handling and directional control performance in an adverse manner.

Owing to the excessive safety risks associated with accidents involving heavy vehicles and increasing demands from the professional drivers, the requirements for improved ride and handling qualities, and high durability and maintainability have been steadily growing [7-11]. A number of advanced control systems have been developed to enhance directional performance and stability of road vehicles through control of the forces and moments in the yaw plane [6, 12, 13]. The applications of such control systems for heavy vehicles, however, have been limited due to associated cost, weight, complex packaging and system reliability concerns [7-11]. Alternatively, design of

vehicle suspension also affects the vehicle performance characteristics in a significant manner by tuning the forces transmitted to the vehicle body and the dynamic wheel loads [3, 6, 14, 15]. The design of a road vehicle suspension, however, involves complex compromises among different measures related to ride vibration, road-holding and directional performance [3, 15]. Apart from these, the anti-roll and anti-pitch characteristics of a vehicle suspension also form a vital design objective to limit the lateral and longitudinal load transfers. The primary goal for heavy vehicle suspension design is thus to seek a satisfying compromise among ride vibration, road-holding, handling, and roll and pitch performances of the vehicle under different maneuvers and external excitations.

The current design practices for heavy vehicles generally utilize leaf or air springs in conjunction with passive anti-roll bars to realize a compromise among ride vibration, roll stability and directional performance [1-3]. Hydraulic dampers are also commonly used to achieve control of the resonant oscillations as well as high frequency vibration [15-17]. Owing to the unreasonable risks associated with potential vehicle rollover, the present design approach emphasizes on realization of high effective roll stiffness, which generally yields stiffer suspension with relatively poor ride comfort. Multiple wheel axle (tandem and tri-axle) suspensions employ load equalizers to evenly distribute the loads on individual tires, while the equalization is limited to either static or low-speed load transfers [18-20]. The transverse mechanical interconnections, such as anti-roll bars, are commonly employed as auxiliary roll stiffeners to achieve high effective roll stiffness and thus lower roll deflection of the vehicle body during steering maneuvers [1-3, 21]. The

use of anti-roll bars, however, tends to add weight, and deteriorates ride responses to some extent [21, 34].

Various hydro-pneumatic struts have been developed to realize compact suspension designs with integrated pneumatic spring and hydraulic damping to achieve improved ride comfort and ride height control. Such suspension struts have been employed in military vehicles for about half a century, and are considered to offer the most significant potential for commercial vehicle applications [14, 22-24]. Moreover, these suspensions offer greater design and tuning flexibilities in either passive or active manners. A few studies have shown that transverse and fore-aft interconnections between the struts can help achieve desirable roll and pitch-attitude control [25-32]. A number of reported studies, however, have employed very large size struts with small effective working area, which would require excessive working pressure [25, 27, 28, 32]. The use of a hydro-pneumatic strut in parallel with passive load-sharing springs has also been suggested in order to reduce operating pressure [29, 31, 32]. The results revealed that the load sharing by the additional springs significantly limits the effectiveness of the roll-interconnections [29]. Moreover, the reported studies have considered strut designs with external gas chamber and damping valves. The reported experimental and analytical studies, however, have clearly shown that hydraulically interconnected suspension struts could help enhance the anti-roll and anti-pitch performance without affecting the vertical ride.

In this dissertation research, the concepts of two integrated suspension struts, namely single-gas-chamber and twin-gas-chamber struts, which comprise gas chamber(s) and damping valves within the same unit, are explored to realize interconnections in the roll and pitch planes. The interconnections are realized through hydraulic, pneumatic or

hybrid fluidic couplings. The most important feature of the compact struts is their large effective working area, which permits relatively lower operating pressure for a given load. The roll-plane, pitch-plane and three dimensional models of a heavy vehicle are developed and validated. The interconnection arrangements in the roll, pitch, and combined roll and pitch planes are proposed and systematically analyzed to study their properties and response characteristics under various excitations. The performance characteristics of the twin-gas-chamber strut suspensions are also explored, in terms of suspension properties and vehicle dynamic responses.

1.2 Literature Review

The formulation and analyses of interconnected vehicle suspension require essential fundamental knowledge of various relevant subjects. These include the ride and handling dynamic behaviors of vehicles, road roughness characterization and tire-road interactions, compressible fluid flows, tire dynamics, suspension design, damping valves, performance requirements and analytical methods in vehicle dynamics. The design, tuning and properties of vehicle suspension strongly influence a wide range of performance measures of the vehicle. Consequently, the vehicle suspension forms an important challenging design task. Heavy vehicle suspension design, and its effects on the roll and pitch dynamics, handling and directional stability, ride dynamics, and vehicle-road interactions of heavy vehicles, typically single-unit vehicles, are reviewed in the following sub-sections. This is followed by a review of design features of various passive as well as controlled interconnected suspensions.

1.2.1 Heavy Vehicle Suspension Design

The design of vehicle suspension strongly affects the ride, handling, suspension travel, road friendliness, roll and directional stability, and braking/traction performance of the vehicle in highly complex and conflicting manners. Owing to the relatively low roll stability limits and large payload variations of heavy vehicles, the design of a suspension forms a more challenging design task. The fundamental issues in suspension design for heavy road vehicles have been discussed by Cole [3], while various advanced controlled suspension systems for commercial vehicles and their feasibilities have been reviewed by Palkovics and Fries [11]. The reported studies [7-9, 33-36] have suggested that while the advanced controlled suspension systems could help improve the vehicle ride and handling performance, recent technical trends in heavy vehicle suspension design are focusing on more cost-effective passive systems. These studies have also concluded that conventional passive suspension designs could not satisfy the various vehicle performance requirements, and must involve compromises among different conflicting measures.

It is well known that natural frequencies of front and rear suspensions should be maintained to be relatively constant under various load conditions [3, 11, 33, 35]. Heavy vehicles, however, exhibit considerably large load variations. Rear suspension of a heavy vehicle could have a loaded/unloaded ratio of 5:1, while that of front suspension is generally about 2:1 [8]. Therefore, it has been suggested that when developing a new suspension concept, the load variation should be taken into account [35]. Heavy vehicles generally employ either leaf or air springs [3, 33-35]. Leaf springs exhibit hysteretic behavior due to interleaf friction, which could considerably deteriorate the ride performance [35]. Alternatively, air or pneumatic springs are being employed more

commonly for their superior ride performance [35]. Compared to leaf springs, air springs exhibit varying spring rates with load changes, low hysteresis and damping, and a relatively constant natural frequency over a wide range of loading conditions by using ride-height leveling valves [35].

The pneumatic suspensions invariably employ hydraulic dampers to achieve adequate control of resonant responses and oscillatory vibrations under different maneuvers and excitations. High damping is desirable for controlling resonant responses of vehicle body and unsprung masses, while the isolation of ride vibrations under random road roughness inputs necessitates low damping. High damping is also beneficial for inhibiting the oscillatory motions of vehicle body during steering and/or braking or acceleration maneuvers. Moreover, asymmetric damping in compression and rebound is desirable to control motions of vehicle body and unsprung masses under abrupt road inputs [116]. Passive hydraulic dampers can be tuned to achieve a compromise among these different conflicting performance requirements. Positioning of the dampers, however, is generally determined by packaging requirements, instead of optimized damping performance, because of which the tuning of roll damping is much less flexible [9].

Similar to air springs, hydro-pneumatic suspensions could also provide superior ride performance, which could conveniently integrate ride-height valves to realize relatively constant suspension natural frequency. Furthermore, hydro-pneumatic suspension offers compact design and integrated damping valves within the same strut. A range of hydro-pneumatic suspensions have been employed in military vehicles, and are regarded to hold the most significant potential for commercial vehicle applications [14, 22-24]. A few studies have suggested that the hydro-pneumatic suspension struts are the key technology

candidates for the development of the future heavy vehicles for military applications [22, 24].

Apart from the basic suspension components (springs and dampers), anti-roll bars are also widely used in heavy vehicle suspension systems to improve vehicle roll stability and to balance the roll moment distribution between the front and rear axles [3]. The use of anti-roll bars permits relatively lower vertical suspension rate for enhanced ride comfort, and provides additional design flexibility for tuning of the handling quality. An anti-roll bar, however, adds considerable weight, and deteriorates ride comfort to some extent [21, 34]. Moreover, the use of very stiff anti-roll bar would significantly reduce effective roll damping, which is undesirable for control of dynamic roll response of heavy vehicles [21].

Owing to the extreme design challenges for the primary suspension for heavy vehicles, Palkovics and Fries [11] have suggested that the ride comfort of driver could be improved by tuning secondary suspensions at the cab and the seat. This could provide an additional freedom to achieve a better compromise between the driver's comfort and the other performance measures. The potential ride improvement by the secondary suspensions, however, is limited by their design spaces. For vehicle ride and handling analysis, Cole [3] suggested that considerations of vehicle motions at frequencies below 25 Hz were adequate for suspension design and tuning. This frequency range essentially incorporates the vibration modes related primarily to rigid-body motions of the vehicle body and unsprung masses, and the first structure bending mode [3]. The bending mode of the chassis frame, which could be in the 6~7 Hz range, is considered only in a few studies, where the nodes occurred close to the attachment points of the suspension system

[3, 35]. The suspension dampers are therefore not effective in controlling such vibration motions [3].

1.2.2 Roll and Pitch Dynamics of Heavy Vehicles

The steering and/or braking maneuvers of heavy vehicles generally induce vehicle roll and/or pitch motions, and therefore lateral and/or longitudinal load transfers [3-6]. While the rotational motions adversely influence the ride comfort, the dynamic load transfers affect the normal tire forces, and thus cornering and braking forces developed by tires in the yaw plane, which directly influence the directional and braking dynamic responses and stability of heavy vehicles [3-6]. Considering the relatively small track width and large wheelbase, and high c.g. location of a heavy vehicle, the roll dynamics and stability limits have been extensively explored in the literature [1-3]. Goldman et al. [37] reviewed roll dynamics of road vehicles. Winkler [2] presented the fundamental aspects associated with rollover dynamics of heavy vehicles. These studies have invariably concluded that heavy vehicles generally exhibit low static rollover threshold (SRT) and could rollover before the tire-road adhesion limit is reached. Due to the fact that some heavy vehicles may exhibit yaw instability at lateral acceleration levels lower than their rollover threshold, El-Gindy [40] redefined SRT as 'the maximum lateral acceleration level in g's beyond which static rollover of a vehicle occurs'. The SRT of a loaded heavy vehicle often lies below 0.5 g [2, 3]. For such vehicles, a relatively small improvement in the physical stability, in terms of rollover threshold, could yield rather large reduction in the rollover accident rates [2, 3]. These studies have also concluded that the improved roll stiffness and roll damping could help improve roll stability of heavy vehicles.

Ervin [1] investigated the influence of size and weight variations on the roll stability of heavy vehicles. It has been observed that the SRT decreases decidedly by increasing the axle load. For a single unit vehicle, a 10% increase in axle load yields an average of 0.025g reduction in the SRT. Roll stability is improved by increasing the width allowance for vehicles. An approximate 3% increase in the roll stability limit can be achieved with only 1% increase in both track width and transverse spring spacing. An increase in the payload c.g. height yields considerable reduction in the roll stability limit, of the order of -0.0024g/cm of increase in payload c.g. height. However, the weights and dimensions of commercial vehicles are governed by the road regulations.

The vehicle roll motion generally involves complex rotations of the sprung and unsprung masses. The sprung mass rolls with respect to the suspension roll center, while the unsprung masses roll about their roll center, respectively, which are often considered to lie in the ground plane [1, 3]. For a typical heavy vehicle, about two third of the total roll angle of the vehicle involves rotation about the suspension roll center [1]. The roll moment consists of primary overturning moment, caused by the lateral acceleration induced by a directional maneuver, and lateral displacement moment, caused by roll motion of the vehicle c.g. A reduction in the roll motion of the sprung mass can thus largely decrease the lateral displacement moment, and thereby improved roll stability limit. In view of the ride quality implications of harder suspension springs, the roll stability limit is generally enhanced by introducing auxiliary roll stiffeners, such as anti-roll bars. Cole [105] investigated the roll control of heavy vehicles using five different suspension configurations through simulations. The study involved relative analyses of different passive and active suspensions, and concluded that an increase in the stiffness of

anti-roll bar of a passive suspension can improve the roll stability, while the ride comfort is decreased. Cebon [21] has suggested that additional roll stiffness of anti-roll bars should be limited such that the SRT of a vehicle does not exceed 90-95% of the static stability factor (SSF). The SSF, also called as track width ratio (TWR), is defined as the ratio of half track width to vehicle c.g. height [37]. Rakheja et al. [41] investigated roll properties of 72 different heavy vehicle configurations, involving different combinations of suspensions, tires and loading, and concluded that the SRT of a heavy vehicle is generally 72% of the SSF, due to compliance of vehicle suspension and tires. Goldman et al. [37] showed that treating a multiple-axle vehicle suspension system as a lumped suspension tends to overestimate the SRT of the vehicle.

Winkler [2] suggested that a heavily loaded semi-trailer could exhibit a roll mode natural frequency as low as 0.5 Hz, which is in the range of excitation frequencies arising from emergency type of steering maneuvers. This suggests the significant importance of roll damping for controlling the roll resonant responses during such emergency maneuvers. Winkler [2] also reported that it is relatively hard for heavy vehicle drivers to perceive their proximity to rollover while driving. The rollover threshold of a heavy vehicle varies continuously with dynamic load transfers in the roll plane, which diminishes the driver's perception of the stability limit of the vehicle. Moreover, the flexible nature of the tractor frame tends to isolate the driver from the roll motions of the trailer, which could serve as an important cue for the impending rollover. The compliances of vehicle's structural frame, suspension and tires can also contribute to the rollover process. A number of studies have established the relative contributions of various vehicle design factors to the vehicle roll stability limit, namely the axle loads,

structure compliance, track width, c.g. height, etc. [1, 2]. These studies have shown that the effect of structural or articulation compliance may be small. The combined effect of all compliances on roll stability could be significant.

Static roll stability is the dominant quality factor affecting the rollover probability of the vehicle. The roll behavior of a vehicle in a dynamic maneuver, however, could differ from the static roll response. A number of measures have thus evolved to assess the dynamic roll behaviors of commercial vehicles. These include the lateral load transfer ratio (LTR), roll safety factor (RSF), effective lateral acceleration (ELA), normalized roll-response of semitrailer sprung mass (NRSSM), etc. [37, 39, 42]. Cooperrider et al. [43] concluded that the lateral acceleration required to induce rollover is a function of the time duration of its application. When the lateral acceleration exceeds the static rollover limit, it needs to be sustained for only a finite time to cause rollover. For instance, for a typical heavy vehicle, a lateral acceleration of 110% of its static limit can produce rollover if sustained for about 1 second, while the acceleration of 120% of the static limit needs to be sustained for only about 0.6 second to cause rollover. For vehicle combinations and tank vehicles, the roll dynamics may play a more important role in rollover [2, 40]. White [38] investigated the influence of ride-height leveling system on roll stability of heavy vehicles with air suspension system, and concluded that the current mechanical ride-height leveling system does not affect the roll stability during a rapid directional maneuver.

While the roll dynamic behavior of heavy vehicles has been extensively reported in the literature, relatively fewer studies have explored the pitch dynamic responses. The performance characteristics of a heavy vehicle are also related to its pitch motion, which

include the ride, handling, suspension stroke and dynamic tire loads. This is partially attributed to the relatively large wheelbase and coupling between the vertical and pitch motions of heavy vehicles. Moreover, heavy vehicles are generally characterized by highly variable gross vehicle weight (GVW) and load distributions, compared with passenger cars. Passenger cars are generally designed to achieve front/rear load distribution ratio and dynamic index (k^2/ab) close to unity [3, 15], where k is the radius of gyration of the sprung mass in pitch, and a and b are the longitudinal distances from the center of gravity (c.g.) to the front and rear wheel centers, respectively. These ratios are significantly different for heavy vehicles, where the dynamic index may assume a value greater than 1 for two-axle vehicles, leading to pitch mode natural frequency lower than the bounce mode frequency [44].

Both the pitch and bounce motions can be induced by the vehicle-road interactions, braking or acceleration. The time delay between the road excitations at the front and rear wheels, which is referred to as wheelbase filtering, contributes to the vehicle pitch. Considering the human ride comfort, the vehicle pitching is perceived as more annoying than bouncing [3, 15]. This is attributed to higher human sensitivity to vibration in the vicinity of the pitch frequency. The vehicle pitch motion predominates around 1 Hz, to which human body is known to be more sensitive in view of the comfort perception [45].

A large number of studies have investigated the pitch responses due to wheelbase filtering effect under constant forward speeds [46, 47], while only a few studies have investigated the influences of suspension properties on pitch dynamic responses of road vehicles. It has been suggested that a relatively softer front axle suspension than the rear suspension could help reduce the pitch motion of an automobile [6]. This design

approach, however, has been argued on the basis of transient responses of a vehicle to a road bump excitation, particularly the phase between the responses caused by interactions of the front and rear ends with the bump, which depends upon the forward speed, the nature of road bump and vehicle wheelbase. Moreover, this approach may induce larger pitch motion due to dynamic load transfer under braking. The suspension design for pitch suppression thus involves complex challenges associated with considerations of wide ranges of operating speeds, road roughness and maneuvers.

Crolla and King [48] investigated this design approach through simulations performed at different speeds in the 10-40 m/s range under random road excitations. The study concluded that this design approach could help reduce pitch motion but deteriorate the vertical ride quality. On the basis of the analysis of a half car pitch plane model, Sharp [47] concluded that this design approach is beneficial in pitch suppression at higher speeds with very little compromise in terms of bounce acceleration response. At lower speeds, however, the compromise between pitch and bounce accelerations was observed. The study further concluded that the suspension stiffnesses implied would be impractical in terms of the attitude control of the automobile. The vast majority of the studies on pitch dynamics have focused on automobiles, while the effects on pitch response of heavy vehicles have been mostly limited to load equalizers for the suspension systems [18, 19].

Although the suspension designs with lower pitch stiffness are preferred for ride comfort, the relatively large wheelbase generally yields higher effective pitch stiffness, which is in contrast with the effective roll stiffness [17]. The use of a fore-aft interconnection between the axle suspensions has thus been suggested to reduce effective

pitch stiffness. The fore-aft load transfer caused by acceleration or braking, however, can be reduced by higher suspension pitch stiffness. A wide range of suspension linkages have also been explored to achieve improved anti-dive and anti-rise performances of the front and rear suspensions, respectively, under vehicle braking, and anti-lift and anti-squat of the front and rear suspensions, respectively, under traction [17, 49]. It has been suggested that anti-pitch suspension geometry tends to induce wheel hop, while adversely affecting the handling dynamics of vehicles [17, 49].

Sharp [50] pointed out the importance of vehicle attitude (roll and pitch motions) control. The driver's perception the path preview is significantly deteriorated in the presence of excessive pitch motions. In order to improve the path perception ability of a driver with minimum effort, the roll and pitch responses of the vehicle body to the maneuvers and excitations arising from road and/or crosswind should be minimized.

For heavy vehicles, a number of concepts and designs in load equalizers have been proposed to equalize the axle loads in a tandem or tri-axle configuration [18, 19]. Such load equalizers, however, do not yield satisfactory dynamic performance [19, 20]. Dahlberg [5] investigated braking-induced pitch motion and longitudinal load transfer, and their effects on yaw dynamics of heavy vehicles. The study concluded that yaw dynamics and stability are strongly influenced by pitch motions and longitudinal load transfer during braking-in-a turn. It has been emphasized that the roll and pitch motions during steering and braking/acceleration should be minimized in order to improve driving safety and comfort of the heavy vehicles [51]. A suspension design with improved roll and pitch performance thus offers considerable potential for improving the ride comfort, handling and directional dynamic performance of heavy vehicles.

1.2.3 Handling and Directional Stability of Heavy Vehicles

The considerations of vehicle dynamics (ride and handling) in the practical vehicle design have been discussed by Crolla [14]. Sharp [50] presented a comprehensive overview of vehicle dynamics and the performance measures. Macadam [63] reviewed and discussed the contributions of human drivers to vehicle handling dynamics and control. Handling and directional dynamic responses and stability of heavy vehicles, especially articulated vehicles, have been reviewed and discussed in a number of studies [62, 100-104]. El-Gindy [40] reviewed the performance measures of heavy commercial vehicles in North America, and suggested that future transportation technology should involve the development of heavy vehicles with measurable and predictable levels of performance in various safety-related maneuvers. Uys et al. [70] briefly reviewed the criteria for handling performance of vehicles, while Crolla et al. [99] investigated the correlations between objective vehicle performance metrics and subjective ratings. These reported studies have concluded that the correlations between objective handling performance measures and subjective evaluations are not well understood yet. These studies also emphasized the handling and directional dynamic responses and stability of heavy vehicles as one of the critical issues in vehicle development and suspension design.

An understeering vehicle is known to be directionally stable, while a vehicle combination with an understeering tractor, the vehicle combination is considered to be directionally stable [6]. It would therefore be desirable for road vehicles to be understeer for various operating conditions [6, 73, 85]. A number of studies have further suggested that the understeer coefficient of a vehicle should be maintained to be relatively constant during both the linear and nonlinear tire slip angle ranges in order to retain consistent

driver's control [72, 86, 88, 92]. Some other studies, however, have preferred the understeer coefficient increasing with an increase in lateral acceleration (or during the nonlinear tire operating range), so as to improve vehicle yaw or directional stability during tight or emergency maneuvers [3, 6, 58, 73].

The suspension design strongly affects the roll moment distribution and thus distribution of load transfer between the axles, which influences the vehicle handling and directional stability [3]. For typical trucks and tractors, the drive axle is much stiffer in roll mode than the steer axle, while it carries larger load with greater c.g. height. This results in the proportion of load transfer within the drive axle greater than the proportion of weight on the drive axle. As the lateral acceleration level increases, the understeering vehicle tends to approach oversteer behavior, causing directional stability limit to decrease. For some vehicles, the usable region of lateral acceleration is determined by potential yaw instability, instead of the SRT [3, 40, 94].

During transient maneuvers, the roll moment distribution depends on the distribution of both effective roll stiffness and roll mode damping between the front- and rear-axle suspensions [86]. Changing the normal load distribution among the four corners of the vehicle also affects the vehicle yaw response. Higher front suspension damping and lower damping of the rear suspension result in greater understeer tendency [91].

The forces and moments arising from steering and braking maneuvers cause lateral and longitudinal dynamic load transfers, which may result in significant reduction in the stability limits and controllability of the vehicle [4-6, 80]. Vehicles tend to be understeer during an acceleration-in-a-turn maneuver, while a braking-in-a-turn maneuver could result in an oversteer tendency. This is considered to be highly undesirable, since

traction-in-a-turn is a normal driving situation, while braking-in-a-turn is generally regarded as a critical driving situation [61]. Apart from dynamic load shifts, variations in static load distributions among different axles could also affect the handling characteristics of a vehicle due to the nonlinear properties of tires [6]. The forces and moments developed by tires govern the handling characteristics of a vehicle. The cornering forces generated by slip and camber mechanisms are responsible for lateral and yaw motions, aligning torques developed at the front tires contribute to steering wheel feel, while the vertical forces affect the roll dynamics of the vehicle [56]. A higher cornering stiffness generally correlates well with a better handling from the subjective evaluation. From the objective performance measures, high cornering stiffness is also considered to be desirable, especially on the rear axle, which tends to improve the vehicle's response time and directional stability [55, 56]. It has also been noted that when the cornering force capability of rear axle tires saturates, yaw rate and sideslip angle of the vehicle increase exponentially, which could possibly cause a directional instability [83].

For the front-wheel-steer road vehicles, a steering maneuver causes increasing slip angles and cornering forces to change the trajectory of the vehicle. The longitudinal path deviations contribute to centrifugal inertia forces that need to be balanced by centrifugal forces on both the front and rear tires. It is at this point that the rear tires develop lateral forces and thus slip angles. The generation of lateral forces on the rear tires therefore lags behind that on the front tires [13, 59].

Although an understeering vehicle is defined as a stable system, a reduction in yaw damping is known to occur above the characteristic speed. The reduced yaw damping

could lead to significantly oscillatory response, particularly at high steering frequency inputs associated with an emergency type of directional maneuver [95]. It has been suggested that reducing the understeer tendency and thus increasing the characteristic speed could make the vehicle response less steering-frequency dependent at relatively high speeds. This reduction in understeer tendency, however, would increase the yaw gain. It is also well known that an understeering vehicle exhibits reduced yaw damping with an increase in vehicle speed [95, 96]. From the driver's perception point of view, an understeering vehicle could thus appear to have a loss of control at the rear especially at relatively high speeds due to higher yaw gain and reduced yaw damping associated with high frequency steering inputs. Moreover, a maneuver-induced large lateral acceleration causes a decrease in yaw response for an understeering vehicle as the steering angle increases. Consequently, an evasive maneuver that necessitates a large steering angle input can be relatively difficult [84].

The vehicle roll motion is strongly coupled with yaw motion [3]. The vehicle roll instability is strongly correlated to the lateral acceleration level, while the yaw instability is strongly influenced by both lateral acceleration and vehicle speed [82]. A vehicle is generally stable in roll when the lateral acceleration is lower than a certain threshold, irrespective of vehicle speed. The yaw instability however, could occur at relatively low lateral accelerations (e.g., 0.1~0.2g) at high vehicle speeds. A roll instability could thus be prevented by limiting the vehicle lateral acceleration, while a yaw instability may still occur. It has been suggested that during a maneuver-induced roll instability situation, the vehicle typically encounters greater oversteer together with significantly large sideslip angle [92]. Oversteer, which is generally followed by a loss of directional control, is

often induced by a rapid change in the steering angle at relatively high speeds. This leads to a rapid change in the direction of the lateral force of the front axle, while the rear axle force may act in the opposite direction due to the time lag. In this relatively short duration, the opposite directions of the front and rear lateral forces would generate a large yaw moment leading to a possible rapid spin-out.

It has been reported that in dynamic rollover tests vehicles generally experience sustained body roll oscillations during a portion of the road edge recovery maneuver, where steering angle is held constant [97]. It has been concluded that these undesirable oscillations are induced by the coupling among the vehicle roll, heave and subsequently yaw modes that result from jacking forces of suspension system. These jacking forces cause bounce motions of vehicle body, which also in turn influence tire normal loads and thus the lateral forces, affecting the vehicle yaw response. Sustained roll, heave and yaw oscillations could therefore occur even during a steady-state portion of maneuver.

The dynamic tire loads induced by the road roughness also affect the vehicle handling dynamics. It has been found that as the surface roughness increases, vehicle handling behavior becomes more erratic [75]. The study concluded that on relatively smooth roads, the overall understeer/oversteer characteristic will not change significantly, up to lateral accelerations of 0.6g. Over a relatively rough road, the understeer/oversteer behavior differs considerably in a wide range of lateral acceleration levels, where the originally understeering vehicle could shift to oversteer behavior.

Vehicle handling and directional dynamics can be generally assessed in three distinct ways: (i) subjective rating of actual vehicles; (ii) objective open-loop tests conducted using an instrumented car; and (iii) analytical methods [57]. Simulation-based design and

analysis methods significantly reduce the development time and cost, and result in prototypes that are much closer to the final product [71, 85, 87, 89, 91-93]. Computer simulations of vehicle dynamics could further provide absolute control of vehicle properties (mass, tire properties, etc.), test repeatability, ability to eliminate the risks associated with track tests, ability to conduct tests that would be physically impossible, ease of varying individual vehicle characteristics, and ability to discriminate small differences in performance.

The levels of required modeling refinements, however, have been long debated in developing vehicle models for handling simulations. Industry analysts and engineering specialists often generate quite complex models to achieve greater accuracy. Experienced academic researchers, however, have put forward the view that typical industry-used vehicle models are too complex and inefficient as design tools [64, 65, 71]. Sharp [65] suggested that models do not possess intrinsic values; an ideal model should possess minimum complexity and be capable of solving the concerned problems with an acceptable accuracy.

The simple linear road vehicle models could provide accurate handling analyses up to a lateral acceleration of 0.3g, while most vehicles tested for handling evaluations experience a lateral acceleration up to 0.8g [54, 68]. A linear analysis for heavy vehicles is valid only up to lateral accelerations of about 0.1g, since such high c.g. vehicles could generate significant load transfers across the axles under lateral acceleration above 0.1g [3]. It has also been noted that the inclusion of longitudinal and lateral load transfers is helpful for predicting handling and directional dynamic responses of road vehicles [6]. The nonlinear 14 degree-of-freedom (DOF) full vehicle model, capturing the basic

vibration modes of rigid-body sprung and unpsrung masses, represents a quite useful tool for predicting the vehicle dynamics without introducing the complexity of multi-body codes. Moreover, it is a good compromise between the requirements of accurate prediction of vehicle response and rapid simulation time [69, 81]. A 14 DOF vehicle model offers the flexibility of modeling nonlinear suspension stiffness and damping components and can further simulate the vehicle responses to normal force inputs, as in the case of a semi-active/active suspension or controlled anti-roll bar systems. Moreover, the 14 DOF model, unlike the conventional 8 DOF model, is capable of evaluating vehicle behavior even after wheel lift-off and thus can be used in developing and testing the validity of rollover prevention strategies. For nonlinear vehicle dynamics analysis, the Magic Formula tire model has been widely accepted as a leading tire model [6, 66, 96].

A variety of maneuvers have been employed to assess vehicle handling and roll characteristics, which can generally be divided into two types: open-loop and closed-loop. For open-loop maneuvers, time history of steering angle input is pre-defined, which is not dependent on the response of the vehicle. In closed-loop maneuvers, the steering angles are computed using paths upon appreciated consideration of vehicle and human driver responses. Automotive industries generally employ closed-loop tests to evaluate the vehicle performance. Such tests, however, are not quite repeatable due to involvement of the human drivers. It is thus often difficult to draw concrete conclusions from the test results [78]. The modeling of an actual driver is also a complex task, due to wide variations in individual perception, reaction and neuromuscular abilities [63, 138]. The use of a simple driver model might, in some cases, hide meaningful results available from open-loop simulation [53, 90]. Moreover, open-loop simulation is inherently repeatable

and thus yields uniform vehicle comparisons and design studies [73, 88]. The open loop stability is definitely desirable. Although the driver might be able to stabilize an inherently unstable vehicle to a certain extent, the added driver's work load might induce fatigue and/or reduced concentration on other driving tasks. Additionally, increasing immunity from external disturbances correlates with the requirements of consistent and robust open loop dynamics of vehicles [54].

For open-loop simulations, two types of steering inputs are generally used: identical or parallel and differential steer angles inputs [53]. A steady turn analysis, based on average parallel steer angle, could result in as much as 5% higher lateral acceleration, compared to that based on differential left and right side values [53]. A property common to most suspension systems is roll steer, which can be appropriately simplified and represented by a constant roll steer coefficient. Apart from axle steer, pitch, bounce, and roll motions of the chassis can also cause small steer angle variations of the left- and right-front wheels. The consideration of these additional steer options is not recommended with the parallel steer analysis [53]. The approximations resulting from the average steer angle analysis would negate the accuracy gained by considering these steer options.

International Organization for Standardization (ISO) has set for the guidance on handling maneuvers and running conditions, in order to facilitate comparisons of different vehicles under more uniform test conditions [106-109]. The standard, however, does not define an evaluation criterion. Consequently, different vehicle manufacturers adopt different performance metrics [79].

The handling qualities are evaluated via subjective ratings and objective measures, while the corrections between objective performance metrics and subjective ratings have not yet been clearly established. A number of objective handling and directional measures, however, have been proposed in the literature [13, 54, 55, 59, 60, 61, 67, 73, 90, 92]. These include: (a) understeer gradient; (b) yaw rate; (c) lateral acceleration; (d) vehicle sideslip angle; (e) time delay in the yaw rate and lateral acceleration responses; (f) roll deflection and rate; (g) pitch deflection and rate; and (h) TB (product of steady-state sideslip angle and yaw rate peak time under a step steer input test) factor, or vehicle characteristic. A number of assessment criteria for good handling and directional behavior have also been suggested, such as: shorter time delay in the yaw rate and lateral acceleration responses, smaller phase lag between the lateral acceleration and the yaw rate, a reasonably good compromise between the requirements of sufficiently high yaw damping and rapid responsiveness of vehicle to steering input, smaller body sideslip angle, higher response immunity to external disturbances, lower roll and pitch motions; and lower TB factor. Although some studies have suggested that the steady state yaw rate gain be maximized for good handling, a too high value would be undesirable since it aggravates nervous behavior of the driver [55].

The optimal steering system gain is dependent upon the aggressiveness of the driver [77]. High steering gain vehicle requires greater alertness and control actions from the driver. On the other hand, low steering gain would increase driver's physical workload to a great extent during evasive maneuvers. A vehicle requiring minimal correction and executing the driver's command accurately is considered to have a good on-center handling [94]. Excessive handwheel activity, uninformative steering feel, and imprecise

vehicle response are the factors contributing to poor on-center handling. Meanwhile, under severe directional maneuvers, the driver's perception of feedback of steering wheel torque is essential, as an indicator of lateral acceleration level that can warn an experienced driver of the lateral force saturation.

El-Gindy [40] summarized eight stability and control measures for heavy vehicle combinations, namely: (1) handling performance; (2) SRT; (3) dynamic rollover stability, in terms of LTR and rearward amplification (RWA); (4) yaw damping ratio (YDR); (5) low- and high-speed friction demands; (6) low- and high-speed lateral friction utilization; (7) low- and high-speed offtracking; and (8) braking performance.

In view of the complexity and urgency of the driver's actions in transient maneuvers, it has been suggested that the driver's psycho-physical vehicle model (the inverse dynamics of the vehicle) be based on the simplest and most basic dynamic states of the vehicle that are consistent with his/her perceptions [54]. A typical driver would be expected to have little or no experience in gauging, estimating or understanding vehicle response during nonlinear operating ranges of tires [72, 73]. Since the driver's experience is mostly limited to normal driving within the linear range of handling behavior, the perception and control limits of the driver may thus be inadequate as the limit of tire-road adhesion is reached. One of the goals of the advanced chassis control systems is to protect the driver from possibly dangerous dynamic instability of the vehicle, by minimizing the difference between the vehicle responses in the linear and nonlinear tire operating ranges. The secondary goal of the chassis control systems is to maintain consistent vehicle behavior, when subject to parameter variations and external disturbances.

The feasibility of four-wheel-steering (4WS) systems in commercial vehicles for enhancement of handling has been discussed by Palkovics and Fries [11]. Steering the rear wheels could help decrease the time delay in the generation of cornering force and permit the independent control of vehicle path and sideslip angle. Moreover, low-speed offtracking can be reduced significantly [59]. The control strategy does not differ significantly from the passenger car systems and could provide advantages in high speed stability and low speed maneuverability. The application of a forced rear axle steering in commercial vehicles, however, is quite complex due to large loads and costs. From the design viewpoint, the steering of dual-tire wheels with heavy load, is a very challenging task. The use of super wide tires can reduce this complexity, which, from the roll stability point of view, also indicates an improved roll stability limit of a heavy vehicle due to the larger effective track width. Such tires, however, are known to transmit excessive dynamic loads to the pavements, which further lead to their rapid wear [3]. The active steering of the trailer wheels is also an option that can considerably improve trailer handling, while the power demand would be excessive [11].

An active steering control can effectively enhance vehicle handling in the linear tire operating range, while the performance gain is limited as the tires saturate at high lateral acceleration levels. Alternatively, the effectiveness of active suspensions in the nonlinear tire operating range has been demonstrated, which is attributed to the suspension ability to actively change the normal tire forces. Such suspensions, however, are not feasible for commercial vehicle applications due to their high cost and weight, packing and maintenance challenges and high power demand [98]. Braking-based stability control systems have also been proposed for enhancement of directional stability limits when

tires operate in the nonlinear range. Braking system is the most vital actuator in the chassis not only for decelerating the vehicle, but also for controlling its lateral movement through differential braking of individual wheels [11, 92]. The braking-based stability control systems can effectively reduce vehicle tendency to oversteer and sideslip velocity of vehicle, and thereby improve the yaw and roll stability limits of the vehicle with minimal external power [92]. It has been reported that braking-based control systems are quite effective in improving vehicle stability and safety, while the effects on the vehicle drivability are ignored [98]. The braking-based control systems could also have a negative impact on the vehicle longitudinal dynamics. Roll moment distribution system is a suspension system control that can improve vehicle handling quality at relatively low power levels than the fully active suspension [98, 139]. It can be realized by employing active roll bars that can provide controllable distribution of roll stiffness among the vehicle axles.

1.2.4 Ride Dynamics of Heavy Vehicles

The driver ride comfort performance of a heavy vehicle forms a vital design goal, since the driver is required to sit in the confined workstation for as much as 10 hours a day. The perception of comfort, however, is a complex function of many workstation design factors, noise and vibration. While the human driver's comfort perception is mostly evaluated through subjective measures, the vibration related comfort performance of a vehicle has been well correlated with the objective measures based on acceleration responses [3, 6, 45, 110, 111]. Gillespie [110] has systematically discussed the ride dynamics and ride comfort of heavy trucks, while a recent review on heavy vehicle ride comfort has been presented by Jiang et al. [111]. Owing to the direct association of

vibration with the comfort perception of the driver and preservation of the cargo, a vast number of studies have emphasized the design of suspensions to realize effective attenuation of road roughness-induced vibration [3, 6, 110, 111]. A large number of analytical and experimental studies have thus been undertaken to study the ride dynamics of commercial freight as well as passenger vehicles, and to assess the ride comfort performance [110, 111].

Tire-interactions with the random road roughness, unlike steering and braking/traction maneuvers that directly relate to vehicle handling quality, serve as the primary excitation when evaluating the ride performance of a suspension together with the suspension stroke requirements and roadholding properties [3, 6, 15]. Moreover, road roughness is a complex input beyond the control of vehicle design engineer and the driver [3]. A thorough understanding of characteristics of the road profiles is thus critical for chassis and vehicle development [112, 113]. The ride properties of vehicles are mostly usually assessed under conditions of constant speed and straight-line travel, while only minimal efforts have been made to study ride during steering and/or braking/acceleration [3]. Ride quality during these maneuvers may strongly affect the driver's perception, reaction on vehicle handling and control, and control abilities of the vehicle.

While the time-histories of road profiles are popularly used as the inputs for analytical vehicle models, road roughness is generally characterized by its power spectral density (PSD) [3, 21, 110]. The PSD of road roughness can be represented in terms of elevation or acceleration against the wave number. For roll dynamics analyses, the roll deflection characteristics of road roughness can be described in terms of the roll-displacement PSD normalized by vertical-displacement PSD, where the roll displacement

refers to the elevation difference between the left- and right-wheel tracks, and the vertical displacement represents the average of both the elevations [21, 110]. It should be noted that the lateral vibrations are considered to be least important for ride comfort evaluations [110]. Unlike the vertical and roll dynamics, road vehicle pitch dynamics are generally characterized by two features, namely coupling between bounce and pitch motions as well as wheelbase filtering [3, 6, 110]. Although suspension design to realize decoupled bounce and pitch modes may indicate a theoretically desirable ride comfort, it cannot be maintained in practice, upon considering variable load conditions of heavy vehicles. It has also been stated the coupled bounce and pitch modes would be helpful for suppressing the pitch motion, and thus improved vehicle ride comfort [110].

The measures of vehicle ride comfort, namely the vertical, pitch and roll motions, are also strongly related to various handling measures of the vehicle [6, 14]. Gillespie [110] pointed out the high driver's position in a heavy vehicle is not desirable for ride comfort, although it is essential for good driver's visibility and maximizing cargo space. The pitch motion of the vehicle thus serves as the dominant source of fore/aft vibrations at the driver's location. A wide range of studies have developed analytical models of varying complexities to study either handling or ride dynamics of heavy vehicles, which consider distinctly different disturbances [3, 6]. Only a few studies have attempted to investigate both sets of measures, although both groups of studies involve comparable modeling considerations. Moreover, the ride dynamic models of heavy vehicles have been effectively applied to study the variations in dynamic tire loads transmitted to the road, which have been related to the road damaging potentials and roadholding performance of heavy vehicles [3, 21]. These models also emphasize the design of vehicle suspension.

The ride dynamic responses of road vehicles have been analyzed through experimental as well as analytical means. The experimental studies focus an assessment of ride performance in terms of acceleration responses, or relative assessments of different suspension systems [6, 111]. The analytical studies involve detailed modeling of vehicle suspension components and inertia/mass distribution. The reported models range simple and linear single- or two-degree-of-freedom (DOF) quarter car models to three-dimensional and nonlinear multi-DOF models. A two-DOF quarter vehicle model is most commonly used to study the vertical dynamics of vehicle, and tuning or role of the suspension components, while it does not permit analyses of roll and pitch motions, and coupling effects of different axles [6]. Linear and nonlinear 4- and 5-DOF half-car roll plane models have also been extensively used to study coupled roll and vertical dynamic performances of road vehicles assuming constant forward velocity [21, 28]. Such models have been applied for analysis of interconnected mechanical suspension systems to achieve a better compromise between the ride properties and roll dynamics [21, 28, 105]. Vertical and pitch dynamic responses of road vehicles have also been widely investigated using 2- or 4-DOF pitch plane models assuming constant forward velocity, while most of them focus on the wheelbase filtering effect [47, 114]. A comprehensive 7-DOF pitch plane model including tire rotations has also been developed to study both vertical and pitch dynamic responses under braking or acceleration [115].

In order to study vertical ride, and roll and pitch dynamic responses of a vehicle more comprehensively, a number of three-dimensional full car models have also been developed [111, 140, 141]. These include linear and nonlinear 7-DOF full car models, comprising heave, roll and pitch motions of the sprung mass, and vertical motions of

independently suspended unsprung masses. The models for heavy vehicles with beam or solid axles invariably consider roll and vertical motions of each axle. The influence of suspension properties on vertical, roll and pitch responses have been widely explored by such ride models. Such models, however, do not include the longitudinal, lateral and yaw motions of the vehicle, and thus cannot predict handling and directional dynamics responses of the vehicle during steering and/or braking maneuvers.

1.2.5 Vehicle-Road Interactions

The normal force developed at the tire-road interface compromises static and dynamic tire force components. The pavement stresses caused by tire loads have been directly related to variations in the tire forces transmitted to the pavement [3, 21]. The dynamic tire loads of a heavy vehicle are strongly related to the static and dynamic properties of the vehicle suspension, including their static load sharing characteristics, apart from the static axle loads. Uneven load sharing could cause high stresses and strains in the pavement and additional pavement damage [21]. The pavement fatigue and failure are affected by a number of factors in a highly complex manner, which are related to the road properties, the vehicle and the environmental conditions. The main types of road damages induced by heavy vehicles are the fatigue cracking and permanent deformations [21]. Road fatigue damage generally increases with axle loads, road roughness and vehicle forward velocity. A thorough review of the literature concerned with tire-road contact forces generated by heavy vehicles and their influences on the road surface response and damage has been presented by Cebon [120].

A number of studies have explored the dynamic tire forces, and road damage potentials of heavy vehicle tire loads [3, 21, 116-119]. The dynamic tire forces are

depended on axle configurations, vehicle geometry, road roughness, forward speed, and suspension and tire properties. Various studies have shown that the dynamic tire loads can be effectively reduced by lowering vertical suspension rate. It has been suggested that a suspension with stiffness about 0.2 times and twice the damping of the current air suspension system would help minimize the road damage [21]. Such a suspension, however, will experience excessive static and dynamic deflections, and exhibit extreme sensitivity to load variations. Anti-roll bars and interconnected hydro-pneumatic suspensions permit the use of relatively softer suspensions. Additionally, soft suspensions might be impractical, considering handling and control requirements. The effects of suspension damping property on the dynamic wheel loads have also been presented in a few studies [116, 118]. These studies have concluded that asymmetric suspension damping cold help reduce dynamic tire loads with only negligible influence on vehicle ride vibration in the ride frequency range.

A number of performance measures have been proposed to assess the relative aggressivity of heavy vehicles and to study the influences of various design and operating factors [21]. These include the dynamic load coefficient (DLC), road stress factor (RSF), etc. The relative road damage potentials of heavy vehicles are mostly assessed in terms of dynamic load coefficient (DLC) of tire forces, which is defined as the ratio of root mean square (RMS) dynamic tire force to the mean tire force. The DLC is also most frequently applied to assess the relative road-friendliness of different vehicle configurations and suspension designs [21, 116, 118]. DLC of heavy vehicles generally ranges from 0.1 to 0.3 under normal straight line driving condition, and increases with increase in road roughness, suspension vertical stiffness, vehicle speed, and tire inflation pressure [21].

Apart from the road-friendliness or road damage potential of heavy vehicles, the other important issue of vehicle-road interactions is roadholding, which strongly influences the longitudinal and lateral forces developed by tires, and thus the handling and directional stability of vehicles. Moreover, roadholding quality of road vehicles also affects the important functions of various steering control and braking-based dynamic stability control systems, since these advanced control systems rely on the tire normal loads to develop adequate forces and moments in the yaw plane. The design of suspension strongly influences the roadholding quality of road vehicles [31, 32, 121-125]. For a full vehicle suspension system, there are four fundamental vibration modes, namely bounce, roll, pitch and warp. It has been well accepted that the warp mode should be designed to be as soft as possible in order to improve the roadholding property [31, 32, 121-125]. For a conventional passive vehicle suspension, these four modes, however, are strongly coupled. The use of anti-roll bars could decouple the roll mode from bounce/pitch, to improve roll stability of vehicles. It, however, also increases the warp mode stiffness of the suspension system, which is detrimental for roadholding property. Therefore, it will be highly desirable to explore the mechanisms by which the four modes can be independently tuned, or partly decoupled in a positive manner.

1.2.6 Passive Interconnected Suspension

Vehicle suspensions involving mechanical interconnections in the roll plane are generally applied to achieve low vertical stiffness and high effective roll stiffness, although there are some examples for reducing roll stiffness, such as the use of Z-bar [17]. Concepts in fluidic interconnections have also been investigated to achieve relatively soft vertical ride, and desirable roll and pitch stiffness and damping properties

[25-30]. Such fluidic interconnections offer considerable potential for realizing soft vertical ride, high roll and pitch stiffness, and tunable damping characteristics. The reported studies on passive interconnected suspensions are discussed below.

Interconnected Mechanical Suspension System

Some studies have explored the performance characteristics of mechanically interconnected suspension system to achieve enhanced anti-roll and anti-pitch responses of automobiles [44, 126, 127]. Interconnected mechanical suspension systems in roll plane are generally implemented to achieve higher roll stiffness through anti-roll bars, and thus enhanced roll stability. Sharp and Dodu [127] presented a kinematic cross-linking suspension system for automobiles, as shown in Figure 1.1. The independent suspension systems are diagonally interconnected in the roll plane (between $p23$ and $p22$; and between $p21$ and $p24$). The study has shown that the roll-interconnected suspension design could reduce roll motion considerably, while the design is relatively sensitive to geometric changes due to load variations.

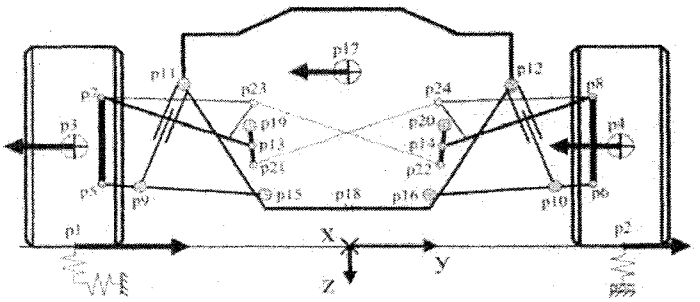

Figure 1.1: A roll-interconnected independent suspension system [127].

A few concepts in mechanically interconnected suspension systems in the fore-aft direction have also been developed to achieve reduced pitch stiffness and thus improved

ride properties by varying the effective spring rates of suspension systems [17, 126]. Figure 1.2 illustrates schematics of two different concepts in pitch-interconnected suspension systems. Lower pitch stiffness, however, results in larger pitch motion of the vehicle due to dynamic load transfer under braking or acceleration.

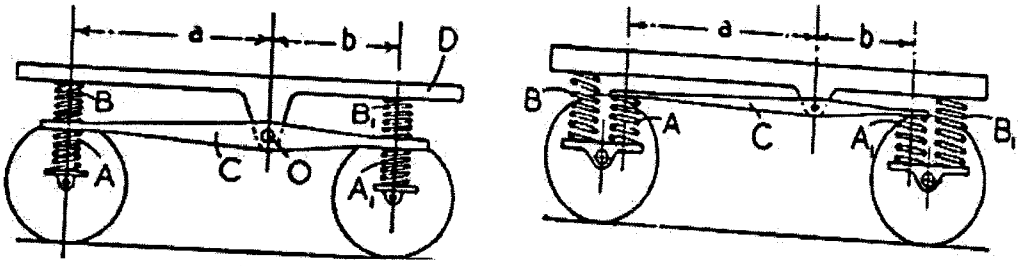

(a) (b)

Figure 1.2: Schematics of pitch-interconnected mechanical suspension systems [126].

Interconnected Hydraulic/Pneumatic Suspension System

The concepts of hydraulic interconnection have also been developed to improve vertical ride, roll and pitch responses [25-30, 128-130]. Moulton and Best [128-130] developed Hydrolastic and its successor, Hydragas suspension units, as shown in Figure 1.3. Compared with the Hydrolastic unit with a built-in rubber spring, the Hydragas suspension strut was developed to replace the rubber spring with the gas spring. The Hydragas suspension units offer simpler means to achieve interconnections between the hydraulic or pneumatic chambers. Figure 1.4 illustrates schematics of a pitch-interconnected Hydragas suspension involving interconnection between the hydraulic chambers. In the bounce mode, no fluid flows between the front and rear Hydragas units, as shown in Figure 1.4(a). But in the pitch mode, the flows through interconnecting pipes could result in lower pitch stiffness of the car, and thus improved ride quality, as shown in Figure 1.4(b). The proposed interconnected suspension, however, exhibits more

sensitivity to dynamic load transfers encountered under braking and acceleration, which may be partly compensated by utilizing suspension linkages.

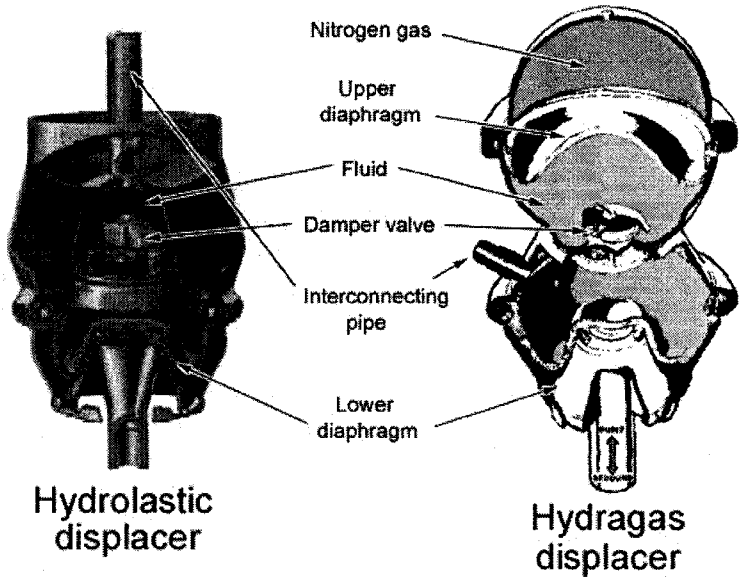

Figure 1.3: Moulton Hydrolastic and Hydragas suspension units [142].

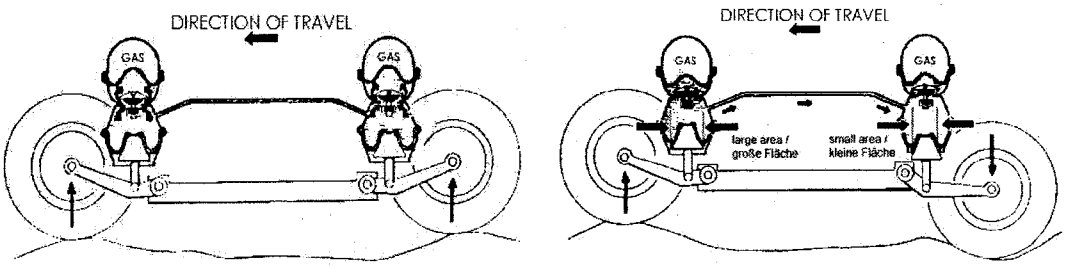

(a) (b)

Figure 1.4: Interconnected Hydragas suspension systems in the pitch plane: (a) bounce; and (b) pitch [130].

A few studies have also investigated the ride properties of vehicles with interconnected pneumatic suspension systems [126, 131]. Figure 1.5 illustrates the schematics of such interconnected suspensions using two different types of air bags [126]. It has been reported that air springs with constant effective working area would be inadequate due to their inability to retain the static equilibrium under load variations caused by braking/acceleration maneuvers. An alternative configuration with variable

effective area, shown in Figure 1.5(b), was considered to be more beneficial in view of ride quality. The use of liquids with significantly less compressibility, instead of air springs, coupled with a gas reservoir (chamber A, shown in Figure 1.5(b)), could yield rapid response time, and improved vertical ride. This concept is similar to the hydro-pneumatic suspension proposed by Moulton and Best [130] and shown in Figure 1.4. Bhave [131] investigated a model of interconnected air suspension in the pitch plane, as shown in Figure 1.6. The study has shown that an optimum capillary flow coefficient exists which could minimize the bounce and pitch mode vibration transmissibilities over the entire frequency range considered. The optimum result, however, might not be applicable for a vehicle operating over a wide range of speeds. Moreover, the effects of the parameters on the suspension rattlespace and roadholding properties were not explored.

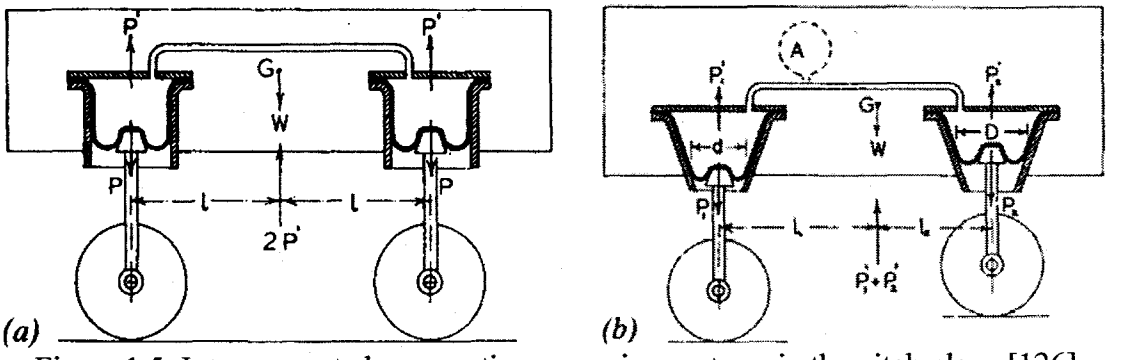

Figure 1.5: Interconnected pneumatic suspension systems in the pitch plane [126].

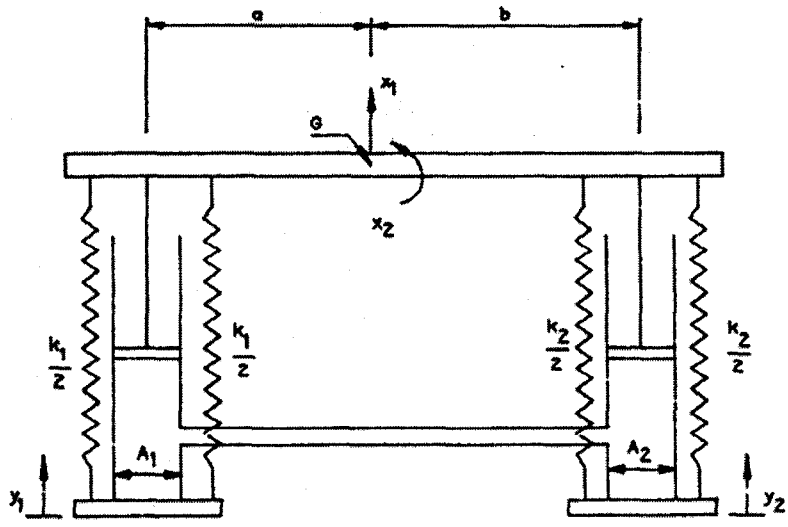

Figure 1.6: Interconnected air suspension system in the pitch plane [131].

The hydraulically or pneumatically interconnected suspensions in the pitch plane, discussed above, invariably resulted in lower pitch stiffness, which is more sensitive to dynamic load transfers encountered during braking/acceleration. Alternative interconnections and couplings, however, can be realized to achieve higher roll and/or pitch stiffness to control the vehicle attitude. The roll-interconnected hydro-pneumatic suspension struts with external gas chambers and damping valves have been investigated in several studies [25, 27, 28]. Figure 1.7 illustrates such interconnected hydro-pneumatic suspension struts in the roll plane. The lower and upper chambers of the left strut are connected to the upper and lower chambers of the right strut, respectively, to achieve high and tunable roll stiffness. These studies have concluded that the ride comfort and anti-roll performance of a vehicle could be considerably enhanced by such interconnections. However, the load carrying capacity of the proposed struts is related to the rod area, and thus a relatively larger strut size or extremely high pressure is required. The hydro-pneumatic struts combined with passive unconnected springs, interconnected

in the roll plane, have also been explored in an attempt to reduce the strut working pressure [29], as shown in Figure 1.8. It has been shown that while the passive unconnected springs could effectively share the load and thus reduce the working pressure, the effectiveness of the interconnected suspension system is significantly reduced.

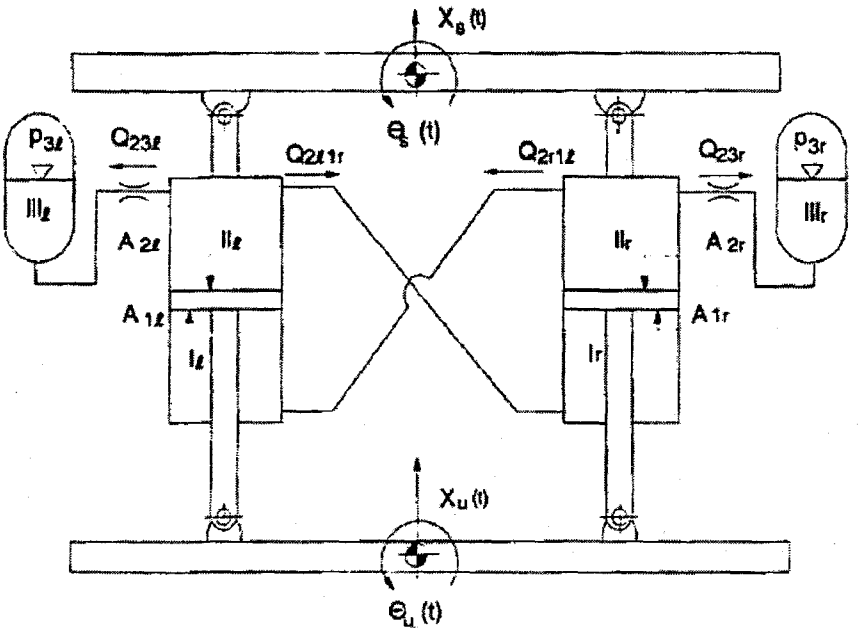

Figure 1.7: Interconnected hydro-pneumatic suspension in the roll plane of a heavy vehicle [25, 27, 28].

Wu [30] proposed a new hydro-pneumatic suspension strut with integrated gas chamber yielding a compact design and a relatively larger working area, thereby reducing the operating pressure. Two configurations of roll-interconnected struts involving connections between different chambers of the left and right struts were investigated to study the resulting vertical and roll mode stiffness and damping properties of the suspension system, as shown in Fig. 1.9. A detailed analysis of one of the configuration involving interconnections between chamber 1 of the left/right strut to the chamber 2 of the right/left struts (as shown in Fig. 1.9(a)), conducted in the course of this dissertation

research revealed uncoupled behavior of such configuration. The configuration involving interconnections between chambers 1 and 3, however, resulted in enhanced roll stiffness and damping properties, as shown in Figure 1.9(b). The reported analyses have considered negligible contributions due to fluid compressibility and seals friction on the suspension properties [25, 27-30].

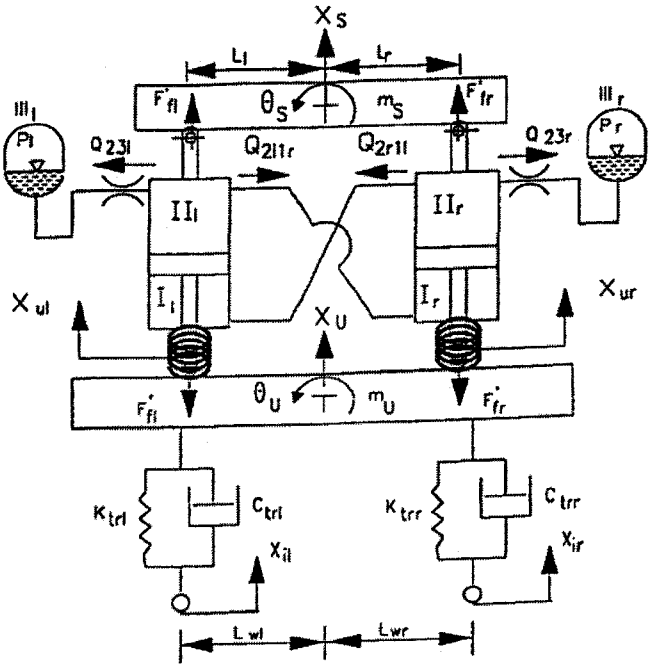

Figure 1.8: Spring loaded interconnected hydro-pneumatic suspension in the roll plane [29].

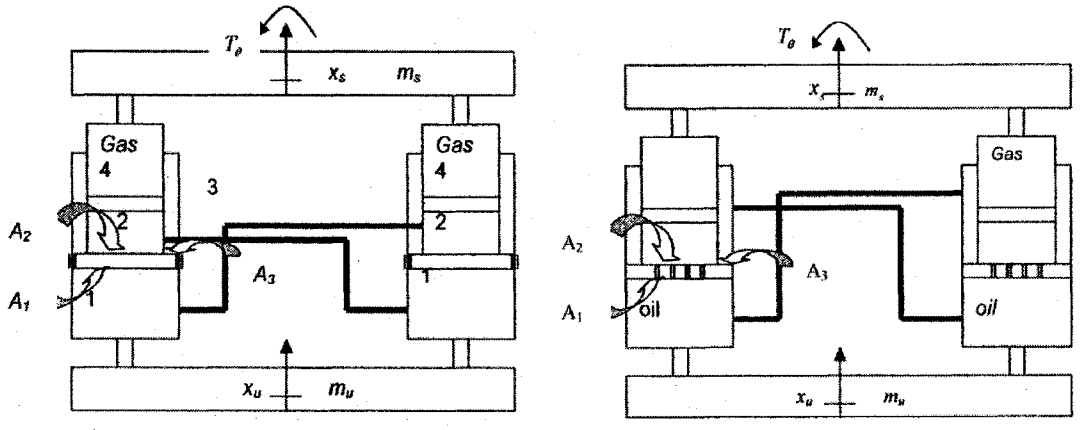

Figure 1.9: Interconnected hydro-pneumatic suspension systems in the roll plane [30].

1.2.7 Semi-Active and Active Interconnected Suspension

Semi-active and active interconnected suspension systems have also been explored to obtain a better compromise among the ride comfort and handling properties. Vast majority of these, however, have investigated different concepts in active anti-roll bars to achieve enhanced roll stability and ride comfort [3, 21, 132]. Only a few studies have analyzed interconnected hydro-pneumatic suspensions incorporating either semi-active or active controll to achieve soft responses to road disturbances, good attitude control and self-leveling [26, 133].

Kusahara et al. [132] investigated the performance of a medium-duty truck with active anti-roll bars through vehicle tests. Figure 1.10 illustrates the control system implemented for the truck, which actuated both the front and rear anti-roll bars by using the steering angle and vehicle speed as the inputs. The test results showed that a significant reduction in roll motion of the truck could be achieved under steady steering and lane change maneuvers, while maintaining soft vertical ride. Semi-active and active interconnected suspensions have also been proposed on the basis of hydraulic or pneumatic interconnections [25, 26, 133]. Felez and Vera [25] investigated an active roll-interconnected hydro-pneumatic suspension system for crane vehicles, as shown in Figure 1.11. The valve was controlled by the pressure difference between the upper chambers of the left and right struts. The simulation results revealed that while the effect of the active interconnected suspension on the vertical ride response of the vehicle was negligible, the roll response of the vehicle was significantly improved.

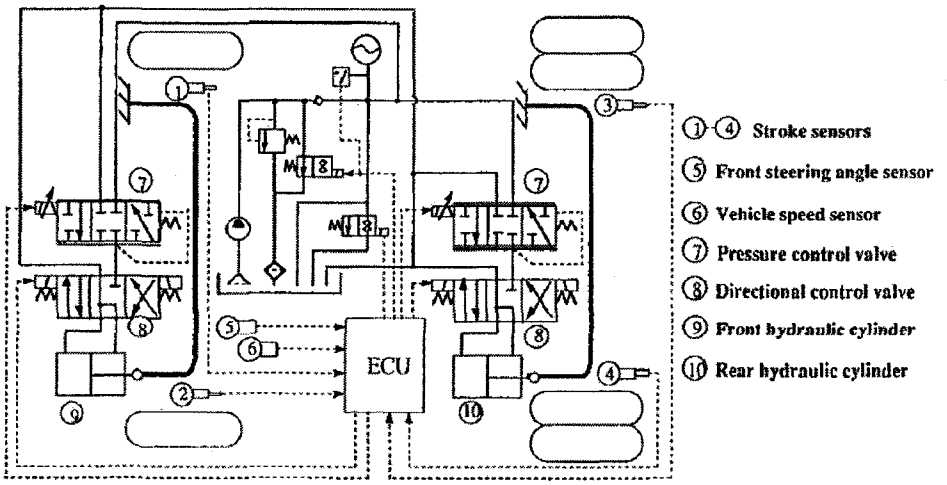

Figure 1.10: Active anti-roll bar control system for a medium-duty truck [132].

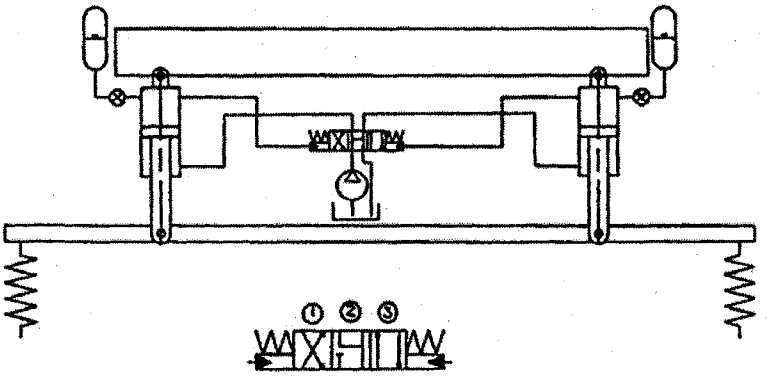

Figure 1.11: Active interconnected hydro-pneumatic suspension system in the roll plane [25].

Active roll control systems based upon interconnected Hydragas suspension units, similar to those proposed by Moulton and Best [128], have also been proposed to achieve reduced roll motions of light vehicles [133, 134]. On the basis of simulation results, Rosam and Darling [133] concluded that a lower bandwidth would be sufficient for roll control of vehicles under severe transient maneuvers. Moreover, a single actuator would be sufficient to achieve the vehicle roll control, when different suspension units are interconnected. This is an attractive feature when compared with a fully-active control system that may require either four actuators or two actuators when active anti-roll bars

are considered. Schumann and Anderson [134] studied the performance of an active interconnected Hydragas suspension for an off-road utility vehicle. The simulation results showed that significant reduction in body roll could be obtained, while the degree of reduction was dependent upon the nature of maneuvers and magnitudes of steering inputs.

A recent study has proposed a semi-active roll-interconnected suspension for automotive application, as shown in Figure 1.12 [135]. Each suspension strut, developed by Advanced Motion Technology, comprised a variable air spring and an electromagnetic damper, which could respond in a fraction of a millisecond. The air springs were pneumatically interconnected to reduce body roll motion, while the roll stiffness could be adjusted by the control valve. Large size diaphragms required lower operating pressure, and thus minimized the energy requirement of the control system. The interconnected pneumatic system in coordination with the electromagnetic dampers could control body roll and pitch motions under acceleration, braking, cornering, and aerodynamic inputs. The proposed system, however, requires large size air bags and an on-board compressor.

Crolla et al. [26, 136] studied a semi-active hydro-pneumatic suspension interconnected in the roll and pitch planes for an agricultural off-road vehicle, which was developed by Automotive Products Limited (AP), as shown in Figure 1.13. Simulations were performed for the passive and semi-active suspension systems based on a 7-DOF full car model. The roll stiffnesses could be conveniently controlled by diagonally interconnecting the upper chambers of the front struts to the lower chambers of the rear struts, and by connecting the upper chambers of the rear struts, as shown in Figure 1.13(a). The damping forces due to the interconnections, however, were not formulated

and investigated. Figure 1.13(b) illustrated the general layout of the AP semi-active suspension. The simulation and experimental results have shown that the proposed semi-active interconnected suspension system could offer improved ride comfort, self-leveling and attitude control of the vehicle.

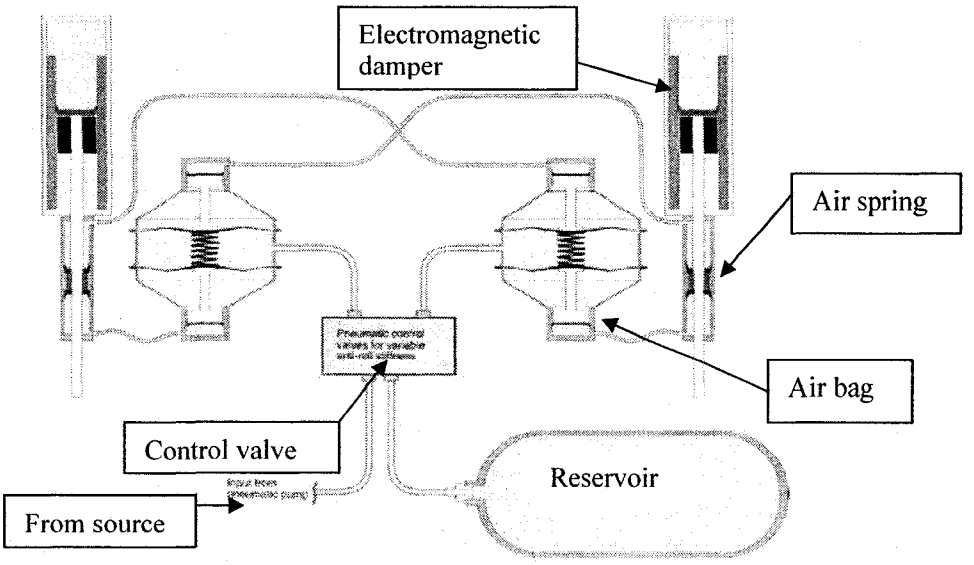

Figure 1.12: Semi-active roll control using interconnected pneumatic system [135].

Fukuda et al. [137] investigated preview control of an interconnected suspension configuration for off-road vehicles, as schematically shown in Figure 1.14. The flow across the interconnected upper and lower chambers was controlled by flow control valves. The analytical and experimental results revealed that the use of preview control of the interconnected suspension system could compensate for the response time delay, and provide improved attitude control of vehicle operating on a rough terrain. Both the concepts proposed by Crolla et. al [26, 136] and Fukuda et al. [137] require considerable power for the hydraulic pump and on-board AC motors.

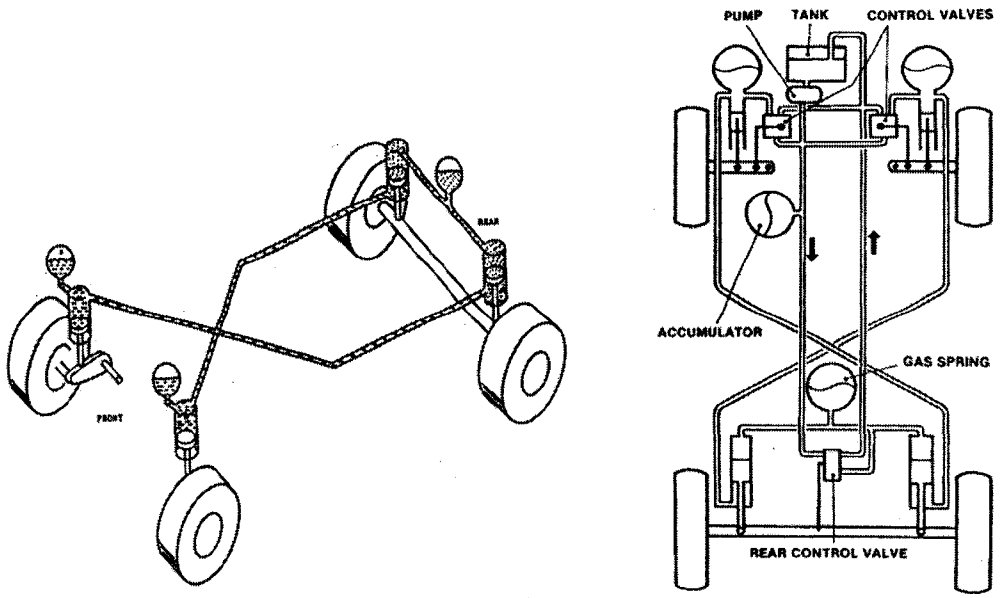

(a) (b)

Figure 1.13: Schematics of AP suspension: (a) Interconnection configuration [26]; and (b) Layout of AP suspension [44].

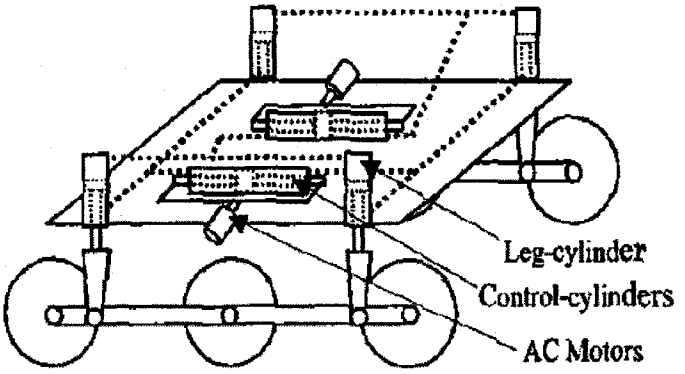

Figure 1.14: Schematic of a full-vehicle semi-active interconnected suspension system [137].

1.3 Scope and Objectives of the Dissertation

From the review of literature, it is apparent that vehicle suspension involves considerable design challenges in order to realize satisfactory roll and pitch motion control, handling and directional responses, ride and tire load performance of the vehicle. The studies also suggest that vehicle suspensions with relatively low vertical stiffness and

variable damping, low warp stiffness, high effective roll stiffness and damping, and variable pitch properties, could help achieve a satisfactory compromise among the concerned measures. Vehicle suspensions interconnected in roll and pitch planes offer considerable potentials for realizing variable roll and pitch stiffness and damping properties in a highly flexible manner, while retaining desirable vertical ride and without deteriorating the warp mode property. Although anti-roll bars have been widely used to achieve additional roll stiffness and thus improved roll stability limits, they tend to add weight, and degrade the ride comfort performance to some extent. The passive fluidic interconnections, on the other hand, offer considerable potential to achieve high roll stiffness and high low speed roll mode damping for improving the roll stability performance, while maintaining a soft vertical ride. Moreover, the fluidic interconnections can also be conveniently implemented in the pitch plane to realize desirable pitch mode properties.

While a few studies have investigated the properties of roll-interconnected hydro-pneumatic suspension systems, the analyses have been limited to incompressible fluids and frictionless main and floating pistons. Moreover, the majority of these studies have employed large size struts to achieve reasonable working area, which is determined by the rod area. The high load carrying requirements of heavy vehicles would thus require high operating pressure and thus additional challenges in design of seals. The use of alternative design of struts with larger effective area is thus desirable for application in interconnected suspension for heavy vehicles. While a few studies have shown considerable potential of pitch-interconnected suspensions in realizing improved anti-

pitch or attitude control, no attempts have been made to characterize the anti-pitch and anti-roll properties of a three-dimensional suspension interconnection.

Objectives of the Dissertation Research

The overall objective of this dissertation research is formulated to investigate the anti-roll and anti-pitch properties of concepts in interconnected hydro-pneumatic suspension systems for a class of heavy vehicles. The properties and performance characteristics of the proposed concepts are investigated for multiple objectives involving ride comfort, tire force variations, and handling and directional dynamics performance. The specific objectives of the proposed dissertation are as follows:

- Propose concepts in roll-, pitch-, and combined roll- and pitch-plane interconnected hydro-pneumatic suspension systems based upon a compact strut design integrating the pneumatic spring and damping valves.
- Formulate analytical models of the two- and three- dimensional interconnected suspensions to derive essential stiffness and damping properties related to anti-roll, anti-pitch, vertical ride and tire load performance characteristics of a vehicle.
- Investigate the effects of hydraulic fluid compressibility on the roll and pitch properties of the interconnected suspension.
- Evaluate performance characteristics of interconnected suspension configuration in two- and three-dimensions under excitations arising from the road roughness, directional maneuvers as well as crosswind.
- Perform parametric sensitivity analyses to identify the desired design parameters and desired variations in the roll and pitch properties of the interconnected suspension systems.
- Explore fundamental guidelines on pitch-plane tuning of a heavy vehicle suspension.
- Investigate the properties of an alternative concept of a twin-gas-chamber strut

through analytical formulations and analyses.

Organization of the Dissertation

This dissertation is organized into seven chapters together with one appendix describing systematic developments and analyses in achieving the above-stated objectives.

Chapter 2 presents conceptual designs of two hydro-pneumatic suspension struts, including a single-gas-chamber strut and a novel twin-gas-chamber strut. The struts integrate the gas chamber(s) and damping valves within the same unit to realize a compact design, while offering considerably larger effective operating area and greater flexibility in realizing interconnections. Both the roll-plane and pitch-plane vehicle models are developed, based on which the strut forces and in-plane properties of different unconnected and interconnected suspension configurations are derived, upon consideration of compressible hydraulic fluid. A generalized model of strut force due to various suspension configurations is further developed.

In Chapter 3, the roll-plane model of a heavy vehicle, employing various configurations of roll-connected and unconnected suspension struts formulated in the previous chapter, is analyzed to investigate the suspension properties, and vertical and roll dynamic responses of the vehicle. The model together with suspension formulations is analyzed under excitations arising from vehicle-road interactions, steering maneuvers and crosswinds. The fundamental properties in the roll plane are evaluated in terms of suspension rate, roll stiffness, and bounce and roll mode damping. Symmetric and asymmetric damping valves are also considered to realize desirable damping properties in

the vertical and roll modes. The design flexibility of the fluidic interconnected suspensions is illustrated through parametric studies. The dynamic responses of the vehicle with different suspension configurations are further explored.

Chapter 4 explores the performance characteristics of different interconnected suspensions, involving pneumatic, hydraulic and hybrid-fluidic couplings in the pitch-plane of the heavy vehicle. The pitch-plane braking model of a heavy vehicle is integrated with various pitch-connected and unconnected suspension configurations formulated in Chapter 2, to investigate the suspension properties, and vehicle vertical and pitch dynamic responses under excitations arising from random road roughness and braking maneuvers. The suspension properties in the pitch plane are evaluated in terms of suspension rate, pitch stiffness, and bounce and pitch mode damping. Parametric studies are also performed to demonstrate the design flexibility of the pitch interconnected suspensions. The dynamic responses of the pitch-plane vehicle model with different suspension configurations are further explored.

Chapter 5 further extensively investigates the performance potentials of the twin-gas-chamber strut suspension arranged in either roll-plane or pitch-plane, in relation to those of the single-gas-chamber strut suspensions. The performance analyses are presented in terms of suspension properties and vehicle responses to different excitations. The design flexibility of the twin-gas-chamber strut suspensions is also explored through parametric studies. The fundamental pitch dynamics and suspension tuning of heavy vehicles are further explored, and a set of suspension tuning rules is proposed (presented in Appendix A).

Chapter 6 focuses on exploring interconnected hydro-pneumatic suspension systems in a full-vehicle arrangement that involves four suspension-strut units. A 14-DOF full-vehicle model is analytically developed and validated using measured data, which facilitates the evaluation and comparison of different suspension systems, either interconnected or unconnected. The feasibilities of various full-vehicle interconnected suspensions involving the two previously-proposed hydro-pneumatic struts are analyzed based on a simplified measure for heavy vehicles. The fundamental suspension properties and vehicle dynamic responses of a hydraulically X-coupled suspension system are investigated and compared with an unconnected suspension system. The suspension stiffness and damping properties are evaluated in terms of four fundamental modes, namely bounce, roll, pitch and warp. The analytical formulations of strut forces and suspension properties due to these two selected suspension systems are derived, based on which the suspension properties are simulated and compared, and vehicle dynamic responses are further evaluated under braking-in-a-turn and split-μ straight-line braking inputs.

The highlights and major conclusions of the dissertation research, and recommendations for the future work are presented in Chapter 7.

CHAPTER 2

MODEL DEVELOPMENT OF IN-PLNAE INTERCONNECTED SUSPENSION

2.1 Introduction

Only a few studies have investigated the performance characteristics of interconnected vehicle suspension systems in different vehicles ranging from conventional passenger cars to extremely challenging World Rally racing vehicles [25-32, 122-124]. These have shown superior performance improvements compared to traditional unconnected suspensions. The most important factor hindering the popular use of such suspension systems is most likely the lack of thorough theoretical formulations for effective design and performance analysis.

While the considerable potential benefits of the fluidic interconnections among different hydro-pneumatic struts have been demonstrated in a few studies [25-32], other studies have highlighted the significant commercial potential of hydro-pneumatic technology applied to vehicle systems [14, 22-24]. A few of these studies have attempted to explore the fundamental properties of interconnected hydro-pneumatic suspensions as well as vehicle dynamic responses, which however have been limited to roll plane analysis alone [28-30]. Moreover, these studies have generally considered a strut design with relatively small effective operating area, and external gas chambers and damping valves. These would lead to a bulky strut or very high gas pressure, which is definitely undesirable for practical applications. Furthermore, the strut forces and suspension properties in these studies were developed by assuming incompressible hydraulic fluid.

In this chapter, conceptual designs of two hydro-pneumatic struts are presented, including a single-gas-chamber strut and a novel twin-gas-chamber strut. The proposed struts integrate the gas chamber(s) and damping valves within the same unit to realize a compact design, while offering considerably larger effective operating area and greater flexibility in realizing interconnections. Roll-plane and pitch-plane vehicle models are developed, based on which the strut forces and in-plane fundamental properties of different unconnected and interconnected suspension configurations are derived, upon consideration of compressible hydraulic fluid. A generalized model of strut force due to various suspension configurations is further developed.

2.2 Hydro-Pneumatic Suspension Struts

Figure 2.1(a) illustrates the schematic of a hydro-pneumatic strut design, referred to as single-gas-chamber strut *B*, which integrates a gas chamber and damping valves within the same unit to realize a compact design [30]. The strut consists of a number of damping orifices in the main piston separating chamber 1 from chambers 2 and 3, while a floating piston isolates the hydraulic fluid in chamber 2 from the nitrogen gas in chamber 4. The shim disc valves, consisting of shim packs, can be employed in conjunction with constant area bleed orifices to achieve variable flow resistance and thus the damping force. Such compact strut design not only eliminates the external gas chamber and external damping valves, but offers a relatively larger effective working area and thus significantly lower operating pressure corresponding to a given load, compared to those reported in the studies [25, 27, 28, 31, 32].

Figure 2.1(b) shows the schematic of a novel hydro-pneumatic strut design, referred to as twin-gas-chamber strut *A*, in which chambers 3 and 4 contain nitrogen gas, and

damping orifices or valves within the main piston provide resistance to hydraulic flows between chambers 1 and 2. Similar to Strut *B*, the twin-gas-chamber strut also offers a compact design with relatively large effective operating area. Under compression stroke, the gas in chamber 4 undergoes compression and tends to dominate the vertical suspension stiffness property. The spring rate in rebound is mostly determined by the gas pressure in chamber 3, which undergoes compression during rebound. The proposed twin-gas-chamber strut design thus offers considerable potential for realizing nearly symmetric spring rates in compression and rebound.

Compared to those reported in the studies [25, 27, 28, 31, 32], these two strut designs further provide considerable flexibilities to conveniently realize various interconnections among different hydraulic/pneumatic chambers of different struts. The interconnected as well as unconnected suspension configurations investigated in this dissertation are therefore based on these two struts.

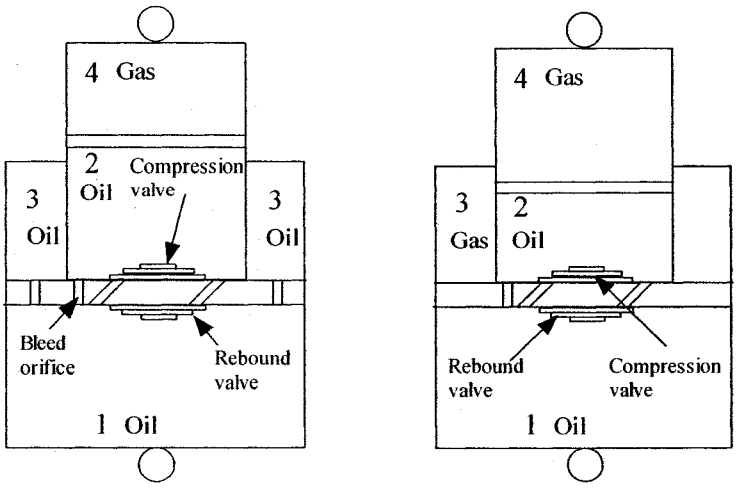

Figure 2.1: Schematics of two strut designs: (a) single-gas-chamber strut *B*; and (b) twin-gas-chamber strut *A*.

2.3 Formulations of Strut Forces in the Roll Plane

The vertical ride and roll dynamics of a vehicle are strongly related to the static and dynamic properties of its suspension system, such as suspension rate, roll stiffness and damping characteristics. The suspension forces, including both stiffness and damping components, combined with roll plane heave vehicle model, can be effectively utilized to derive the bounce and roll properties of different suspension configurations involving unconnected and interconnected struts, and roll and ride dynamic responses.

2.3.1 Roll Plane Model of a Heavy Vehicle

A generalized nonlinear roll plane model of a heavy vehicle is formulated to investigate the relative vertical and roll properties of hydro-pneumatic suspension struts, and vertical ride and roll dynamic responses. The roll plane model, shown in Figure 2.2, comprises two suspension units that may involve transverse interconnections between them. The model considers a beam axle with vertical (z_u), lateral (y_u) and roll (θ_u) degrees-of-freedom (DOF), and a lumped sprung mass with vertical (z_s) and roll (θ_s) DOF. The sprung mass (m_s) is considered to roll about its roll center (RC_1), fixed to the unsprung mass (m_u). The vertical compliance of the tires is represented by linear stiffness (k_t) and damping (c_t) elements, assuming point contact with the road. Series-connected stiffness (k_l) and damping (c_l) elements are used to represent the lateral compliance of each tire [143]. The total forces developed by the left- and right-suspension struts are represented by f_L and f_R, respectively. The equations of motion can be expressed as:

$$m_s \ddot{z}_s = -f_L - f_R + m_s g$$

$$(I_{xxs}+m_s h_2^2)\ddot{\theta}_s + m_s h_2\left[\ddot{y}+(h-h_2)\ddot{\theta}_u\right] = m_s g h_2\theta_s - l_s f_L + l_s f_R + F_y h_2$$

$$m_u \ddot{z}_u = f_L + f_R + k_t(z_{0l}+z_{0r}-2z_u) + c_t(\dot{z}_{0l}+\dot{z}_{0r}-2\dot{z}_u) + m_u g$$

$$\left[I_{xxu}+m_u h_1^2 + m_s(h-h_2)^2\right]\ddot{\theta}_u + m_s h_2(h-h_2)\ddot{\theta}_s + \left[m_u h_1 + m_s(h-h_2)\right]\ddot{y} =$$

$$l_s(f_L - f_R) + F_y(h-h_2) + m_u g h_1\theta_u + l_t\left[k_t(z_{0l}-z_{0r}-2l_t\theta_u) + c_t(\dot{z}_{0l}-\dot{z}_{0r}-2l_t\dot{\theta}_u)\right]$$

$$(m_u+m_s)\ddot{y} + m_s h_2\ddot{\theta}_s + \left[m_u h_1 + m_s(h-h_2)\right]\ddot{\theta}_u = F_y - 2k_l(y-y_c)$$

$$k_l(y-y_c) - c_l\dot{y}_c = 0 \qquad (2.1)$$

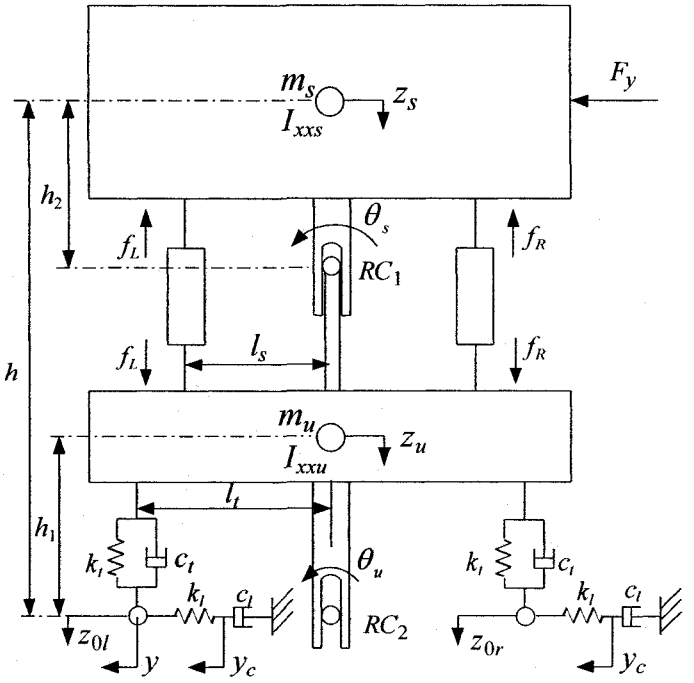

Figure 2.2: Roll plane model of a heavy vehicle.

where I_{xxs} and I_{xxu} are the roll mass moments of inertia due to the sprung and unsprung masses, respectively, g is acceleration due to gravity, and z_{0l} and z_{0r} represent the road elevations at the left and right tire-road interfaces, respectively. F_y is the centrifugal force acting on the sprung mass that may arise from a directional maneuver or crosswind, h and h_1 are the c.g. heights of the sprung and unsprung masses from the ground, respectively, l_s and l_t are half suspension-spacing and half track-width, respectively. h_2 is the vertical distance between the RC_1 and the sprung mass c.g.

2.3.2 Interconnected and Unconnected Strut forces

Figures 2.3(a) and (b) illustrate the two unconnected suspension configurations, B_{UR} and A_{UR}, which employ two single-gas-chamber struts B and two twin-gas-chamber struts A, respectively. The schematics of two suspension configurations involving hydraulic and pneumatic interconnections are presented in Figures 2.3(c) and (d), respectively. The hydraulic interconnections are realized by connecting the hydraulic fluid chambers 1 and 3 of the left strut to 3 and 1 of the right strut, respectively, as shown in Figure 2.3(c) and referred to as B_{IR}. For the pneumatic interconnection, the gas replaces the hydraulic fluid in chamber 3, where chambers 3 and 4 of the left strut are connected to chambers 4 and 3 of the right strut, respectively. This configuration (referred to as A_{IR}) is shown in Figure 2.3(d). The suspension forces developed by struts in each suspension configuration are derived upon considerations of the continuity equations, flows through damping orifices and interconnecting pipes when presented, and the relative vertical and roll motions of the sprung and unsprung masses.

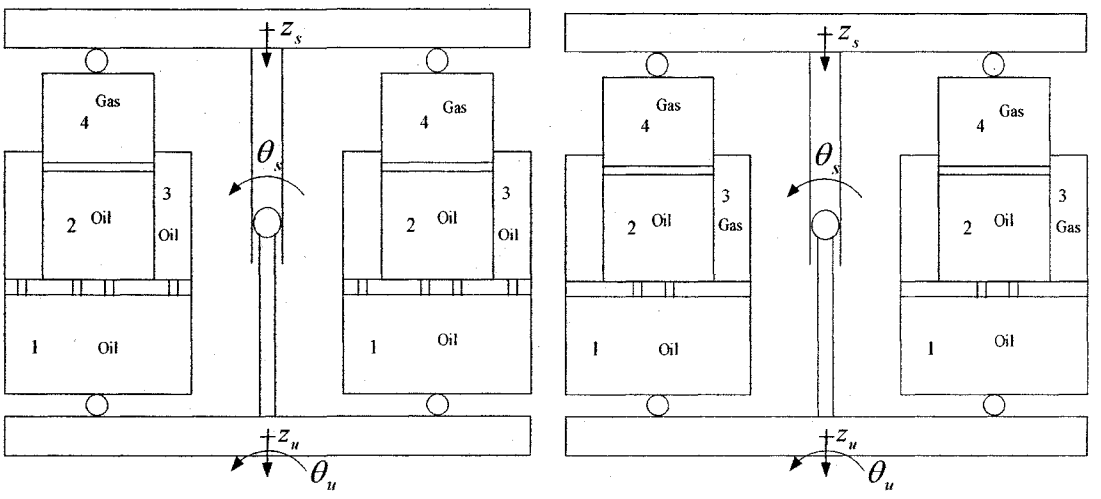

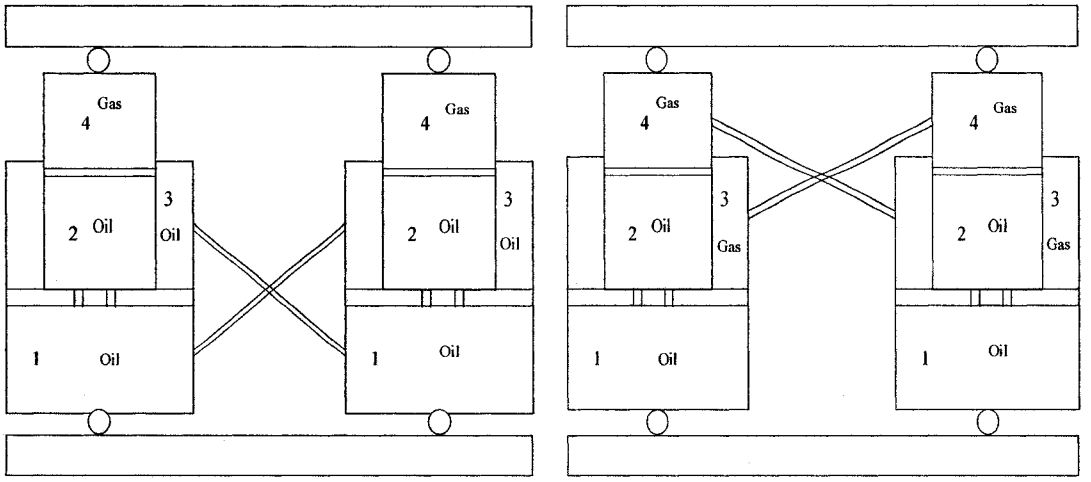

(c) (d)

Figure 2.3: Unconnected and interconnected hydro-pneumatic suspension configurations in the roll plane: (a) unconnected single-gas-chamber strut suspension, B_{UR}; (b) unconnected twin-gas-chamber strut suspension, A_{UR}; (c) hydraulic interconnection, B_{IR}; and (d) pneumatic interconnection, A_{IR}.

FORMULATIONS OF HYDRAULICALLY CONNECTED STRUT FORCES (B_{IR})

The major assumptions made in formulating the forces developed by roll-interconnected struts (B_{IR}) include: (i) ideal friction between the floating and main pistons seals and the cylinder; (ii) compressible hydraulic fluid; (iii) turbulent flows through damping orifices; (iv) laminar flows through interconnecting pipes; (v) polytropic process of the gas in the gas chambers; (vi) negligible leakage across the pistons; and (vii) negligible thermal expansion of the cylinder, piston and oil.

The static load supported by a strut is related to the static gas pressure P_0 and the effective working area, such that:

$$w_i = (P_0 - P_a)A_{2i} \quad (i = l, r) \tag{2.2}$$

where the subscripts l and r refer to left- and right-struts, respectively, w_i is the static load supported by the strut i (i=l,r), P_a is atmospheric pressure, and A_{ji} is the effective piston area reflected on the chamber j (j=1,2,3) side of the strut i (i=l,r).

Equations of fluid flow

The instantaneous volume of fluid V_{1l} of chamber 1 of strut l can be expressed as:

$$V_{1l} = -V_{12l} - V_{1l3r} + \Delta V_{c1l} + V_{10l} \tag{2.3}$$

where V_{12l} is the change in volume due to flows through damping orifices from chamber 1 to 2, V_{1l3r} is fluid volume due to flows through interconnecting pipes from chamber 1 of strut l to chamber 3 of strut r, ΔV_{c1l} is the volume change due to fluid compressibility, and V_{10l} is the initial fluid volume in chamber 1 of strut l. The equation of fluid flow can thus be obtained as:

$$Q_{1l} = -Q_{12l} - Q_{1l3r} + dV_{c1l} / dt \tag{2.4}$$

where Q_{1l} is the rate of change of fluid volume in chamber 1 of strut l, and Q_{12l} and Q_{1l3r} are the flow rate across the damping orifices and the interconnecting pipes, respectively.

The rate of change of fluid volume due to its compressibility can be obtained from the fluid bulk modulus E, and the rate of change of fluid pressure P_{1l} in the same chamber [144]:

$$\frac{dV_{c1l} / dt}{V_{1l}} = -\frac{dP_{1l} / dt}{E} \tag{2.5}$$

The rate of change of fluid volume in chamber 1 of strut l can be further related to the relative velocity $\dot{x}_l$ across the strut l and the effective area on the chamber 1 side A_{1l}, such that:

$$Q_{1l} = A_{1l}\dot{x}_l \tag{2.6}$$

where $\dot{x}_l = \dot{z}_u + l_s\dot{\theta}_u - \dot{z}_s - l_s\dot{\theta}_s$, assuming small motions with positive direction being upward.

The fluid flow rates between the struts l and r can be derived assuming laminar flows through the interconnecting pipes, such that [28, 144]:

$$Q_{1l3r} = \frac{\pi D^4}{128\mu L}(P_{1l} - P_{3r}); \; Q_{1r3l} = \frac{\pi D^4}{128\mu L}(P_{1r} - P_{3l}) \tag{2.7}$$

where P_{ji} is the pressure of fluid in chamber j (j=1,2,3,4) of strut i (i=l,r), μ represents the dynamic viscosity of fluid, and L and D represent the length and diameter of the interconnecting pipes, respectively.

The flow rates Q_{12i} across the damping orifices from chamber 1 to 2 of the same strut are formulated assuming turbulent flows [28, 144]:

$$Q_{12i} = C_d a_{12i}\sqrt{2|P_{1i} - P_{2i}|/\rho}\,\mathrm{sgn}(P_{1i} - P_{2i}) \qquad (i = l, r) \tag{2.8}$$

where C_d is the discharge coefficient, a_{12i} is the total area of damping orifices between chambers 1 and 2 of strut i (i=l,r), and ρ is the mass density of hydraulic fluid. The *sgn* function describes the direction of fluid flow.

Pressure equations

The pressure of fluid in chamber 1 of both struts is derived from Eqs. (2.4)~(2.6), such that:

$$\frac{dP_{1l}}{dt} = E\left(\frac{-A_{1l}\dot{x}_l - Q_{12l} - Q_{1l3r}}{A_{1l}x_{10l} + A_{1l}x_l}\right); \; \frac{dP_{1r}}{dt} = E\left(\frac{-A_{1r}\dot{x}_r - Q_{12r} - Q_{1r3l}}{A_{1r}x_{10r} + A_{1r}x_r}\right) \tag{2.9}$$

The pressures of fluids in chambers 2 and 3 of both the struts are also derived in a similar manner and expressed as:

$$\frac{dP_{2l}}{dt} = E\left(\frac{A_{2l}\dot{x}_{4l} + Q_{12l}}{A_{2l}x_{20l} - A_{2l}x_{4l}}\right); \; \frac{dP_{3l}}{dt} = E\left(\frac{A_{3l}\dot{x}_l + Q_{1r3l}}{A_{3l}x_{30l} - A_{3l}x_l}\right)$$

$$\frac{dP_{2r}}{dt} = E\left(\frac{A_{2r}\dot{x}_{4r} + Q_{12r}}{A_{2r}x_{20r} - A_{2r}x_{4r}}\right); \quad \frac{dP_{3r}}{dt} = E\left(\frac{A_{3r}\dot{x}_r + Q_{1/3r}}{A_{3r}x_{30r} - A_{3r}x_r}\right) \tag{2.10}$$

where x_{j0i} is the initial length of chamber j (j=1,2,3) of strut i (i=l,r), and x_{4i} is the relative displacement of the floating piston with respect to the main piston of the strut i, with positive direction being downward.

The instantaneous pressure of gas in chamber 4 is derived assuming polytropic process of the gas:

$$P_{4i} = P_0\left(\frac{V_{40i}}{V_{40i} + A_{2i}x_{4i}}\right)^n \quad (i=l,r) \tag{2.11}$$

where n is polytropic exponent of gas and V_{40i} is the initial gas volume in chamber 4.

Equations of motion of the floating pistons

Assuming ideal Coulomb friction due to seals, the equations of motion of the floating pistons within the struts can be formulated as:

$$m_{fi}\ddot{x}_{4i} = (P_{4i} - P_{2i})A_{2i} + m_{fi}g - F_{c2i}\,\mathrm{sgn}(\dot{x}_{4i}) \quad (i=l,r) \tag{2.12}$$

where m_{fi} is the mass of the floating piston within strut i, and F_{c2i} is the magnitude of the Coulomb friction force due to the floating piston seals.

Effective damping orifice areas

The vehicle suspension dampers, invariably, exhibit variable damping properties with velocity, which are realized by varying the effective damping orifice areas. Suspension dampers generally exhibit high damping coefficients at low velocities due to flows through bleed orifices, and relatively lower damping coefficients at higher velocities due to flows through additional blow-off valves [144]. Moreover, the damping force in

rebound is generally considerably higher than that in compression to realize improved handling performance. Such variations in damping forces could be realized by linearly varying the effective flow areas of shim disc valves, as shown in Figure 2.1 [144]. Asymmetric damping force in compression and rebound could be achieved by selecting different flow areas and values of threshold and maximum pressure differentials of valves in compression and extension, such that:

$$a_{12i} = \begin{cases} a_{12c} & -P_{esl} \le P_{1i} - P_{2i} \le P_{csl} \\ a_{12c} + a_{12vc} \dfrac{\left(|P_{1i} - P_{2i}| - P_{csl}\right)}{P_{csh} - P_{csl}} & P_{csl} < P_{1i} - P_{2i} \le P_{csh} \\ a_{12c} + a_{12vc} & P_{1i} - P_{2i} > P_{csh} \\ a_{12c} + a_{12ve} \dfrac{\left(|P_{1i} - P_{2i}| - P_{esl}\right)}{P_{esh} - P_{esl}} & P_{esl} < P_{2i} - P_{1i} \le P_{esh} \\ a_{12c} + a_{12ve} & P_{2i} - P_{1i} > P_{esh} \end{cases} \tag{2.13a}$$

where a_{12c} is the bleed orifice area, a_{12vc} and a_{12ve} are maximum effective flow areas of valves in compression and extension, respectively. P_{csl} and P_{esl} are the lower limits or thresholds of pressure differential in compression and extension, which cause deflections of shim discs to initiate valve opening. P_{csh} and P_{esh} are the pressures that cause maximum valve openings, namely a_{12vc} and a_{12ve}. The symmetric damping property in compression and rebound can be easily achieved by letting the parameters: P_{csl}=P_{esl}, P_{csh}=P_{esh} and a_{12vc}=a_{12ve}.

The piecewise linear variations in the flow areas could yield non-differential variations in the fluid pressures in the vicinity of the transition pressures. The preset pressures are also a function of the strut velocity, as evident from Eqs. (2.6)~(2.10). A

refined model is thus developed to smoothen the variations in the flow areas around the transition values, such that:

$$a_{12i}=\begin{cases} a_{12c} & -P_{esl}\le P_{1i}-P_{2i}\le P_{csl} \\ a_{12c}+a_{12vc}\left\{\dfrac{\left(\left|P_{1i}-P_{2i}\right|-P_{csl}\right)}{P_{csh}-P_{csl}}-\dfrac{1}{2\pi}\sin\left[\dfrac{2\pi\left(\left|P_{1i}-P_{2i}\right|-P_{csl}\right)}{P_{csh}-P_{csl}}\right]\right\} & P_{csl}<P_{1i}-P_{2i}\le P_{csh} \\ a_{12c}+a_{12vc} & P_{1i}-P_{2i}>P_{csh} \\ a_{12c}+a_{12ve}\left\{\dfrac{\left(\left|P_{1i}-P_{2i}\right|-P_{esl}\right)}{P_{esh}-P_{esl}}-\dfrac{1}{2\pi}\sin\left[\dfrac{2\pi\left(\left|P_{1i}-P_{2i}\right|-P_{esl}\right)}{P_{esh}-P_{esl}}\right]\right\} & P_{esl}<P_{2i}-P_{1i}\le P_{esh} \\ a_{12c}+a_{12ve} & P_{2i}-P_{1i}>P_{esh} \end{cases} \tag{2.13b}$$

Dynamic suspension forces (B_{IR})

The dynamic force F_i developed by strut i can be expressed as:

$$F_i=(P_{1i}-P_a)A_{1i}-(P_{3i}-P_a)A_{3i}-F_{c1i}\,\mathrm{sgn}(\dot{x}_i)-(P_0-P_a)A_{2i}\quad(i=l,r) \tag{2.14a}$$

where F_{c1i} is the magnitude of the Coulomb friction force due to rod and main piston seals within strut i. Equation (2.14a) can be expressed as functions of the floating piston dynamics and pressure differentials, such that:

$$\begin{aligned} F_l&=(P_{4l}-P_0)A_{1l}-(P_{4r}-P_0)A_{3l}+P_{12l}A_{1l}-(P_{12r}-P_{1r3l})A_{3l}-F_{c1l}\,\mathrm{sgn}(\dot{x}_l) \\ &\quad+\frac{A_{1l}}{A_{2l}}\left[m_{fl}g-m_{fl}\ddot{x}_{4l}-F_{c2l}\,\mathrm{sgn}(\dot{x}_{4l})\right]-\frac{A_{3l}}{A_{2r}}\left[m_{fr}g-m_{fr}\ddot{x}_{4r}-F_{c2r}\,\mathrm{sgn}(\dot{x}_{4r})\right] \\ F_r&=(P_{4r}-P_0)A_{1r}-(P_{4l}-P_0)A_{3r}+P_{12r}A_{1r}-(P_{12l}-P_{1l3r})A_{3r}-F_{c1r}\,\mathrm{sgn}(\dot{x}_r) \\ &\quad+\frac{A_{1r}}{A_{2r}}\left[m_{fr}g-m_{fr}\ddot{x}_{4r}-F_{c2r}\,\mathrm{sgn}(\dot{x}_{4r})\right]-\frac{A_{3r}}{A_{2l}}\left[m_{fl}g-m_{fl}\ddot{x}_{4l}-F_{c2l}\,\mathrm{sgn}(\dot{x}_{4l})\right] \end{aligned} \tag{2.14b}$$

where $P_{12i}=P_{1i}-P_{2i}$ is the pressure drop between chambers 1 and 2 of strut i, and P_{1l3r} and P_{1r3l} are the pressure drops across the connecting chambers 1 and 3. It is evident that the dynamic suspension force developed by a single strut is related to the relative motion

responses of both the interconnected struts, and the floating pistons. In the above equations, the first two terms relate to the dynamic restoring forces developed by the gas chambers and reveal strong coupling between the two struts. The following two terms describe the dissipative forces developed due to flows through damping orifices and interconnecting pipes, which further show the damping feedback effect of the interconnections. The last three terms relate to friction forces due to rod and main piston seals, and the floating pistons seals in a coupled manner.

Equation (2.14b) could be significantly simplified upon consideration of negligible contributions of seals friction, fluid compressibility and floating piston dynamics, such that:

$$\begin{aligned}
F_l &= P_0\left\{A_{1l}\left[\left(\frac{V_{40l}}{V_{40l}+A_{1l}x_l-A_{3r}x_r}\right)^n-1\right]-A_{3l}\left[\left(\frac{V_{40r}}{V_{40r}+A_{1r}x_r-A_{3l}x_l}\right)^n-1\right]\right\} \\
&+\frac{\rho A_{1l}\left|A_{3r}\dot{x}_r-A_{1l}\dot{x}_l\right|(A_{3r}\dot{x}_r-A_{1l}\dot{x}_l)}{2C_d^2a_{12l}^2}-\frac{\rho A_{3l}\left|A_{3l}\dot{x}_l-A_{1r}\dot{x}_r\right|(A_{3l}\dot{x}_l-A_{1r}\dot{x}_r)}{2C_d^2a_{12r}^2}-\frac{128\mu LA_{3l}^2\dot{x}_l}{\pi D^4} \\
F_r &= P_0\left\{A_{1r}\left[\left(\frac{V_{40r}}{V_{40r}+A_{1r}x_r-A_{3l}x_l}\right)^n-1\right]-A_{3r}\left[\left(\frac{V_{40l}}{V_{40l}+A_{1l}x_l-A_{3r}x_r}\right)^n-1\right]\right\} \\
&+\frac{\rho A_{1r}\left|A_{3l}\dot{x}_l-A_{1r}\dot{x}_r\right|(A_{3l}\dot{x}_l-A_{1r}\dot{x}_r)}{2C_d^2a_{12r}^2}-\frac{\rho A_{3r}\left|A_{3r}\dot{x}_r-A_{1l}\dot{x}_l\right|(A_{3r}\dot{x}_r-A_{1l}\dot{x}_l)}{2C_d^2a_{12l}^2}-\frac{128\mu LA_{3r}^2\dot{x}_r}{\pi D^4}
\end{aligned} \tag{2.15}$$

The above equations clearly show that the dynamic suspension force developed by a strut is dependent upon the relative displacements and velocities of both the struts due to the coupling effects of the interconnections.

The forces due to unconnected suspension struts (B_{UR}) are also derived in a similar but considerably simpler manner, while the detailed derivation is not presented. Assuming negligible contributions due to seals friction, fluid compressibility and floating piston dynamics, the simplified dynamic strut forces of configuration B_{UR} are given by:

$$F_i = P_{40i}A_{2i}\left\{\left[\frac{V_{40i}}{V_{40i}+A_{2i}x_i}\right]^n - 1\right\} - \frac{\rho A_{2i}^3}{2C_d^2 a_{12i}^2}|\dot{x}_i|\dot{x}_i - \frac{\rho A_{3i}^3}{2C_d^2 a_{13i}^2}|\dot{x}_i|\dot{x}_i \quad (i=l,r) \tag{2.16}$$

It should be noted that the struts in this configuration employ additional bleed orifices between chambers 1 and 3 of area a_{13i}, as evident in Figure 2.3(a).

FORMULATIONS OF PNEUMATICALLY CONNECTED STRUT FORCES (A_{IR})

The dynamic forces developed due to pneumatic roll-interconnections involving chambers 3 and 4, as shown in Figure 2.3(d), are derived using similar flow and pressure equations. Unlike the hydraulic interconnection, the gas flows through the interconnecting pipes are modeled by considering mass flow rates.

Equations of mass flow rate of gas

The rate of change of fluid mass in chamber 4 of strut i can be expressed as [145]:

$$\frac{dm_{4i}}{dt} = \frac{d(\rho_{4i}V_{4i})}{dt} = V_{4i}\frac{d\rho_{4i}}{dt} + \rho_{4i}\frac{dV_{4i}}{dt} \quad (i=l,r) \tag{2.17}$$

where m_{ji} and ρ_{ji} are the mass and density of gas in chamber j (j=3,4) of strut i (i=l,r), respectively.

The instantaneous volume of gas in chamber 4 of the strut i can be related to the floating piston displacement, such that:

$$V_{4i} = V_{40i} + A_{2i}x_{4i} \quad (i=l,r) \tag{2.18}$$

The rate of change of volume of gas in chamber 4 can thus be derived as:

$$dV_{4i}/dt = A_{2i}\dot{x}_{4i} \quad (i=l,r) \tag{2.19}$$

Assuming polytropic process of the gas in chamber 4, the density of gas in chamber 4 can be expressed as:

$$\rho_{4i} = \frac{P_0}{RT_0}\left(\frac{P_{4i}}{P_0}\right)^{\frac{1}{n}} \quad (i = l, r) \tag{2.20}$$

where R is the gas constant and T_0 is the absolute temperature.

Equations (2.17)~(2.20) yield the following expression for the rate of change of fluid mass in chamber 4 of strut i:

$$\frac{dm_{4i}}{dt} = \frac{(P_0)^{\frac{n-1}{n}}}{nRT_0}(P_{4i})^{\frac{1-n}{n}}(V_{40i} + A_{2i}x_{4i})\frac{dP_{4i}}{dt} + \frac{A_{2i}P_0}{RT_0}\left(\frac{P_{4i}}{P_0}\right)^{\frac{1}{n}}\dot{x}_{4i} \quad (i = l, r) \tag{2.21}$$

The rate of change of fluid mass in chamber 3 of the strut i is also derived in a similar manner as:

$$\frac{dm_{3i}}{dt} = \frac{(P_0)^{\frac{n-1}{n}}}{nRT_0}(P_{3i})^{\frac{1-n}{n}}(V_{30i} - A_{3i}x_i)\frac{dP_{3i}}{dt} - \frac{A_{3i}P_0}{RT_0}\left(\frac{P_{3i}}{P_0}\right)^{\frac{1}{n}}\dot{x}_i \quad (i = l, r) \tag{2.22}$$

For the proposed roll plane interconnections, $dm_{4l}/dt = -dm_{3r}/dt$ and $dm_{4r}/dt = -dm_{3l}/dt$. The gas pressures in the right and left struts can thus be related as:

$$\frac{(P_{4l})^{\frac{1-n}{n}}}{n}(V_{40l} + A_{2l}x_{4l})\frac{dP_{4l}}{dt} + A_{2l}(P_{4l})^{\frac{1}{n}}\dot{x}_{4l} = -\frac{(P_{3r})^{\frac{1-n}{n}}}{n}(V_{30r} - A_{3r}x_r)\frac{dP_{3r}}{dt} + A_{3r}(P_{3r})^{\frac{1}{n}}\dot{x}_r \tag{2.23}$$

$$\frac{(P_{4r})^{\frac{1-n}{n}}}{n}(V_{40r} + A_{2r}x_{4r})\frac{dP_{4r}}{dt} + A_{2r}(P_{4r})^{\frac{1}{n}}\dot{x}_{4r} = -\frac{(P_{3l})^{\frac{1-n}{n}}}{n}(V_{30l} - A_{3l}x_l)\frac{dP_{3l}}{dt} + A_{3l}(P_{3l})^{\frac{1}{n}}\dot{x}_l \tag{2.24}$$

The mass flow rates of gas from chamber 4 of the left/right strut to chamber 3 of the right/left strut can also be related by considering the flows through the interconnecting pipes [131, 146], such that:

$$-\frac{dm_{4l}}{dt} = \frac{\pi D^4}{256\mu LRT_0}(P_{4l}^2 - P_{3r}^2);\ -\frac{dm_{4r}}{dt} = \frac{\pi D^4}{256\mu LRT_0}(P_{4r}^2 - P_{3l}^2) \tag{2.25}$$

Equations (2.21)~(2.25) yield following relationships for the gas pressures in the two struts:

$$\frac{\pi D^4}{256\mu L}(P_{4l}^2 - P_{3r}^2) = \frac{(P_0)^{\frac{n-1}{n}}}{n}(P_{3r})^{\frac{1-n}{n}}(V_{30r} - A_{3r}x_r)\frac{dP_{3l}}{dt} - A_{3r}P_0\left(\frac{P_{3r}}{P_0}\right)^{\frac{1}{n}}\dot{x}_r \tag{2.26}$$

$$\frac{\pi D^4}{256\mu L}(P_{4r}^2 - P_{3l}^2) = \frac{(P_0)^{\frac{n-1}{n}}}{n}(P_{3l})^{\frac{1-n}{n}}(V_{30l} - A_{3l}x_l)\frac{dP_{3r}}{dt} - A_{3l}P_0\left(\frac{P_{3l}}{P_0}\right)^{\frac{1}{n}}\dot{x}_l \tag{2.27}$$

Dynamic suspension forces (A_{IR})

The dynamic force F_i developed by strut i, described in Eq. (2.14a), can be expressed as functions of the floating piston dynamics and pressure differentials for the pneumatically interconnected struts in the following manner:

$$\begin{aligned} F_l &= (P_{3r} - P_0)A_{1l} - (P_{3l} - P_0)A_{3l} + (P_{12l} + P_{4l3r})A_{1l} + \frac{A_{1l}}{A_{2l}}\left[m_{fl}g - m_{fl}\ddot{x}_{4l} - F_{c2l}\,\mathrm{sgn}(\dot{x}_{4l})\right] - F_{c1l}\,\mathrm{sgn}(\dot{x}_l) \\ F_r &= (P_{3l} - P_0)A_{1r} - (P_{3r} - P_0)A_{3r} + (P_{12r} + P_{4r3l})A_{1r} + \frac{A_{1r}}{A_{2r}}\left[m_{fr}g - m_{fr}\ddot{x}_{4r} - F_{c2r}\,\mathrm{sgn}(\dot{x}_{4r})\right] - F_{c1r}\,\mathrm{sgn}(\dot{x}_r) \end{aligned} \tag{2.28}$$

where P_{4l3r} and P_{4r3l} are the pressure drops across the connecting chambers 4 and 3. For the A_{IR} configuration, the above equations suggest that the dynamic suspension force developed by a single strut is related to the relative motions of both the struts, and the floating pistons. In the above equations, the first two terms relate to the dynamic restoring forces developed by the gas chambers and reveal strong coupling between the two struts. The following term describes the damping forces developed due to flows through damping orifices and interconnecting pipes, which relate to the damping feedback effect of the interconnections. The last two terms relate to friction forces due to main and floating pistons seals, and the floating piston inertial forces.

Considering that the dynamic viscosity of the nitrogen gas is significantly smaller than that of the hydraulic fluid, the damping forces due to flows through the

interconnecting pipes can be neglected. The resulting dynamic forces in Eq. (2.28) could be further simplified by assuming negligible contributions due to seals friction, fluid compressibility and floating piston dynamics, such that:

$$F_l = P_0 A_{1l}\left[\left(\frac{V_{40l}+V_{30r}}{V_{40l}+V_{30r}+A_{1l}x_l-A_{3r}x_r}\right)^n-1\right]-P_0 A_{3l}\left[\left(\frac{V_{40r}+V_{30l}}{V_{40r}+V_{30l}+A_{1r}x_r-A_{3l}x_l}\right)^n-1\right]-\frac{\rho A_{1l}^3|\dot{x}_l|(\dot{x}_l)}{2C_d^2\alpha_{12l}^2}$$

$$F_r = P_0 A_{1r}\left[\left(\frac{V_{40r}+V_{30l}}{V_{40r}+V_{30l}+A_{1r}x_r-A_{3l}x_l}\right)^n-1\right]-P_0 A_{3r}\left[\left(\frac{V_{40l}+V_{30r}}{V_{40l}+V_{30r}+A_{1l}x_l-A_{3r}x_r}\right)^n-1\right]-\frac{\rho A_{1r}^3|\dot{x}_r|(\dot{x}_r)}{2C_d^2\alpha_{12r}^2} \quad (2.29)$$

The above formulations clearly show the coupling effects of the two struts, where dynamic suspension force developed by a strut is dependent not only upon its relative displacement and velocity, but also on the relative displacements of the connected strut.

2.3.3 Twin-Gas-Chamber Strut Forces

The solutions of Eqs. (2.14b) and (2.28) revealed negligible effect of hydraulic fluid compressibility due to its high bulk modulus on the suspension stiffness properties. The subsequent formulations for the suspension forces developed by twin-gas-chamber suspension configuration A_{UR} are thus derived assuming incompressible hydraulic fluid.

Static equilibrium equations

The static loads supported by the struts in the twin-gas-chamber strut suspension configuration A_{UR} are related to the static gas pressures and effective working areas of the struts, such that:

$$w_i = (P_{40i} - P_a)A_{1i} - (P_{30i} - P_a)A_{3i} \quad (i = l, r) \quad (2.30)$$

where P_{40i} and P_{30i} are static gas pressures in chambers 4 and 3 of strut i, respectively.

Fluid flow equations

The rate of change of fluid volume in chamber 1 of each strut, Q_{1i}, can be expressed as:

$$Q_{1i} = -Q_{12i} \quad (i = l, r) \tag{2.31}$$

The rate of change of fluid volume in chamber 1 of strut *i* is also related to the relative velocity $\dot{x}_i$ across the strut *i*, such that:

$$Q_{1i} = A_{1i}\dot{x}_i \quad (i = l, r) \tag{2.32}$$

The flow rates across the damping orifices from chamber 1 to 2 of the same strut are derived assuming turbulent flows:

$$Q_{12i} = -A_{1i}\dot{x}_i = C_d a_{12i}\sqrt{2 \mid P_{1i} - P_{2i} \mid / \rho}\,\mathrm{sgn}(P_{1i} - P_{2i}) \quad (i = l, r) \tag{2.33}$$

Pressure equations

The pressure differential P_{12i} associated with fluid flows across the damping orifices of strut *i* can be expressed in terms of relative velocity $\dot{x}_i$:

$$P_{12i} = -\frac{\rho}{2}\left(\frac{A_{1i}}{C_d a_{12i}}\right)^2 |\dot{x}_i|\dot{x}_i \quad (i = l, r) \tag{2.34}$$

Assuming polytropic process for the gas, the instantaneous pressure and volume of gas in chambers 3 and 4 can be related as:

$$P_{3i}V_{3i}^n = P_{30i}V_{30i}^n;\ P_{4i}V_{4i}^n = P_{40i}V_{40i}^n \quad (i = l, r) \tag{2.35}$$

where V_{j0i} and V_{ji} are the initial and instantaneous volumes of gas in chamber j of strut i, respectively. Equation (2.35) can be manipulated to yield instantaneous gas pressure as a function of the strut deflection:

$$P_{4i} = P_{40i}\left(\frac{V_{40i}}{V_{40i} + A_{1i}x_i}\right)^n ;\ P_{3i} = P_{30i}\left(\frac{V_{30i}}{V_{30i} - A_{3i}x_i}\right)^n \quad (i = l, r) \tag{2.36}$$

Assuming negligible friction due to floating piston seals and negligible mass, the pressure of gas in chamber 4 would be identical to that of the hydraulic fluid in chamber 2, such that $P_{2i} = P_{4i}$. Furthermore, the fluid pressure in chamber 2 is related to the pressure differential across the damping orifices, such that $P_{2i} = P_{1i} - P_{12i}$.

Dynamic suspension forces (A_{UR})

The dynamic suspension forces developed by the left and right struts can be expressed as:

$$F_i = (P_{1i} - P_{40i})A_{1i} - (P_{3i} - P_{30i})A_{3i} \quad (i = l, r) \tag{2.37}$$

which can be further expressed in terms of gas pressure, and strut deflection and velocity, using Eqs. (2.34)~(2.36), such that:

$$F_i = P_{40i}A_{1i}\left\{\left[\frac{V_{40i}}{V_{40i} + A_{1i}x_i}\right]^n - 1\right\} - P_{30i}A_{3i}\left\{\left[\frac{V_{30i}}{V_{30i} - A_{3i}x_i}\right]^n - 1\right\} \quad (i = l, r) \tag{2.38}$$
$$- \frac{\rho A_{1i}^3}{2C_d^2 a_{12i}^2}|\dot{x}_i|\dot{x}_i$$

2.4 Modeling of Roll Plane Properties of Suspension Systems

On the basis of roll plane vehicle model and strut forces developed for different suspension configurations in the above section, the roll plane suspension stiffness and

damping properties can be derived, in terms of suspension rate, roll stiffness, and bounce and roll mode damping.

2.4.1 Properties of Interconnected and Unconnected Suspensions

Suspension rate property

The suspension rate of a hydro-pneumatic suspension is derived from the pressure-deflection relationships of the gas springs. The suspension rate k_{vi} of the strut i is dependent upon the deflections of the both struts, such that:

$$k_{vi} = -dF_{si} / dx_i \quad (i = l, r) \tag{2.39}$$

where F_{si} is the restoring force due to strut i, which is a function of deflections (x_l and x_r) of both the struts, as evident from the first two terms in Eq. (2.15). The suspension rate of the interconnected suspension is evaluated through solutions of the coupled differential equations of motion (Eq. (2.1)) under a pure vertical displacement input ($x_\ell = x_r = x$). The considerations of the symmetric load distribution on the left and right struts and negligible seals friction yield the identical geometry of left and right struts and $x_{4\ell} = x_{4r} = x_4$. Furthermore, the steady state solutions would yield $P_{1\ell} = P_{3r} = P_\ell$, $P_{1r} = P_{3l} = P_r$ and $P_l = P_r$. The restoring force due to strut i can thus be derived from Eq. (2.14) as:

$$F_{si} = (P_{1i} - P_a)A_1 - (P_{3i} - P_a)A_3 = (P_i - P_a)A_2 \quad (i = l, r) \tag{2.40}$$

The suspension rate of each strut ($k_{vl} = k_{vr} = k_v$) can thus be rewritten as:

$$k_{vi} = -A_2 \, dP_i / dx \quad (i = l, r) \tag{2.41}$$

Owing to the identical motions of both the struts, the total mass of the hydraulic fluid remains unchanged. The change of hydraulic fluid volume in each strut can thus be expressed as:

$$xA_2 - x_4 A_2 = \Delta V_{comp} \tag{2.42}$$

where xA_2 represents the total change in fluid volume in the strut, $x_4 A_2$ is the change in gas chamber volume, and ΔV_{comp} is the change in hydraulic fluid volume due to fluid compressibility, which can be related to fluid pressure:

$$\Delta V_{comp} = -\frac{V}{E}(P_i - P_0) \quad (i = l, r) \tag{2.43}$$

where V is the total hydraulic fluid volume in chambers 1, 2 and 3 of strut i. Equations (2.42) and (2.43) yield following relationship between the motions of strut and the floating piston:

$$x_4 = x + \frac{V}{EA_2}(P_i - P_0) \quad (i = l, r) \tag{2.44}$$

Upon substituting for x_4 in Eq. (2.11), the fluid pressure in strut i can be expressed by:

$$\phi(P_i, x) = P_i\left[x_{40} + x + \frac{V}{EA_2}(P_i - P_0)\right]^n - P_0 x_{40}^n = 0 \quad (i = l, r) \tag{2.45}$$

The change in fluid pressure of fluid in strut i with respect to its relative vertical displacement can be derived as:

$$\frac{dP_i}{dx} = -\frac{\partial\phi/\partial x}{\partial\phi/\partial P_i} = \frac{-nP_i}{x_{40} + x + \frac{V}{EA_2}[(n+1)P_i - P_0]} \quad (i = l, r) \tag{2.46}$$

The suspension rate of the hydraulically interconnected strut can thus be formulated upon considerations of Eqs. (2.41) and (2.46), such that:

$$k_{vi} = \frac{nP_i A_2}{x_{40} + x + \frac{V}{EA_2}\left[(n+1)P_i - P_0\right]} \quad (i = l, r) \tag{2.47}$$

The suspension rate of each strut can be obtained through simultaneous solutions of Eqs. (2.45) and (2.47). The suspension rates of pneumatic interconnection and unconnected suspensions can be developed in a very similar manner. Assuming incompressible hydraulic fluid, the suspension rate of the hydraulically interconnected struts B_{IR} can be simplified as:

$$k_{vi} = nP_i V_{40}^n A_2^2 \frac{1}{\left(V_{40} + A_2 x\right)^{n+1}} \quad (i = l, r) \tag{2.48}$$

While the vertical suspension rate of unconnected suspension configuration B_{UR} is identical to that described in Eqs. (2.47) and (2.48), the suspension rate of the pneumatically connected strut (A_{IR}) can be achieved from the simultaneous solutions of Eqs. (2.49) and (2.50):

$$\phi(P_i, x) = P_i\left[V_{40} + V_{30} + A_2 x + \frac{V}{E}(P_i - P_0)\right]^n - P_0 V_{40}^n = 0 \quad (i = l, r) \tag{2.49}$$

$$k_{vi} = -\frac{dF_{si}}{dx} = \frac{nP_i A_2^2}{V_{40} + V_{30} + A_2 x + \frac{V}{E}\left[(n+1)P_i - P_0\right]} \quad (i = l, r) \tag{2.50}$$

Roll stiffness property

The effective roll stiffness k_R can be derived from the restoring roll moment developed by the struts and the relative roll deflection, such that:

$$k_R = dM_R / d\theta \tag{2.51}$$

where M_R is the restoring roll moment developed due to restoring forces of both the struts, and $\theta = \theta_s - \theta_u$, which is the relative roll deflection of the sprung mass with respect to the unsprung mass. The roll stiffness of interconnected suspension, derived using Eq. (2.51) and the static equilibrium equation in the vertical direction, is evaluated through simultaneous solutions of these equations under out-of-phase vertical displacement inputs ($x_l = -x_r$).

For suspension configuration B_{IR}, the total mass of hydraulic fluid in chambers 1, 2 of one strut and chamber 3 of the connected strut remains unchanged. The restoring roll moment developed due to the restoring forces of both the struts can be expressed as:

$$M_R = (P_{4\ell} - P_{4r})(A_1 + A_3)l_s \tag{2.52}$$

The consideration of the volume of fluid in chambers 1, 2 and 4 of the left strut and chamber 3 of the right strut yields following relationship:

$$x_l A_1 - x_r A_3 = x_{4l} A_2 + \Delta V_{coml} \tag{2.53}$$

where the term $x_l A_1 - x_r A_3$ represents the change in total fluid volume in strut l, and $x_{4l} A_2$ is the change in gas volume of chamber 4 in the left strut. ΔV_{coml} is the hydraulic fluid volume change due to fluid compressibility. Equations (2.43) and (2.53) yield:

$$zA_2 - l_s\theta(A_1 + A_3) = x_{4l} A_2 + \frac{V}{E}(P_0 - P_{4l}) \tag{2.54}$$

where $z = z_u - z_s$.

Similarly, for chambers 1, 2 and 4 of the right strut and chamber 3 of the left strut, the following expression can also be obtained as:

$$zA_2 + l_s\theta(A_1 + A_3) = x_{4r} A_2 + \frac{V}{E}(P_0 - P_{4r}) \tag{2.55}$$

The static equilibrium of vertical motion can be expressed as:

$$2P_0A_2 = (P_{4l} + P_{4r})A_2 \tag{2.56}$$

Equations (2.11) and (2.53)~(2.56) yield following relationship:

$$\psi(P_{4l},\theta) = \left[\left(\frac{P_0}{2P_0 - P_{4l}}\right)^{\frac{1}{n}} - \left(\frac{P_0}{P_{4l}}\right)^{\frac{1}{n}}\right]A_2x_{40} + \frac{2V}{E}(P_{4l} - P_0) - 2l_s\theta(A_1 + A_3) = 0 \tag{2.57}$$

The change in pressure of fluid in the left strut with respect to the relative roll deflection can thus be derived, such that:

$$\frac{dP_{4l}}{d\theta} = -\frac{\partial\psi/\partial\theta}{\partial\psi/\partial P_{4l}} = \frac{2l_s(A_1 + A_3)}{\left[(2P_0 - P_{4l})^{-(\frac{1}{n}+1)} + (P_{4l})^{-(\frac{1}{n}+1)}\right]\frac{A_2x_{40}\sqrt[n]{P_0}}{n} + \frac{2V}{E}} \tag{2.58}$$

Equation (2.52) can be rewritten upon consideration of Eq. (2.56), such that:

$$M_R = 2(P_{4\ell} - P_0)(A_1 + A_3)l_s \tag{2.59}$$

The roll stiffness of hydraulically interconnected suspension can be formulated upon considerations of Eqs. (2.51), (2.58) and (2.59), such that:

$$k_R = 2l_s(A_1 + A_3)\frac{dP_{4l}}{d\theta} = \frac{4l_s^2(A_1 + A_3)^2}{\left[(2P_0 - P_{4l})^{-(\frac{1}{n}+1)} + (P_{4l})^{-(\frac{1}{n}+1)}\right]\frac{A_2x_{40}\sqrt[n]{P_0}}{n} + \frac{2V}{E}} \tag{2.60}$$

The roll stiffness of hydraulically interconnected suspension B_{IR} is therefore obtained through simultaneous solutions of Eqs. (2.57) and (2.60).

The roll stiffness properties of unconnected (B_{UR}) and pneumatically interconnected (A_{IR}) suspensions are also derived in a similar manner. For unconnected suspension B_{UR}, the roll stiffness can be achieved through simultaneous solutions of Eqs. (2.61) and (2.62), given below:

$$k_R = 2l_s A_2 \frac{dP_{4l}}{d\theta} = \frac{4A_2^2 l_s^2}{\left[(2P_0 - P_{4l})^{-(\frac{1}{n}+1)} + (P_{4l})^{-(\frac{1}{n}+1)}\right]\frac{A_2 x_{40}\sqrt[n]{P_0}}{n} + \frac{2V}{E}} \tag{2.61}$$

$$\varphi(P_{4l},\theta) = \left[\left(\frac{P_0}{2P_0 - P_{4l}}\right)^{\frac{1}{n}} - \left(\frac{P_0}{P_{4l}}\right)^{\frac{1}{n}}\right] A_2 x_{40} + \frac{2V}{E}(P_{4l} - P_0) - 2l_s\theta A_2 = 0 \tag{2.62}$$

Similarly, the roll stiffness property of pneumatically roll-interconnected suspension A_{IR} can be derived from Eqs. (2.63) and (2.64), such that:

$$k_R = \frac{4l_s^2(A_1 + A_3)^2}{\left[(2P_0 - P_{4l})^{-(\frac{1}{n}+1)} + (P_{4l})^{-(\frac{1}{n}+1)}\right]\frac{(V_{40} + V_{30})\sqrt[n]{P_0}}{n} + \frac{2V}{E}} \tag{2.63}$$

$$\phi(P_{4l},\theta) = \left[\left(\frac{P_0}{2P_0 - P_{4l}}\right)^{\frac{1}{n}} - \left(\frac{P_0}{P_{4l}}\right)^{\frac{1}{n}}\right](V_{40} + V_{30}) + \frac{2V_{all}}{E}(P_{4l} - P_0) - 2l_s\theta(A_1 + A_3) = 0 \tag{2.64}$$

The roll stiffness of hydraulically interconnected suspension B_{IR} can be expressed by assuming incompressible hydraulic fluid, such that:

$$k_R = nP_0V_{40}^n(A_1 + A_3)\ell_s\left\{\frac{(A_1 + A_3)\ell_s - (A_1 - A_3)\frac{dx}{d\theta}}{[V_{40} + A_1(x - \ell_s\theta) - A_3(x + \ell_s\theta)]^{n+1}} + \frac{(A_1 + A_3)\ell_s + (A_1 - A_3)\frac{dx}{d\theta}}{[V_{40} + A_1(x + \ell_s\theta) - A_3(x - \ell_s\theta)]^{n+1}}\right\} \tag{2.65}$$

$$\psi(x,\theta) = \frac{1}{[V_{40} + A_1(x - \ell_s\theta) - A_3(x + \ell_s\theta)]^n} + \frac{1}{[V_{40} + A_1(x + \ell_s\theta) - A_3(x - \ell_s\theta)]^n} - \frac{2}{V_{40}^n} = 0 \tag{2.66}$$

$$\frac{dx}{d\theta} = \frac{A_1 + A_3}{A_1 - A_3}\ell_s\left\{\frac{[V_{40} + A_1(x + \ell_s\theta) - A_3(x - \ell_s\theta)]^{n+1} - [V_{40} + A_1(x - \ell_s\theta) - A_3(x + \ell_s\theta)]^{n+1}}{[V_{40} + A_1(x + \ell_s\theta) - A_3(x - \ell_s\theta)]^{n+1} + [V_{40} + A_1(x - \ell_s\theta) - A_3(x + \ell_s\theta)]^{n+1}}\right\} \tag{2.67}$$

The static roll stiffness properties of hydraulically interconnected suspension (k_{R0I}) and unconnected suspension (k_{R0U}) at the design ride height can be expressed as:

$$k_{R0I} = \frac{2nP_0(A_1 + A_3)^2\ell_s^2}{V_{40}} \tag{2.68}$$

$$k_{ROU} = \frac{2nP_0(A_1 - A_3)^2 \ell_s^2}{V_{40}} \tag{2.69}$$

Upon considerations of Eqs. (2.68) and (2.69), the roll stiffness amplification factor (RSAF) proposed in [28] can be expressed as:

$$RSAF = \frac{k_{ROI}}{k_{ROU}} = \frac{(A_1 + A_3)^2}{(A_1 - A_3)^2} \tag{2.70}$$

RSAF described in Eq. (2.70) clearly indicates that the static roll stiffness of the interconnected suspension at the design ride height can be considerably enhanced compared to that of the unconnected suspension when both the suspensions are selected to have identical suspension rates.

Bounce and roll mode damping properties

Assuming incompressible hydraulic fluid and negligible friction, the analytical models of the bounce and roll mode damping forces of different suspensions can be developed under in-phase ($\dot{x}_l = \dot{x}_r = \dot{x}$) and out-of-phase ($\dot{x}_l = -\dot{x}_r = \dot{x}$) vertical velocity inputs, respectively. The roll mode damping property of the suspension can be presented in terms of the damping force developed by the strut under a pure or dominant roll motion of the suspension and vehicle masses.

For the hydraulically roll-interconnected suspension B_{IR}, selections of hydraulic fluid with relative small dynamic viscosity and large diameter of the interconnecting pipes could take much advantage of the damping valves. Bounce mode damping force could therefore be simplified as:

$$F_{vd} = \frac{\rho(A_1 - A_3)^3}{2C_d^2 a_{12}^2} \dot{x}|\dot{x}| \tag{2.71}$$

The roll mode damping force can also be simplified as:

$$F_{rd} = \frac{\rho(A_1 + A_3)^3}{2C_d^2 a_{12}^2}\dot{x}|\dot{x}| \tag{2.72}$$

For unconnected single-gas-chamber strut suspension B_{UR}, the bounce and roll mode damping forces are identical, such that:

$$F_{Ud} = \frac{\rho(A_1 - A_3)^3}{2C_d^2 a_{12}^2}\dot{x}|\dot{x}| \tag{2.73}$$

For pneumatic roll-interconnection configuration A_{IR}, the simplified bounce and roll mode damping forces are identical, such that:

$$F_{Ad} = \frac{\rho A_1^3}{2C_d^2 a_{12}^2}\dot{x}|\dot{x}| \tag{2.74}$$

Equations (2.71)~(2.74) suggest that for the identical bounce mode damping properties, the hydraulic interconnection could improve roll mode damping due to the hydraulic fluid coupling effect, compared to the unconnected suspension and pneumatic interconnection.

2.4.2 Properties of Twin-Gas-Chamber Suspension

Suspension rate property

The suspension rate of twin-gas-chamber suspension configuration A_{UR} can be derived from Eqs. (2.38) and (2.39), such that:

$$k_{vi} = \frac{nP_{40i}A_{1i}^2 V_{40i}^n}{(V_{40i} + A_{1i}x_i)^{n+1}} + \frac{nP_{30i}A_{3i}^2 V_{30i}^n}{(V_{30i} - A_{3i}x_i)^{n+1}} \quad (i = l, r) \tag{2.75}$$

Roll stiffness property

Assuming symmetric load distribution on the left- and right-struts, the restoring roll moment developed by the twin-gas-chamber strut suspension configuration A_{UR} due to the restoring forces of both the struts is derived from Eqs. (2.36) and (2.37):

$$M_R = \frac{P_{40}\ell_s A_1 V_{40}^n}{\left[V_{40} + A_1(z - \ell_s\theta)\right]^r} - \frac{P_{30}\ell_s A_3 V_{30}^n}{\left[V_{30} - A_3(z - \ell_s\theta)\right]^r} - \frac{P_{40}\ell_s A_1 V_{40}^n}{\left[V_{40} + A_1(z + \ell_s\theta)\right]^r} + \frac{P_{30}\ell_s A_3 V_{30}^n}{\left[V_{30} - A_3(z + \ell_s\theta)\right]^r} \tag{2.76}$$

where $z = z_u - z_s$. The first two terms relate to the forces developed due to compression/extension of gas in chambers 4/3 of the left strut, under a pure roll deflection θ>0. The last two terms relate to the forces developed by the right strut due to extension/compression of gas in chambers 4/3.

The effective roll stiffness of the suspension A_{UR} can therefore be formulated upon consideration of Eq. (2.51), such that:

$$k_R = nP_{40}\ell_s A_1^2 V_{40}^n \left\{ \frac{l_s - \frac{dz}{d\theta}}{\left[V_{40} + A_1(z - \ell_s\theta)\right]^{n+1}} + \frac{\ell_s + \frac{dz}{d\theta}}{\left[V_{40} + A_1(z + \ell_s\theta)\right]^{n+1}} \right\} + nP_{30}\ell_s A_3^2 V_{30}^n \left\{ \frac{\ell_s - \frac{dz}{d\theta}}{\left[V_{30} - A_3(z - \ell_s\theta)\right]^{n+1}} + \frac{\ell_s + \frac{dz}{d\theta}}{\left[V_{30} - A_3(z + \ell_s\theta)\right]^{n+1}} \right\} \tag{2.77}$$

Under a constant roll deflection, the forces developed by a strut depend upon both the relative vertical (z) and roll (θ) motions. A function relating the forces with z and θ can be derived from the equation of the corresponding static equilibrium:

$$(P_{4\ell} + P_{4r})A_1 - (P_{3\ell} + P_{3r})A_3 = 2P_{40}A_1 - 2P_{30}A_3 - 2P_a A_2 \tag{2.78}$$

Upon substituting for fluid pressures from Eq. (2.36), the above equation yields static equilibrium as a function of z and θ:

$$g(z,\theta) = P_{40}A_1V_{40}^n\left\{\frac{1}{\left[V_{40}+A_1(z-\ell_s\theta)\right]^n}+\frac{1}{\left[V_{40}+A_1(z+\ell_s\theta)\right]^n}\right\}-P_{30}A_3V_{30}^n$$
$$\left\{\frac{1}{\left[V_{30}-A_3(z-\ell_s\theta)\right]^n}+\frac{1}{\left[V_{30}-A_3(z+\ell_s\theta)\right]^n}\right\}-2P_{40}A_1+2P_{30}A_3+2P_aA_2=0 \tag{2.79}$$

which further yields:

$$\frac{dz}{d\theta} = -\frac{\partial g/\partial\theta}{\partial g/\partial z} = \ell_s\frac{(\lambda_1-\lambda_2)+(\eta_1-\eta_2)}{(\lambda_1+\lambda_2)+(\eta_1+\eta_2)} \tag{2.80}$$

where $\lambda_1 = \dfrac{P_{40}A_1^2V_{40}^n}{\left[V_{40}+A_1(z-\ell_s\theta)\right]^{n+1}}$, $\lambda_2 = \dfrac{P_{40}A_1^2V_{40}^n}{\left[V_{40}+A_1(z+\ell_s\theta)\right]^{n+1}}$, $\eta_1 = \dfrac{P_{30}A_3^2V_{30}^n}{\left[V_{30}-A_3(z-\ell_s\theta)\right]^{n+1}}$, and

$\eta_2 = \dfrac{P_{30}A_3^2V_{30}^n}{\left[V_{30}-A_3(z+\ell_s\theta)\right]^{n+1}}$.

The effective roll stiffness of suspension configuration A_{UR} is then obtained through simultaneous solutions of Eqs. (2.77), (2.79) and (2.80).

Assuming incompressible hydraulic fluid, the restoring roll moment developed by the unconnected single-gas-chamber suspension configuration B_{UR} is derived in a similar manner and expressed as:

$$M_R = P_{40}V_{40}^nA_2\ell_s\left\{\frac{1}{\left[V_{40}+A_2(z-\ell_s\theta)\right]^n}-\frac{1}{\left[V_{40}+A_2(z+\ell_s\theta)\right]^n}\right\} \tag{2.81}$$

The effective roll stiffness is then derived from the restoring roll moment developed under a roll deflection, as described in Eq. (2.51), such that:

$$k_R = nP_{40}V_{40}^nA_2^2\ell_s\left\{\frac{\ell_s-\dfrac{dz}{d\theta}}{\left[V_{40}+A_2(z-\ell_s\theta)\right]^{n+1}}+\frac{\ell_s+\dfrac{dz}{d\theta}}{\left[V_{40}+A_2(z+\ell_s\theta)\right]^{n+1}}\right\} \tag{2.82}$$

The static equilibrium of suspension system corresponding to a given roll deflection, $(P_\ell - P_0)A_2 + (P_r - P_0)A_2 = 0$, yields following relationship as a function of x and θ:

$$g(z,\theta) = \frac{1}{[V_{40} + A_2(z - \ell_s\theta)]^n} + \frac{1}{[V_{40} + A_2(z + \ell_s\theta)]^n} - \frac{2}{V_{40}^n} = 0 \tag{2.83}$$

which yields,

$$\frac{dz}{d\theta} = \ell_s \left\{ \frac{[V_{40} + A_2(z + \ell_s\theta)]^{n+1} - [V_{40} + A_2(z - \ell_s\theta)]^{n+1}}{[V_{40} + A_2(z + \ell_s\theta)]^{n+1} + [V_{40} + A_2(z - \ell_s\theta)]^{n+1}} \right\} \tag{2.84}$$

The effective roll stiffness of the unconnected single-gas-chamber suspension B_{UR} can then be computed through simultaneous solutions of Eqs. (2.82)~(2.84).

Bounce and roll mode damping properties

For unconnected twin-gas-chamber strut suspension A_{UR}, the bounce and roll mode damping forces are identical, and expressed as:

$$F_{Ud} = \frac{\rho A_1^3}{2C_d^2 a_{12}^2} \dot{x}|\dot{x}| \tag{2.85}$$

Analyses of suspension rate properties

The suspension rate characteristics of configurations A_{UR} and B_{UR} are analyzed using the above formulations. The properties of configuration B_{UR} are also investigated in conjunction with an anti-roll bar, referred to as B_{URbar}. The relative properties of the resulting three configurations are evaluated on the basis of identical load carry capacity, while assuming symmetric load distribution on the left and right struts.

The change in the suspension rate of suspension A_{UR}, with respect to relative deflection of the struts, is evaluated from Eq. (2.75), over a practical range of deflection, such that:

$$\frac{dk_{vi}}{dx_i} = -n(n+1)\left[\frac{P_{40}A_1^3V_{40}^n}{(V_{40}+A_1x_i)^{n+2}} - \frac{P_{30}A_3^3V_{30}^n}{(V_{30}-A_3x_i)^{n+2}}\right] \tag{2.86}$$

Above can be simplified to realize the rate near static ride height (x_i=0):

$$\left.\frac{dk_{vi}}{dx_i}\right|_{x_i=0} = -n(n+1)\left[\frac{P_{40}A_1^3}{V_{40}^2} - \frac{P_{30}A_3^3}{V_{30}^2}\right] \tag{2.87}$$

The above formulation suggests that the suspension rate would approach its maxima or minima at the static ride height, when $P_{40}A_1^3/V_{40}^2 = P_{30}A_3^3/V_{30}^2$. It should be noted that the chamber 3 is independent of the other chambers, and P_{30} may differ from P_{40} even under a static condition. This configuration could thus offer added design flexibility. The above formulations also show that the rate of change of suspension rate is negative $(dk_v/dx < 0)$ during a compression stroke (x<0), since:

$$\frac{P_{40}A_1^3V_{40}^n}{(V_{40}+A_1x)^{n+2}} > \frac{P_{40}A_1^3}{V_{40}^2} \text{ and } \frac{P_{30}A_3^3V_{30}^n}{(V_{30}-A_3x)^{n+2}} < \frac{P_{30}A_3^3}{V_{30}^2} \tag{2.88}$$

Similarly, it can be shown that the rate of change of suspension rate remains positive $(dk_v/dx > 0)$ during the rebound stroke (x>0), since:

$$\frac{P_{40}A_1^3V_{40}^n}{(V_{40}+A_1x)^{n+2}} < \frac{P_{40}A_1^3}{V_{40}^2} \text{ and } \frac{P_{30}A_3^3V_{30}^n}{(V_{30}-A_3x)^{n+2}} > \frac{P_{30}A_3^3}{V_{30}^2} \tag{2.89}$$

The above formulations suggest that the suspension rate is a minimum point near the static ride height, while the suspension rate exhibits hardening effects in both

compression and rebound directions. It is thus possible to achieve a lower suspension rate at the design ride height.

The change in suspension rate of the struts in configuration B_{UR} is derived in a similar manner from the suspension rate in Eq. (2.48):

$$\frac{dk_v}{dx} = \frac{-n(n+1)P_{40}A_1^3V_{40}^n}{(V_{40}+A_1x)^{n+2}} \tag{2.90}$$

The above yields a softening property in rebound (x>0) and a hardening effect in compression (x<0). The presence of an anti-roll bar is characterized by additional roll stiffness, while it does not affect the vertical suspension rate.

2.5 Pitch Plane Modeling of a Heavy Vehicle and Model Validation

The pitch plane road vehicle model is formulated to explore the pitch properties of different suspension configurations, as well as dynamic responses of the vehicle under straight-line braking inputs and road roughness excitations. The model, shown in Figure 2.4, incorporates: longitudinal motion (x_v) of the vehicle, vertical motions of the front and rear unsprung masses (z_{uf}, z_{ur}), vertical (z_s) and pitch (φ_s) motions of the sprung mass, and angular velocities of the front and rear wheels (ω_f, ω_r). The vertical properties of tires are represented by linear stiffness and damping elements, assuming point-contact with the road surface, as in the case of the roll-plane model. Figure 2.4(b) illustrates the forces and moments acting on a wheel and tire assembly under a braking input.

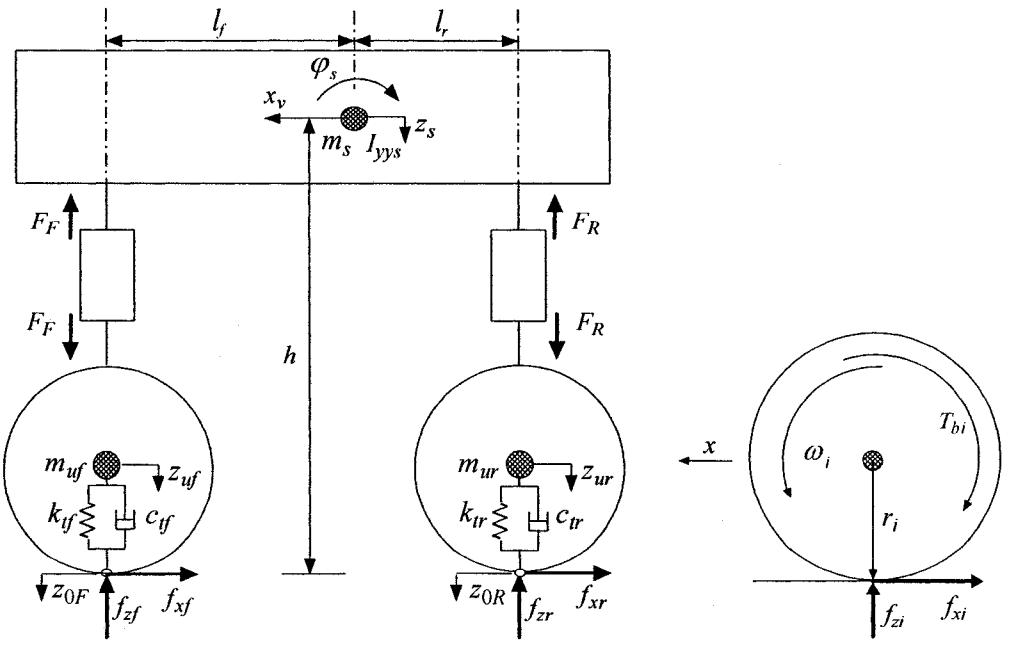

Figure 2.4: (a) Pitch plane model of a two-axle road vehicle; and (b) forces and moments acting on a wheel and tire assembly under braking.

The equations of motion for the vehicle model are formulated under excitations arising from the vehicle-road interactions and the braking torque. The pitch plane formulations include total forces developed by suspension struts, comprising the static as well as dynamic components of the front (F_F) and rear (F_R) struts. Assuming small pitch motions, the equations of motion can be summarized as:

$$m_s\ddot{z}_s = -F_F - F_R + m_s g$$

$$I_{yys}\ddot{\phi}_s = F_F l_f - F_R l_r - f_{xf}(h + z_{0F} - z_s) - f_{xr}(h + z_{0R} - z_s)$$

$$m_{uf}\ddot{z}_{uf} = F_F + k_{tf}(z_{0F} - z_{uf}) + c_{tf}(\dot{z}_{0F} - \dot{z}_{uf}) + m_{uf} g$$

$$m_{ur}\ddot{z}_{ur} = F_R + k_{tr}(z_{0R} - z_{ur}) + c_{tr}(\dot{z}_{0R} - \dot{z}_{ur}) + m_{ur} g$$

$$(m_s + m_{uf} + m_{ur})\ddot{x}_v = -(f_{xf} + f_{xr}) - m_s g\phi_s$$

$$I_{wi}\dot{\omega}_i = f_{xi} \cdot r_i - T_{bi} \quad (i = f, r) \tag{2.91}$$

where the subscripts f and r refer to front and rear suspension struts, respectively, I_{yys} is the pitch mass moment of inertia of the sprung mass, and m_{uf} and m_{ur} are front and rear

unsprung masses, respectively. Lengths l_f and l_r define longitudinal distances between sprung mass c.g. and front and rear axles, respectively; k_{ti} and c_{ti} (i=f,r) are vertical stiffness and damping coefficients of tires, respectively; z_{0F} and z_{0R} represent road elevations in the vicinity of front and rear tire-road contacts, respectively; f_{xf} and f_{xr} are braking efforts developed by the front- and rear-axle tires, respectively, and f_{zf} and f_{zr} are the respective normal forces applied to the road surface; h is vehicle c.g. height from the ground; T_{bi} is applied braking torque; r_i is effective radius of tire i; and I_{wi} is polar mass moment of inertia of wheel i. The Magic Formula tire model is used to derive the braking forces developed by the tires, as a function of slip and normal load [147, 148].

The validity of the simplified pitch plane model of the vehicle is examined using the measured data reported in [20]. Equations of motion were solved under the known conditions reported in [20] to compute the stopping distance and the vehicle pitch deflection. The analyses were performed for three different load conditions, and initial speeds of 48 and 80 km/h on a dry road surface. The three load conditions include: (*a*) no-load; (*b*) a low c.g. load; and (*c*) a high c.g. load. Figures 2.5, 2.6 and 2.7 illustrate comparisons of model results with the measured data under the three load conditions and both the speeds, respectively. Each figure illustrates stopping distance as a function of braking pressure for the two initial speeds, and vehicle pitch deflection against deceleration. Comparisons of stopping distance and pitch angle responses attained from the model show reasonably good agreement with the measured data for all load and speed conditions.

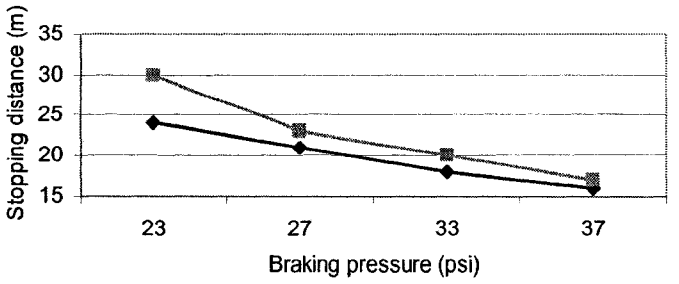

(a)

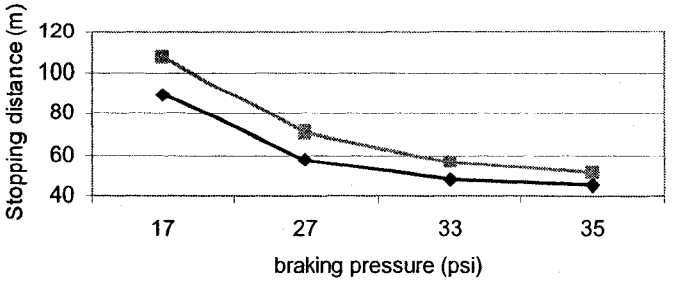

(b)

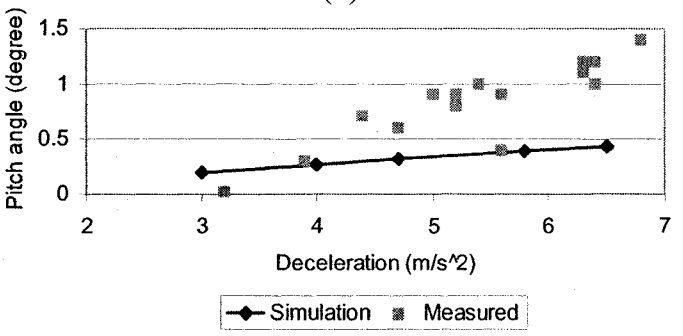

(c)

Figure 2.5: Comparison of pitch plane model responses with the measured data under the no-load condition: (a) stopping distance vs braking pressure (48 km/h); (b) stopping distance vs braking pressure (80 km/h); and (c) vehicle pitch response vs deceleration.

The results suggest that the stopping distance responses predicted by the model are only slightly lower than the measured data for the no-load condition, irrespective of the initial speed considered. The model results, however, are higher than the measured values for the other loading conditions. These deviations are possibly attributed to: (*a*) inappropriate braking system parameters that directly affect the braking torque gains; and (*b*) consideration of constant braking torque distribution for all the load conditions considered. The results further show that magnitude of sprung mass pitch increases

nearly linearly with deceleration magnitude. For the no-load and low c.g. load conditions, the sprung mass pitch responses of the model tend to be lower than the measured data, while a good agreement with the measured data is obtained for the high c.g. load condition, as evident in Figures 2.5(c), 2.6(c) and 2.7(c).

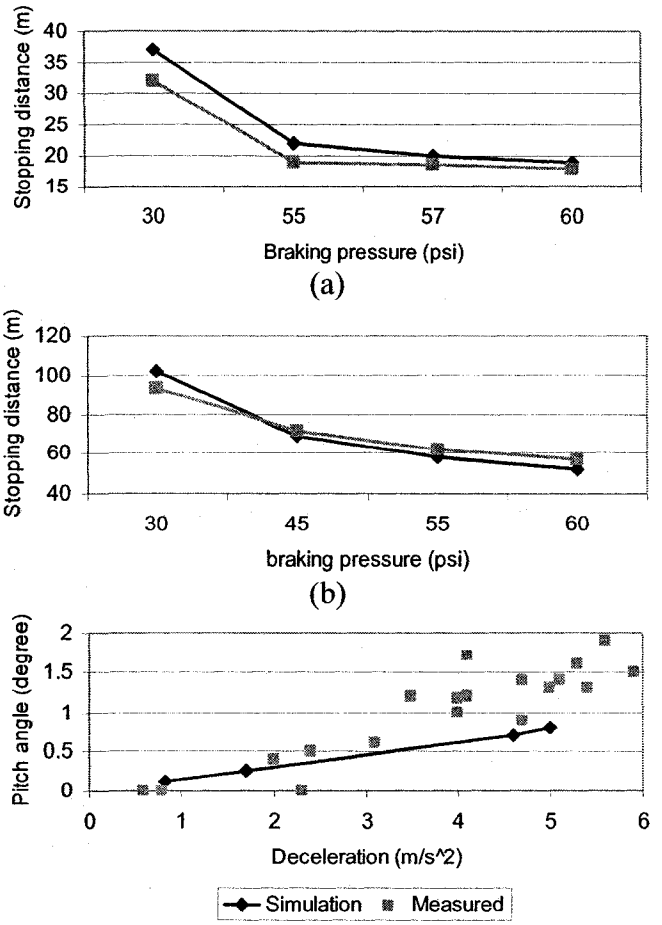

Figure 2.6: Comparison of pitch plane model responses with the measured data under the low c.g. loading condition: (a) stopping distance vs braking pressure (48 km/h); (b) stopping distance vs braking pressure (80 km/h); and (c) vehicle pitch response vs deceleration.

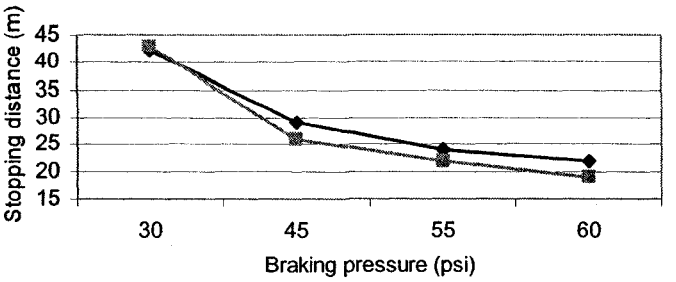

(a)

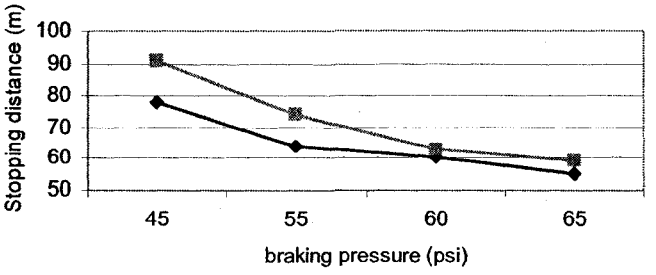

(b)

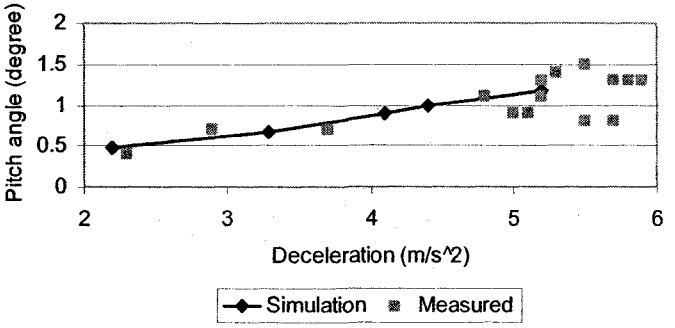

(c)

Figure 2.7: Comparison of pitch plane model responses with the measured data under the high c.g. loading condition: (a) stopping distance vs braking pressure (48 km/h); (b) stopping distance vs braking pressure (80 km/h); and (c) vehicle pitch response vs deceleration.

2.6 Development of a Generalized Model of Suspension Forces

The proposed single-gas-chamber and twin-gas-chamber struts could be employed in an unconnected manner in the pitch plane of the vehicle, as illustrated in Figure 2.8. The configuration A_{UP} employs two twin-gas-chamber struts, while B_{UP} comprises two single-gas-chamber struts. A hybrid configuration H_{UP} is also shown combining struts A and B.

Figure 2.9 illustrates a few interconnection configurations considered for analyses. Configurations A_{IP4}, A_{IP3} and A_{IP34} involve pneumatic interconnections between the gas

chambers of struts A, while B_{IP13} involves connections between the hydraulic fluid chambers of struts B. The configurations A_{IP4} and A_{IP3} are realized by connecting the gas chambers 4 and 3 of the two struts, respectively. The arrangements A_{IP34} and B_{IP13} involve pneumatic and hydraulic couplings, respectively, between gas chambers 3 and 4 of the opposite struts (A) and between hydraulic fluid chambers 1 and 3 of the struts (B).

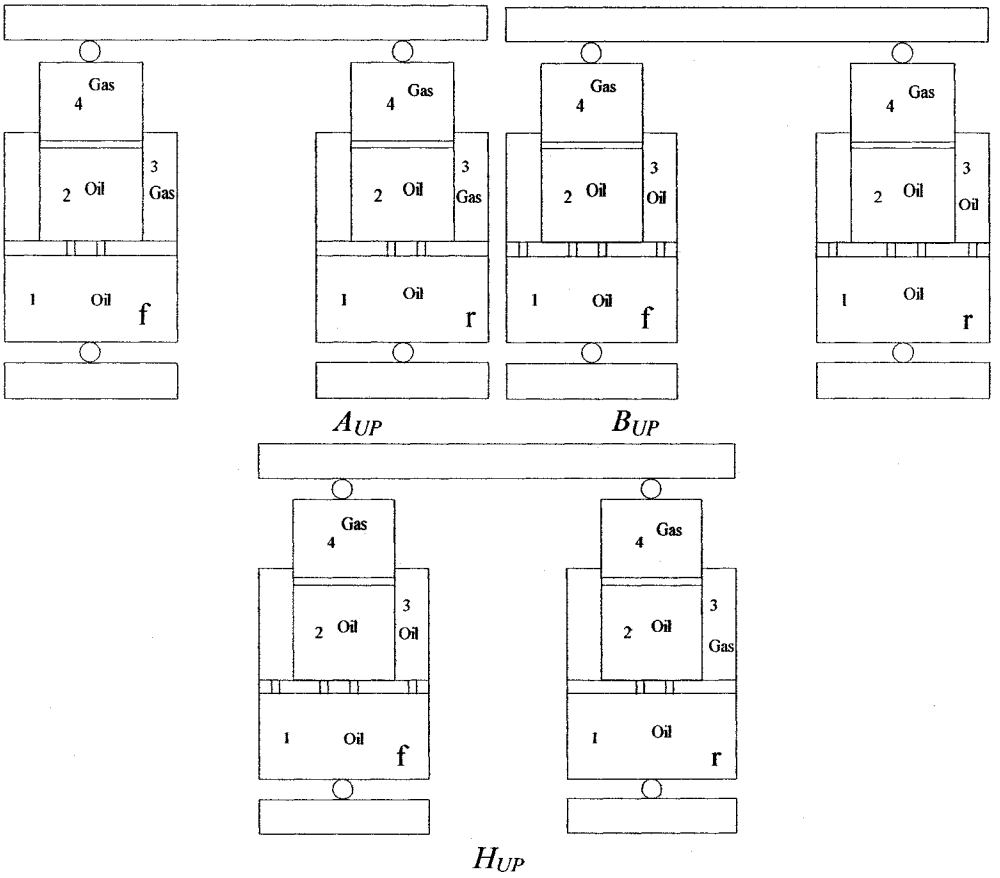

Figure 2.8: Unconnected suspension configurations in the pitch plane.

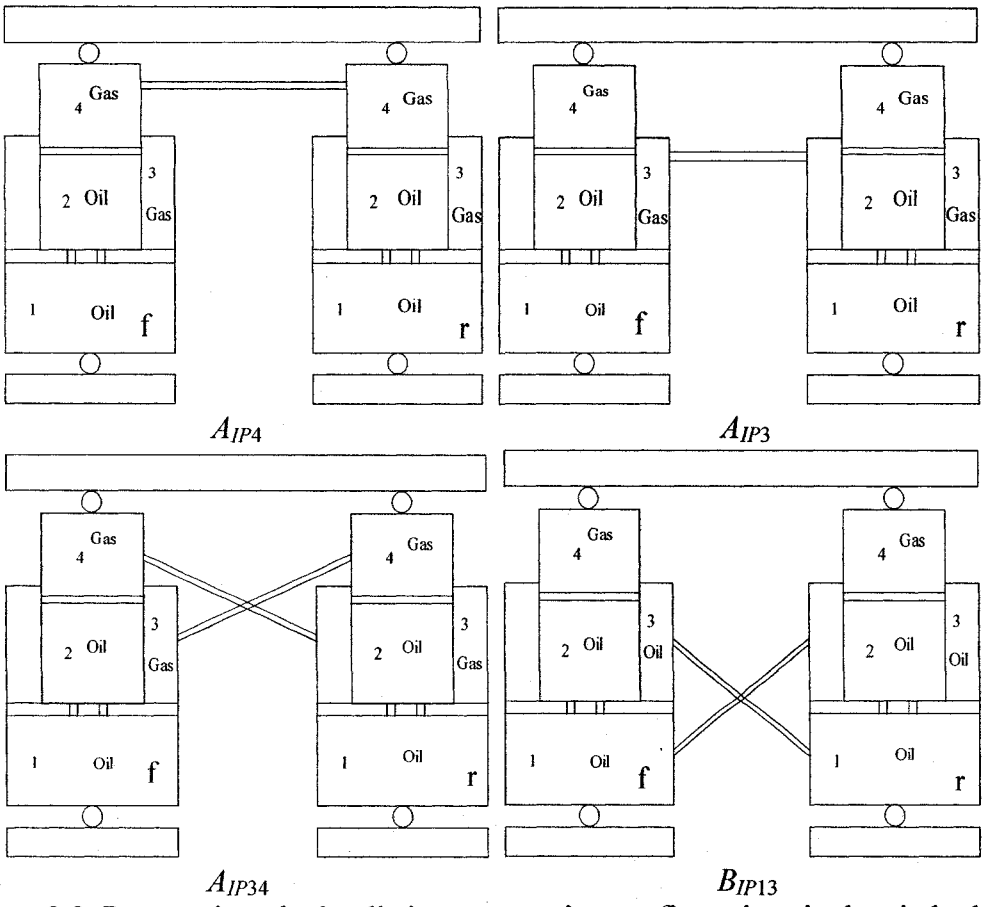

Figure 2.9: Pneumatic or hydraulic interconnection configurations in the pitch plane.

Alternate interconnection configurations may be realized using combinations of both the struts *A* and *B*. Figure 2.10 presents a few hybrid interconnection configurations. Configuration H_{IP4} is formed by connecting gas chambers 4 of struts *A* and *B*. H_{IP134} involves interconnections of gas chambers 4 of both the struts, while the chamber 3 of strut *B* is hydraulically connected to chamber 1 of strut *A*. The configuration $H_{IP1\text{-}4}$, in a similar manner, couples gas chamber 4 of strut *B* to chamber 3 of strut *A*, and chamber 3 of strut *B* is hydraulically connected to chamber 1 of strut *A*.

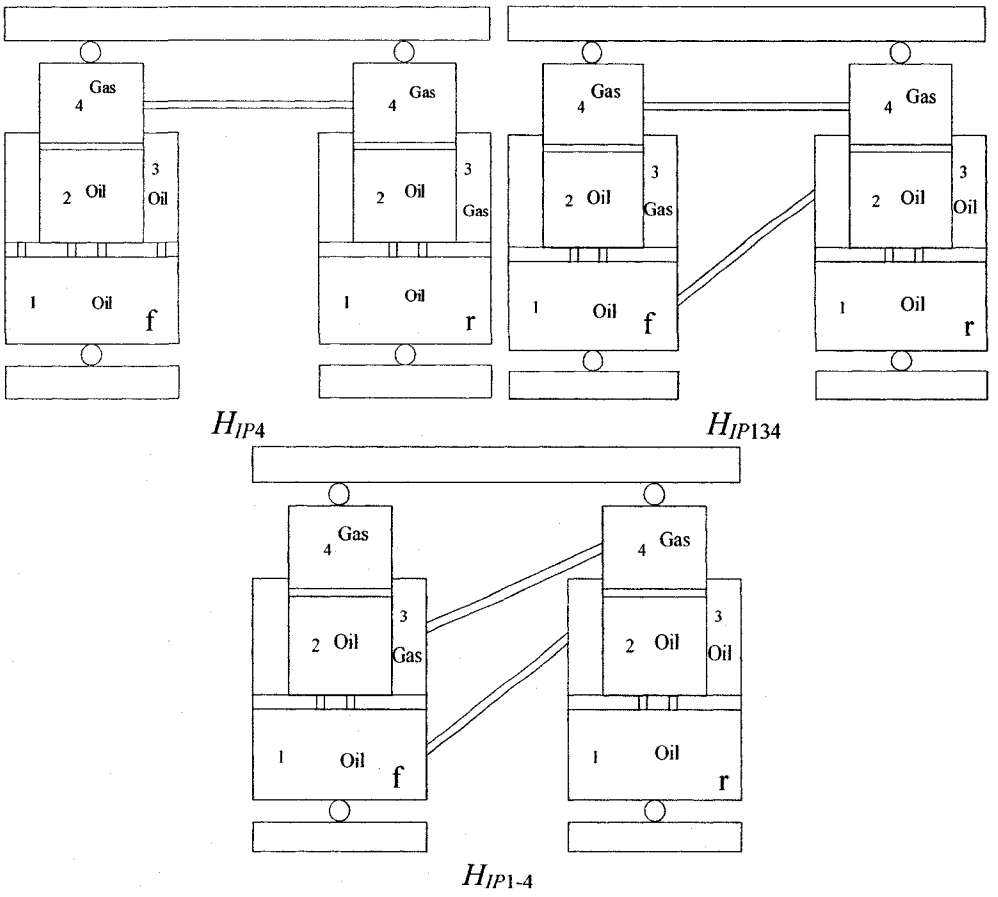

Figure 2.10: Hybrid fluidic interconnection configurations in the pitch plane.

2.6.1 A Generalized Model of Suspension Forces

Generalized mathematical formulations of the strut forces and pitch plane properties of different hydro-pneumatic suspension configurations involving struts *A* and/or *B* are derived, which may be applied to either unconnected or interconnected struts in both the roll and pitch planes. The generalized forces are derived assuming: (*a*) turbulent flows through damping orifices between the hydraulic chambers within the same strut; (*b*) laminar flows through hydraulic interconnections between the two struts, when present; (*c*) negligible damping effect of pneumatic flows through interconnections, when present; (*d*) polytropic gas process; (*e*) incompressible hydraulic fluid; (*f*) negligible leakage and

thermal expansion of the struts and hydraulic fluid; and (g) negligible effect of floating piston dynamics and seal friction.

The dynamic force F_i due to a strut is formulated, assuming identical static charge pressure in all the chambers of the same strut, such that:

$$F_i = (P_{1i} - P_0)A_{1i} - (P_{3i} - P_0)A_{3i} \quad (i = f, r) \tag{2.92}$$

where P_{ji} is the fluid pressure in chamber j (j=1,2,3,4) of strut i (i=f,r), A_{ji} is the effective piston area reflected on chamber j (j=1,2,3) side of strut i.

Figure 2.11 illustrates the generalized model of the strut forces due to different suspension configurations, including unconnected and connected, in which x_i and $\dot{x}_i$ are the relative displacement and velocity across strut i, respectively. For the pitch plane arrangement, $\dot{x}_f = \dot{z}_{uf} - \dot{z}_s + l_f\dot{\varphi}_s$ and $\dot{x}_r = \dot{z}_{ur} - \dot{z}_s - l_r\dot{\varphi}_s$, assuming small motions with positive direction being upward. The blocks in the upper row of the generalized model relate to gas spring forces, where C_p refers to the number of gas chambers in a particular suspension configuration, give by:

$$C_p = \begin{bmatrix} C_{4f} & 0 & 0 & 0 \\ 0 & C_{3f} & 0 & 0 \\ 0 & 0 & C_{4r} & 0 \\ 0 & 0 & 0 & C_{3r} \end{bmatrix} \tag{2.93}$$

where C_{ji}=1, when chamber j (j=3,4) of strut i (i=f,r) is filled with gas, otherwise C_{ji}=0.

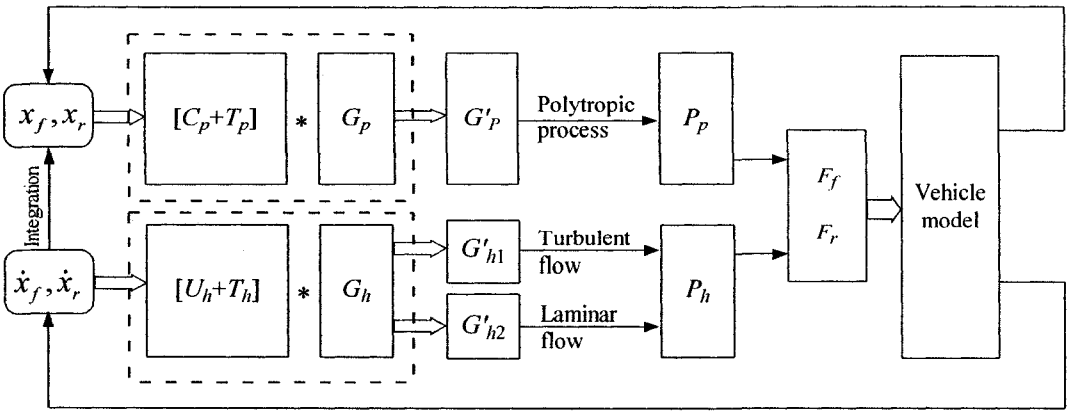

Figure 2.11: A generalized model for deriving suspension strut forces.

The matrix T_P in Figure 2.11, describes the nature of coupling between various chambers of the strut suspension and is defined in Eq. (2.94). Subscripts used with coefficient T denote the coupled chambers within a strut or across the front and rear suspension struts in a pitch connected suspension. T_{4f3r}, for example, is a coefficient related to coupling between chamber 4 of front strut and chamber 3 of the rear strut. The coefficient T_{43f}, on the other hand, refers to coupling between chambers 3 and 4 of the front strut alone. The coefficient T_{ji} assumes a unity value when the two fluidic chambers are coupled (directly or indirectly); and a 0 value in the absence of a coupling. A direct coupling implies interconnections of two chambers through interconnecting pipes, while an indirect coupling occurs when the fluids in two chambers attain identical pressure under static equilibriums, such as those coupled through damping orifices or floating piston. The dimension of matrix T_P is governed by the number of chambers that may be coupled, such that:

$$T_p = \begin{bmatrix} 0 & C_{4f}T_{43f} & C_{4f}T_{4f4r} & C_{4f}T_{4f3r} \\ C_{3f}T_{34f} & 0 & C_{3f}T_{3f4r} & C_{3f}T_{3f3r} \\ C_{4r}T_{4r4f} & C_{4r}T_{4r3f} & 0 & C_{4r}T_{43r} \\ C_{3r}T_{3r4f} & C_{3r}T_{3r3f} & C_{3r}T_{34r} & 0 \end{bmatrix} \tag{2.94}$$

Changes in volumes of gas chambers G'_p are related to matrices C_p and T_p:

$$G'_P = \left[C_p + T_p\right] G_p \tag{2.95}$$

where G'_p is a vector of variations in gas volumes in different chambers of both struts, while G_P defines the change in fluid volume attributed to struts deflections:

$$G_p = \begin{bmatrix} A_{1f} x_f \\ -A_{3f} x_f \\ A_{1r} x_r \\ -A_{3r} x_r \end{bmatrix} \tag{2.96}$$

In the generalized model (Figure 2.11), P_p is matrix of gas pressures in different chambers, derived from volume change vector G'_p and the gas laws. It needs to be noted that the coupled gas chambers are assumed to possess identical gas pressure.

Similarly, for the coupled hydraulic fluid chambers, matrix U_h describing the number of hydraulic fluid chambers is defined as:

$$U_h = \begin{bmatrix} U_{1f} & 0 & 0 & 0 \\ 0 & U_{1r} & 0 & 0 \\ 0 & 0 & U_{3f} & 0 \\ 0 & 0 & 0 & U_{3r} \end{bmatrix} \tag{2.97}$$

where U_{ji}=1, when a chamber j (j=1,3) of strut i (i=f,r) is filled with hydraulic fluid, otherwise it is 0. Damping matrix T_h, computed from hydraulic flow continuity equations for the hydraulically coupled chambers, is derived as:

$$T_h = \begin{bmatrix} 0 & 0 & U_{3f} S_{13f} & U_{3r} S_{1f3r} \\ 0 & 0 & U_{3f} S_{1r3f} & U_{3r} S_{13r} \\ 0 & 0 & 0 & 0 \\ 0 & 0 & 0 & 0 \end{bmatrix} \tag{2.98}$$

where the coefficient S=1, when two hydraulic fluid chambers are coupled through either interconnecting pipes or damping orifices, otherwise S=0. The flow rates are determined from the rates of change of fluid volumes in hydraulic fluid chambers, expressed by G_h:

$$G_h = \begin{bmatrix} U_{1f}A_{1f}\dot{x}_f \\ U_{1r}A_{1r}\dot{x}_r \\ -U_{3f}A_{3f}\dot{x}_f \\ -U_{3r}A_{3r}\dot{x}_r \end{bmatrix} \tag{2.99}$$

In the generalized model (Figure 2.11), vector G'_{h1} defines the flow rates of hydraulic fluid to/from the chambers within the same strut coupled through damping valves/orifices. The hydraulic fluid flow rates between chambers of different struts through interconnecting pipes are described by the flow rate vector G'_{h2}. The vectors G'_{h1} and G'_{h2} can be derived from Eqs. (2.97)~(2.99), which further yield pressure drops (P_h) across the flow paths (orifices or connecting pipes).

Applications of the generalized model for pneumatic, hydraulic and hybrid interconnections are illustrated in the following sections.

2.6.2 Forces due to Pneumatic Configuration (A_{IP})

The dynamic forces developed by a strut within an unconnected or interconnected suspension can be easily derived from the above generalized model. Dynamic suspension forces developed by the struts in the pneumatic interconnection arrangement A_{IP} are developed from Eq. (2.92), as an example, such that:

$$F_f = (P_{1f} - P_0)A_{1f} - (P_{3f} - P_0)A_{3f} = (P_{4f} + P_{12f} - P_0)A_{1f} - (P_{4r} - P_0)A_{3f}$$

$$F_r = (P_{1r} - P_0)A_{1r} - (P_{3r} - P_0)A_{3r} = (P_{4r} + P_{12r} - P_0)A_{1r} - (P_{4m} - P_0)A_{3r} \tag{2.100}$$

where $P_{jki} = P_{ji} - P_{ki}$ is pressure differential of fluids in chambers j and k of strut i, which are derived from coefficient matrices C_p and T_p, defined in Eqs. (2.93) and (2.94), respectively, and the volume change vector G_p, defined in Eq. (2.96). For configuration A_{IP}, these matrices can be derived as:

$$C_p = \begin{bmatrix} 1 & 0 & 0 & 0 \\ 0 & 1 & 0 & 0 \\ 0 & 0 & 1 & 0 \\ 0 & 0 & 0 & 1 \end{bmatrix}; \; T_p = \begin{bmatrix} 0 & 0 & 0 & 1 \\ 0 & 0 & 1 & 0 \\ 0 & 1 & 0 & 0 \\ 1 & 0 & 0 & 0 \end{bmatrix} \tag{2.101}$$

The vector G'_p that describes the changes in the volume of fluids in gas chambers of both the struts can be obtained from Eqs. (2.96) and (2.101), such that:

$$G'_p = \begin{bmatrix} A_{1f}x_f - A_{3r}x_r \\ A_{1r}x_r - A_{3f}x_f \\ A_{1r}x_r - A_{3f}x_f \\ A_{1f}x_f - A_{3r}x_r \end{bmatrix} \tag{2.102}$$

Matrices T_p and G'_p show the coupling effects in restoring forces developed due to gas chambers of both the struts. The gas pressures in different chambers can be derived assuming polytropic gas law, such that:

$$P_{4f} = P_{3r} = P_0 \left(\frac{V_{40f} + V_{30r}}{V_{40f} + V_{30r} + A_{1f}x_f - A_{3r}x_r} \right)^n$$

$$P_{4r} = P_{3f} = P_0 \left(\frac{V_{40r} + V_{30f}}{V_{40r} + V_{30f} + A_{1r}x_r - A_{3f}x_f} \right)^n \tag{2.103}$$

The flow rates of hydraulic fluids through the damping orifices/valves (G'_{h1}) and interconnecting pipes (G'_{h2}) are derived from matrices U_h and T_h, defined in Eqs. (2.97) and (2.98), and the vector G_h containing changes in fluid volumes in hydraulic fluid

chambers. The flow and volume change matrices for this configuration can be expressed as:

$$U_h = \begin{bmatrix} 1 & 0 & 0 & 0 \\ 0 & 1 & 0 & 0 \\ 0 & 0 & 0 & 0 \\ 0 & 0 & 0 & 0 \end{bmatrix}; \; T_h = \begin{bmatrix} 0 & 0 & 0 & 0 \\ 0 & 0 & 0 & 0 \\ 0 & 0 & 0 & 0 \\ 0 & 0 & 0 & 0 \end{bmatrix}; \; G_h = \begin{bmatrix} A_{1f}\dot{x}_f \\ A_{1r}\dot{x}_r \\ 0 \\ 0 \end{bmatrix} \tag{2.104}$$

The rates of change of hydraulic fluid volumes, associated with turbulent flows through damping restrictions G'_{h1} and laminar flows through connecting pipes G'_{h2} are then derived as:

$$G'_{h1} = \begin{bmatrix} A_{1f}\dot{x}_f \\ A_{1r}\dot{x}_r \end{bmatrix}; \; G'_{h2} = \begin{bmatrix} 0 \\ 0 \end{bmatrix} \tag{2.105}$$

The damping forces due to turbulent flows within the same strut are related to pressure drop and the effective orifice area a_{12i} due to bleed orifice and the valves. Assuming turbulent flows, the pressure drops across the damping restrictions of the two struts are expressed as:

$$P_{12f} = -\frac{\rho A_{1f}^2 |\dot{x}_f|(\dot{x}_f)}{2C_d^2 a_{12f}^2}; \; P_{12r} = -\frac{\rho A_{1r}^2 |\dot{x}_r|(\dot{x}_r)}{2C_d^2 a_{12r}^2} \tag{2.106}$$

Upon substituting for pressure differentials from Eqs. (2.103) and (2.106) in Eq. (2.100), the dynamic force developed by each strut within the pneumatically coupled suspension configuration can be formulated as:

$$F_f = P_0 A_{1f}\left[\left(\frac{V_{40f}+V_{30r}}{V_{40f}+V_{30r}+A_{1f}x_f - A_{3r}x_r}\right)^n - 1\right] - P_0 A_{3f}\left[\left(\frac{V_{40r}+V_{30f}}{V_{40r}+V_{30f}+A_{1r}x_r - A_{3f}x_f}\right)^n - 1\right] - \frac{\rho A_{1f}^3 |\dot{x}_f|(\dot{x}_f)}{2C_d^2 a_{12f}^2}$$

$$F_r = P_0 A_{1r}\left[\left(\frac{V_{40r}+V_{30f}}{V_{40r}+V_{30f}+A_{1r}x_r-A_{3f}x_f}\right)^n-1\right]-P_0 A_{3r}\left[\left(\frac{V_{40f}+V_{30r}}{V_{40f}+V_{30r}+A_{1f}x_f-A_{3r}x_r}\right)^n-1\right]$$
$$-\frac{\rho A_{1r}^3|\dot{x}_r|(\dot{x}_r)}{2C_d^2a_{12r}^2} \tag{2.107}$$

The above formulations of strut forces are identical to those developed in the roll plane suspension, where the formulations were derived from flow continuous and pressure equations, presented in Eq. (2.28).

2.6.3 Forces due to Hydraulic Configuration (B_{IP})

The dynamic force developed by each strut within the hydraulically connected suspension configuration B_{IP} is derived in a similar manner, such that:

$$F_f = P_0 A_{1f}\left[\left(\frac{V_{40f}}{V_{40f}+A_{1f}x_f-A_{3r}x_r}\right)^n-1\right]-P_0 A_{3f}\left[\left(\frac{V_{40r}}{V_{40r}+A_{1r}x_r-A_{3f}x_f}\right)^n-1\right]-\frac{\rho A_{1f}|A_{1f}\dot{x}_f-A_{3r}\dot{x}_r|(A_{1f}\dot{x}_f-A_{3r}\dot{x}_r)}{2C_d^2a_{12f}^2}$$
$$+\frac{\rho A_{3f}|A_{1r}\dot{x}_r-A_{3f}\dot{x}_f|(A_{1r}\dot{x}_r-A_{3f}\dot{x}_f)}{2C_d^2a_{12r}^2}-\frac{128\mu L A_{3f}^2\dot{x}_f}{\pi D^4}$$
$$F_r = P_0 A_{1r}\left[\left(\frac{V_{40r}}{V_{40r}+A_{1r}x_r-A_{3f}x_f}\right)^n-1\right]-P_0 A_{3r}\left[\left(\frac{V_{40f}}{V_{40f}+A_{1f}x_f-A_{3r}x_r}\right)^n-1\right] \tag{2.108}$$
$$-\frac{\rho A_{1r}|A_{1r}\dot{x}_r-A_{3f}\dot{x}_f|(A_{1r}\dot{x}_r-A_{3f}\dot{x}_f)}{2C_d^2a_{12r}^2}+\frac{\rho A_{3r}|A_{1f}\dot{x}_f-A_{3r}\dot{x}_r|(A_{1f}\dot{x}_f-A_{3r}\dot{x}_r)}{2C_d^2a_{12f}^2}-\frac{128\mu L A_{3r}^2\dot{x}_r}{\pi D^4}$$

The above formulations clearly show that hydraulic interconnections yield strong stiffness couplings between the two struts, as evident from the first two terms, similar to configuration A_{IP}. Unlike configuration A_{IP}, the hydraulically connected configuration induces strong coupling effect in dissipative forces, attributed to flows through interconnections, as evident from the last three terms of the above equations.

2.6.4 Forces due to Hybrid Configuration (H_{IP})

The dynamic forces developed by the struts in hybrid pitch-interconnection configuration H_{IP} involving pneumatic and hydraulic fluid couplings are also formulated in a similar manner and given by:

$$\begin{aligned}
F_f &= P_0 A_{1f}\left[\left(\frac{V_{40f}}{V_{40f}+A_{1f}x_f-A_{3r}x_r}\right)^n-1\right]-P_0A_{3f}\left[\left(\frac{V_{40r}+V_{30f}}{V_{40r}+V_{30f}+A_{1r}x_r-A_{3f}x_f}\right)^n-1\right]-\frac{\rho A_{1f}\left|A_{1f}\dot{x}_f-A_{3r}\dot{x}_r\right|(A_{1f}\dot{x}_f-A_{3r}\dot{x}_r)}{2C_d^2a_{12f}^2}\\
F_r &= P_0 A_{1r}\left[\left(\frac{V_{40r}+V_{30f}}{V_{40r}+V_{30f}+A_{1r}x_r-A_{3f}x_f}\right)^n-1\right]-P_0A_{3r}\left[\left(\frac{V_{40f}}{V_{40f}+A_{1f}x_f-A_{3r}x_r}\right)^n-1\right]-\frac{\rho A_{1r}^3|\dot{x}_r|\dot{x}_r}{2C_d^2a_{12r}^2}\\
&+\frac{\rho A_{3r}\left|A_{1f}\dot{x}_f-A_{3r}\dot{x}_r\right|(A_{1f}\dot{x}_f-A_{3r}\dot{x}_r)}{2C_d^2a_{12f}^2}-\frac{128\mu LA_{3r}^2\dot{x}_r}{\pi D^4}
\end{aligned} \tag{2.109}$$

Equation (2.109) also shows strong couplings in the restoring forces developed by the two struts. Moreover, the hybrid fluidic interconnection yields coupled damping forces developed by the struts, as seen in case of hydraulic interconnection B_{IP}.

2.6.5 Forces due to Unconnected Configuration (B_{UP})

The dynamic for developed by an unconnected strut can also be formulated in a similar manner, upon considering turbulent flows through damping orifices/valves and polytropic gas process:

$$F_i = P_0 A_{2i}\left[\left(\frac{V_{40i}}{V_{40i}+A_{2i}x_i}\right)^n-1\right]-\frac{\rho A_{2i}^3|\dot{x}_i|\dot{x}_i}{2C_d^2a_{12i}^2}-\frac{\rho A_{3i}^3|\dot{x}_i|\dot{x}_i}{2C_d^2a_{13i}^2} \quad (i=f,r) \tag{2.110}$$

2.6.6 Forces due to Twin-Gas-Chamber Suspension (A_{UP})

The dynamic force developed by twin-gas-chamber strut suspension A_{UP} can also be formulated in a similar manner, such that:

$$F_i = P_0 A_{1i}\left[\left(\frac{V_{40i}}{V_{40i}+A_{1i}x_i}\right)^n-1\right]-P_0A_{3i}\left[\left(\frac{V_{30i}}{V_{30i}-A_{3i}x_i}\right)^n-1\right]-\frac{\rho A_{1i}^3|\dot{x}_i|\dot{x}_i}{2C_d^2a_{12i}^2} \quad (i=f,r) \tag{2.111}$$

2.7 Modeling of Pitch Plane Properties of Different Suspension Systems

The pitch plane properties of different suspension configurations are derived upon consideration of the pitch plane vehicle model and generalized mathematical formulations of strut forces. The properties of selected suspension configurations are derived in terms of suspension rate, pitch stiffness, and bounce and pitch mode damping.

2.7.1 Suspension Rate Property

The suspension rate of a strut in a pitch-interconnected suspension could be conveniently evaluated from Eq. (2.39), under a pure vertical displacement input, such that $x_f = x_r = x$.

PNEUMATIC PITCH-INTERCONNECTION CCONFIGURATION (A_{IP}):

The restoring forces due to the pneumatically pitch-interconnected suspension A_{IP} can be obtained from Eq. (2.107), such that:

$$F_f = P_0 A_{1f}\left[\left(\frac{V_{40f}+V_{30r}}{V_{40f}+V_{30r}+A_{1f}x_f-A_{3r}x_r}\right)^n-1\right]-P_0 A_{3f}\left[\left(\frac{V_{40r}+V_{30f}}{V_{40r}+V_{30f}+A_{1r}x_r-A_{3f}x_f}\right)^n-1\right]$$

$$F_r = P_0 A_{1r}\left[\left(\frac{V_{40r}+V_{30f}}{V_{40r}+V_{30f}+A_{1r}x_r-A_{3f}x_f}\right)^n-1\right]-P_0 A_{3r}\left[\left(\frac{V_{40f}+V_{30r}}{V_{40f}+V_{30r}+A_{1f}x_f-A_{3r}x_r}\right)^n-1\right] \quad (2.112)$$

The suspension rates of front (k_{vf}) and rear (k_{vr}) struts of suspension configuration A_{IP} are thus expressed as:

$$k_{vf} = nP_0\left(V_{40f}+V_{30r}\right)^n \frac{A_{1f}^2 - A_{1f}A_{3r}\dfrac{dx_r}{dx_f}}{\left[V_{40f}+V_{30r}+A_{1f}x_f - A_{3r}x_r\right]^{n+1}} + nP_0\left(V_{40r}+V_{30f}\right)^n \frac{A_{3f}^2 - A_{1r}A_{3f}\dfrac{dx_r}{dx_f}}{\left[V_{40r}+V_{30f}+A_{1r}x_r - A_{3f}x_f\right]^{n+1}}$$

$$k_{vr} = nP_0\left(V_{40r}+V_{30f}\right)^n \frac{A_{1r}^2 - A_{1r}A_{3f}\dfrac{dx_f}{dx_r}}{\left[V_{40r}+V_{30f}+A_{1r}x_r - A_{3f}x_f\right]^{n+1}} + nP_0\left(V_{40f}+V_{30r}\right)^n \frac{A_{3r}^2 - A_{1f}A_{3r}\dfrac{dx_f}{dx_r}}{\left[V_{40f}+V_{30r}+A_{1f}x_f - A_{3r}x_r\right]^{n+1}} \quad (2.113)$$

Under identical vertical displacements of both the front and rear struts $x_f = x_r = x$, the relationship $dx_r/dx_f = dx_f/dx_r = 1$ can be achieved to yield suspension rates as:

$$k_{vf} = nP_0\left(V_{40f}+V_{30r}\right)^n \frac{A_{1f}^2 - A_{1f}A_{3r}}{\left[V_{40f}+V_{30r}+A_{1f}x - A_{3r}x\right]^{n+1}} + nP_0\left(V_{40r}+V_{30f}\right)^n \frac{A_{3f}^2 - A_{1r}A_{3f}}{\left[V_{40r}+V_{30f}+A_{1r}x - A_{3f}x\right]^{n+1}}$$

$$k_{vr} = nP_0\left(V_{40r}+V_{30f}\right)^n \frac{A_{1r}^2 - A_{1r}A_{3f}}{\left[V_{40r}+V_{30f}+A_{1r}x - A_{3f}x\right]^{n+1}} + nP_0\left(V_{40f}+V_{30r}\right)^n \frac{A_{3r}^2 - A_{1f}A_{3r}}{\left[V_{40f}+V_{30r}+A_{1f}x - A_{3r}x\right]^{n+1}} \quad (2.114)$$

The suspension rate properties of the other selected suspension configurations are also derived in a similar manner and summarized below:

HYDRAULIC PITCH-INTERCONNECTION (B_{IP}):

$$k_{vf} = nP_0V_{40f}^n \frac{A_{1f}^2 - A_{1f}A_{3r}}{\left[V_{40f}+A_{1f}x - A_{3r}x\right]^{n+1}} + nP_0V_{40r}^n \frac{A_{3f}^2 - A_{1r}A_{3f}}{\left[V_{40r}+A_{1r}x - A_{3f}x\right]^{n+1}}$$

$$k_{vr} = nP_0V_{40r}^n \frac{A_{1r}^2 - A_{1r}A_{3f}}{\left[V_{40r}+A_{1r}x - A_{3f}x\right]^{n+1}} + nP_0V_{40f}^n \frac{A_{3r}^2 - A_{1f}A_{3r}}{\left[V_{40f}+A_{1f}x - A_{3r}x\right]^{n+1}} \quad (2.115)$$

HYBRID FLUIDIC PITCH-INTERCONNECTION (H_{JP}):

$$k_{vf} = nP_0V_{40f}^n \frac{A_{1f}^2 - A_{1f}A_{3r}}{\left[V_{40f} + A_{1f}x - A_{3r}x\right]^{n+1}} + nP_0\left(V_{40r} + V_{30f}\right)^n \frac{A_{3f}^2 - A_{1r}A_{3f}}{\left[V_{40r} + V_{30f} + A_{1r}x - A_{3f}x\right]^{n+1}}$$

$$k_{vr} = nP_0\left(V_{40r} + V_{30f}\right)^n \frac{A_{1r}^2 - A_{1r}A_{3f}}{\left[V_{40r} + V_{30f} + A_{1r}x - A_{3f}x\right]^{n+1}} + nP_0V_{40f}^n \frac{A_{3r}^2 - A_{1f}A_{3r}}{\left[V_{40f} + A_{1m}x - A_{3r}x\right]^{n+1}} \quad (2.116)$$

UNCONNECTED CONFIUGRATION (B_{UP}):

$$k_{vi} = nP_0V_{40i}^n \frac{A_{2i}^2}{\left[V_{40i} + A_{2i}x\right]^{n+1}} \qquad (i = f, r) \quad (2.117)$$

TWIN-GAS-CHAMBER SUSPENSION CONFIUGRATION (A_{UP}):

$$k_{vi} = nP_0V_{40i}^n \frac{A_{1i}^2}{\left[V_{40i} + A_{1i}x_i\right]^{n+1}} + nP_0V_{30i}^n \frac{A_{3i}^2}{\left[V_{30i} - A_{3i}x_i\right]^{n+1}} \qquad (i = f, r) \quad (2.118)$$

2.7.2 Pitch Stiffness Property

The effective pitch stiffness k_P of a suspension configuration can be derived from the restoring pitch moment developed by the struts and pitch deflection of the sprung mass, such that:

$$k_P = dM_P / d\varphi \quad (2.119)$$

where M_P is restoring pitch moment developed due to restoring forces of both the struts, and φ is relative pitch deflection across the suspension, which is derived from pitch axis of the sprung mass.

The suspension pitch rate can be conveniently evaluated under a pitch deflection input. It needs to be noted that a pitch deflection input would also yield relative vertical deflection of each strut due to coupling between the bounce and pitch modes of the vehicle. The suspension pitch rate analysis thus involves simultaneous solutions of Eq. (2.119) with the static equilibrium of the vehicle, as described below for configuration A_{IP}, considering the generally coupled bounce and pitch vibration modes of vehicles.

PNEUMATIC PITCH-INTERCONNECTION (A_{IP}):

The restoring pitch moment due to pneumatically connected suspension is formulated upon considering restoring forces of both the front and rear suspension struts, such that:

$$\begin{aligned} M_P &= -P_{4f}(A_{1f}l_f + A_{3r}l_r) + P_{4r}(A_{1r}l_r + A_{3f}l_f) \\ &= -P_0(A_{1f}l_f + A_{3r}l_r)\left(\frac{V_{40f}+V_{30r}}{V_{40f}+V_{30r}+A_{1f}(x+l_f\varphi)-A_{3r}(x-l_r\varphi)}\right)^n \\ &+ P_0(A_{1r}l_r + A_{3f}l_f)\left(\frac{V_{40r}+V_{30f}}{V_{40r}+V_{30f}+A_{1r}(x-l_r\varphi)-A_{3f}(x+l_f\varphi)}\right)^n \end{aligned} \tag{2.120}$$

Assuming a vertical displacement z_u of a point on the pitch axis of the unsprung masses beneath the sprung mass c.g., the pitch angle $\varphi_u = (z_{ur} - z_{uf})/(l_f + l_r)$. Letting $\varphi = \varphi_s - \varphi_u$ and $z = z_s - z_u$ yields strut deflections as: $x_f = z + l_f\phi$, $x_r = z - l_r\phi$. The suspension pitch rate can thus be derived from Eqs. (2.119) and (2.120) as:

$$k_p = nP_0\left(A_{1F}l_f + A_{3r}l_r\right)\left(V_{40f}+V_{30r}\right)^n \frac{\left(A_{1f}l_f + A_{3r}l_r\right)+\left(A_{1f}-A_{3r}\right)\dfrac{dz}{d\phi}}{\left[V_{40f}+V_{30r}+A_{1f}\left(z+l_f\phi\right)-A_{3r}\left(z-l_r\phi\right)\right]^{n+1}}$$
$$+nP_0\left(A_{1r}l_r + A_{3f}l_f\right)\left(V_{40r}+V_{30f}\right)^n \frac{\left(A_{1r}l_r + A_{3f}l_f\right)-\left(A_{1r}-A_{3f}\right)\dfrac{dz}{d\phi}}{\left[V_{40r}+V_{30f}+A_{1r}\left(z-l_r\phi\right)-A_{3f}\left(z+l_f\phi\right)\right]^{n+1}} \tag{2.121}$$

where $\dfrac{dz}{d\phi}$ can be obtained from quasi-static equilibrium of the sprung mass corresponding to a given input φ, such that:

$$\begin{aligned} g(z,\phi) &= P_{4f}(A_{1f}-A_{3r})+P_{4r}(A_{1r}-A_{3f})-P_0(A_{2f}+A_{2r}) \\ &= \left(A_{1f}-A_{3r}\right)\left(\frac{V_{40f}+V_{30r}}{V_{40f}+V_{30r}+A_{1f}\left(z+l_f\phi\right)-A_{3r}\left(z-l_r\phi\right)}\right)^n \\ &+\left(A_{1r}-A_{3f}\right)\left(\frac{V_{40r}+V_{30f}}{V_{40r}+V_{30f}+A_{1r}\left(z-l_r\phi\right)-A_{3f}\left(z+l_f\phi\right)}\right)^n-(A_{2f}+A_{2r})=0 \end{aligned} \tag{2.122}$$

Above equilibrium equation yields the following relationship between z and φ:

$$\begin{aligned} \frac{dz}{d\phi} &= -\frac{\partial g/\partial\phi}{\partial g/\partial z} \\ &= \frac{\dfrac{-\left(A_{1f}-A_{3r}\right)\left(A_{1f}l_f+A_{3r}l_r\right)\left(V_{40f}+V_{30r}\right)^n}{\left[V_{40f}+V_{30r}+A_{1f}\left(z+l_f\phi\right)-A_{3r}\left(z-l_r\phi\right)\right]^{n+1}}+\dfrac{\left(A_{1r}-A_{3f}\right)\left(A_{1r}l_r+A_{3f}l_f\right)\left(V_{40r}+V_{30f}\right)^n}{\left[V_{40r}+V_{30f}+A_{1r}\left(z-l_r\phi\right)-A_{3f}\left(z+l_f\phi\right)\right]^{n+1}}}{\dfrac{\left(A_{1f}-A_{3r}\right)^2\left(V_{40f}+V_{30r}\right)^n}{\left[V_{40f}+V_{30r}+A_{1f}\left(z+l_f\phi\right)-A_{3r}\left(z-l_r\phi\right)\right]^{n+1}}+\dfrac{\left(A_{1r}-A_{3f}\right)^2\left(V_{40r}+V_{30f}\right)^n}{\left[V_{40r}+V_{30f}+A_{1r}\left(z-l_r\phi\right)-A_{3f}\left(z+l_f\phi\right)\right]^{n+1}}} \end{aligned} \tag{2.123}$$

The simultaneous solution of Eqs. (2.121)~(2.123) yields effective pitch rate of the pitch-connected suspension A_{IP}. The pitch stiffness properties of the other suspension configurations are also derived in a similar manner, together with the quasi-static equilibrium equation, and summarized below.

HYDRAULIC PITCH-INTERCONNECTION (B_{IP}):

For suspension configuration B_{IP}, suspension pitch rate and quasi-static equilibrium are obtained as:

$$k_P = nP_0\left(A_{1f}l_f + A_{3r}l_r\right)V_{40f}^n \frac{\left(A_{1f}l_f + A_{3r}l_r\right)+\left(A_{1f} - A_{3r}\right)\dfrac{dz}{d\phi}}{\left[V_{40f} + A_{1f}\left(z + l_f\phi\right) - A_{3r}\left(z - l_r\phi\right)\right]^{n+1}}$$
$$+nP_0\left(A_{1r}l_r + A_{3f}l_f\right)V_{40r}^n \frac{\left(A_{1r}l_r + A_{3f}l_f\right)-\left(A_{1r} - A_{3f}\right)\dfrac{dz}{d\phi}}{\left[V_{40r} + A_{1r}\left(z - l_r\phi\right) - A_{3f}\left(z + l_f\phi\right)\right]^{n+1}} \tag{2.124}$$

$$g(z,\phi) = \left(A_{1f} - A_{3r}\right)\left(\frac{V_{40f}}{V_{40f} + A_{1f}\left(z + l_f\phi\right) - A_{3r}\left(z - l_r\phi\right)}\right)^n$$
$$+\left(A_{1r} - A_{3f}\right)\left(\frac{V_{40r}}{V_{40r} + A_{1r}\left(z - l_r\phi\right) - A_{3f}\left(z + l_f\phi\right)}\right)^n - (A_{2f} + A_{2r}) = 0 \tag{2.125}$$

$$\frac{dz}{d\phi} = -\frac{\partial g/\partial\phi}{\partial g/\partial z} = \frac{\dfrac{-\left(A_{1f} - A_{3r}\right)\left(A_{1f}l_f + A_{3r}l_r\right)V_{40f}^n}{\left[V_{40f} + A_{1f}\left(z + l_f\phi\right) - A_{3r}\left(z - l_r\phi\right)\right]^{n+1}} + \dfrac{\left(A_{1r} - A_{3f}\right)\left(A_{1r}l_r + A_{3f}l_f\right)V_{40r}^n}{\left[V_{40r} + A_{1r}\left(z - l_r\phi\right) - A_{3f}\left(z + l_f\phi\right)\right]^{n+1}}}{\dfrac{\left(A_{1f} - A_{3r}\right)^2 V_{40f}^n}{\left[V_{40f} + A_{1f}\left(z + l_f\phi\right) - A_{3r}\left(z - l_r\phi\right)\right]^{n+1}} + \dfrac{\left(A_{1r} - A_{3f}\right)^2 V_{40r}^n}{\left[V_{40r} + A_{1r}\left(z - l_r\phi\right) - A_{3f}\left(z + l_f\phi\right)\right]^{n+1}}} \tag{2.126}$$

The simultaneous solutions of above equation yield pitch rate of the hydraulic interconnection configuration B_{IP}.

HYBRID FLUIDIC PITCH-INTERCONNECTION (H_{IP}):

The pitch stiffness of the hybrid fluidic interconnection configuration H_{IP} is similarly derived from simultaneous solutions of following equations.

$$k_P = nP_0\left(A_{1f}l_f + A_{3r}l_r\right)V_{40f}^n \frac{\left(A_{1f}l_f + A_{3r}l_r\right)+\left(A_{1f}-A_{3r}\right)\dfrac{dz}{d\phi}}{\left[V_{40f}+A_{1f}\left(z+l_f\phi\right)-A_{3r}\left(z-l_r\phi\right)\right]^{n+1}}$$
$$+nP_0\left(A_{1r}l_r + A_{3f}l_f\right)\left(V_{40r}+V_{30f}\right)^n \frac{\left(A_{1r}l_r + A_{3f}l_f\right)-\left(A_{1r}-A_{3f}\right)\dfrac{dz}{d\phi}}{\left[V_{40r}+V_{30f}+A_{1r}\left(z-l_r\phi\right)-A_{3f}\left(z+l_f\phi\right)\right]^{n+1}} \tag{2.127}$$

$$g(z,\phi)=\left(A_{1f}-A_{3r}\right)\left(\frac{V_{40f}}{V_{40f}+A_{1f}\left(z+l_f\phi\right)-A_{3r}\left(z-l_r\phi\right)}\right)^n$$
$$+\left(A_{1r}-A_{3f}\right)\left(\frac{V_{40r}+V_{30f}}{V_{40r}+V_{30f}+A_{1r}\left(z-l_r\phi\right)-A_{3f}\left(z+l_f\phi\right)}\right)^n-\left(A_{2f}+A_{2r}\right)=0 \tag{2.128}$$

$$\frac{dz}{d\phi}=-\frac{\partial g/\partial\phi}{\partial g/\partial z}=\frac{\dfrac{-\left(A_{1f}-A_{3r}\right)\left(A_{1f}l_f+A_{3r}l_r\right)V_{40f}^n}{\left[V_{40f}+A_{1f}\left(z+l_f\phi\right)-A_{3r}\left(z-l_r\phi\right)\right]^{n+1}}+\dfrac{\left(A_{1r}-A_{3f}\right)\left(A_{1r}l_r+A_{3f}l_f\right)\left(V_{40r}+V_{30f}\right)^n}{\left[V_{40r}+V_{30f}+A_{1r}\left(z-l_r\phi\right)-A_{3f}\left(z+l_f\phi\right)\right]^{n+1}}}{\dfrac{\left(A_{1f}-A_{3r}\right)^2V_{40f}^n}{\left[V_{40f}+A_{1f}\left(z+l_f\phi\right)-A_{3r}\left(z-l_r\phi\right)\right]^{n+1}}+\dfrac{\left(A_{1r}-A_{3f}\right)^2\left(V_{40r}+V_{30f}\right)^n}{\left[V_{40r}+V_{30f}+A_{1r}\left(z-l_r\phi\right)-A_{3f}\left(z+l_f\phi\right)\right]^{n+1}}} \tag{2.129}$$

UNCONNECTED SUSPENSION (B_{UP}):

$$k_P = nP_0A_{2f}l_fV_{40f}^n\frac{A_{2f}l_f+A_{2f}\dfrac{dz}{d\phi}}{\left[V_{40f}+A_{2f}\left(z+l_f\phi\right)\right]^{n+1}}+nP_0A_{2r}l_rV_{40r}^n\frac{A_{2r}l_r-A_{2r}\dfrac{dz}{d\phi}}{\left[V_{40r}+A_{2r}\left(z-l_r\phi\right)\right]^{n+1}} \tag{2.130}$$

$$g(z,\phi)=A_{2f}\left(\frac{V_{40f}}{V_{40f}+A_{2f}\left(z+l_f\phi\right)}\right)^n+A_{2r}\left(\frac{V_{40r}}{V_{40r}+A_{2r}\left(z-l_r\phi\right)}\right)^n-\left(A_{2f}+A_{2r}\right)=0 \tag{2.131}$$

$$\frac{dz}{d\phi}=-\frac{\partial g/\partial\phi}{\partial g/\partial z}=\frac{\dfrac{-A_{2f}^2V_{40f}^nl_f}{\left[V_{40f}+A_{2f}\left(z+l_f\phi\right)\right]^{n+1}}+\dfrac{A_{2r}^2V_{40r}^nl_r}{\left[V_{40r}+A_{2r}\left(z-l_r\phi\right)\right]^{n+1}}}{\dfrac{A_{2f}^2V_{40f}^n}{\left[V_{40f}+A_{2f}\left(z+l_f\phi\right)\right]^{n+1}}+\dfrac{A_{2r}^2V_{40r}^n}{\left[V_{40r}+A_{2r}\left(z-l_r\phi\right)\right]^{n+1}}} \tag{2.132}$$

The pitch rate of unconnected suspension B_{UP} can be achieved from simultaneous solutions of Eqs. (2.130) to (2.132).

TWIN-GAS-CHAMBER SUSPENSION (A_{UP}):

$$k_P = nP_0A_{1f}l_fV_{40f}^n\frac{A_{1f}l_f + A_{1f}\dfrac{dz}{d\phi}}{\left[V_{40f} + A_{1f}\left(z + l_f\phi\right)\right]^{n+1}} + nP_0A_{1r}l_rV_{40r}^n\frac{A_{1r}l_r - A_{1r}\dfrac{dz}{d\phi}}{\left[V_{40r} + A_{1r}\left(z - l_r\phi\right)\right]^{n+1}}$$
$$+nP_0A_{3f}l_fV_{30f}^n\frac{A_{3f}l_f + A_{3f}\dfrac{dz}{d\phi}}{\left[V_{30f} - A_{3f}\left(z + l_f\phi\right)\right]^{n+1}} + nP_0A_{3r}l_rV_{30r}^n\frac{A_{3r}l_r - A_{3r}\dfrac{dz}{d\phi}}{\left[V_{30r} - A_{3r}\left(z - l_r\phi\right)\right]^{n+1}} \tag{2.133}$$

$$g(z,\phi) = P_{4f}A_{1f} + P_{4r}A_{1r} - P_{3f}A_{3f} - P_{3r}A_{3r} - P_0(A_{2f} + A_{2r})$$
$$= A_{1f}\left(\frac{V_{40f}}{V_{40f} + A_{1f}\left(z + l_f\phi\right)}\right)^n + A_{1r}\left(\frac{V_{40r}}{V_{40r} + A_{1r}\left(z - l_r\phi\right)}\right)^n \tag{2.134}$$
$$-A_{3f}\left(\frac{V_{30f}}{V_{30f} - A_{3f}\left(z + l_f\phi\right)}\right)^n - A_{3r}\left(\frac{V_{30r}}{V_{30r} - A_{3r}\left(z - l_r\phi\right)}\right)^n - (A_{2f} + A_{2r}) = 0$$

$$\frac{dz}{d\phi} = -\frac{\partial g/\partial\phi}{\partial g/\partial z} = \frac{l_r\left(\lambda_2 + \lambda_4\right) - l_f\left(\lambda_1 + \lambda_3\right)}{\sum_{m=1}^{4}\lambda_m} \tag{2.135}$$

where $\lambda_1 = \dfrac{A_{1f}^2V_{40f}^n}{\left[V_{40f} + A_{1f}\left(z + l_f\phi\right)\right]^{n+1}}$, $\lambda_2 = \dfrac{A_{1r}^2V_{40r}^n}{\left[V_{40r} + A_{1r}\left(z - l_r\phi\right)\right]^{n+1}}$, $\lambda_3 = \dfrac{A_{3f}^2V_{30f}^n}{\left[V_{30f} - A_{3f}\left(z + l_f\phi\right)\right]^{n+1}}$,

and $\lambda_4 = \dfrac{A_{3r}^2V_{30r}^n}{\left[V_{30r} - A_{3r}\left(z - l_r\phi\right)\right]^{n+1}}$. Simultaneous solution of Eqs. (2.133) to (2.135) yields effective pitch stiffness of the twin-gas-chamber strut suspension A_{UP}.

2.7.3 Bounce and Pitch Mode Damping Properties

The bounce and pitch mode damping forces of different suspension configurations can be derived upon considering in-phase ($\dot{x}_f = \dot{x}_r = \dot{x}$) and out-of-phase ($\dot{x}_f = -\dot{x}_r = \dot{x}$) vertical velocity inputs, respectively. The pitch mode damping property of the suspension can be presented in terms of the damping moment, $M_d = l_f F_{df} - l_r F_{dr}$, where F_{di} (i=f,r) is the dissipative force developed by strut i.

PNEUMATIC PITCH-INTERCONNECTION (A_{IP}):

Owing to uncoupled damping property of the pneumatically connected configuration A_{IP}, the damping force and moment are derived from Eq. (2.107), as:

$$F_{di} = \frac{\rho A_{1i}^3 |\dot{x}|(\dot{x})}{2C_d^2 a_{12i}^2} \quad (i = f,r); \; M_d = \frac{\rho l_f A_{1f}^3 |\dot{x}|(\dot{x})}{2C_d^2 a_{12f}^2} + \frac{\rho l_r A_{1r}^3 |\dot{x}|(\dot{x})}{2C_d^2 a_{12r}^2} \tag{2.136}$$

UNCONNECTED CONFIGURATION (B_{UP}):

The suspension struts employed in this configuration generate damping force due to fluid flows through bleed orifices and damping valves between chambers 1 and 2, and bleed orifices between chambers 1 and 3. The variations in damping force could be realized from flows through damping valves. The damping force developed by valve flows could be emphasized by selecting relatively larger effective damping area a_{13i}. This would yield damping force and moment similar to those in Eq. (2.136), assuming

negligible contribution due to fluid flows through large size bleed orifices between chambers 1 and 3, such that:

$$F_{di} \approx \frac{\rho A_{2i}^3 |\dot{x}|(\dot{x})}{2C_d^2 a_{12i}^2} \quad (i = f, r) \; ; \quad M_d \approx \frac{\rho l_f A_{2i}^3 |\dot{x}|(\dot{x})}{2C_d^2 a_{12i}^2} + \frac{\rho l_r A_{2r}^3 |\dot{x}|(\dot{x})}{2C_d^2 a_{12r}^2} \tag{2.137}$$

HYDRAULIC PITCH-INTERCONNECTION (B_{JP}):

The damping forces developed by the hydraulically connected struts are expressed as:

$$F_{df} = \frac{\rho A_{1f} |A_{1f}\dot{x} - A_{3r}\dot{x}|(A_{1f}\dot{x} - A_{3r}\dot{x})}{2C_d^2 a_{12f}^2} - \frac{\rho A_{3f} |A_{1r}\dot{x} - A_{3f}\dot{x}|(A_{1r}\dot{x} - A_{3f}\dot{x})}{2C_d^2 a_{12r}^2} + \frac{128\mu L A_{3f}^2 \dot{x}}{\pi D^4}$$

$$F_{dr} = \frac{\rho A_{1r} |A_{1r}\dot{x} - A_{3f}\dot{x}|(A_{1r}\dot{x} - A_{3f}\dot{x})}{2C_d^2 a_{12r}^2} - \frac{\rho A_{3r} |A_{1f}\dot{x} - A_{3r}\dot{x}|(A_{1f}\dot{x} - A_{3r}\dot{x})}{2C_d^2 a_{12f}^2} + \frac{128\mu L A_{3r}^2 \dot{x}}{\pi D^4} \tag{2.138a}$$

The above equations suggest negative damping feedback effect due to hydraulic coupling, and viscous damping due to flows through pipes. The effect of damping valves and the coupling feedback could be emphasized by selecting large diameter connecting pipes so as to reduce the contributions due to viscous damping. The resulting damping force and moment may thus be expressed as:

$$F_{df} \approx \frac{\rho A_{1f} |A_{1f}\dot{x} - A_{3r}\dot{x}|(A_{1f}\dot{x} - A_{3r}\dot{x})}{2C_d^2 a_{12f}^2} - \frac{\rho A_{3f} |A_{1r}\dot{x} - A_{3f}\dot{x}|(A_{1r}\dot{x} - A_{3f}\dot{x})}{2C_d^2 a_{12r}^2}$$

$$F_{dr} \approx \frac{\rho A_{1r} |A_{1r}\dot{x} - A_{3f}\dot{x}|(A_{1r}\dot{x} - A_{3f}\dot{x})}{2C_d^2 a_{12r}^2} - \frac{\rho A_{3r} |A_{1f}\dot{x} - A_{3r}\dot{x}|(A_{1f}\dot{x} - A_{3r}\dot{x})}{2C_d^2 a_{12f}^2} \tag{2.138b}$$

$$M_d \approx l_f\left(\frac{\rho A_{1f}\left|A_{1f}\dot{x}+A_{3r}\dot{x}\right|(A_{1f}\dot{x}+A_{3r}\dot{x})}{2C_d^2a_{12f}^2}+\frac{\rho A_{3f}\left|-A_{1r}\dot{x}-A_{3f}\dot{x}\right|(A_{1r}\dot{x}+A_{3f}\dot{x})}{2C_d^2a_{12r}^2}\right)$$
$$+l_r\left(\frac{\rho A_{1r}\left|-A_{1r}\dot{x}-A_{3f}\dot{x}\right|(A_{1r}\dot{x}+A_{3f}\dot{x})}{2C_d^2a_{12r}^2}+\frac{\rho A_{3r}\left|A_{1f}\dot{x}+A_{3r}\dot{x}\right|(A_{1f}\dot{x}+A_{3r}\dot{x})}{2C_d^2a_{12f}^2}\right) \quad (2.139)$$

HYBRID FLUIDIC PITCH-INTERCONNECTION (H_{IP}):

The damping force developed by each strut in configuration H_{IP} can be directly obtained from Eq. (2.109), and expressed as:

$$F_{df}=\frac{\rho A_{1f}\left|A_{1f}\dot{x}-A_{3r}\dot{x}\right|(A_{1f}\dot{x}-A_{3r}\dot{x})}{2C_d^2a_{12f}^2}$$

$$F_{dr}=\frac{\rho A_{1r}^3\left|\dot{x}\right|(\dot{x})}{2C_d^2a_{12r}^2}-\frac{\rho A_{3r}\left|A_{1f}\dot{x}-A_{3r}\dot{x}\right|(A_{1f}\dot{x}-A_{3r}\dot{x})}{2C_d^2a_{12f}^2}+\frac{128\mu LA_{3r}^2\dot{x}}{\pi D^4} \quad (2.140a)$$

Similar to configuration B_{IP}, the contribution due to damping valve and coupling feedback effect could be easily emphasized by reducing the viscous damping effect in F_{dr}. Selection of relatively large diameter of pipe coupling, and chambers $1f$ to $2r$ would yield identical expression for F_{df}, while F_{dr} reduces to:

$$F_{dr}\approx\frac{\rho A_{1r}^3\left|\dot{x}\right|(\dot{x})}{2C_d^2a_{12r}^2}-\frac{\rho A_{3r}\left|A_{1f}\dot{x}-A_{3r}\dot{x}\right|(A_{1f}\dot{x}-A_{3r}\dot{x})}{2C_d^2a_{12f}^2} \quad (2.140b)$$

The corresponding pitch damping moment is thus derived as:

$$M_d\approx\frac{\rho l_f A_{1f}\left|A_{1f}\dot{x}+A_{3r}\dot{x}\right|(A_{1f}\dot{x}+A_{3r}\dot{x})}{2C_d^2a_{12f}^2}+\frac{\rho l_r A_{1r}^3\left|\dot{x}\right|(\dot{x})}{2C_d^2a_{12r}^2}+\frac{\rho l_r A_{3r}\left|A_{1f}\dot{x}+A_{3r}\dot{x}\right|(A_{1f}\dot{x}+A_{3r}\dot{x})}{2C_d^2a_{12f}^2} \quad (2.141)$$

TWIN-GAS-CHAMBER STRUT SUSPENSION CONFIGURATION (A_{UP}):

The damping force developed by each strut in twin-gas-chamber suspension configuration A_{UP} can be directly obtained from Eq. (2.111), and expressed as:

$$F_{di} = \frac{\rho A_{1i}^3 |\dot{x}|(\dot{x})}{2C_d^2 a_{12i}^2} \quad (i = f,r); \quad M_d = \frac{\rho l_f A_{1i}^3 |\dot{x}|(\dot{x})}{2C_d^2 a_{12i}^2} + \frac{\rho l_r A_{1r}^3 |\dot{x}|(\dot{x})}{2C_d^2 a_{12r}^2} \tag{2.142}$$

2.8 Summary

Two hydro-pneumatic strut designs, which integrate gas chamber(s) and damping valves within the same units, are proposed to obtain a compact deign with considerably larger effective operating area, based on which various fluidic interconnections can be conveniently realized. The novel twin-gas-chamber strut design could further provide potential benefit in realizing nearly symmetric suspension rate in compression and rebound, and improved roll stiffness. Both the roll- and pitch-plane vehicle models are developed for facilitating the investigation of fundamental properties of different unconnected as well as interconnected suspension configurations, and vehicle dynamic responses. A number of roll- and pitch-interconnected and unconnected suspension configurations, based on the two strut designs, are analyzed to develop the strut forces and suspension properties. A generalized model of strut forces is further formulated to unify different suspension configurations in an integrated frame, which may further provide a foundation for exploring common characteristics of various suspension configurations in a theoretical manner.

CHAPTER 3

PERFORMANCE ANALYSIS OF ROLL-INTERCONNECTED SUSPENSIONS

3.1 Introduction

The rollover propensity of heavy vehicles can be greatly minimized by enhancing their suspension roll stiffness and roll mode damping [2, 21]. Conventional passive suspensions thus employ lateral mechanical interconnections, such as anti-roll bars, to achieve enhanced roll stiffness. The use of anti-roll bars, however, tends to add mass and degrade ride comfort properties to some extent [21]. Alternatively, a number of active mechanisms have been proposed to achieve improved compromise between the roll and ride dynamic performances, while their applications have been prohibitive due to the associated high cost and weight. Passive roll-interconnected hydro-pneumatic suspension systems could offer considerable potential for improved anti-roll properties, while preserving the soft vertical ride [25, 27-30].

In this chapter, the roll plane model of a heavy vehicle, employing various configurations of roll-connected and unconnected suspension struts formulated in the previous chapter, is analyzed to investigate the suspension properties, and vertical and roll dynamic responses of the vehicle. It should be noted that roll dynamic responses of a vehicle can be effectively evaluated using a roll plane model of the vehicle [1, 3, 21, 25, 28]. The generalized roll plane heavy vehicle model formulated in Section 2.3.1 permits for analysis of both the roll and ride dynamic performances coupled with either interconnected or unconnected suspension system, and can also easily integrate an anti-

roll bar. The model together with suspension formulations is analyzed under excitations arising from vehicle-road interactions, steering maneuvers and crosswinds. The fundamental properties in the roll plane are evaluated in terms of suspension rate, roll stiffness, and bounce and roll mode damping. Symmetric and asymmetric damping valves are also considered to realize desirable damping properties in the vertical and roll modes. The design flexibility of the fluidic interconnected suspensions is illustrated through parametric studies. The dynamic responses of the vehicle with different suspension configurations are further explored.

3.2 Simulation Parameters and Excitations

Table 3.1 summarizes the simulation parameters for the roll plane analysis of the vehicle model (Figure 2.2) with different suspension configurations. The vehicle parameters are adopted from the measured and estimated data of a heavy vehicle [152], while the unsprung mass is considered to be the sum of the front and rear unsprung masses. The parameters of suspension struts are designed to achieve reasonable size and static gas charge pressure with properties that are comparable to the conventional suspension systems. The struts parameters are further chosen to yield identical static vertical rates for the roll-connected and unconnected suspension configurations.

3.2.1 Excitations

The analyses of vertical ride and roll dynamic responses of the vehicle model require identification of excitations arising from vehicle-road interactions and various directional maneuvers. This section describes the nature of excitations employed in the simulation.

Table 3.1: Simulation parameters for the vehicle model and the suspensions.

Parameter	Value	Parameter	Value
Vehicle model			
m_s	15753 kg	k_t	921607 N/m
m_u	1550 kg	c_t	8000 Ns/m
I_{xxs}	40976 kgm^2	h	1.2 m
I_{xxu}	850 kgm^2	h_1	0.5 m
k_l	1264500 N/m	h_2	0.6 m
c_l	31614 Ns/m	g	9.81 m^2/s
l_t	1.03 m	l_s	0.78 m
Suspension			
n	1.38	L	1.5 m
ρ	912 kg/ m^3	D	0.03 m
P_a	101300 Pa	E	7×10^8 Pa
μ	0.082 Ns/m^2	C_d	0.7
k_{bar}	859000 Nm/rad	A_2	0.01194 m^2
P_0	3337000 Pa	A_3	0.0024 m^2

Random and transient road inputs

The measured road roughness data of three different roads in Quebec (Canada) are considered for relative ride dynamic analyses of different suspension configurations [152]. The measured data of road elevations consisted of both the roughness variations and the local road gradients of the left and right tracks. The contributions due to low-frequency variations associated with changes in the local gradients are often attenuated by using a high-pass filter. A high pass filter with a cut-off frequency 0.3 Hz was applied to process the measured raw road data [152]. The filtered roughness data of the selected three road profiles are used for the dynamic analyses in this thesis.

Figure 3.1 illustrates the elevations of the left- and right-track profiles of the three roads as a function of longitudinal distance, as well as their corresponding spatial displacement power spectral density (PSD) characteristics, over a total longitudinal distance of 579 m. On the basis of the spatial displacement PSD characteristics, the selected three roads are classified as "*smooth*" (Figure 3.1(a)), "*medium-rough*" (Figure 3.1(b)) and "*rough*" (Figure 3.1(c)) roads. The elevations as a function of the distance show that the left tracks are relatively smoother than the right tracks for the *smooth* and *medium-rough* roads, while both the left and right tracks are comparable throughout the longitudinal distance measured for the *rough* road. These are further evident from their corresponding spatial displacement PSD characteristics. For both the *smooth* and *medium-rough* roads, the PSD of the right track is higher than that of the left track. The PSDs of the left and right tracks of the *rough* road, however, are similar, as seen in Figure 3.1(c). The spatial displacement PSD characteristics of the selected three roads exhibit similar trends to those reported in [6, 21, 110].

Figure 3.2 further illustrates the vertical displacement and acceleration temporal PSD characteristics of the three road profiles at a speed of 70 km/h. For the profiles of the three roads considered, the amplitude of road elevation decreases with increasing frequency, while an increase in frequency causes larger amplitude of the acceleration of road roughness. Such characteristics are consistent with those in the reported study [110]. Both the PSD amplitude and the predominant frequencies of elevations also depend upon the forward speed.

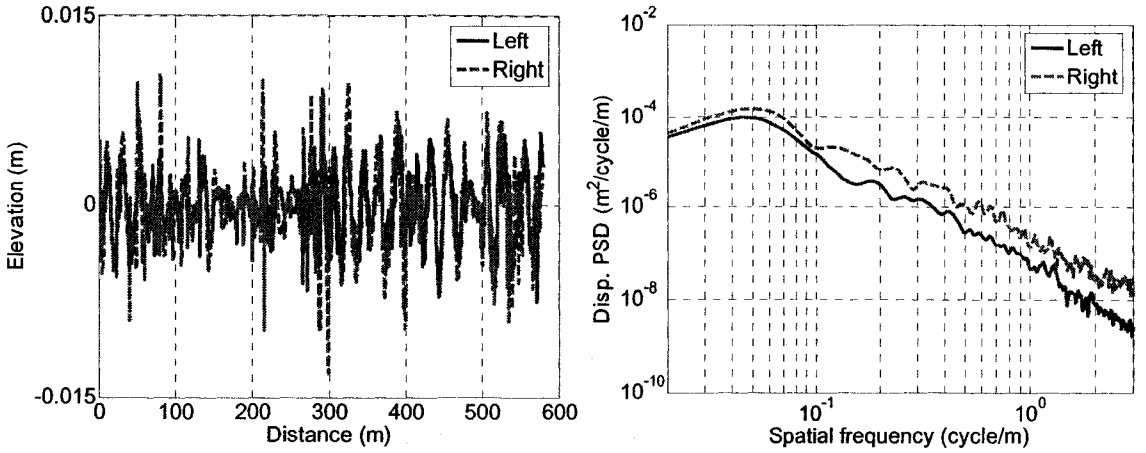

(a)

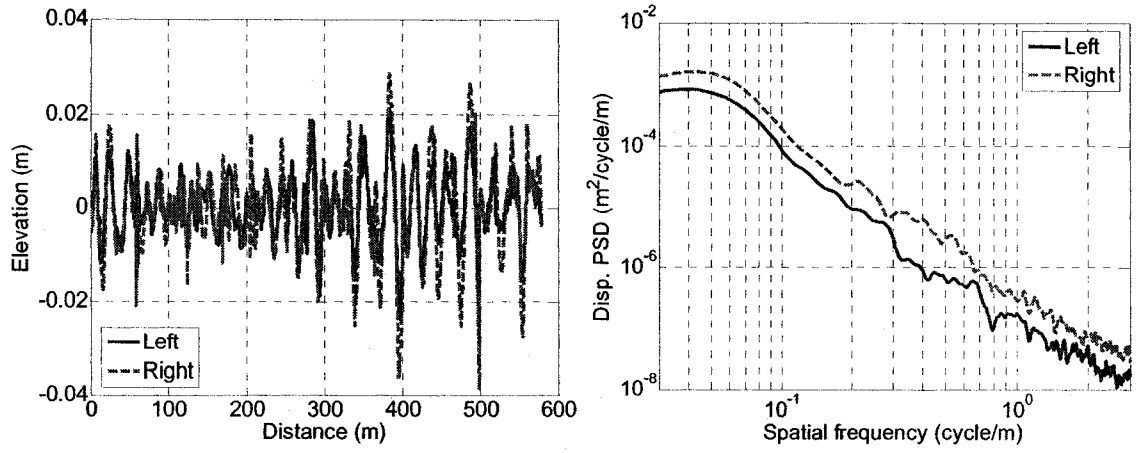

(b)

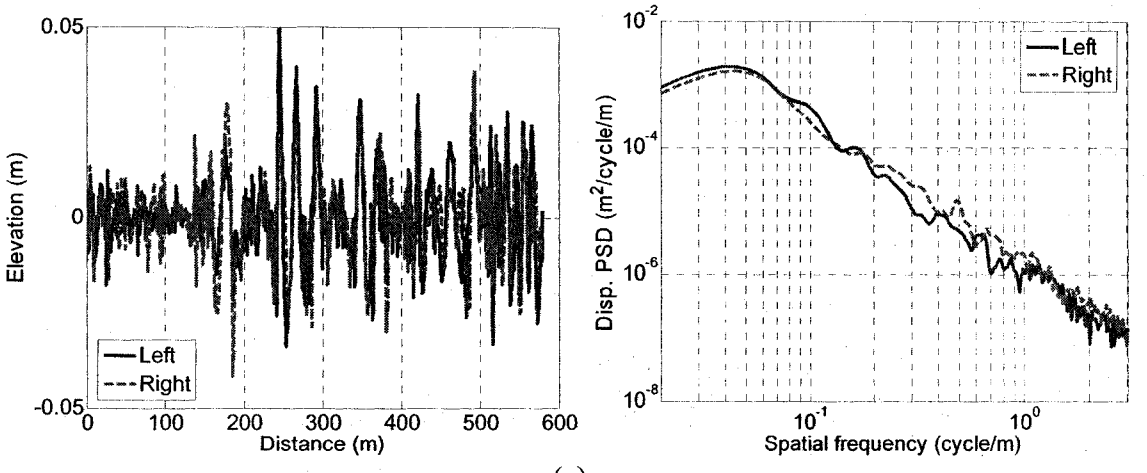

(c)

Figure 3.1: Elevations as a function of the longitudinal distance and spatial PSD of different road profiles along the left- and right-tracks: (a) smooth; (b) medium-rough; and (c) rough.

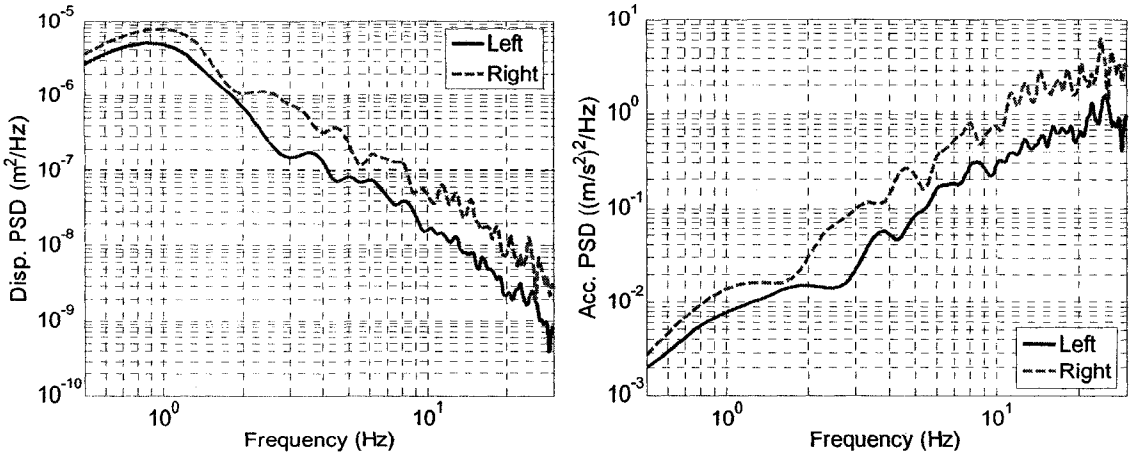

(a)

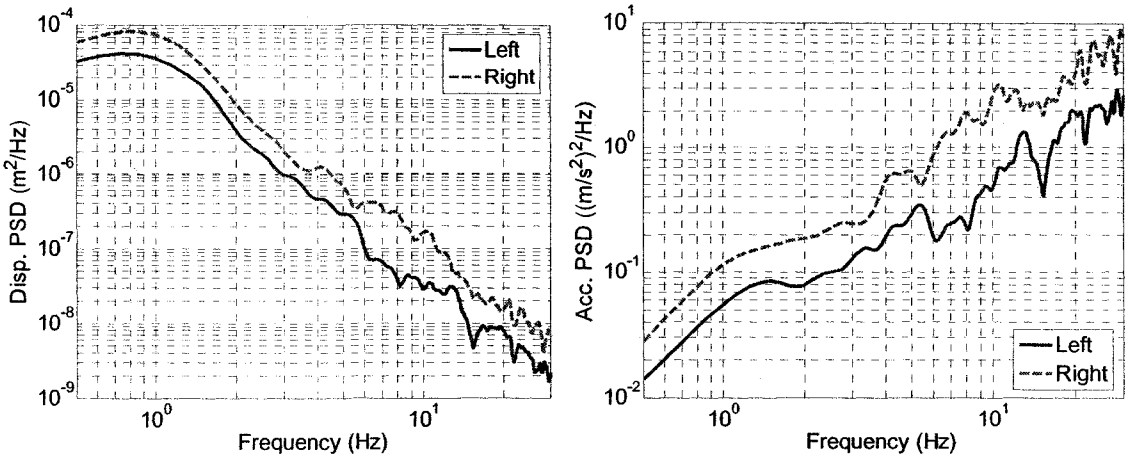

(b)

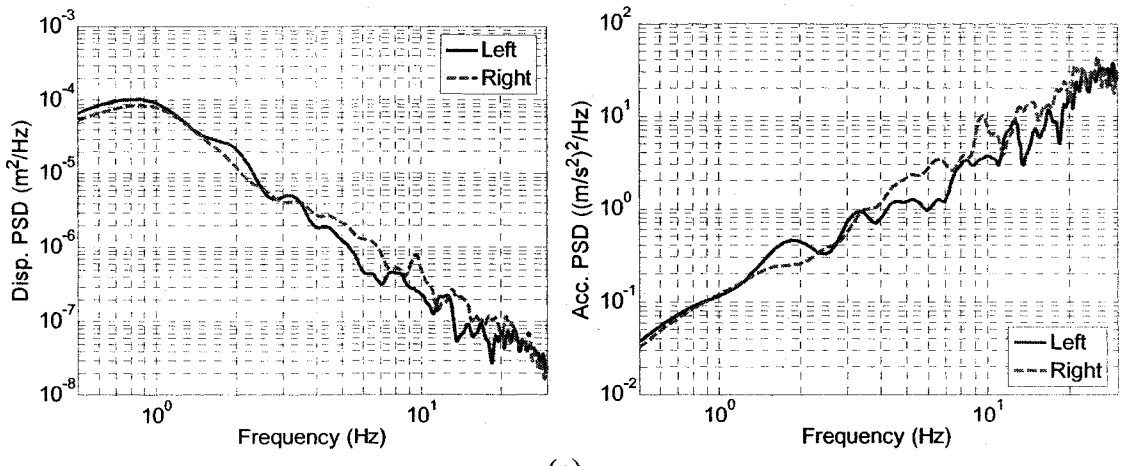

(c)

Figure 3.2: Vertical displacement and acceleration temporal PSD characteristics of the selected three road profiles at a speed of 70 km/h: (a) smooth; (b) medium-rough; and (c) rough.

Apart from the random road inputs, deterministic road profiles, such as road bumps and potholes, are also considered for evaluating shock isolation performance of different suspension configurations.

Centrifugal acceleration inputs

Steering maneuvers, such as steady turning and lane change maneuvers, can be conveniently expressed by the effective lateral accelerations experienced by the vehicle [21, 42]. Heavy vehicles may experience relative high magnitudes of transient lateral acceleration encountered under a lane change maneuver, depending upon the driving speed and rate of steering. Field measurements of a highway bus revealed the peak lateral acceleration during a lane change maneuver in the order of 0.3 g [28]. The lateral acceleration induced by a steady steering maneuver or crosswinds can be approximated by a rounded-step function, while that during a high speed lane change can be represented by a sine function [153], as illustrated in Figures 3.3(a) and (b), respectively. These functions can be expressed as:

$$a_y(t) = \begin{cases} A_{\max}\left[1 - e^{-\sigma t}(1+\sigma t)\right]; & rounded-step \\ A_{\max}\sin 2\pi f_s t; \quad (t_0 \le t \le t_0 + T); & lane-change \end{cases} \tag{3.1}$$

where a_y is the effective lateral acceleration, A_{max} is the magnitude of acceleration, chosen as 3 m/s^2, σ is the parameter describing the slope of lateral acceleration before reaching steady-state value, and f_s is the steering frequency of a lane change maneuver, t_0 refers to time when a lane change steering is initiated and T is the duration of steering input. The analyses are performed to study the relative anti-roll characteristics of different suspension configurations.

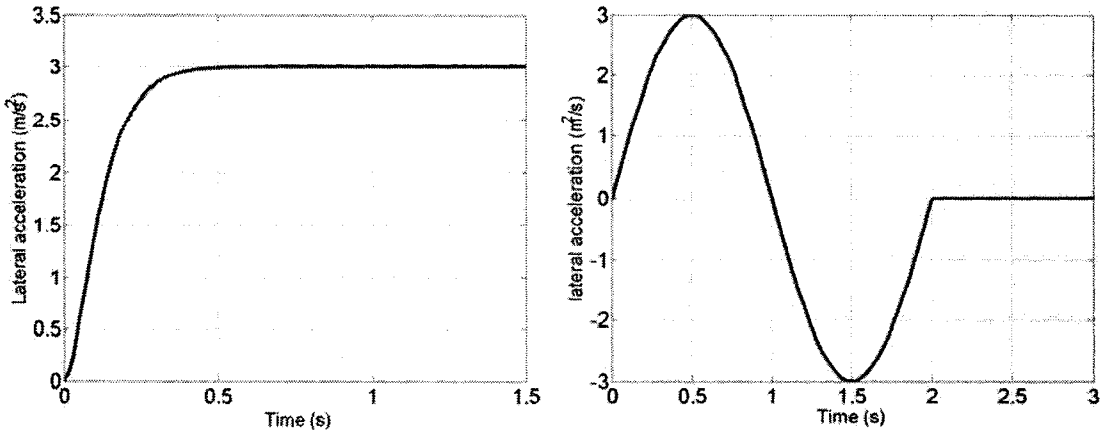

(a) (b)

Figure 3.3: Idealized lateral acceleration excitations: (a) rounded-step; and (b) lane change.

3.3 Relative Roll Plane Properties of Different Suspension Configurations

The roll plane vehicle model is analyzed to determine the roll plane properties of different suspension configurations, including: (i) unconnected hydro-pneumatic strut suspension without an anti-roll bar (B_{UR}); (ii) unconnected suspension with an anti-roll bar (B_{URbar}); (iii) hydraulically roll-interconnected suspension (B_{IR}); and (iv) pneumatically roll-interconnected suspension (A_{IR}). The strut forces developed by these suspensions have been presented in Section 2.3.2. The left and right struts are assumed to support identical loads. The strut parameters for all the suspension configurations are chosen to achieve identical load carrying capacity, static suspension rate and effective static deflection. The chosen parameters revealed undamped sprung mass bounce natural frequency in the order of 1.54 Hz at the design ride height. The parameters of the B_{URbar}, B_{IR} and A_{IR} configurations were further selected to obtain identical static roll stiffness. The static properties of these suspension systems at the design ride position are summarized in Table 3.2. The relative properties of different suspension configurations are further evaluated and compared as functions of the relative vertical and roll motions

of the sprung mass with respect to the unsprung mass. The dynamic properties are evaluated and compared under the inputs defined in the previous chapter, in terms of suspension rate, roll stiffness, and bounce and roll mode damping.

Table 3.2: Static properties of different suspension configurations.

	B_{UR}	B_{URbar}, B_{IR}, A_{IR}
Load carrying capacity (kg)	15753	15753
Effective static deflection (m)	0.0105	0.0105
Suspension rate (kN/m)	1466	1466
Roll stiffness (kNm/rad)	892	1751

3.3.1 Suspension Rate

The vertical suspension rate of each suspension configuration is evaluated under identical vertical inputs at the right and left struts, as described in Section 2.4.1. Figure 3.4 illustrates the suspension rates of all the four suspension configurations as a function of relative displacement across the struts. All the suspension configurations exhibit identical suspension rates over the deflection range considered, when hydraulic fluid is assumed to be incompressible (E=∞). The suspensions exhibit progressively hardening properties in compression and softening effects in rebound, which is attributed to the force-deflection characteristics of the gas spring. The figure further illustrates the effect of hydraulic fluid bulk modulus on the vertical force-deflection characteristics. The suspension rates due to the configurations B_{UR}, B_{URbar} and B_{IR} are quite close to those derived for the incompressible hydraulic fluid, when the nominal fluid bulk modulus (E=7e+8 Pa) is considered. The suspension rates, however, decrease considerably when a lower value of the fluid bulk modulus (7e+7 Pa) is considered, particularly in compression where the operating pressure becomes significantly higher. The effect of fluid compressibility on the suspension rate of the pneumatically interconnected

configuration A_{IR} is nearly identical to that observed for the configurations B_{UR}, B_{URbar} and B_{IR}, for the deflection range considered. This is due to the very small difference between the total volumes of hydraulic fluid in struts A and B.

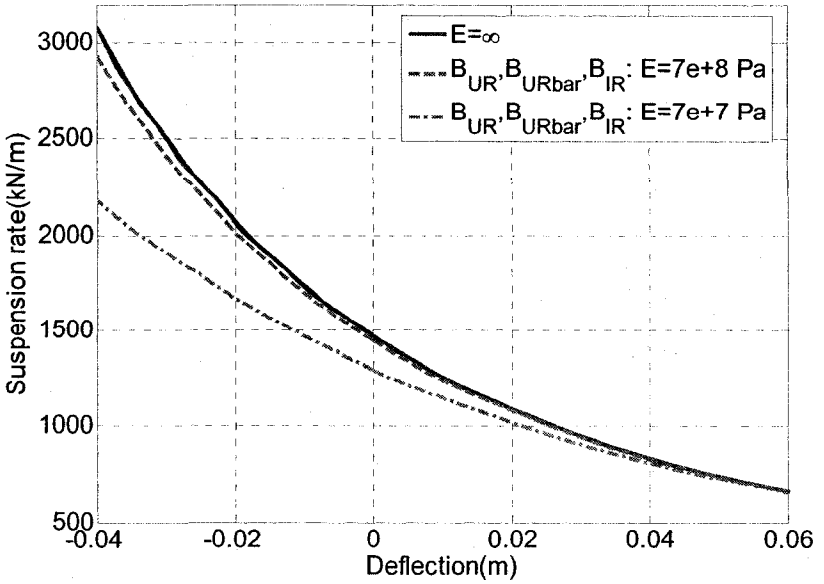

Figure 3.4: Suspension rates of different configurations and effects of compressibility of hydraulic fluid.

3.3.2 Roll Stiffness

The effective roll stiffness properties of the selected suspension configurations are evaluated under out-of-phase deflections of right and left struts, as described in Section 2.4.1. Figure 3.5 compares the roll stiffness characteristics of the four suspension configurations as a function of the relative roll deflection of the sprung mass with respect to the unsprung mass, assuming incompressible hydraulic fluid. The use of anti-roll bar or roll plane interconnections yields significantly higher static roll stiffness when compared to that of the unconnected suspension B_{UR}. While the B_{URbar}, B_{IR} and A_{IR} configurations yield identical static roll stiffness, both the fluidic interconnections B_{IR} and A_{IR} exhibit softening effect in roll with increasing roll deflection, which is attributed to

the nonlinear force-deflection properties of the gas spring. The results suggest that the roll stiffness properties of the suspension could be significantly enhanced through hydraulic and pneumatic coupling effects of the interconnections. Moreover, such interconnections do not affect the vertical spring rate, as evident in Figure 3.4. The enhanced anti-roll property could be realized without the additional mass and design space requirements of the anti-roll bar. The effect of variations in the fluid compressibility on the roll stiffnesses of both the hydraulically- and pneumatically-interconnected suspensions was observed to be nearly identical. Figure 3.6, as an example, illustrates the effects of fluid compressibility on the roll stiffness of the suspension configuration B_{IR}. Fluid compressibility tends to reduce the effective roll stiffness, as observed for the vertical spring rate. The reduction in the roll stiffness is relatively small for the nominal bulk modulus (E=7e+8 Pa) considered in the study. Significantly lower roll stiffness, however, is observed with a further reduction in the fluid bulk modulus.

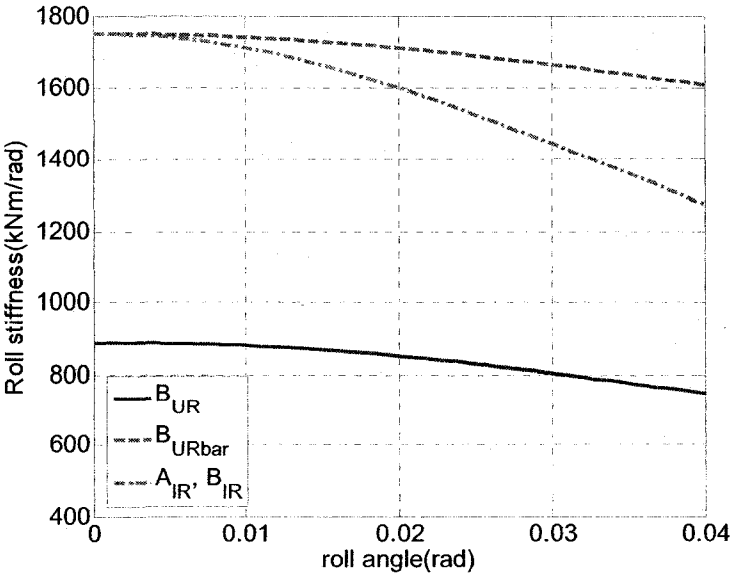

Figure 3.5: Relative roll stiffness characteristics of the different unconnected and connected suspension configurations, assuming incompressible hydraulic fluid.

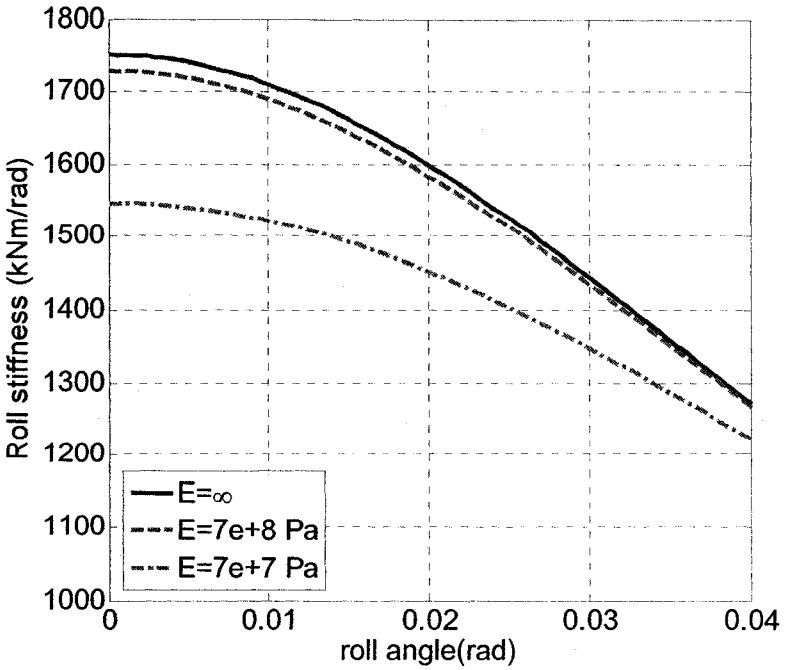

Figure 3.6: Effect of variations in fluid bulk modulus on the roll stiffness characteristics of the suspension configuration B_{IR}.

The roll stiffness of a hydraulically-interconnected suspension can also be expressed by its roll stiffness index (RSI), defined as the ratio of its roll stiffness to that of the corresponding unconnected suspension with the same strut dimensions and roll deflection. The RSI thus defines a measure of the gain in effective roll stiffness that could be realized through the roll-plane coupling. Figure 3.7 illustrates the RSI of the hydraulically interconnected configuration B_{IR} as a function of the fluid compressibility. The results indicate that the hydraulic interconnections could yield nearly twice the static roll stiffness of the unconnected suspension. The RSI of the suspension decreases with increasing roll deflection, while a lower bulk modulus fluid yields higher gain in the effective roll stiffness, when compared to the unconnected suspension with identical fluid.

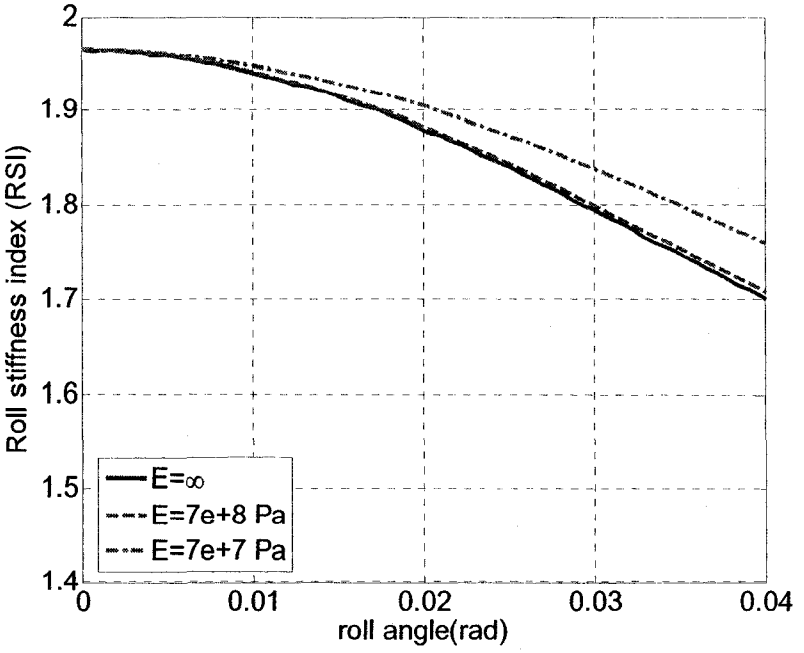

Figure 3.7: Variations in roll stiffness index (RSI) of the hydraulically interconnection configuration B_{IR} with roll deflection and fluid bulk modulus.

3.3.3 Bounce and Roll Mode Damping Properties

The relative damping properties of the suspension configurations are evaluated in the bounce and roll modes under in-phase and out-of-phase relative velocity excitations, respectively. The resulting force-velocity characteristics are evaluated using Equations (2.71)~(2.74) for both symmetric and asymmetric valves, described in Equation (2.13). The transition velocity at which the fluid flow initiates through the shim-disc valves is chosen as 0.08 m/s, while the valves become fully open at a velocity of 1.5 m/s. Such damping valves have been widely employed in vehicle suspension dampers to achieve variable damping properties [144]. A few studies have investigated the damping properties of the hydro-pneumatic struts with constant area damping orifices, which yield excessive damping forces at higher strut velocities [28-30]. The use of damping valves could significantly reduce the effective high speed damping for improved ride comfort,

while retaining adequately high low-speed damping for improved roll and handling performance.

The unconnected configurations (B_{UR} and B_{URbar}) and connected pneumatic suspension (A_{IR}) exhibit nearly identical force-velocity properties of the struts in the bounce and roll modes, as evident in Figure 3.8, for the symmetric and asymmetric damping valves. The hydraulic interconnection (B_{IR}), however, offers considerably larger damping in the entire velocity range, and greater flexibility in realizing vertical mode damping comparable to the unconnected suspension and significantly higher roll mode damping, as shown in Figure 3.8. Higher roll mode damping is attributed to the hydraulic coupling between the two struts, as evident in Equation (2.15). The pneumatically connected configuration A_{IR}, however, does not provide any gain in damping force due to negligible damping effects of the gas flows through the interconnecting pipes. The results thus suggest that the roll-interconnections do not affect the vertical mode damping properties of the suspensions, while the hydraulic interconnection could provide significantly higher roll stiffness and damping properties due to hydraulic fluid couplings.

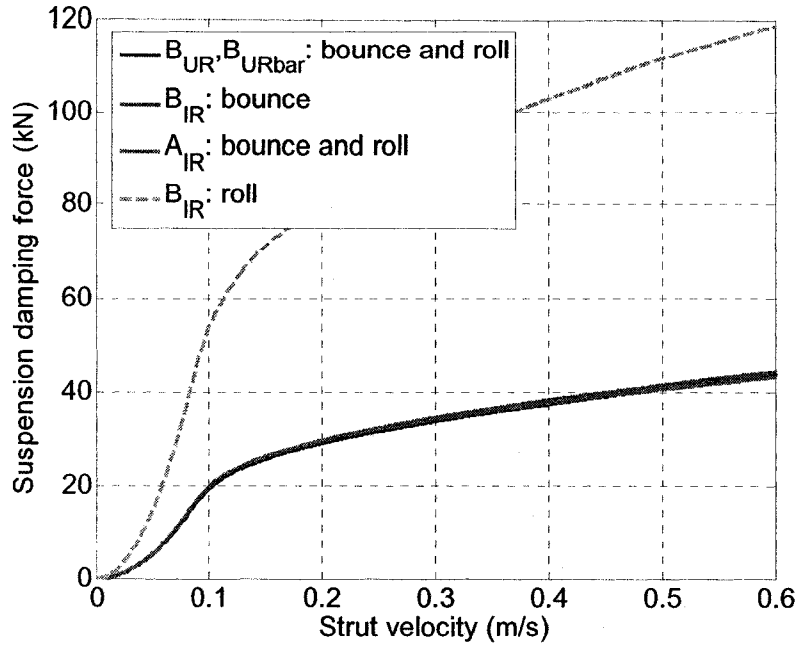

(a)

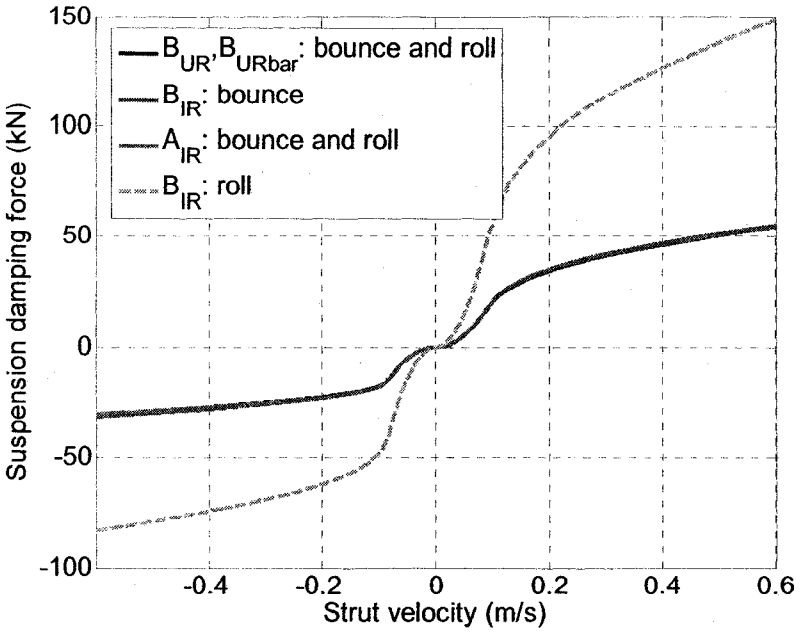

(b)

Figure 3.8: Bounce and roll mode damping properties of the suspension struts: (a) symmetric valves; and (b) asymmetric valves.

3.3.4 Design Flexibility of Roll-Interconnected Suspensions

The hydro-pneumatic suspension offers greater tuning flexibility in vertical and roll mode stiffness and damping properties. This flexibility is attributed to the sensitivity of

the vertical and roll mode properties to variations in design parameters of the struts and the interconnecting pipes, and the fluid properties. The influences of variations in the design parameters on the resulting bounce and roll properties are thus investigated, while the load carrying capacity is held fixed in order to demonstrate the superior design flexibility of the interconnected hydro-pneumatic suspension. The results attained may be further applied for identification of more desirable interconnected suspension design parameters.

Figures 3.9~3.12 illustrate the influences of variations in static charge pressure (P_0) and annular piston area (A_3) of the strut on the suspension stiffness properties of B_{IR} and A_{IR} configurations. The static charge pressure is varied about the nominal value, while the main and floating piston areas, A_1 and A_2, are also varied to ensure the same load carrying capacity, and identical annular piston area (A_3). In a similar manner, the variations in the annular area A_3 are realized by varying the main piston area A_1, while the floating piston area A_2 and the static charge pressure remain the same to yield identical load carrying capacity.

An increase in the gas charge pressure could yield significantly higher roll stiffness of the pneumatically as well as hydraulically interconnected suspensions, as illustrated in Figure 3.9. The variations in P_0 have negligible effects on the vertical suspension rates of both the fluidic interconnected suspensions, due to consideration of constant load carrying capacity and corresponding changes in area A_2. This is also applicable for the unconnected suspension configurations B_{UR} and B_{URbar}. A higher roll stiffness of the unconnected suspension could also be realized through a relatively stiffer anti-roll bar, which however tend to impose considerable additional weight.

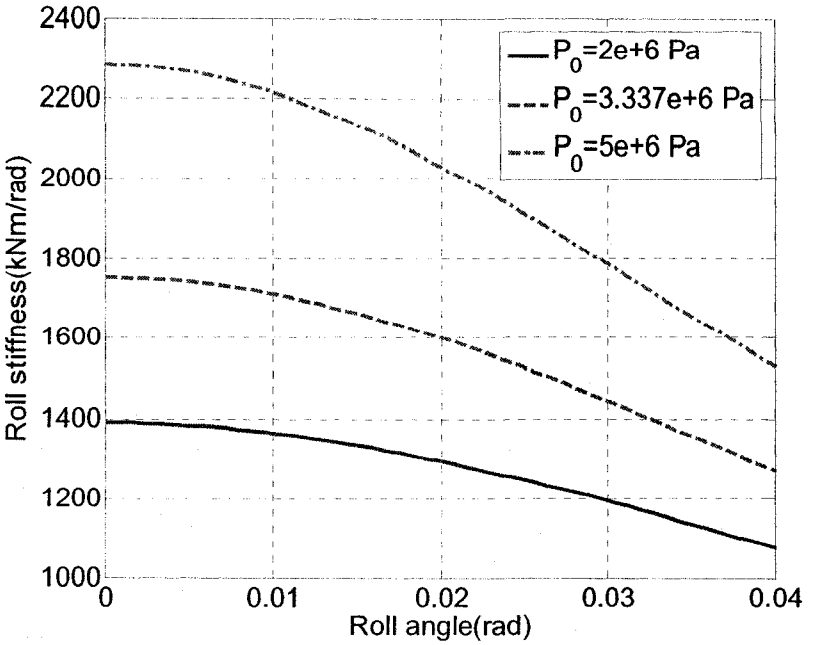

Figure 3.9: Effects of variations in the static gas pressure on the roll stiffness properties of the hydraulically and pneumatically connected suspension configurations (B_{IR} and A_{IR}).

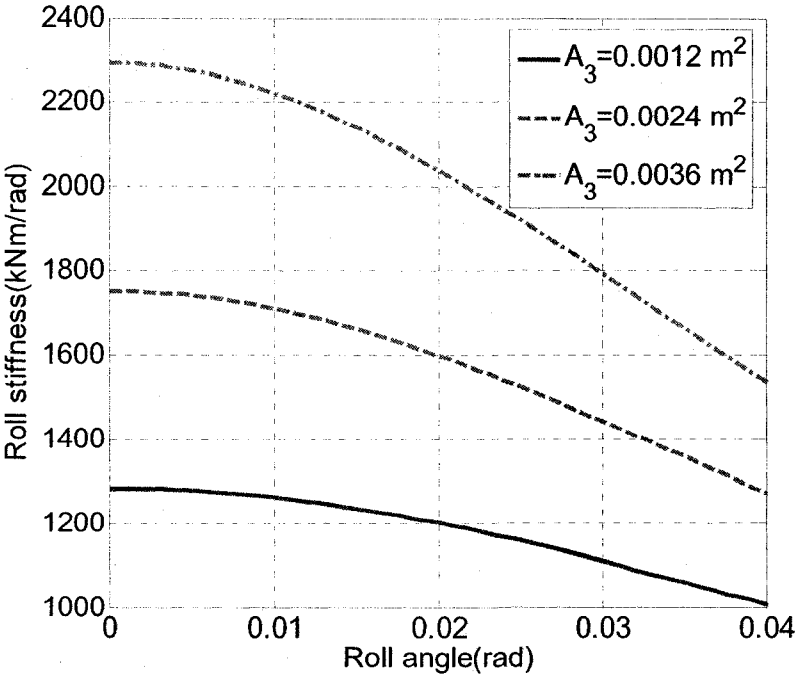

Figure 3.10: Effects of variations in the annular piston area A_3 on the roll stiffness of the hydraulically interconnected suspension configurations B_{IR}.

Figures 3.10 and 3.11 present the influence of variations in the main piston area, realized by varying A_3 alone, on the roll stiffness properties of the suspension configurations B_{IR} and A_{IR}, respectively. It should be noted that these results are attained

for constant effective area A_2 and static charge pressure to ensure identical load carrying capacity. The results show that an increase in A_3 yields stronger coupling effects of the right and left struts and thus considerably higher roll stiffness of both the configurations. The variations in A_3, however, do not affect the vertical spring rate of the suspension B_{IR}, while the effect is relatively small for the A_{IR} configuration, as evident in Figure 3.12. An increase in A_3 exhibits somewhat greater softening effect of the suspension rate of the A_{IR} configuration, especially in compression. The results suggest that the roll stiffnesses of the hydraulically and pneumatically suspensions can be greatly enhanced by increasing the annular piston area or the gas charge pressure.

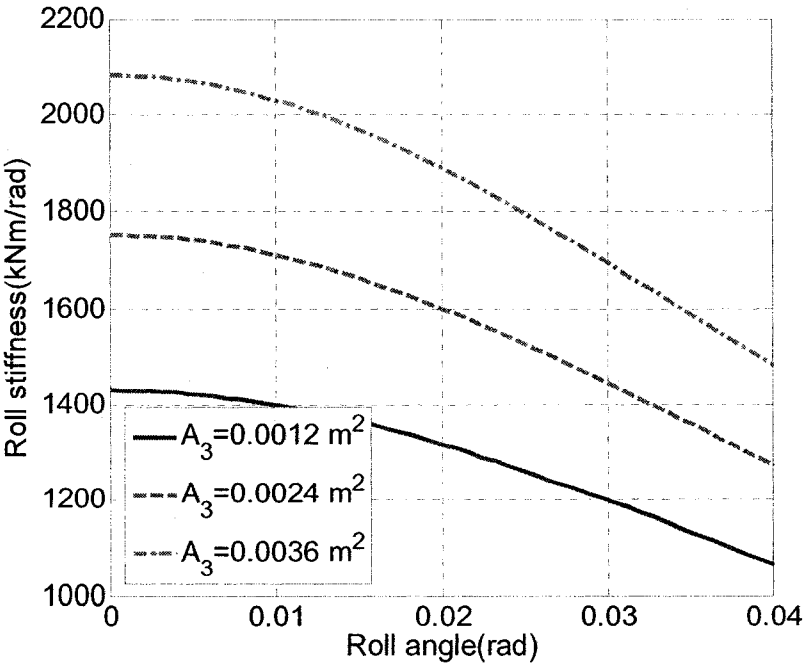

Figure 3.11: Effects of variations in the annular piston area A_3 on the roll stiffness of the pneumatically interconnected suspension configurations A_{IR}.

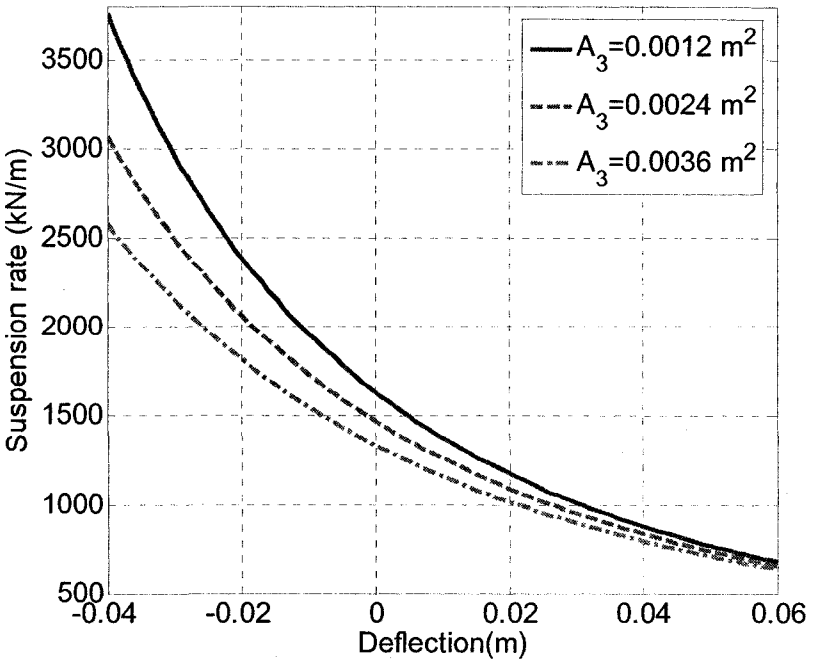

Figure 3.12: Effects of variations in the annular piston area A_3 on the suspension rate of the hydraulically interconnected suspension configurations A_{IR}.

Parameters of interconnecting pipes

Due to the laminar flow characteristics across the interconnecting pipes employed in the hydraulically interconnected suspension B_{IR}, the damping force attributed to flows through the pipes is directly proportional to the length of pipes and inversely proportional to the fourth power of the diameter of pipes [28]. The influence of variations in length of pipes would thus be relatively negligible, compared to those in the pipe diameter. For the hydraulic interconnections, an increase in the pipe diameter affects the bounce and roll mode damping forces only slightly, since the parameters are designed to ensure the total damping forces dominated by the flows through the damping orifices in the main piston. Such design could maximize the benefit of damping valves in realizing variable damping. A reduction in the pipe diameter, however, could result in an increase in the linear bounce and roll mode damping properties of the interconnected suspension, when the damping resistance offered by the interconnection flows predominates over that caused

by the orifice flows. The damping forces developed by the flows through the interconnecting pipes in the A_{IR} suspension are negligible due to significantly smaller dynamic viscosity of the gas.

Fluid properties

The use of higher density hydraulic fluid can improve damping forces developed by the damping orifices, while the use of hydraulic fluid with higher dynamic viscosity can improve the damping forces developed by the interconnecting pipes. Since the dynamic viscosity of hydraulic fluid is relatively more sensitive to variations in temperature, the damping force due to damping orifices is considered to be relatively more robust under a wide range of temperature variations, although thermal expansion of the fluid and changes in the gas pressure could yield considerable variations in damping force [154].

3.4 Roll Dynamic Responses of the Vehicle Model with Roll-Connected Suspensions

The vertical ride and roll performance characteristics of the vehicle model with unconnected and roll-interconnected suspension systems are evaluated through solutions of the equations of motion for the vehicle model (Section 2.3.1), together with mathematical formulations of the dynamic forces developed by the suspension struts (Section 2.3.2). The dynamic responses of the vehicle model with five selected suspension configurations (B_{URS}, B_{URSbar}, A_{IRS}, B_{IRS} and B_{IRE}) are investigated and compared under excitations arising from vehicle-road interactions, and centrifugal accelerations due to directional maneuvers and crosswinds. The analyses are performed for both the symmetric and asymmetric damping valves. The subscripts 'S' and 'E' refer to symmetric and asymmetric damping valves (Figure 3.8), respectively. The notations

B_{URS} and B_{URSbar} thus refer to the unconnected suspension without and with anti-roll bars, respectively, coupled with symmetric damping valves in compression and rebound (Figure 3.8(a)). The configurations B_{IRS} and A_{IRS}, in a similar manner, refer to roll-connected suspensions with symmetric damping properties, while the configuration B_{IRE} represents the hydraulically interconnected suspension with damping valves asymmetric in compression and rebound (Figure 3.8(b)). The configuration B_{IRE} is realized by increasing annular piston area A_3 by 50%, for which A_3=0.0036 m^2. The roll stiffness of the suspension B_{IRE} is shown in Figure 3.10.

3.4.1 Performance Measures

The relative ride and roll dynamic performance characteristics of different suspension configurations, coupled with the vehicle model, are evaluated in terms of following measures under the selected excitations:

- Human perception of ride comfort related to vertical vibration is known to be associated with root mean square (rms) vertical acceleration responses of the sprung mass under excitations arising from random road undulations [3, 6, 15, 45]. The peak acceleration response can also be associated with the human annoyance and potential injury risks to the spine and supporting structure [45]. The rms and peak vertical acceleration responses of the vehicle model subject to the three different roads are thus considered as effective measures for relative vertical ride evaluations of the suspension configurations. Although the assessment of human perception of ride vibration requires the use of acceleration levels at the human seat interface and the frequency-weights defined in ISO-2631-1 [45], the relative vertical ride perceptions of different suspension configurations can be effectively evaluated from the rms and peak values of the unweighted bounce acceleration response of the sprung mass.

- Peak sprung mass roll angle and lateral load transfer ratio (LTR) under centrifugal accelerations induced by directional maneuvers and/or crosswinds, have been widely used to evaluate the roll dynamics and stability performances of heavy vehicles [21, 40, 42, 151]. The LTR is defined as the ratio of the absolute value of the difference between left (F_{zl}) and right (F_{zr}) tire normal loads to the sum of the left and right tire normal loads, such that [40, 42]:

$$LTR = \frac{|F_{zl} - F_{zr}|}{F_{zl} + F_{zr}} \tag{3.2}$$

- The relative responses to transient road inputs are evaluated in terms of vertical shock acceleration ratio (SAR) and roll displacement ratio (RSR). The SAR, defined as the ratio of peak sprung mass vertical acceleration to peak acceleration of the transient road input, describes the shock isolation performance of the suspension system, describes the shock isolation performance of the suspension, while the RSR, the ratio of peak sprung mass roll angle to the equivalent peak roll input of transient road input applied at only one wheel, describes the roll motion isolation property.

3.4.2 Dynamic Responses

The vertical and roll dynamic responses of the vehicle model with the defined five suspensions are performed and compared under excitations arising from the vehicle-road interactions and centrifugal accelerations.

Responses under random road inputs

The equations of motion of the vehicle model together with formulations of different suspension configurations are solved under excitations arising from the three random roads (Figures 3.1 and 3.2) at two different constant vehicle speeds of 70 and 100 km/h. The resulting time-histories of the responses of the vehicle involving different suspension configurations are analyzed to evaluate the vertical ride quality, in terms of rms and peak bounce accelerations of the sprung mass, assuming incompressible hydraulic fluid, as shown in Figure 3.13. The results show that all the suspension configurations yield nearly identical rms sprung mass acceleration response, irrespective of forward speed and road roughness, suggesting only very little influence of interconnections and anti-roll bar on the vertical ride performance of the vehicle. An increase in the road roughness or the vehicle speed causes higher rms and peak magnitudes of the sprung mass vertical

accelerations. The B_{IRE} configuration with asymmetric damping yields slightly higher peak sprung mass vertical accelerations on the *medium-rough* and *rough* roads, when compared to those of the suspensions with symmetric damping. This could in part be attributed to relatively higher damping of the suspension B_{IRE} in rebound.

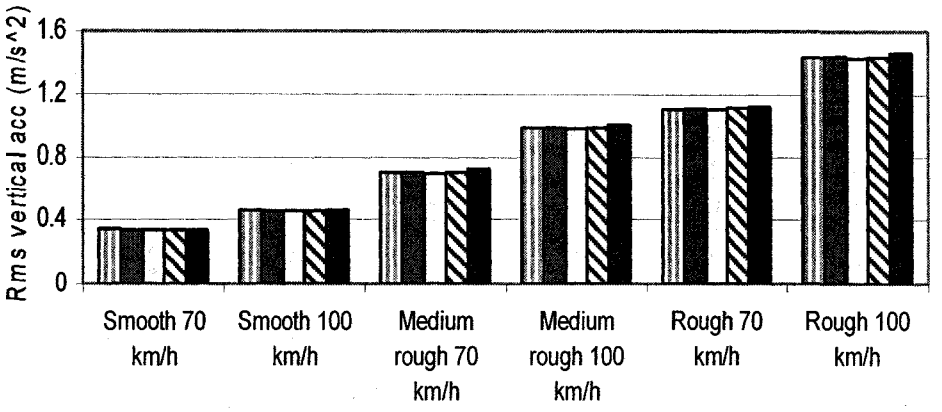

(a)

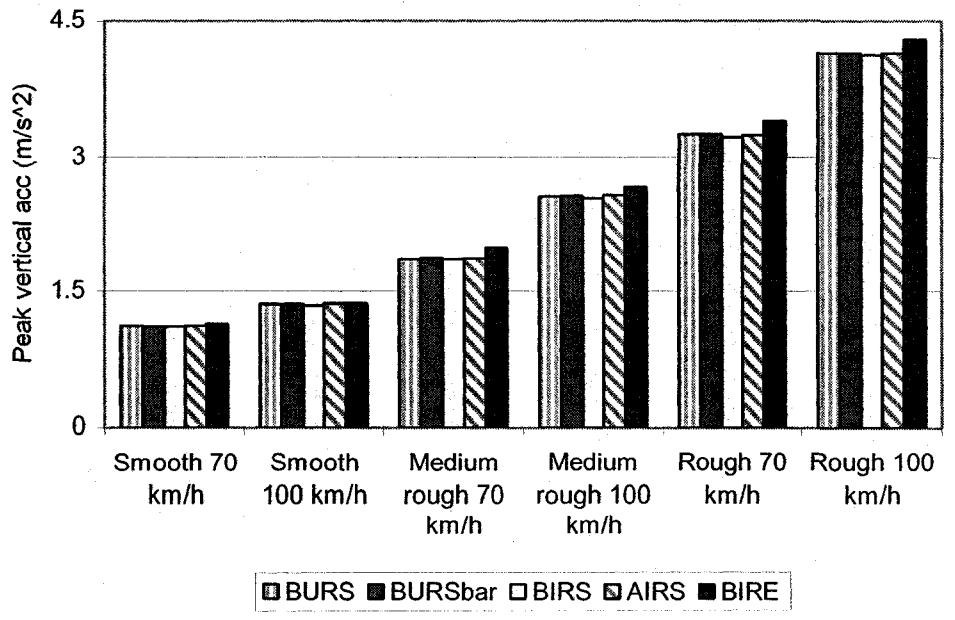

(b)

Figure 3.13: Comparisons of vertical acceleration responses of the sprung mass due to different suspension configurations: (a) rms acceleration; and (b) peak acceleration.

Responses under centrifugal acceleration inputs

Figure 3.14 presents comparisons of the sprung mass roll angle and LTR responses of the vehicle with the selected suspension configurations, when subjected to the 3 m/s^2 rounded step lateral acceleration input. The results show that the unconnected suspension B_{URS} without an anti-roll bar yields significantly larger sprung mass roll angle compared with the interconnected suspension configurations. The pneumatic interconnection A_{IRS} and the configuration with anti-roll bar B_{URSbar} yield similar roll angle responses, which are larger than that of the hydraulically interconnected suspension B_{IRS}. The hydraulically interconnected suspension B_{IRS} yields lower peak roll angle, which tends to decay relatively more quickly due to its enhanced roll mode damping properties. The suspension B_{IRE} yields the lowest peak sprung mass roll angle, which also decays most rapidly, attributed to its considerably improved roll stiffness and damping properties. The LTR responses exhibit trends similar to the sprung mass roll angle responses for the five suspension configurations considered.

Figure 3.15 compares the variations in the sprung mass roll angle and LTR responses of the vehicle with different suspension configurations, under a 3 m/s^2 sinusoidal input (lane change maneuver) at a forward speed of 100 km/h. The results suggest that the hydraulically connected suspension with its higher roll mode damping yields lower peak roll angle and LTR. The B_{IRE} configuration with its enhanced roll stiffness and damping properties, yields lowest peak sprung mass roll angle and LTR. The results indicate that the hydraulically roll-interconnected suspensions could considerably improve the anti-roll property of heavy vehicles, while maintaining the soft vertical ride.

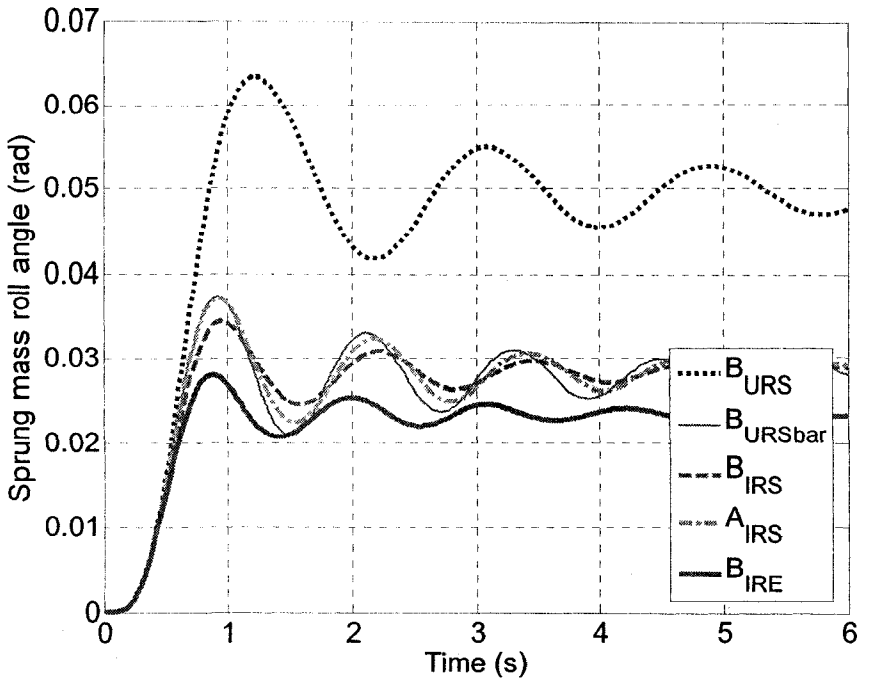

(a)

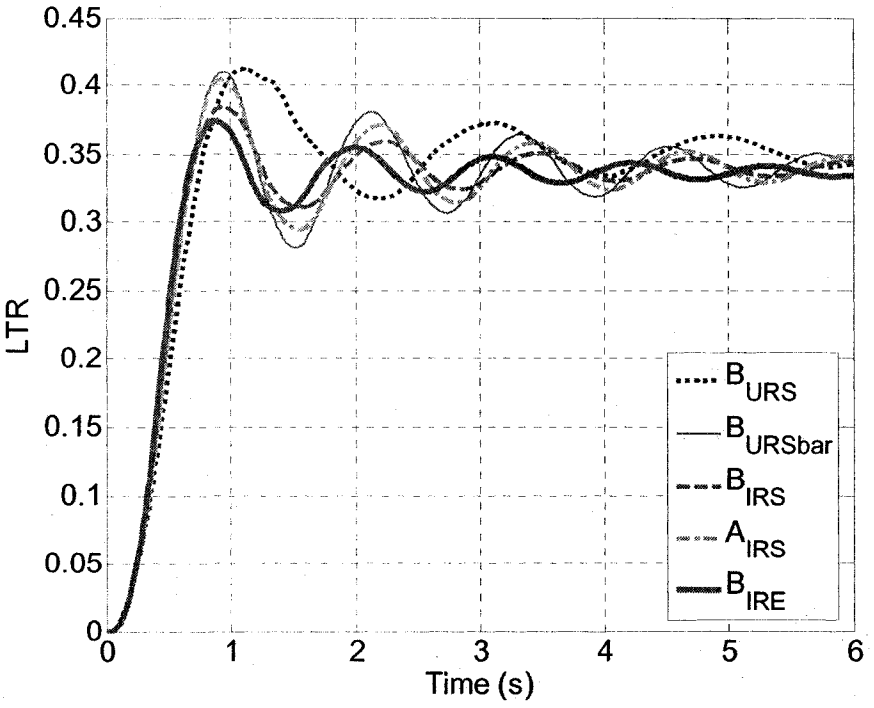

(b)

Figure 3.14: Responses under the rounded-step lateral acceleration: (a) sprung mass roll angle; and (b) LTR.

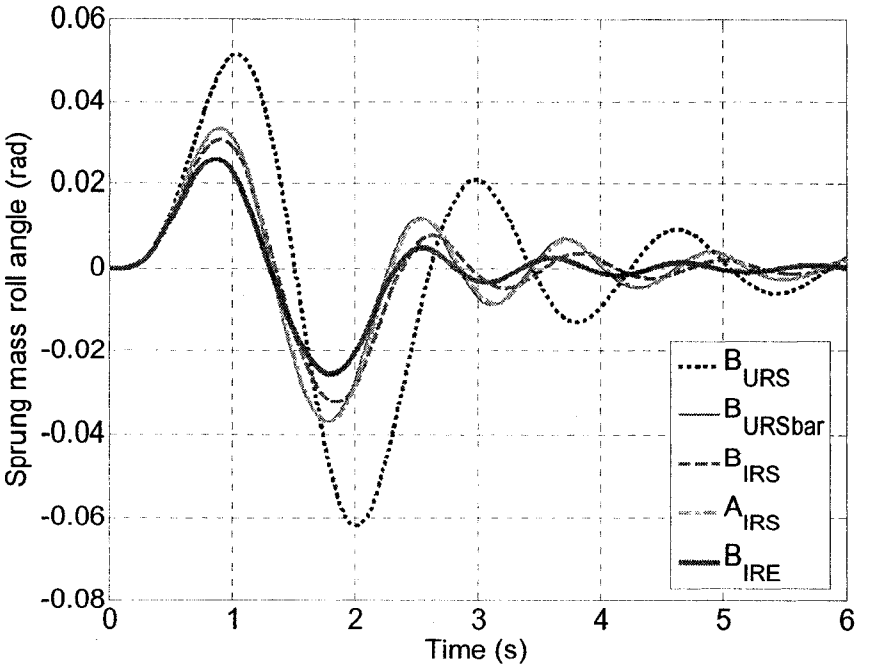

(a)

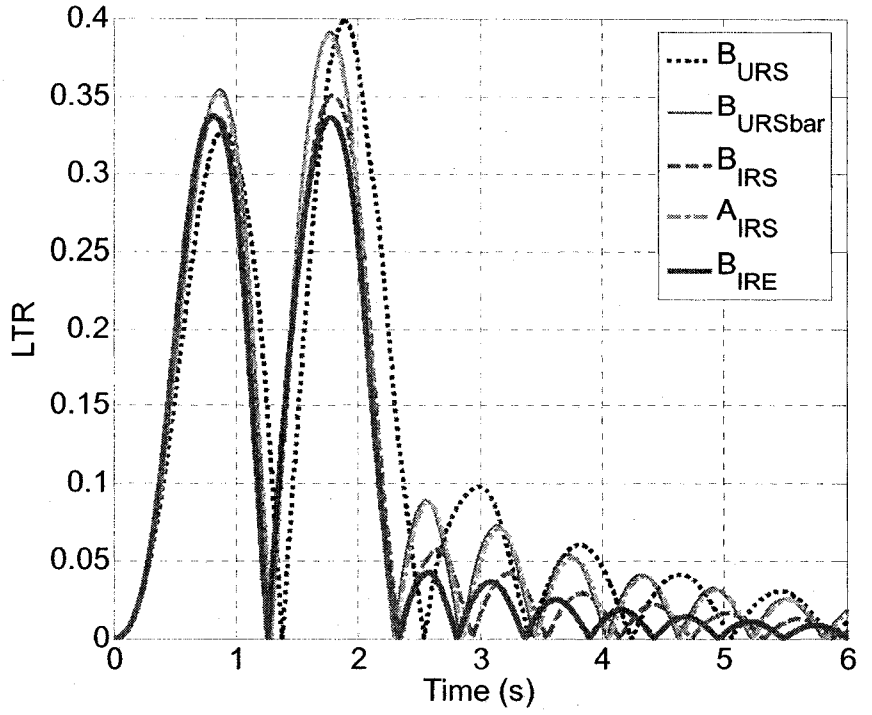

(b)

Figure 3.15: Responses under the centrifugal acceleration excitation arising from a lane change maneuver: (a) sprung mass roll angle; and (b) LTR.

Responses under transient road inputs

The relative roll and vertical responses of different suspensions are further evaluated under a discrete road input characterized by a versed-sine displacement pulse. Considering the wide possible variations in vehicle speed and length of the road bump, the analyses are performed by considering the time duration of the bump excitation. The road bump is initially applied to the left-wheel alone to study the roll responses and is modeled by a 0.04 s duration versed-sine displacement pulse with amplitude of 0.1 m. The vertical response is evaluated by applying a road bump to both wheels, which is modeled by a 0.08 s duration versed-sine displacement pulse with amplitude of 0.05 m. The shock isolation and roll motion performance characteristics of the vehicle with different suspension configurations are evaluated in terms of the two performance measures: SAR and RSR.

Table 3.3 summarizes the SAR and RSR responses of the vehicle model employing the five different suspension configurations under the defined road bump excitations. While the unconnected suspension configurations (B_{URS}, B_{URSbar}) and pneumatic interconnection (A_{IRS}) exhibit nearly identical SAR responses, the hydraulic configurations B_{IRS} and B_{IRE} with symmetric and asymmetric damping valves yield relatively lower values. The hydraulic interconnection B_{IRE} exhibits nearly 16% lower SAR response, when compared to those of the B_{URS}, B_{URSbar} and A_{IRS} configurations. The hydraulic interconnection B_{IRE} also yields the lowest RSR compared to the other four configurations. Moreover, the sprung mass roll response decays most rapidly with this suspension configuration. For the in-phase road bump inputs, the suspension

configurations B_{URS}, B_{URSbar}, A_{IRS} and B_{IRS} exhibit almost identical SAR values, while the suspension B_{IRE} yields slightly lower SAR, partly due to its asymmetric damping property, as evident in Table 3.3.

Table 3.3: Shock and roll motion isolation characteristics of different suspension configurations under transient road inputs.

Performance measures	**Bump excitations**	B_{URS}	B_{URSbar}	B_{IRS}	A_{IRS}	B_{IRE}
SAR	Left wheel	0.0090	0.0090	0.0084	0.0089	0.0075
	In-phase	0.0482	0.0482	0.0479	0.0481	0.0466
RSR	Left wheel	0.208	0.194	0.206	0.2	0.192

Responses under combined centrifugal acceleration and random road inputs

The roll dynamic responses of the vehicle model employing different suspension configurations are further investigated under the combined 3 m/s^2 centrifugal acceleration arising from a lane change maneuver, and three different random road inputs. The simulations are performed under two different constant forwards speeds of 70 and 100 km/h, while the relative roll response is evaluated only in terms of the peak sprung mass roll angle. Figure 3.16 illustrates comparisons of peak sprung mass roll angle responses of the vehicle model with the five different suspension configurations. The sprung mass roll is mostly caused by the centrifugal acceleration excitation, and the results suggest that the hydraulic interconnections B_{IRS} and B_{IRE} invariably yield lower peak sprung mass roll angle compared with the pneumatic interconnection A_{IRS} and the unconnected suspension with anti-roll bar B_{URSbar}. The B_{URSbar} and A_{IRS} configurations yield comparable peak sprung mass roll angles. While the configuration B_{IRE} yields the lowest peak sprung mass roll angle, irrespective of the forward speed and road roughness considered, the unconnected suspension B_{URS} yields the largest response. The effects of

road roughness on the sprung mass roll angle are not clear, which is dependent upon the local road profiles during a directional maneuver.

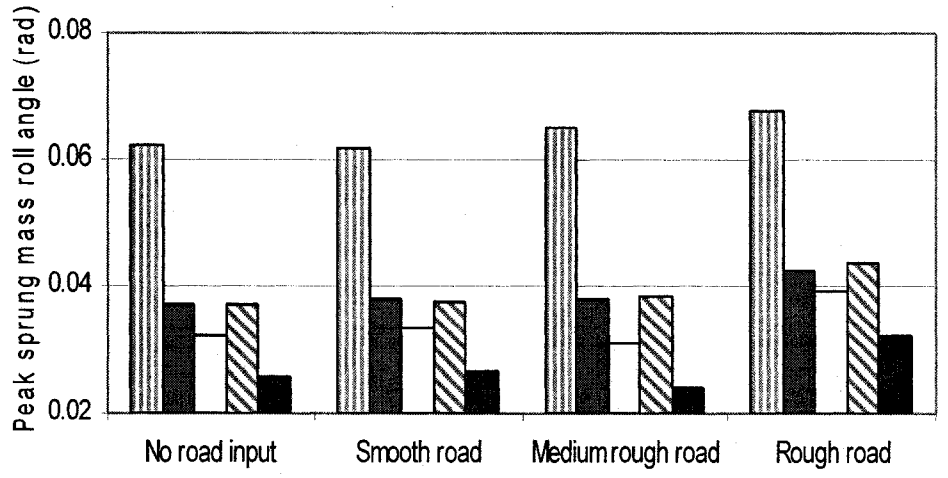

(a)

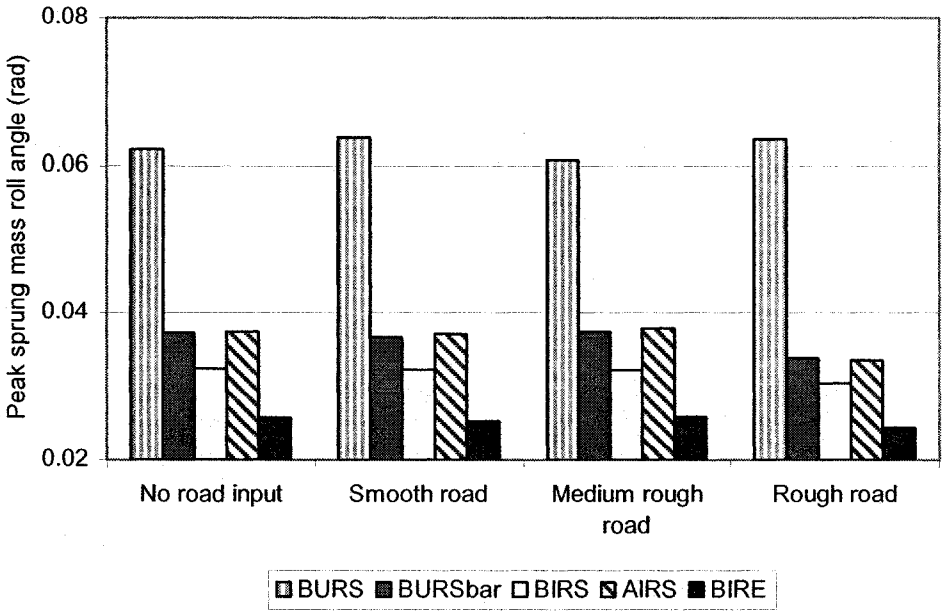

(b)

Figure 3.16: Peak sprung mass roll angle responses of the vehicle model with different suspensions under combined lane change and random road inputs: (a) 70 km/h; and (b) 100 km/h.

3.5 Summary

The roll plane suspension properties and dynamic responses of a vehicle are analyzed and compared for five different suspension configurations. These include four configurations with symmetric damping: unconnected with and without an anti-roll bar, hydraulically interconnected, and pneumatically interconnected. An additional hydraulically interconnected configuration with asymmetric damping and increased roll stiffness is also considered. Comparisons of roll plane properties of different suspension configurations demonstrate that both hydraulically and pneumatically interconnected suspensions yield enhanced roll stiffness while maintaining soft vertical ride. The hydraulic interconnection further offers improved roll mode damping attributed to the hydraulic coupling effect. The results attained from the parametric studies show the superior design flexibility of the fluidic interconnections. The roll stiffness of the connected struts could be conveniently improved by varying the design parameters of the struts, which is unlike the use of anti-roll bar that could add weight and pose a challenge in view of the design space.

The relative vertical and roll responses of the vehicle model with different suspension configurations are evaluated under excitations arising from tire interactions with random road profiles and discrete bumps, and centrifugal accelerations corresponding to steady turning and lane change maneuvers, and crosswinds. From the results, it is concluded that fluidic interconnections yield improved roll response, with negligible influence on the vertical ride performance, irrespective of driving speed and road roughness. For the centrifugal acceleration excitations, the roll responses of the vehicle evaluated in terms of the sprung mass roll angle and LTR are nearly identical

with pneumatic interconnection and unconnected suspension with anti-roll bar. The hydraulic interconnections yield much lower roll angle responses, which tend to decay more rapidly and can be attributed to its enhanced roll mode damping and stiffness properties. The asymmetric damping coupled with hydraulic interconnections also yields improved shock and roll motion isolation performance under the deterministic road inputs considered.

CHAPTER 4

PERFORMANCE ANALYSIS OF PITCH-INTERCONNECTED SUSPENSIONS

4.1 Introduction

The results presented in the previous chapters demonstrated considerable performance benefits of the fluidic interconnections between the roll-plane suspension struts in terms of enhanced roll-mode stiffness and damping, and thus the roll dynamics and stability, with only negligible influence on the vertical ride performance. These further indicate the superior potential of the passive interconnections among different suspension units in achieving independent or partially-independent tuning of various suspension properties, and thus the enhanced flexibility in realizing an improved performance compromise. In the pitch plane, the bounce and pitch vibration modes of road vehicles are strongly coupled [3, 6]. Even greater coupling between the two modes could be observed under certain load conditions of heavy vehicles. The wheelbase filtering effect coupled with a wide range of vehicle speeds and loads may pose additional difficulties in realizing a desirable compromise in various performance requirements associated with pitch-plane vehicle dynamics, such as vertical, ride, braking, longitudinal load transfer and vehicle dive. The pitch plane requirements of the suspension system design may therefore be more complex compared to those associated with roll plane dynamics of the vehicle.

This chapter explores the performance characteristics of different interconnected suspensions, involving pneumatic, hydraulic and hybrid fluidic couplings in the pitch plane of the heavy vehicle. The pitch plane braking model of a heavy vehicle (developed

in Section 2.5) is integrated with various pitch-connected and unconnected suspension configurations formulated in Chapter 2, to investigate the suspension properties, and vehicle vertical and pitch dynamic responses under excitations arising from random road roughness and braking maneuvers. The fundamental suspension properties in the pitch plane are evaluated in terms of suspension rate, pitch stiffness, and bounce and pitch mode damping, which have been defined and formulated in Section 2.7. Parametric studies are also performed to demonstrate the design flexibility of the pitch interconnected suspensions. The dynamic responses of the pitch plane vehicle model with different suspension configurations are further explored.

4.2 Simulation Parameters and Static Properties

Table 4.1 summarizes the simulation parameters for the pitch plane analysis of the vehicle model (Figure 2.4) together with different suspension configurations, while the vehicle parameters are adopted from the measured and estimated data of a heavy vehicle [152]. The design parameters of the struts employed in the ten different unconnected and pitch-interconnected suspension configurations (shown in Figures 2.8~2.10) were selected to achieve identical load carrying capacity corresponding to a particular load distribution condition $l_f/(l_f+l_r)=0.653$.

Further attempts were also made to attain identical spring rates due to both struts of each configuration. This condition, however, could not be realized for the configurations H_{IP4} and H_{IP134} (Figure 2.10), which is attributed to the coupling effects of the gas chambers of the front and rear suspension struts. Configuration H_{IP4} involves coupling between gas chambers 4 of struts A and B. H_{IP134} involves interconnections of gas

chambers 4 of both the struts, while the chamber 3 of strut *B* is hydraulically connected to chamber 1 of strut *A*. The selected parameters of the rear struts of all the ten configurations revealed bounce natural frequency of the rear suspension in the order of 1.5 Hz at the design ride height. The static suspension rates of the front struts of all the configurations, with the exception of the hybrid configurations H_{IP4} and H_{IP134}, also resulted in the same bounce mode natural frequencies (1.5 Hz) of the front suspension at the design ride height. The configuration H_{IP4} resulted in a lower front suspension rate, while the H_{IP134} configuration provided a higher front suspension rate, as shown in Table 4.2.

Table 4.1: Simulation parameters for the pitch plane vehicle model and the struts.

Parameter	Value	Parameter	Value
Vehicle model			
m_s	15753 kg	k_t	921607 N/m
m_{uf}	675 kg	c_t	8000 Ns/m
m_{uf}	875 kg	l_f	4.05 m
I_{yys}	175034 kgm^2	l_r	2.15 m
I_{wf}	30 kgm^2	r_f	0.5 m
I_{wr}	60 kgm^2	r_r	0.5 m
Suspension			
L	6.5 m	P_0	3000000 Pa
A_{2f}	0.00924 m^2	A_{2r}	0.01741 m^2
A_{3f}	0.00231 m^2	A_{3r}	0.00231 m^2

Table 4.2: Static pitch plane properties at the design ride height.

Parameter	*All**	H_{IP4}	H_{IP134}
Load carrying capacity (kg)	15753	15753	15753
Front suspension rate (kN/m)	485	383	733
Rear suspension rate (kN/m)	913	913	913

*All**: includes configurations A_{UP}, B_{UP}, H_{UP}, A_{IP34}, B_{IP13}, $H_{IP1\text{-}4}$, A_{IP4}, and A_{IP3}.

Table 4.3 summarizes the static pitch stiffness characteristics of different suspension configurations, including those of the unconnected suspension configurations A_{UP}, B_{UP}, and H_{UP}. The table classifies the pitch interconnected suspension configurations by their pitch stiffness being either higher or lower than those of the unconnected suspensions. It can be seen that the three unconnected configurations (A_{UP}, B_{UP}, and H_{UP}) yield identical static pitch stiffness at the design height. The interconnected configurations A_{IP4}, A_{IP3}, H_{IP4} and H_{IP134} involving interconnections of identical gas chambers of different struts, could yield significantly lower static pitch stiffness, compared to the unconnected suspensions. Alternatively, the interconnected suspension configurations A_{IP34} (pneumatic), B_{IP13} (hydraulic) and $H_{IP1\text{-}4}$ (hybrid fluidic) yield higher pitch stiffness, which would be beneficial for pitch attitude control of road vehicles, and thus improving vehicle braking and directional performances. These three interconnected suspension configurations, together with unconnected configuration B_{UP}, are therefore selected for further investigations of suspension properties and vehicle dynamic responses.

Table 4.3: Static pitch stiffness properties of different suspension configurations

		Static pitch stiffness (kNm/rad)
Unconnected	A_{UP}, B_{UP}, H_{UP}	12170
Higher	A_{IP34}, B_{IP13}, $H_{IP1\text{-}4}$	23270
Lower	A_{IP4}	3730
	A_{IP3}	8910
	H_{IP4}	347
	H_{IP134}	1630

4.3 Pitch Plane Suspension Properties

The pitch-plane stiffness and damping properties of the four selected configurations (B_{UP}, A_{IP34}, B_{IP13} and $H_{IP1\text{-}4}$) are evaluated as functions of relative vertical and pitch

deflection responses of the vehicle model. The sizes of damping orifices and valves were also chosen to achieve identical vertical bounce mode damping properties of the front as well as rear suspensions for the four configurations (B_{UP}, A_{IP34}, B_{IP13} and $H_{IP1\text{-}4}$). An additional configuration of the hydraulically pitch-interconnected suspension is also synthesized using asymmetric damping, referred to as B_{IPE13}.

Figures 4.1(a) and 4.1(b) present comparisons of bounce mode stiffness and damping properties, respectively, of the four basic suspension configurations. All the configurations (B_{UP}, A_{IP34}, B_{IP13} and $H_{IP1\text{-}4}$) yield identical front as well as rear suspension rates throughout the suspension deflection range considered, which exhibit softening effect in extension and aggressively hardening characteristic in compression, as evident in Figure 4.1(a). The vertical mode damping properties are evaluated for constant orifice areas, as well as symmetric valves. All the four suspension configurations yield identical damping force-velocity characteristics of the front and rear suspensions, for both the constant orifices and damping valves. The flows through the damping valves are initiated, when the strut velocity either approaches or exceeds 0.08 m/s, and the valves become fully open at 1.5 m/s. For the dynamic responses of the vehicle in this chapter, the configurations B_{UP}, A_{IP34}, B_{IP13} and $H_{IP1\text{-}4}$ employ the symmetric damping valves, the characteristics of which are presented in Figure 4.1(b). The additional hydraulically pitch-interconnected configuration B_{IPE13} also resulted in identical suspension rate, while its bounce mode damping properties are asymmetric in compression and rebound, which will be presented in Figure 4.3.

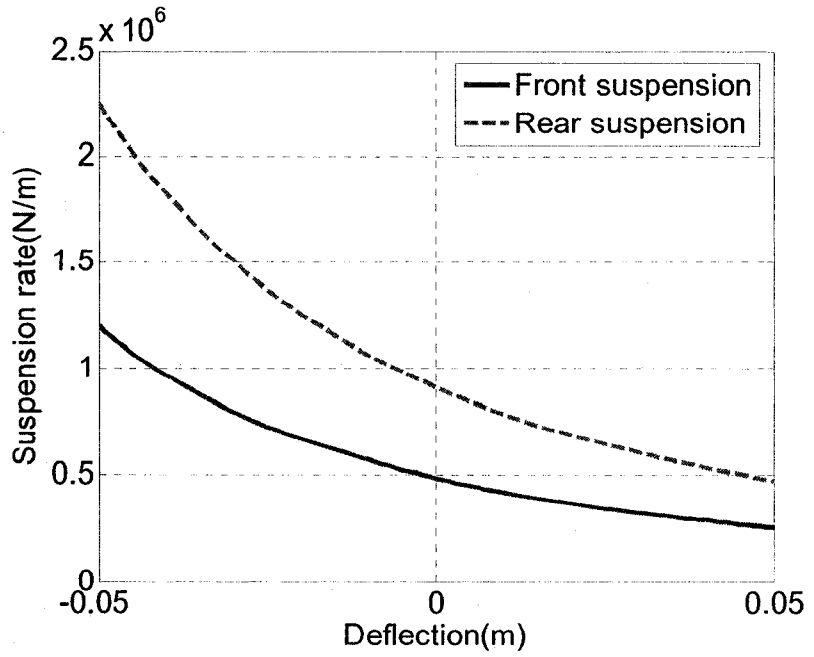

(a)

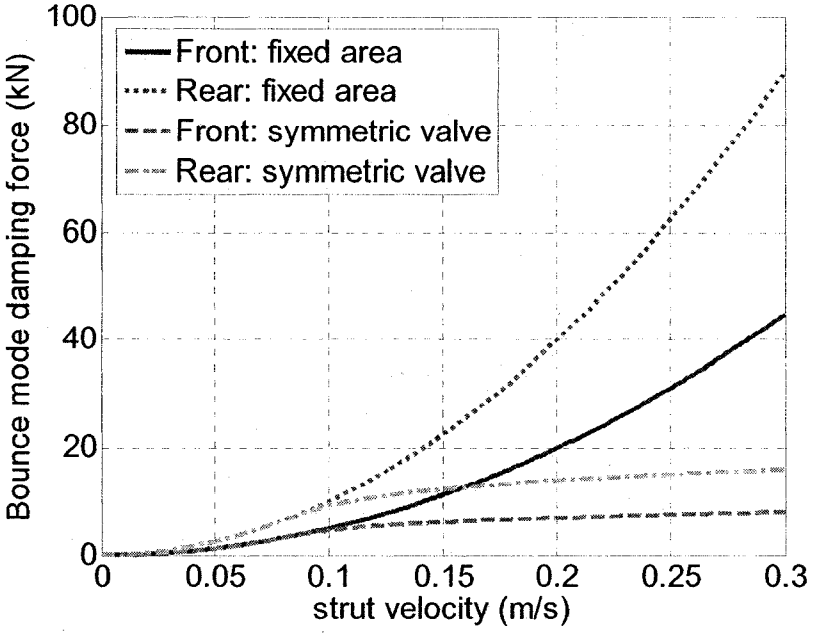

(b)

Figure 4.1: Bounce mode properties of different suspension configurations: (a) suspension rate; and (b) symmetric bounce mode damping.

Figures 4.2(a) and 4.2(b) illustrate the pitch mode stiffness and damping properties, respectively, of the selected suspension configurations. The analysis of damping properties, however, is limited to design involving symmetric damping valves. It should

be noted that the pitch damping moment are derived upon imposing discrete values of out-of-phase velocities across the front and rear struts. The pitch mode damping property can be presented in terms of magnitude of the strut velocity, which can be expressed in terms of its pitch velocity, $\dot{\varphi} = (\dot{x}_f - \dot{x}_r)/(l_f + l_r)$. The results again show identical pitch stiffness of all the interconnected configurations (A_{IP34}, B_{IP13}, $H_{IP1\text{-}4}$ and B_{IPE13}), which is considerably higher than that of the unconnected configuration B_{UP}. The pitch stiffness properties of the unconnected and interconnected configurations are evidently nonlinear with peak values occurring at different pitch deflections, which is attributed to coupling between the bounce and pitch vibration modes. The variation in pitch stiffness is dependent upon the longitudinal load transfers, and it assumes a peak value when the loads on two axles approach identical values.

For the symmetric pitch-mode damping property, the unconnected and pneumatically-interconnected suspensions B_{UP} and A_{IP34} yield identical pitch mode damping, due to the assumed negligible effect of flow through pneumatic interconnections in configuration A_{IP34}. While the hybrid fluidic interconnection $H_{IP1\text{-}4}$ could provide considerably higher pitch mode damping, compared to configurations B_{UP} and A_{IP34}, the hydraulic interconnection configuration B_{IP13} yields significantly larger pitch damping, which is attributed to the fully hydraulic couplings. The results in Figures 4.1 and 4.2 suggest that the proposed pitch-connected suspensions could realize enhanced pitch stiffness and tunable pitch mode damping properties, without affecting the suspension rate characteristics. Moreover, the pitch-interconnections can provide added design flexibility to achieve desired pitch mode damping without influencing the bounce mode damping properly under a predominantly vertical input. These suggest that

interconnected suspensions could offer independent or partially-independent tunings for the suspension pitch and bounce mode properties.

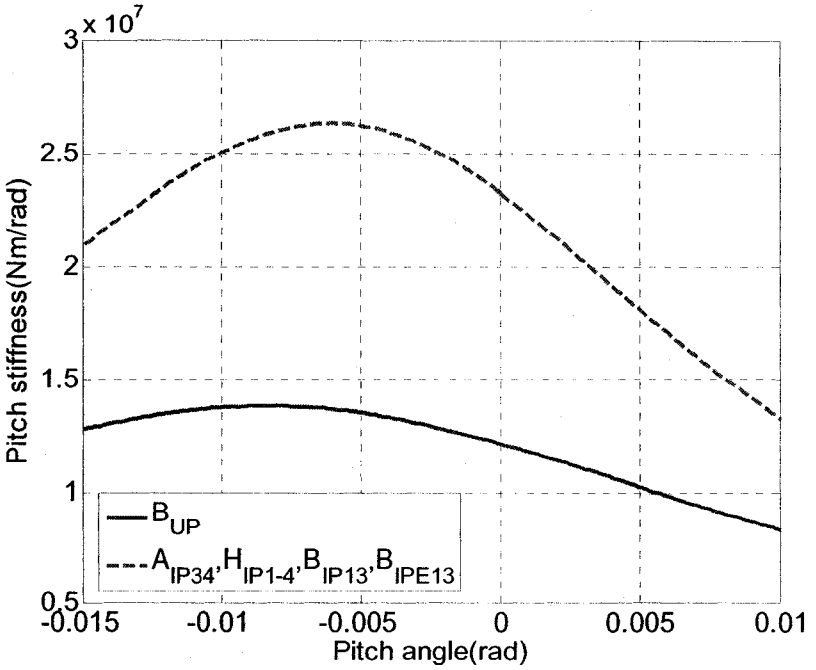

(a)

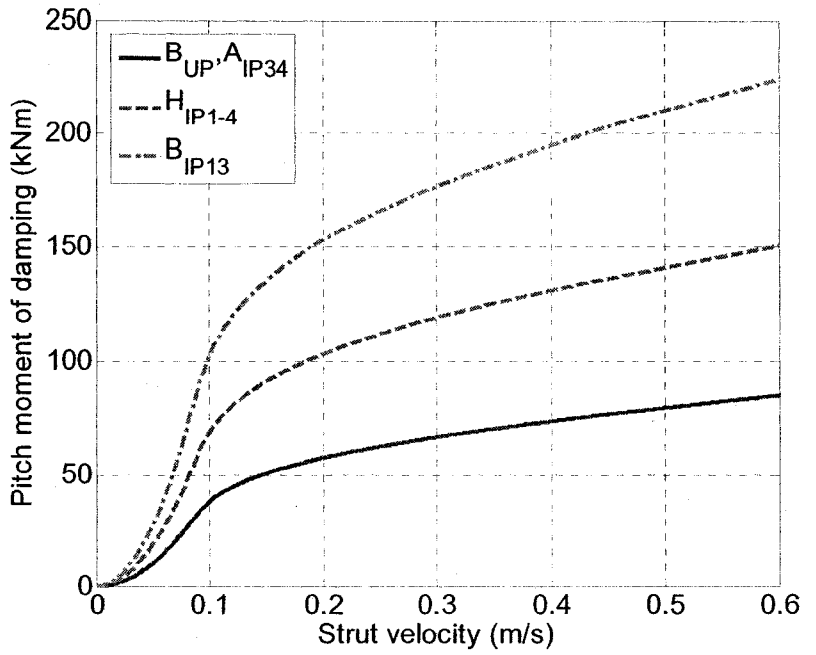

(b)

Figure 4.2: Pitch mode properties of different suspension configurations: (a) pitch stiffness; and (b) symmetric pitch mode damping with damping valves.

Figure 4.3 further compares the asymmetric damping properties of configuration B_{IPE13} with the symmetric damping characteristics of configuration B_{IP13}. The asymmetric damping properties were realized by selecting different areas of orifices in compression a_{12vc} and in extension a_{12ve}, as described in Eq. (2.13b). While the bounce mode damping force-velocity relationships of the configurations B_{IP13} and B_{IPE13} are quite different, both the configurations yield nearly similar pitch mode damping properties. This is attributed to the fact that pitch mode damping moment is formulated by the forces developed by the two struts, which act in opposite rebound/compression directions. This suggests that the asymmetric damping in bounce would yield nearly symmetric pitch mode damping for both connected and unconnected suspensions.

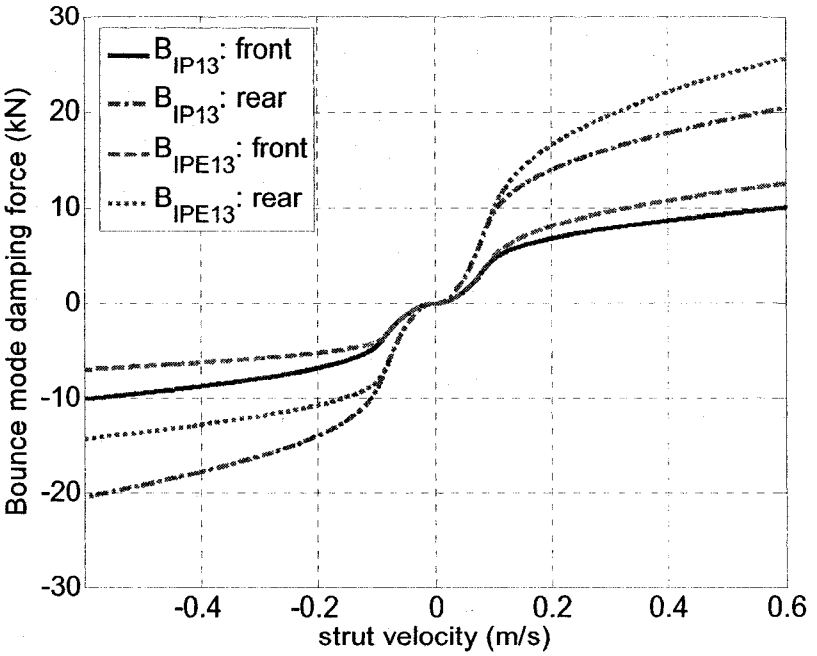

(a)

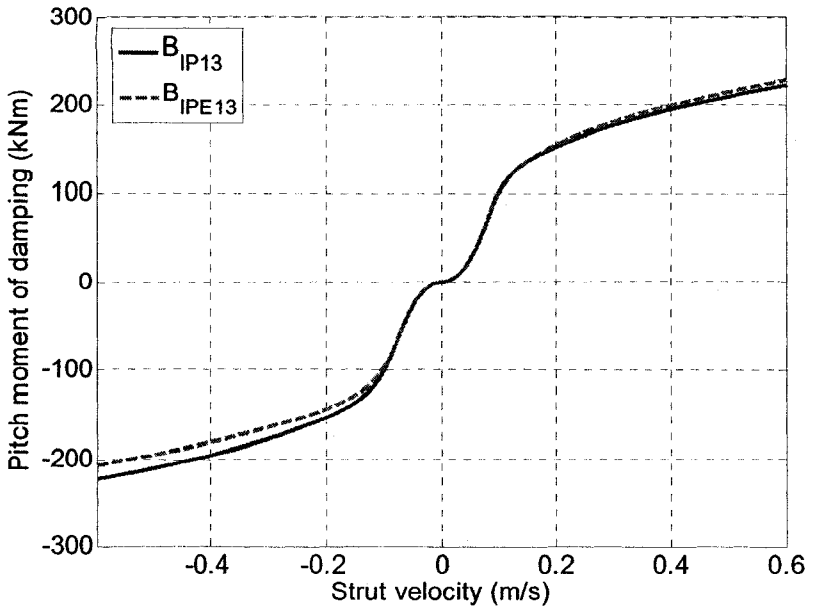

(b)

Figure 4.3: Comparison of symmetric and asymmetric damping properties due to the configurations B_{IP13} and B_{IPE13}: (a) bounce mode damping; and (b) pitch mode damping.

4.4 Design Flexibility of Pitch Interconnected Suspensions and Discussions

The analytical formulations for the interconnected suspensions, presented in Section 2.7, show that the pitch properties are closely related to strut design parameters, especially the static gas pressure (P_0) and the annular piston area (A_3) of chambers 3, which directly affect the couplings. All the pitch interconnected suspensions were configured with identical annular piston area A_3 to achieve identical stiffness characteristics, as observed in Figures 4.1 and 4.2. The design flexibility of the pitch interconnected suspensions is investigated through a parameter variation analysis involving P_0 and A_3.

The effects of variations in the static gas pressure P_0 on the vertical and pitch stiffness properties of the interconnected suspensions are illustrated in Figure 4.4. The results are attained by varying P_0 by $\pm 20\%$ about its nominal value (Table 4.1). As

expected, an increase in P_0 would increase both the front and rear suspension rates, as well as pitch stiffness throughout the deflection ranges considered. The influence of variations in annular piston area A_3 on the stiffness characteristics of the interconnected suspensions is illustrated in Figure 4.5. The results indicate that both the front and rear suspension rates are less sensitive to variations in A_3, compared to variations in the static gas pressure (P_0). While the suspension rates in rebound are mostly insensitive to variations in A_3, only slight variations in compression mode could be observed for both the front and rear suspension rates, as seen in Figures 4.5(a) and 4.5(b). The variations in A_3, however, strongly affect the pitch stiffness of the interconnected suspensions. A 20% increase in A_3 could yield up to 8% reduction in the front suspension rate in compression, while the corresponding pitch rate is increased by nearly 8%. Moreover, the pitch rate tends to increase in the entire pitch deflection range considered. This suggests a stronger coupling between the front and rear suspensions. The results presented in Figures 4.1 to 4.5 demonstrate the considerable design flexibility potentials of pitch-interconnected suspensions in realizing desired pitch stiffness and damping properties, without affecting the bounce mode properties.

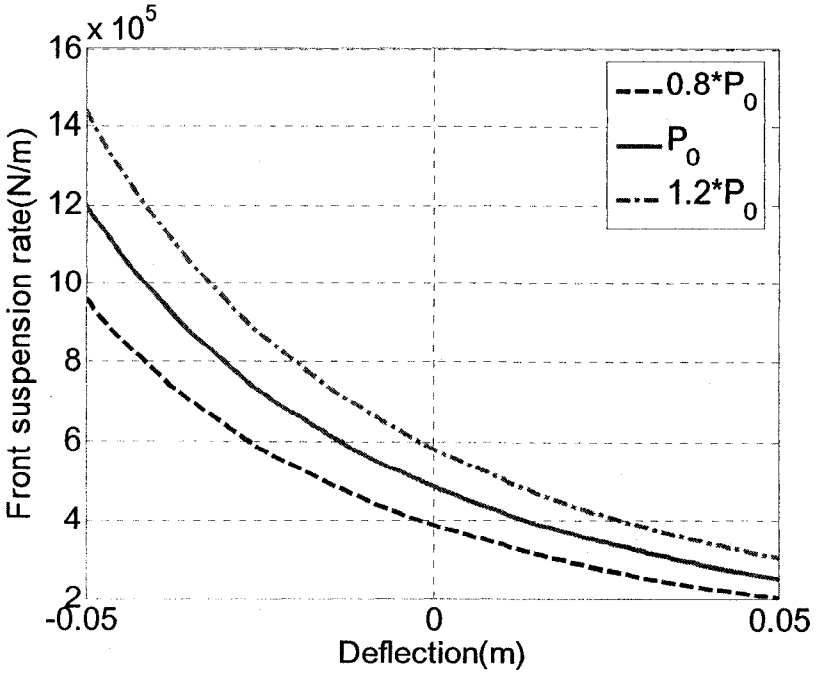
x 10^5
16
14
12
10
8
6
4
2
Front suspension rate(N/m)
-0.05
0
0.05
Deflection(m)
---0.8*P0
—P0
-·- 1.2*P0

(a)

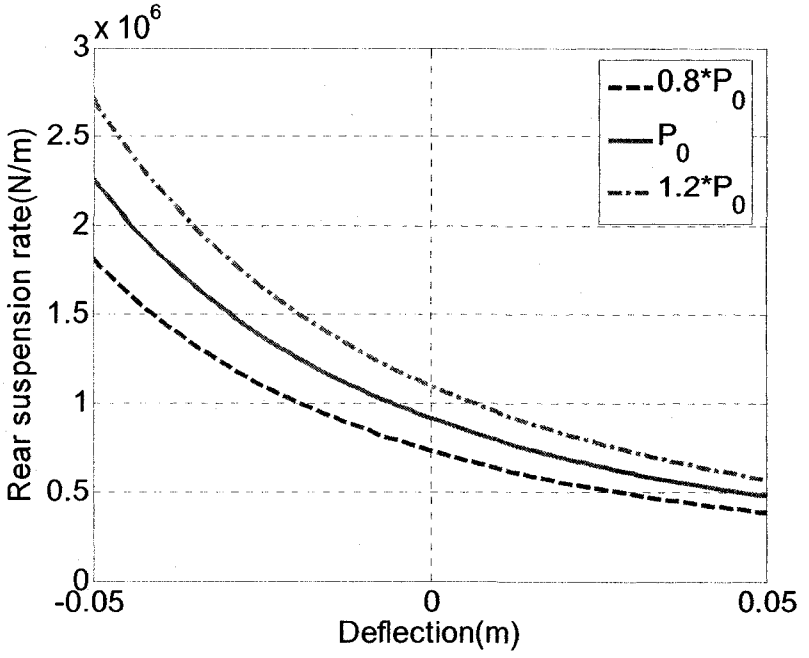
x 10^6
3
2.5
2
1.5
1
0.5
0
Rear suspension rate(N/m)
-0.05
0
0.05
Deflection(m)
---0.8*P0
—P0
-·- 1.2*P0

(b)

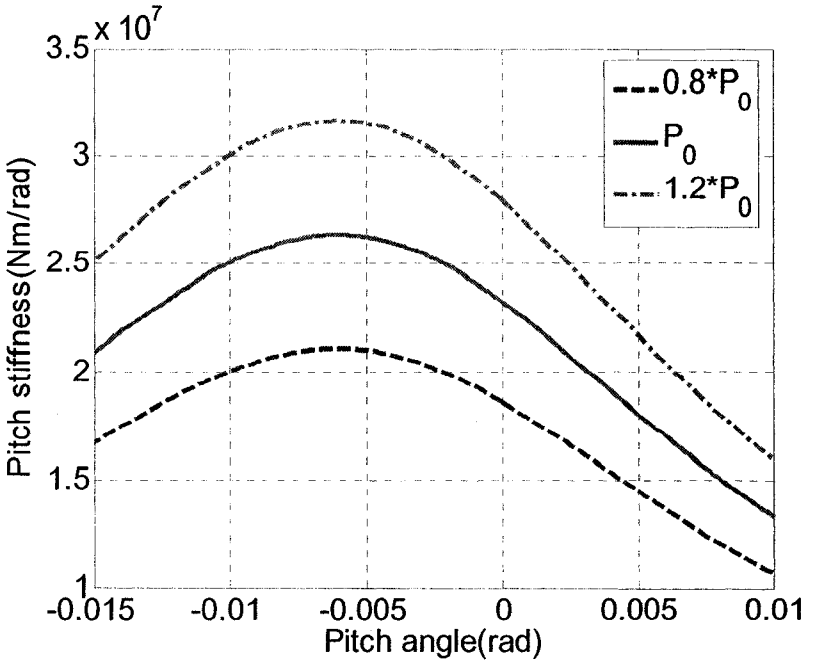

(c)

Figure 4.4: Influence of variations in static gas pressure P_0 on: (a) front suspension rate; (b) rear suspension rate; and (c) pitch stiffness.

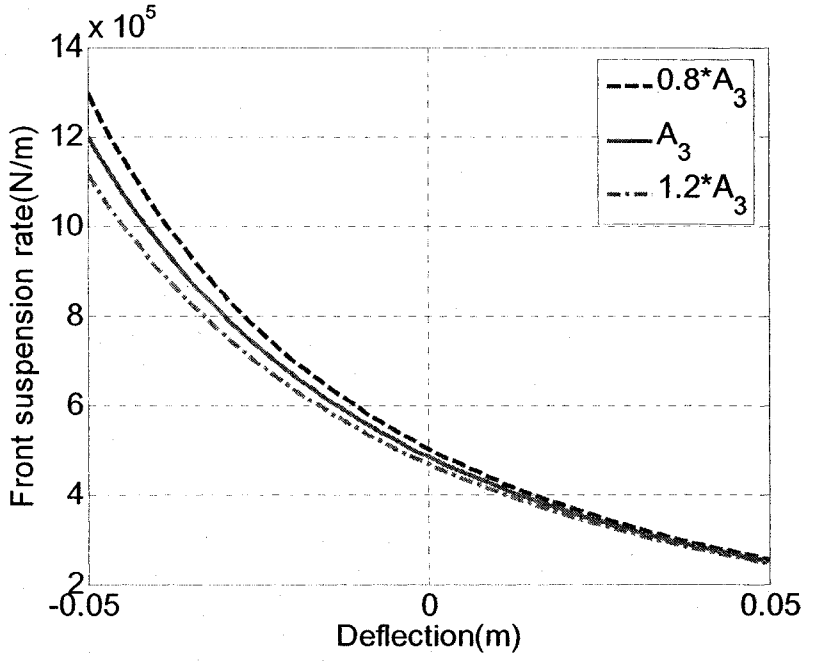

(a)

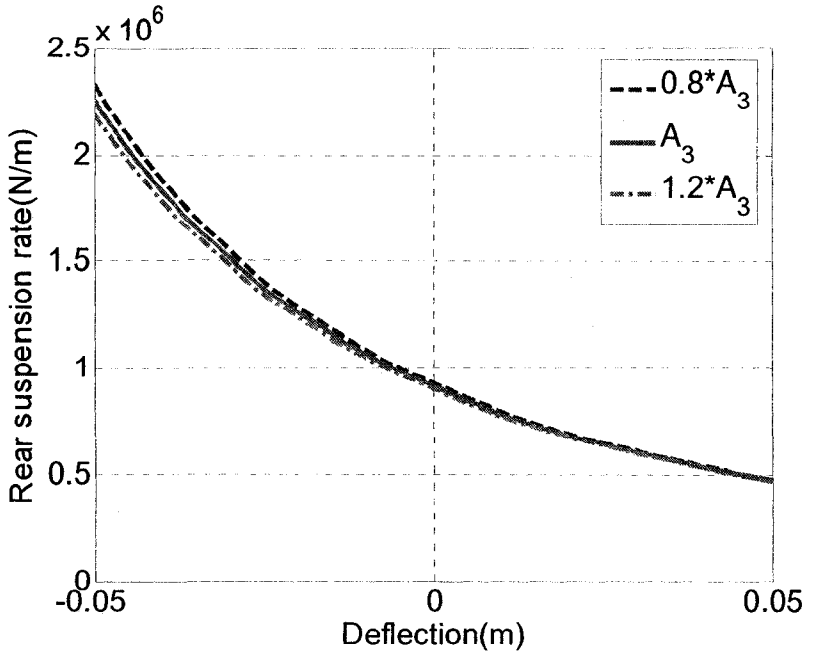

(b)

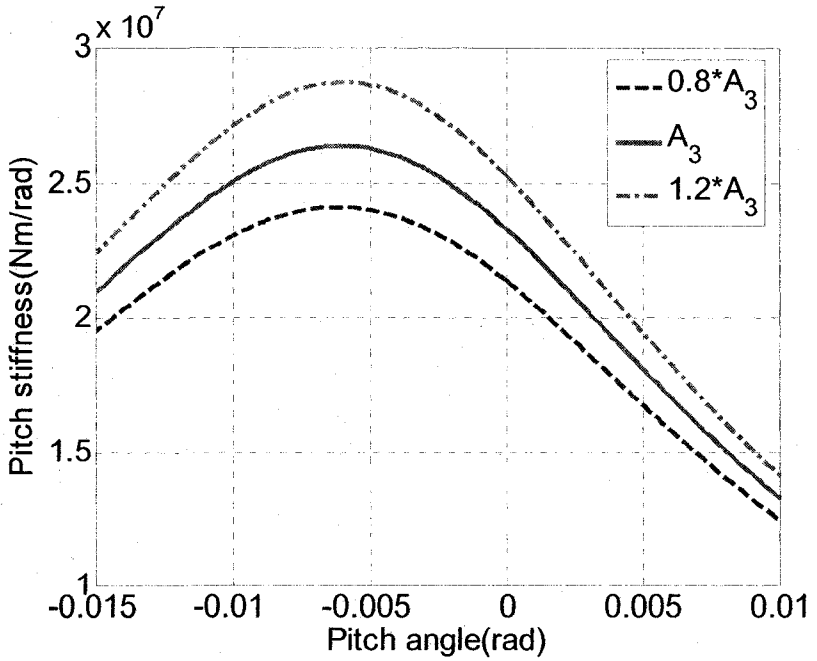

(c)

Figure 4.5: Influence of variations in annular piston area A3 on: (a) front suspension rate; (b) rear suspension rate; and (c) pitch stiffness.

4.5 Pitch Dynamic Responses of the Vehicle Model with Different Suspension Configurations

The relative performance potentials of the proposed interconnected suspension configurations are evaluated in terms of dynamic responses of the vehicle under straight-

line braking inputs as well as random road roughness excitations. The equations of motion for the heavy vehicle equipped with different suspension configurations are analyzed through simultaneous solutions of Eq. (2.91) together with those of dynamic strut forces derived in Section 2.6.

4.5.1 Excitations and Performance Measures

The characteristics of the three random road profiles used in the simulation have been presented in Section 3.2.1. Under the random road roughness excitations, the relative performance characteristics of different suspension configurations can be evaluated in terms of: (i) rms sprung mass bounce acceleration, a simplified and effective measure of vertical ride quality; (ii) rms pitch angle of the sprung mass, a measure of the vehicle dive; and (iii) peak front and rear suspension travels based on 99% probability, which could serve as an indicator for the rattlespace design requirement.

Performance evaluations of heavy vehicles under braking inputs are dependent upon the functions of braking maneuvers, which are generally classified as: (a) normal stops; (b) speed corrections; (c) downhill descents; and (d) emergency stop [155]. Braking maneuvers intended for speed corrections are frequently encountered under various road conditions. The responses to such inputs can be evaluated in terms of sprung mass pitch angle and front and rear suspension travels. In this study, the initial vehicle speed for the analyses is set as 90 km/h, while the braking torque distribution is selected to be proportional to the static weight distribution between the two axles of the vehicle [100].

The modeling of braking torque has been extremely difficult due to the complexities associated with the brake fade effect [100, 155]. The constant braking torque with a

transient response in the absence of brake fade, therefore, has been generally utilized to provide a first-order approximation [4, 100, 155-157]. A novel braking torque model is proposed in this thesis in an attempt to represent the characteristics of brake fade:

$$T_b = b_1 \left\{ e^{-\left[b_5(t-b_7/2)\right]^{b_3}} - b_2 e^{-\left[b_6(t-b_8/2)\right]^{b_4}} \right\} \tag{4.1}$$

where T_b is braking torque, and b_i (i=1,2,...,8) are constant parameters that determine the variations in the braking torque.

The baseline parameters for a braking torque input are summarized in Table 4.4. The variations in these constants can help realize various braking torque properties, as evident in Figure 4.6. The results suggest that the parameter b_1 is a gain factor that directly controls the amplitude of braking torque. The constants b_2, b_4 and b_6 are chosen to achieve desired brake fade effect, while constant b_3 determines the rise and fall rates of the braking torque. Constant b_5 determines the time duration of braking torque, while b_7 and b_8 provide asymmetric rise and fall characteristics of the braking torque. The above equation can be effectively applied to incorporate various brake fade characteristics.

Table 4.4: Baseline parameters for the braking torque model incorporating fade effect.

Parameters	b_1	b_2	b_3	b_4	b_5	b_6	b_7	b_8
Value	20000	0.1	16	4	1	1.4	5	5

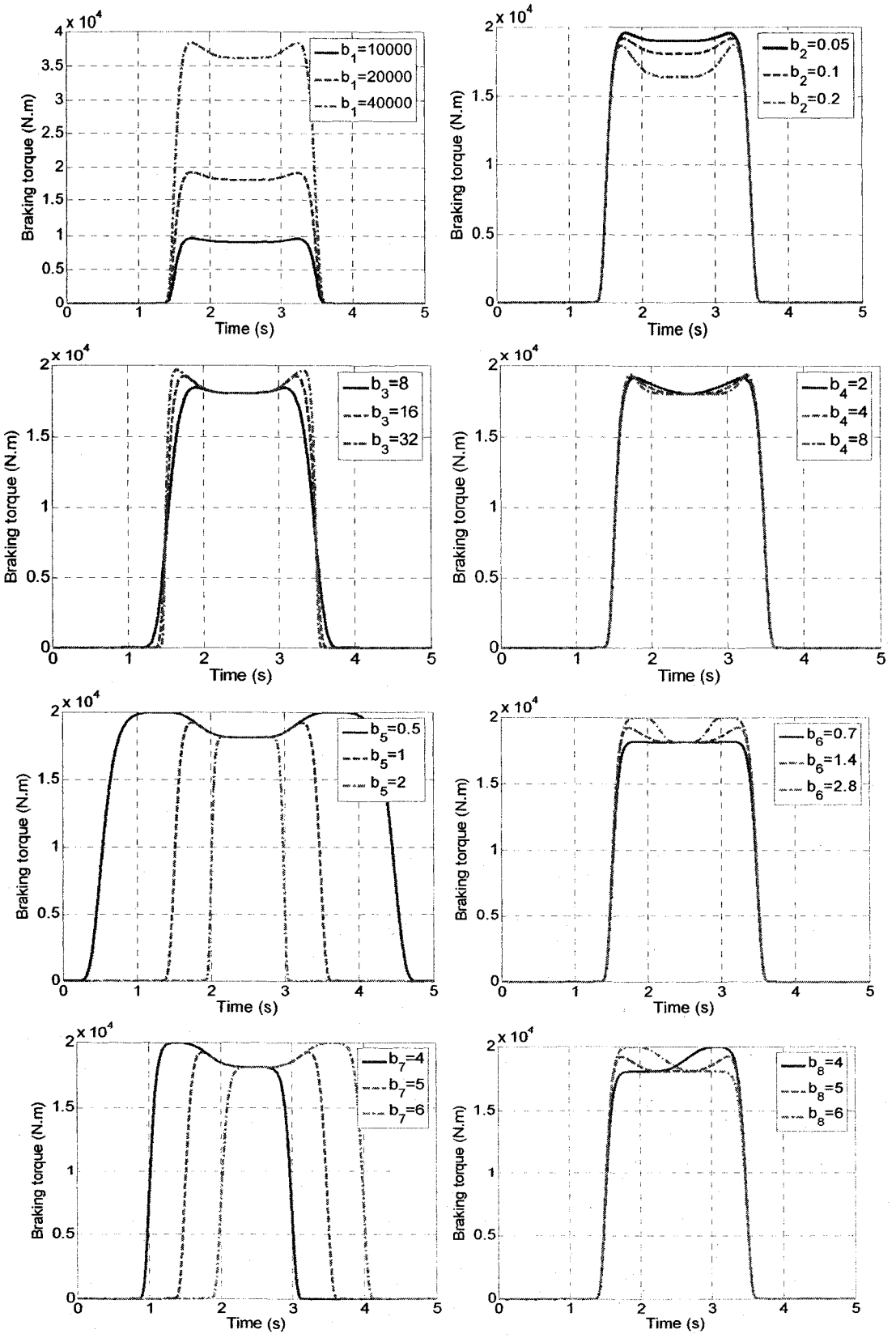

Figure 4.6: Influences of tuning parameters on the braking torque derived from the proposed braking input model.

The braking response analyses are performed using the Magic Formula tire model whose parameters were identified from the available tire data [158], using the MATLAB™ Optimization Toolbox. Two road surfaces with different friction characteristics are considered for dynamic analyses: (i) a dry road with friction coefficient of 0.9, referred to as '*dry surface*'; and (ii) a wet road with friction coefficient of 0.5, referred to as '*wet surface*'.

4.5.2 Responses to Braking Inputs

Figure 4.7 presents the dynamic responses of the vehicle model integrating different suspensions under application of a braking torque input, described by Eq. (4.1), on the *dry surface*. The braking torques applied for the front and rear wheels are shown in Figure 4.7(a). The responses in terms of sprung mass pitch angle, and front and rear suspension travels, are illustrated in Figures 4.7(b), 4.7(c) and 4.7(d), respectively. The results indicate that all the four pitch-connected suspension configurations (A_{IP34}, B_{IP13}, $H_{IP1\text{-}4}$ and B_{IPE13}) yield considerably lower sprung mass pitch angle and suspension travels, compared to those due to the unconnected suspension B_{UP}. The hydraulic interconnection configurations (B_{IP13} and B_{IPE13}) could further improve the transient responses with relatively faster decay of responses, compared to A_{IP34} and $H_{IP1\text{-}4}$ configurations. This is attributed to the enhanced pitch mode damping properties of configurations B_{IP13} and B_{IPE13}.

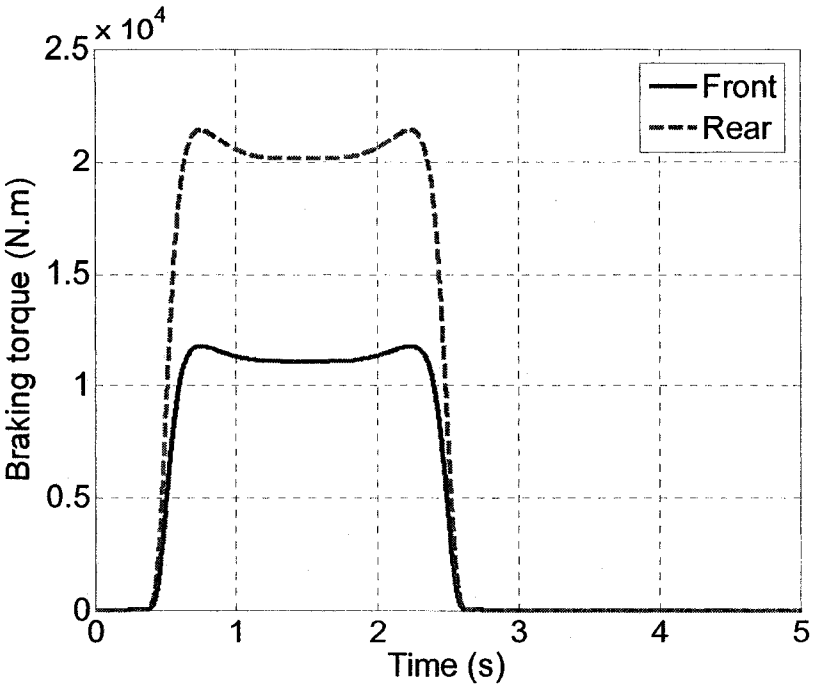
x 10^4
2.5
2
1.5
1
0.5
0
Braking torque (N.m)
0
1
2
3
4
5
Time (s)
Front
Rear

(a)

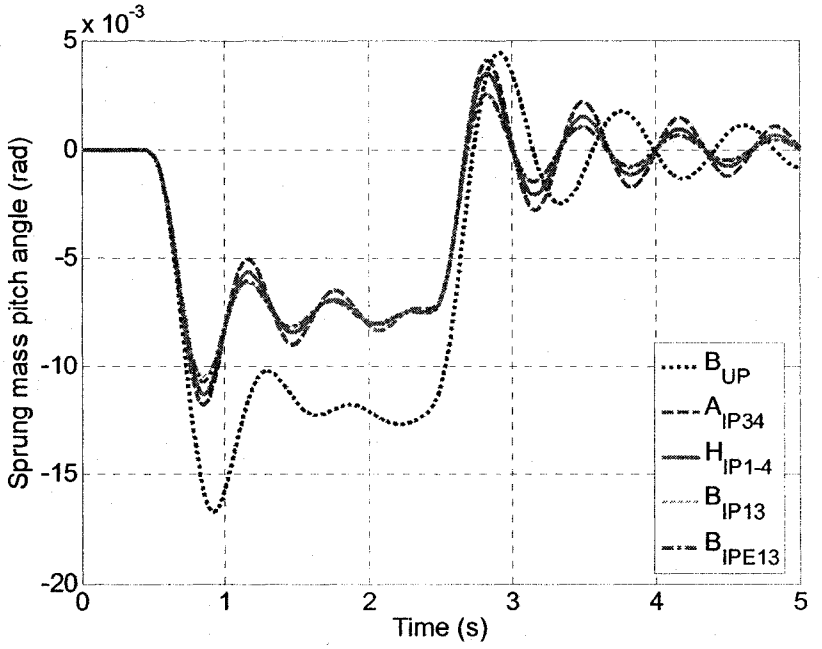
x 10^-3
5
0
-5
-10
-15
-20
Sprung mass pitch angle (rad)
0
1
2
3
4
5
Time (s)
B_UP
A_IP34
H_IP1-4
B_IP13
B_IPE13

(b)

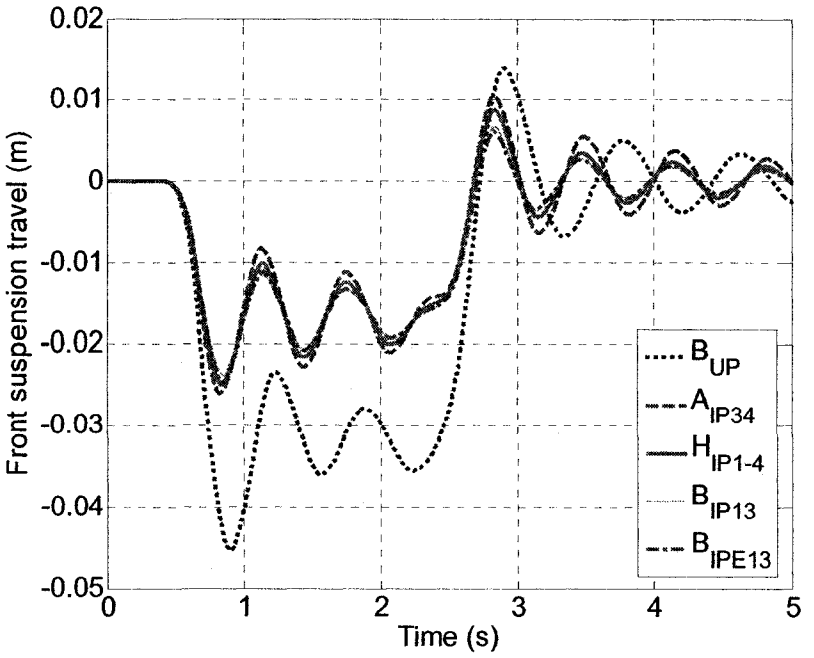

(c)

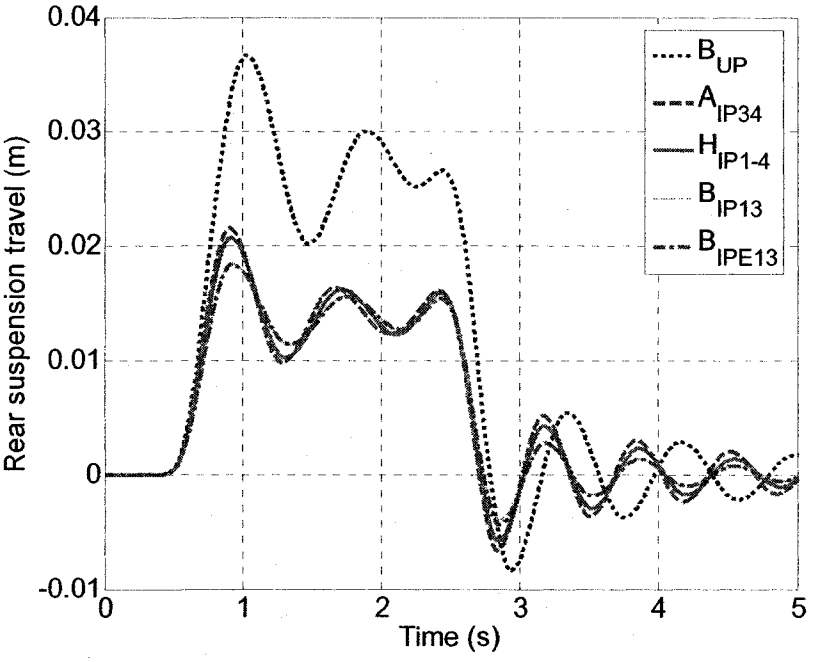

(d)

Figure 4.7: Dynamic responses of the heavy vehicle with different suspension configurations on the dry surface: (a) braking torque; (b) sprung mass pitch angle; (c) front suspension travel; and (d) rear suspension travel.

Similar performance gains of the interconnected suspensions were also observed under braking inputs on the *wet surface* (results not shown). While the control of vehicle

pitch attitude is known to help improve handling quality, the inhibition of suspension travel could reduce the risk of compression or bump stop impacts. Interactions with the bump stops would cause a sudden change in the suspension stiffness and shock motions, which may deteriorate the vehicle handling as well as ride quality. Braking responses attained for the dry as well as wet road surfaces suggest that the pitch-interconnected suspensions could offer considerable potential for improving both the handling and ride characteristics under braking inputs via passive means, irrespective of road adhesion conditions.

4.5.3 Responses to Random Road Inputs

The relative dynamic responses of different suspension configurations are further evaluated under the three random road roughness inputs. Considering the practical vehicle operations, different vehicle speeds are chosen for different road profiles: 70 and 90 km/h for *smooth* road; 50 and 70 km/h for *medium-rough* road; and 30 and 50 km/h for *rough* road.

Figure 4.8 illustrates dynamic responses of the vehicle with different suspension configurations under different road and vehicle speed inputs. The results show the responses in terms of rms bounce acceleration, rms pitch deflection, rms deflections of the front and rear suspensions, as functions of road roughness and speed. All the suspension configurations yield nearly similar rms sprung mass bounce acceleration responses, which is attributed to their identical front and rear suspension rates and bounce mode damping properties. The rms pitch deflection responses of the sprung mass with hydraulically interconnected configurations (B_{IP13} and B_{IPE13}) tend to be only slightly

lower than that with unconnected suspension B_{UP}. The pneumatic interconnection A_{IP34} yields slightly higher pitch response, which is partially attributed to its lower pitch damping, compared to B_{IP13} and B_{IPE13} configurations. The pitch-interconnected suspensions (A_{IP34}, B_{IP13}, $H_{IP1\text{-}4}$ and B_{IPE13}) generally yield lower magnitudes of peak suspension travel compared to those of the unconnected configuration B_{UP}, under a wide range of operating conditions with only a few exceptions. The hydraulically interconnected configurations (B_{IP13} and B_{IPE13}) with their higher pitch mode damping yield lower peak suspension travels, compared to the pneumatic (A_{IP34}) and hybrid fluidic ($H_{IP1\text{-}4}$) interconnections, as seen in Figures 4.8(c) and 4.8(d). The results suggest that the pitch-interconnected suspensions could reduce suspension travel and sprung mass pitch angle responses without greatly affecting the vertical ride performance.

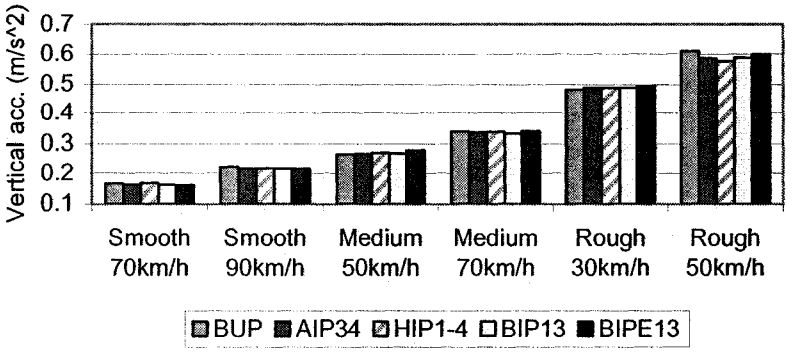

(a)

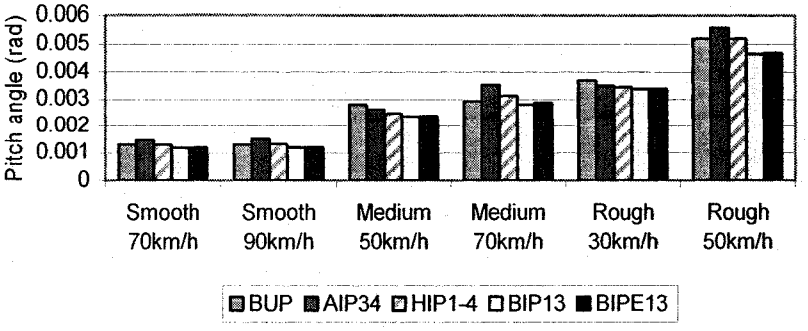

(b)

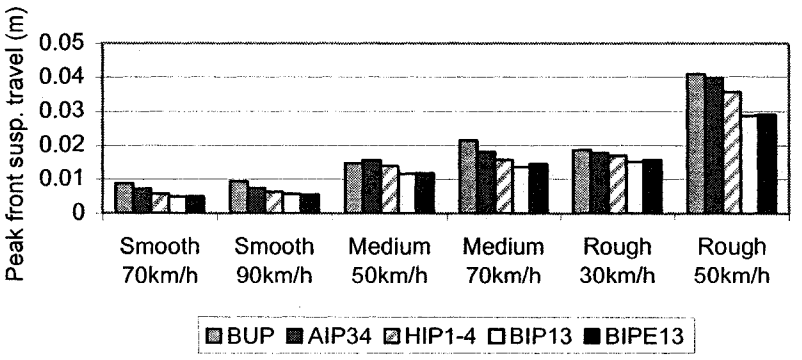

(c)

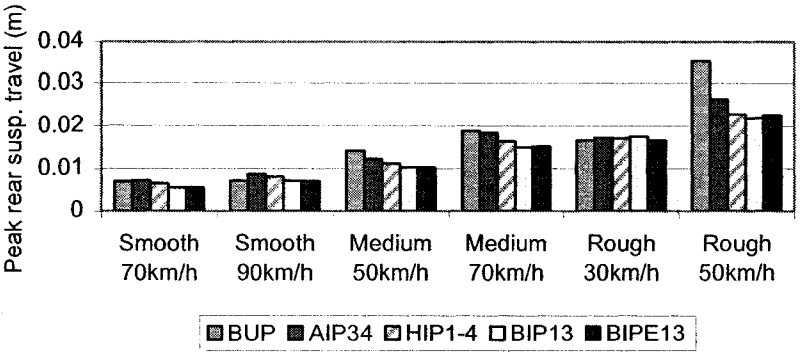

(d)

Figure 4.8: Dynamic responses of the vehicle with different suspensions under random road inputs: (a) rms sprung mass bounce acceleration; (b) rms sprung mass pitch angle; (c) peak front suspension travel; and (d) peak rear suspension travel.

4.6 Ride Height Leveling

Heavy vehicles employ ride height leveling systems to achieve constant ride height under a wide range of load variations. It has also been stated that a ride height control could help achieve a relatively constant natural frequency of the sprung mass [159]. Conventional ride height valves can be easily incorporated within the unconnected suspension configuration B_{UP}. For some of the interconnected suspension configurations, a static equilibrium may not be achievable when ride height valves are used. This is attributed to the coupling effects of the front and rear struts. It is therefore necessary to

investigate the ride height leveling abilities of the proposed pitch-interconnected suspension configurations.

The static equilibrium for the pitch-interconnected suspension struts within the configurations (A_{IP34}, B_{IP13}, $H_{IP1\text{-}4}$ and B_{IPE13}) can be expressed as:

$$P_{1f}A_{1f} - P_{1r}A_{3f} = W_f + P_aA_{4f}$$

$$P_{1r}A_{1r} - P_{1f}A_{3r} = W_r + P_aA_{4r} \tag{4.2}$$

where W_i is the static load on axle i (i=f,r) and P_a is atmospheric pressure. Considering that $A_{1i} > A_{3i}$, the above equations can be manipulated to derive fluid pressures in chambers 1 under the static equilibrium:

$$P_{1f} = \frac{(W_f + P_0A_{4f})A_{1r} + (W_r + P_0A_{4r})A_{3f}}{A_{1f}A_{1r} - A_{3f}A_{3r}} > 0$$

$$P_{1r} = \frac{(W_f + P_0A_{4f})A_{3r} + (W_r + P_0A_{4r})A_{1f}}{A_{1f}A_{1r} - A_{3f}A_{3r}} > 0 \tag{4.3}$$

Above static equilibrium equations suggest that the gas pressure in each strut corresponding to a given load can always be realized ($P_{1i} = P_{4i}$). All the four configurations cinsdeired can thus provide ride height control.

4.6.1 Effects of Load Variations on Suspension Properties and Vehicle Responses

Heavy vehicles generally encounter variable loading conditions, which may influence the suspension properties and thus the vehicle responses to external excitations. The effects of load variations on the properties of different suspension configurations and dynamic vehicle responses to braking inputs and road excitations are thus investigated. The analyses are performed in conjunction with the ride height leveling ability of each

configuration. The essential baseline vehicle parameters (m_s=15753 kg, and $l_f/(l_f+l_r)=0.653$) were varied to achieve two different load conditions: (i) m_s=12000 kg, and $l_f/(l_f+l_r)=0.55$; and (ii) m_s=17000 kg, and $l_f/(l_f+l_r)=0.7$. The former loading condition yields nearly 36% lower load on the rear axle and nearly similar front axle load, when compared to the baseline parameters. The latter loading condition yields 16% higher load on the rear axle, and approximately 6.7% lighter load on the front axle.

Figures 4.9 and 4.10 present the stiffness properties due to different suspension configurations corresponding to two loading conditions involving sprung masses of 12000 kg and 17000 kg, respectively. For different load conditions, the front and rear suspension rates due to the unconnected configuration B_{UP} and the interconnected configurations (A_{IP34}, B_{IP13}, $H_{IP1\text{-}4}$ and B_{IPE13}) are nearly identical; slight variations in the suspension rates are attributed to atmospheric pressure effect considered in the formulations. The pitch stiffness due to all the interconnected configurations for both loading conditions is considerably higher than that of the unconnected suspension B_{UP}. The peak values of pitch stiffness, however, occur at different pitch deflections, which are directly related to the load distributions. The effective pitch rates of all the configurations tend to increase with increasing sprung mass due to corresponding variations in the strut forces and the mass center coordinate. The suspension rates of individual struts also increase with the load, which demonstrates the leveling ability of the suspensions that may lead to relatively constant bounce mode natural frequency.

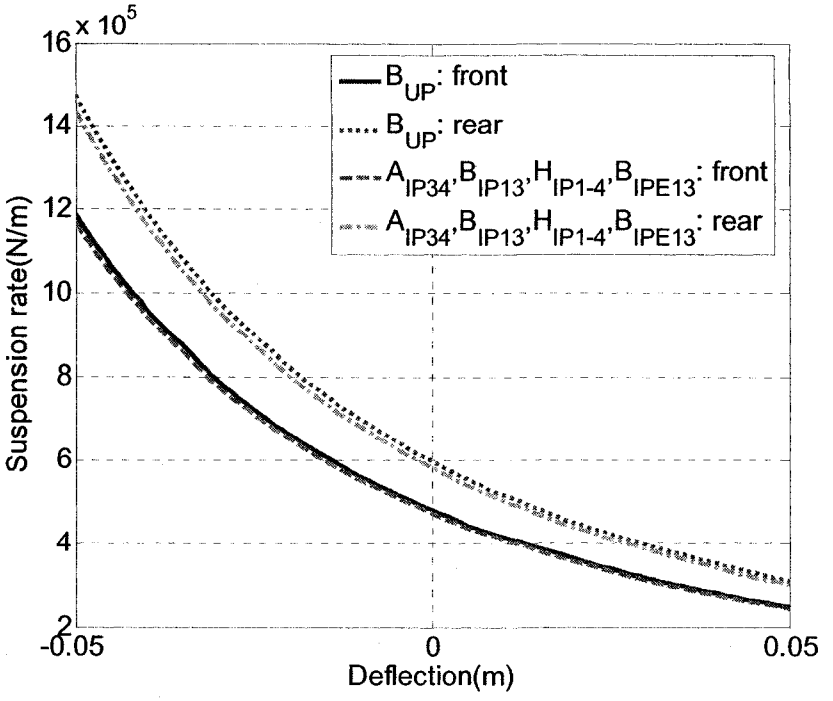

(a)

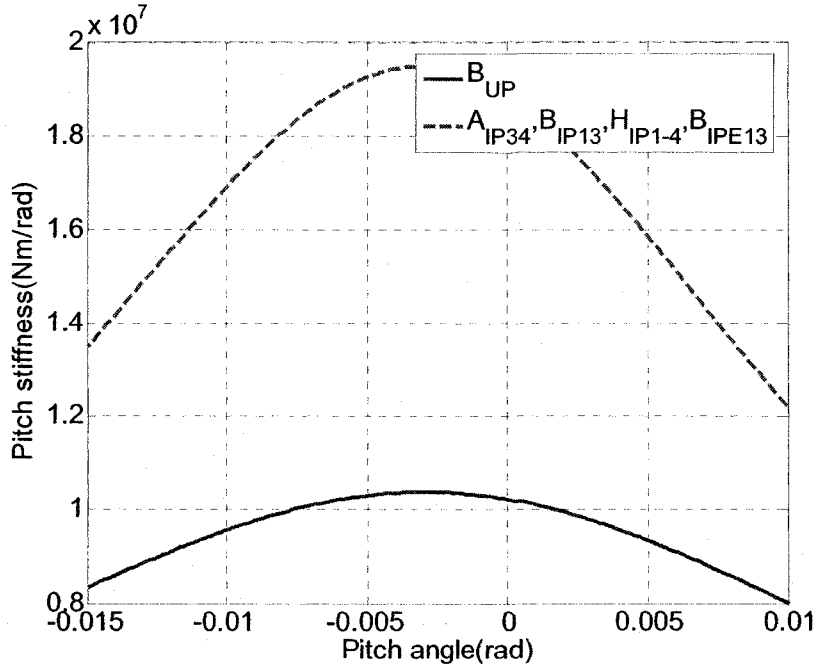

(b)

Figure 4.9: Stiffness properties of different suspension configurations under loading condition, m_s=12000 kg and $l_f/(l_f+l_r)=0.55$: (a) suspension rate; and (b) pitch stiffness.

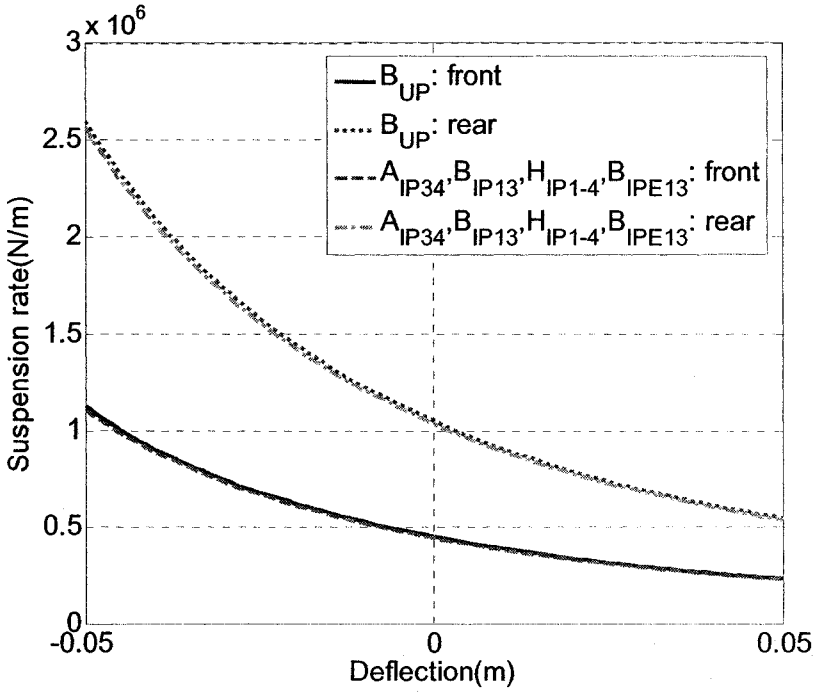

(a)

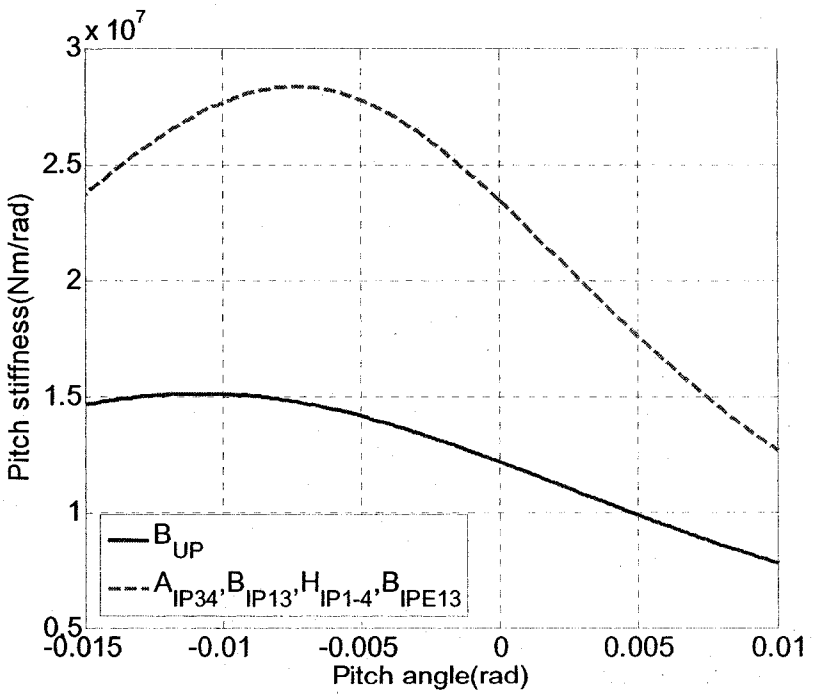

(b)

Figure 4.10: Stiffness properties of different suspension configurations under loading condition, m_s=17000 kg and $l_f/(l_f+l_r)=0.7$: (a) suspension rate; and (b) pitch stiffness.

Figures 4.11 and 4.12 illustrate the effects of load variations on the dynamic responses under an identical braking input, defined in Eq. (4.1), for the *dry surface*. Since all the interconnected configurations yield quite similar responses, the figures show the vehicle responses only with B_{UP} and B_{IP13} suspension configurations. The results attained for the two loading conditions are quite similar to those presented in Figure 4.7 for the nominal load. The peak pitch deflections tend to be smaller for both the loading conditions than that observed for the nominal vehicle. Moreover, the magnitudes of oscillations in the rear strut deflection tend to be significantly smaller under the light load condition (Figure 4.11), which is attributed to higher effective rear strut damping ratio of this configuration. The results suggest that the pitch-interconnected suspension configurations with a ride height leveling system could offer similar braking performance under various load conditions.

Figures 4.13 and 4.14 illustrate ride dynamic responses of the vehicle model with unconnected and interconnected suspensions, corresponding to the two loading conditions. The results again are presented only for B_{UP} and B_{IP13} configurations, while the excitations due to *smooth*, *medium-rough* and *rough* roads are considered at different driving speeds. The vehicle with unconnected (B_{UP}) or hydraulically-interconnected (B_{IP13}) suspension configurations exhibits very similar rms sprung mass bounce acceleration responses, for both the loading conditions, as it was observed for the nominal vehicle. The configuration B_{IP13} yields lower rms sprung mass pitch angle responses, compared to B_{UP} suspension, especially for rougher roads, irrespective of the loading conditions considered, as evident in Figures 4.8, 4.13 and 4.14. The results suggest that the pitch-interconnected suspensions integrating a ride height leveling

system could yield slight improvement in the sprung mass pitch responses with only negligible influence on the vertical ride, under different loading conditions.

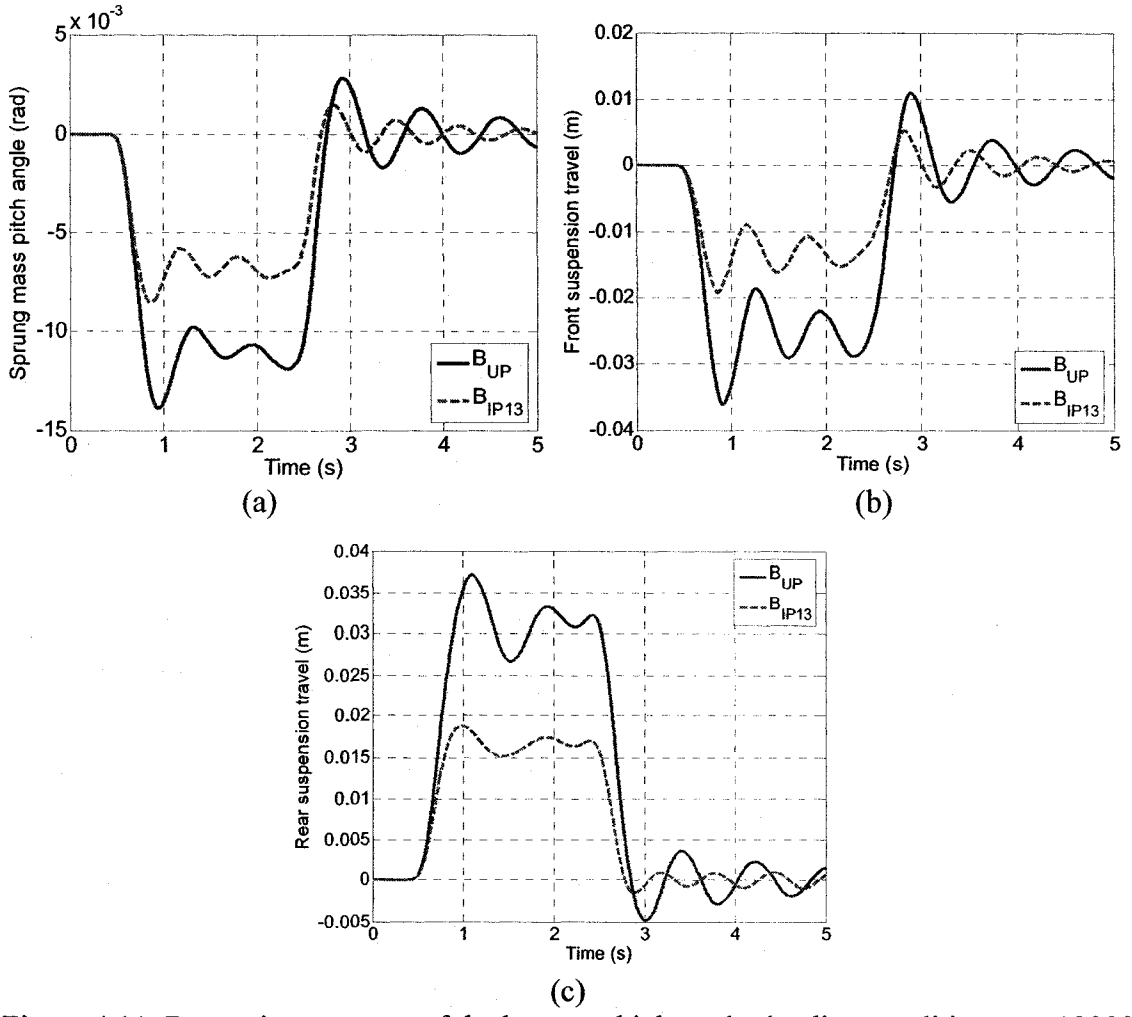

Figure 4.11: Dynamic responses of the heavy vehicle under loading condition, m_s=12000 kg and $l_f/(l_f+l_r)=0.55$ on the dry surface: (a) sprung mass pitch angle; (b) front suspension travel; and (c) rear suspension travel.

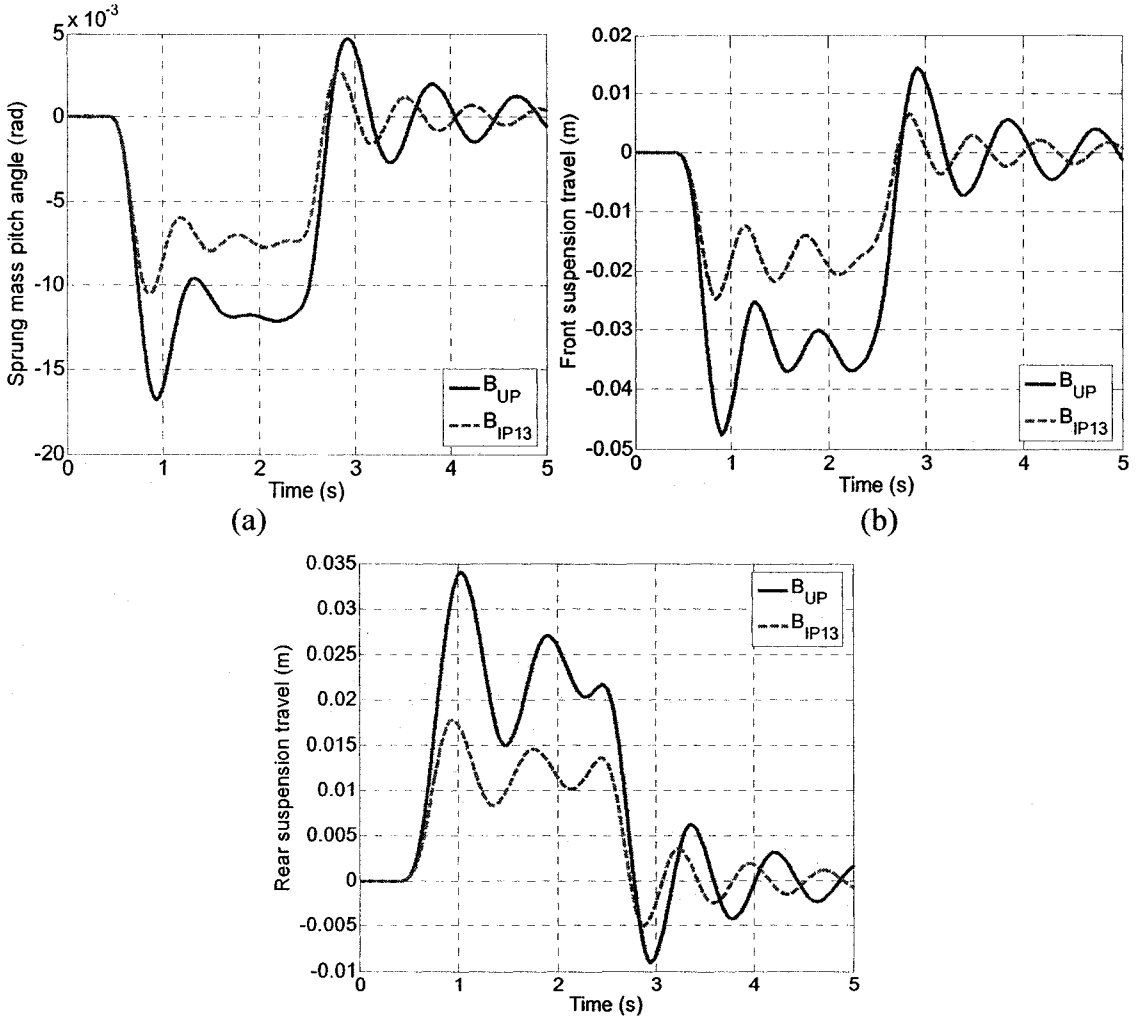

Figure 4.12: Dynamic responses of the heavy vehicle under loading condition, m_s=17000 kg and $l_f/(l_f+l_r)=0.7$ on the dry surface: (a) sprung mass pitch angle; (b) front suspension travel; and (c) rear suspension travel.

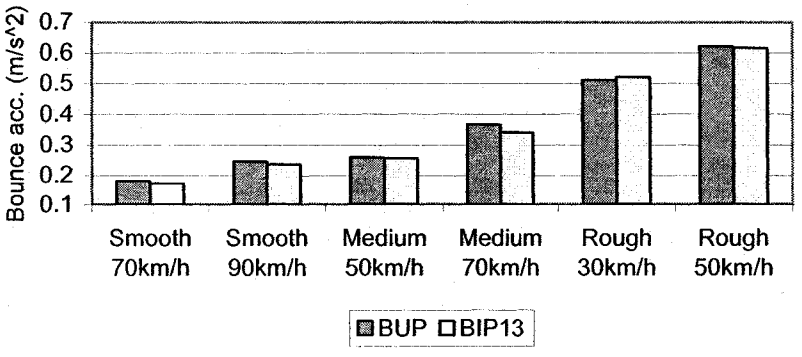

(a)

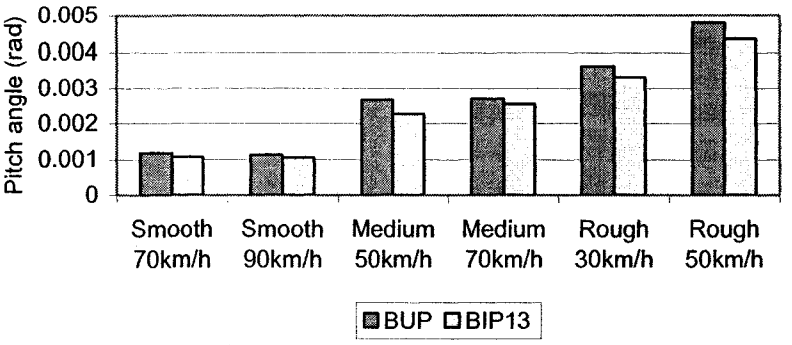

(b)

Figure 4.13: Dynamic responses of the heavy vehicle under loading condition, m_s=12000 kg and $l_f/(l_f+l_r)=0.55$, subjected to random road inputs: (a) rms sprung mass bounce acceleration; and (b) rms sprung mass pitch angle.

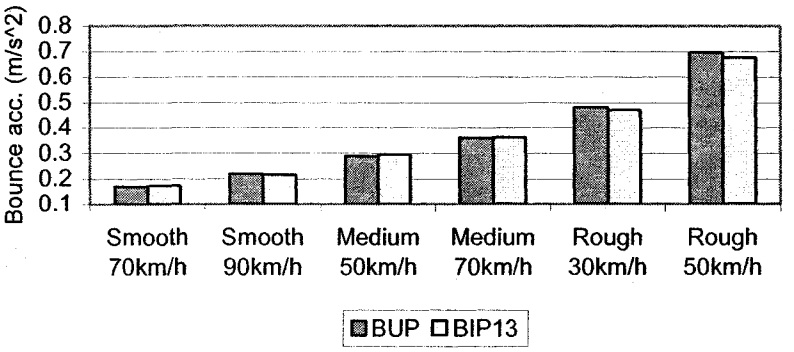

(a)

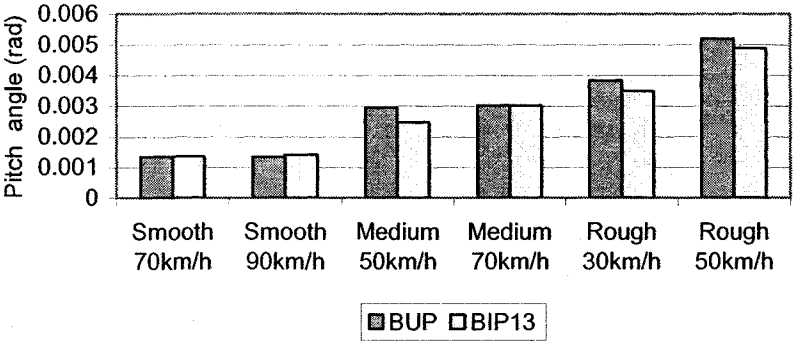

(b)

Figure 4.14: Dynamic responses of the heavy vehicle under loading condition, m_s=17000 kg and $l_f/(l_f+l_r)=0.7$, subjected to random road inputs: (a) rms sprung mass bounce acceleration; and (b) rms sprung mass pitch angle.

4.7 Summary

The fundamental pitch plane suspension properties and dynamic responses of the vehicle model with different pitch-interconnected suspensions configurations were investigated, subject to the braking inputs and random road roughness excitations. These interconnected suspension configurations involved pneumatic, hydraulic and hybrid fluidic interconnections between the front and rear struts. The essential properties of the pitch-connected configurations were evaluated in terms of front and rear suspension rates, pitch stiffness, and bounce and pitch mode damping characteristics, and compared with those of the unconnected suspension. The results suggested that the pitch-interconnections, either hydraulic or pneumatic, can yield significantly higher pitch stiffness without affecting the vertical suspension rates and bounce damping, which could thus achieve improved anti-dive performance and reduce dynamic longitudinal load transfers under braking inputs. The hydraulic interconnections further permit considerably higher pitch mode damping compared to the unconnected suspension, pneumatically and hybrid-fluidically interconnected configurations. The most significant benefits of pitch-connected suspension arise from its design flexibility. The results attained from parametric analyses revealed that the proposed struts and interconnections can be easily tuned to achieve desired pitch properties with negligible influence on the bounce properties. The improved anti-dive performance could thus be realized with soft vertical ride.

The dynamic responses of a heavy vehicle with proposed suspension configurations were also evaluated under braking inputs and random road roughness excitations. A novel braking torque model was proposed to characterize the brake fade effects. The ride

height control ability of pitch-interconnected suspensions was also analytically proven. The effects of load variations on the performance of the vehicle with different suspensions as well as ride height leveling system were further investigated. The results demonstrated that the proposed pitch-interconnected suspensions could considerably inhibit vehicle attitude and suspension travels during straight-line braking maneuvers intended for speed corrections. The interconnected suspensions also revealed reduced suspension travel without greatly affecting the vertical ride under excitations arising from random roads of varying surface roughness. The braking and ride responses showed only little sensitivity to load variations. From the results, it was concluded that pitch-connected suspension offers significant potential for enhancing the vehicle pitch performance, irrespective of various operating and load conditions considered. Moreover, these offer greater design flexibility for realizing desired pitch mode stiffness and damping without affecting the bounce properties.

CHAPTER 5

ROLL AND PITCH DYNAMIC ANALYSIS OF TWIN-GAS-CHAMBER STRUT SUSPENSION

5.1 Introduction

The analyses of the proposed roll-connected and pitch-connected hydro-pneumatic suspension struts in the previous three chapters have demonstrated their superior design flexibility and potentials in enhancing vehicle performance. It was shown that both the unconnected and interconnected suspension configurations of the single-gas-chamber struts yield asymmetric hardening and softening vertical stiffness properties in compression and extension motions, respectively, attributed to the gas property. Such properties help inhibit the motions in compression but may yield larger motions and wheel-hop in rebound. Furthermore, the asymmetric force-deflection properties of the unconnected suspension configurations (B_{UR}, B_{UP}) revealed a softening effect on the effective roll or pitch stiffness with increasing roll or pitch deflection, respectively. This softening effect would be undesirable in view of the roll stability and vehicle attitude control, particularly under large roll and pitch deflections. Although the proposed interconnected suspension configurations, including roll-connected (B_{IR}, A_{IR}) and pitch-connected (A_{IP34}, B_{IP13}, $H_{IP1\text{-}4}$), also yield a softening effect in the effective roll or pitch stiffness, the effective stiffnesses are considerably higher than those of the unconnected configurations. Such characteristics in the roll stiffness were also observed for the reported roll-connected suspension configurations employing different types of hydro-pneumatic struts explored in the studies [25, 27-29].

Alternatively, the twin-gas-chamber struts, proposed in Section 2.2, could overcome the suspension softening effect in rebound, which would also reduce the softening effect in effective roll and pitch stiffnesses. Similar to the single-gas-chamber strut (*B*), the design of a twin-gas-chamber strut (*A*) could also be realized in a compact manner with considerably larger effective working area when compared to those reported in [25, 27, 28, 31, 32]. Additionally, the twin-gas-chamber strut involves two gas chambers that dominate the suspension stiffness in compression and rebound motions, respectively, and thereby can offer nearly symmetric vertical stiffness properties. Through the mathematical formulations, presented in Section 2.4, it was analytically proven that the twin-gas-chamber strut suspension can provide suspension hardening effect in the vertical stiffness in both compression and rebound directions, while retaining a lower suspension rate in the vicinity of the design ride height.

This chapter further extensively investigates the performance potentials of the twin-gas-chamber strut suspension arranged in either roll-plane (A_{UR}) or pitch-plane (A_{UP}), in relation to those of the single-gas-chamber strut suspensions (B_{UR} and B_{UP}), shown in Figures 2.3 and 2.8. Since the conventional vehicle suspension systems are unconnected (with the exception of the anti-roll bars coupling in the roll plane), the relative performance analyses are limited only to the unconnected suspension configurations. The performance analyses are presented in terms of suspension properties and vehicle responses to different excitations, which would demonstrate the relative performance potentials of the twin-gas-chamber strut suspension over the single-gas-chamber strut suspension. The design flexibility of the twin-gas-chamber strut suspensions is also explored through parametric studies. The fundamental pitch dynamics and suspension

tuning of heavy vehicles are further explored, and a set of suspension tuning rules is proposed.

5.2 Roll Plane Analysis of Twin-Gas-Chamber Strut Suspension

Roll plane analysis of the twin-gas-chamber strut suspension is performed, based on the roll plane vehicle model (Figure 2.2) together with the analytical formulations of static and dynamic characteristics of the twin-gas-chamber struts, presented in Sections 2.3.3 and 2.4.2. Simulation parameters of the vehicle model are identical to those applied for the single-gas-chamber strut suspension (B_{UR}), which have been presented in Table 3.1. The design parameters of the twin-gas-chamber strut suspension A_{UR} that differ from those of the single-gas-chamber strut configuration are summarized in Table 5.1. The strut parameters were selected to attain identical static vertical rates for both the suspension configurations (A_{UR} and B_{UR}), and identical load carrying capacities. A comparison of the parameters of the two strut suspensions shows that for the identical load carrying capacity, the twin-gas-chamber strut would yield relatively larger piston areas and thus require considerably lower static charge pressure. The relative analyses are also performed for the single-gas-chamber strut suspension with an anti-roll bar B_{URb}, which would represent a conventional vehicle suspension with an anti-roll bar. The roll stiffness of the anti-roll bar was selected as 200 kNm/rad. The selected roll stiffness is different from that of the configuration B_{URbar} investigated in Chapter 3, where the anti-roll bar geometry was selected to attain roll stiffness identical to the static roll stiffness of the connected suspensions.

The selected simulation parameters for the three suspension configurations (A_{UR}, B_{UR} and B_{URb}) resulted in identical static properties, namely the load carrying capacity, static suspension rate and static deflection. The chosen parameters revealed undamped bounce mode natural frequency of the sprung mass in the order of 1.5 Hz at the design ride height for all the three suspension configurations.

Table 5.1: Simulation parameters for the twin-gas-chamber strut suspension.

Parameter	Value
P_0	2.248 MPa
A_2	0.018 m^2
A_3	0.002 m^2

5.2.1 Roll-Plane Property Analysis

The roll plane properties of the selected suspension configurations are obtained using the methodologies described in Section 2.4. Figure 5.1(a) illustrates a comparison of the suspension rates of the three selected suspension configurations. The results show identical suspension rates for all the configurations at the design ride height, while the configurations B_{UR} and B_{URb} yield identical suspension rates over the entire deflection range. These two configurations exhibit softening and hardening effects in extension and compression, respectively, similar to those reported for commercial air springs [118, 160]. The twin-gas-chamber strut suspension A_{UR}, however, shows hardening effects in both compression and rebound, which is also consistent with that obtained from the analytical formulations in Equations (2.86) to (2.90) in Section 2.4.2.

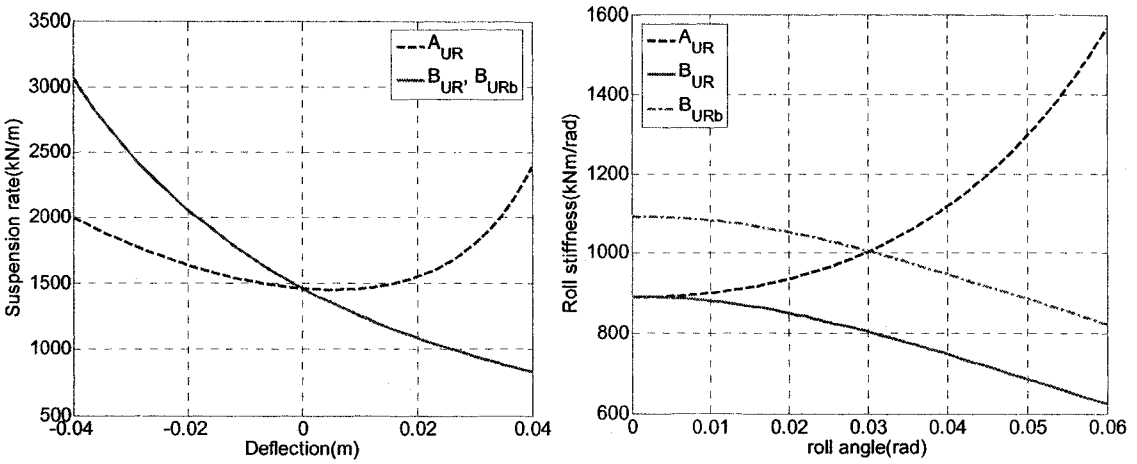

Figure 5.1: Stiffness characteristics of different suspension configurations: (a) suspension rate; and (b) roll stiffness.

Figure 5.1(b) presents the roll stiffness characteristics of different suspension configurations. While the suspensions A_{UR} and B_{UR} yield identical static roll stiffness, the suspension B_{UR} exhibits softening tendency with increasing roll deflection, which is attributed to hardening and softening spring rates of the struts. The twin-gas-chamber strut suspension A_{UR}, however, exhibits progressively increasing roll stiffness with increasing roll angle, which is in part attributed to hardening spring rates of the struts in compression as well as rebound, as evident in Figure 5.1(a). The use of an anti-roll bar could augment the static roll stiffness of the suspension system, as seen in Figure 5.1(b). The roll stiffness of configuration B_{URb}, however, decreases with roll deflection and could approach a value lower than that of configuration A_{UR}. The results clearly show that the proposed twin gas chamber strut suspension could yield enhanced stiffness over the entire range of the roll deflection, while the use of a relatively stiffer anti-roll bar would add weight to the vehicle.

5.2.2 Design Flexibility of the Twin-Gas-Chamber Strut Suspension

The vertical and roll stiffness properties of the twin-gas-chamber strut suspension A_{UR} are strongly dependent upon the static charge pressure, initial lengths and effective working areas of the gas chambers 3 and 4, as evident from Eqs. (2.38) and (2.77). The proposed struts thus offer considerable design flexibility potential to realize varying roll stiffness for enhancement of roll stability limits of vehicles, while retaining a soft vertical ride in the vicinity of the static ride height. Moreover, it can yield nearly symmetric vertical spring rates in compression and rebound. The influences of the above-stated design parameters on the resulting vertical and roll stiffness properties of the twin-gas-chamber strut suspension configuration A_{UR} are explored and discussed to demonstrate its suspension design flexibility.

The suspension rate and roll stiffness of the baseline configuration (Figure 5.1) were attained assuming $P_{30}= P_{40}$. The influences of variations in the static charge pressure on the vertical and roll stiffness properties are evaluated by varying the charge pressure by ±20% about the baseline value, while all other parameters are held fixed. Such variations in the charge pressure would also alter the load carrying capacity of the suspension. The results presented in Figures 5.2(a) and (b) show that an increase in the static charge pressure yields higher suspension rate and roll stiffness throughout the deflection ranges considered, while the degree of symmetry or asymmetry in the suspension rate remains nearly unchanged.

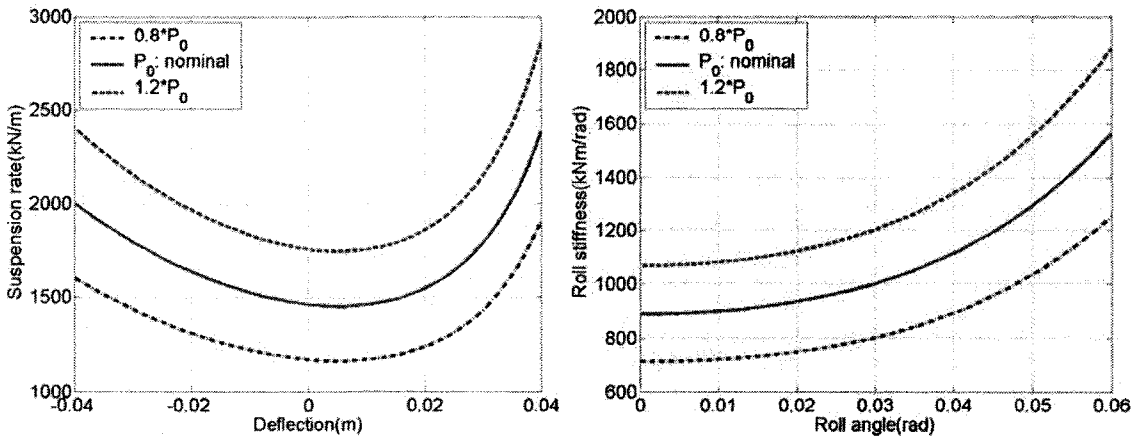

(a) (b)

Figure 5.2: Effects of variations in the static charge pressure on the stiffness properties of the twin-gas-chamber strut suspension A_{UR}: (a) suspension rate; and (b) roll stiffness.

Figures 5.3(a) and (b) illustrate the influence of variations in the initial length of the gas chamber 3 on the vertical and roll stiffness properties of the suspension A_{UR}, while the annular piston area A_3 and charge pressure are held to their nominal values. The results show only negligible effect on suspension rate in the compression stroke, while the suspension rate in rebound increases significantly with lower chamber length or gas volume. A lower gas volume in chamber 3 yields considerable asymmetry in the spring rate, which is attributed to its significantly higher spring rate in rebound. This also results in considerably higher roll stiffness with increasing roll deflection, as evident in Figure 5.3(b).

A variation in the initial length of gas chamber 4 yields an opposite effect on the suspension spring rate, as shown in Figure 5.4(a). Reducing the chamber 4 length and thus the volume V_{40} causes higher suspension rate in compression with relative small effect on the rebound stroke stiffness property. This also yields higher suspension roll stiffness, which increases with roll deflection, as shown in Figure 5.4(b).

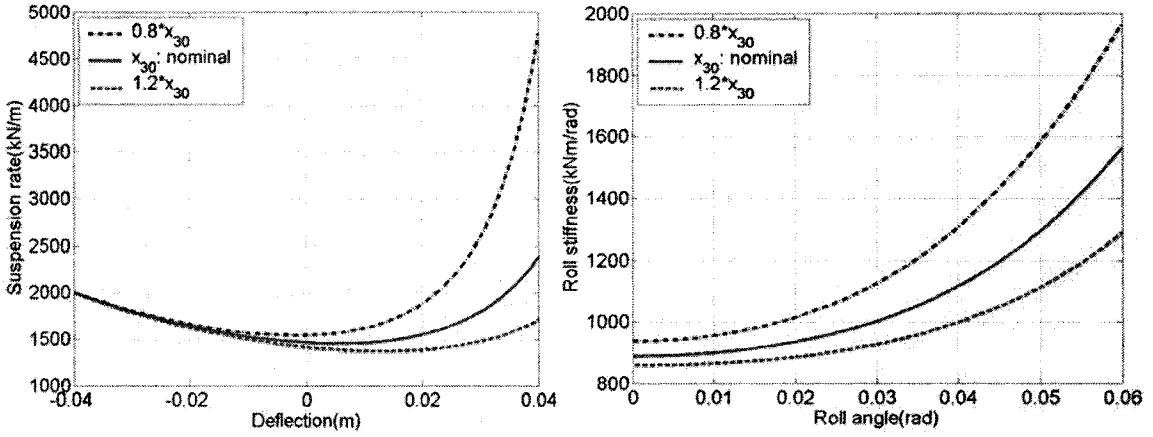

(a) (b)

Figure 5.3: Effects of variations in the initial length of chamber 3 on the stiffness properties of the twin-gas-chamber strut suspension A_{UR}: (a) suspension rate; and (b) roll stiffness.

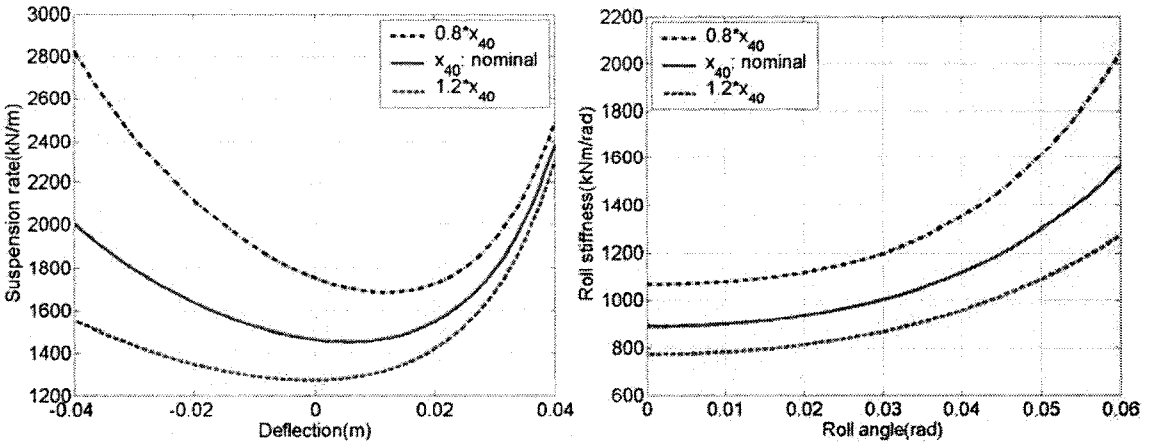

(a) (b)

Figure 5.4: Effects of variations in the initial length of chamber 4 on the stiffness properties of the twin-gas-chamber strut suspension A_{UR}: (a) suspension rate; and (b) roll stiffness.

The proposed twin-gas-chamber strut design also offers flexibility in varying the piston area without affecting the load carrying capacity and the operating pressure. The design load carrying capacity can be ensured by keeping the constant floating piston area, while the main piston area can be changed by varying the annular area A_3. Figures 5.5(a) and (b) present the effects of variations in the annular piston area on the vertical and roll stiffness characteristics of the suspension, where the area is varied by ±20% about its

nominal value. The results show that a reduction in A_3 yields lower suspension rate and roll stiffness in the deflection ranges considered. Moreover, a change in A_3 yields nearly parallel shifts in the suspension rate and the roll stiffness, as seen in Figure 5.5. This property of the proposed struts can be effectively applied to achieve desired stiffness properties and thus the natural frequencies without imposing additional rattle space demand, and without affecting the load carrying capacity and operating pressure.

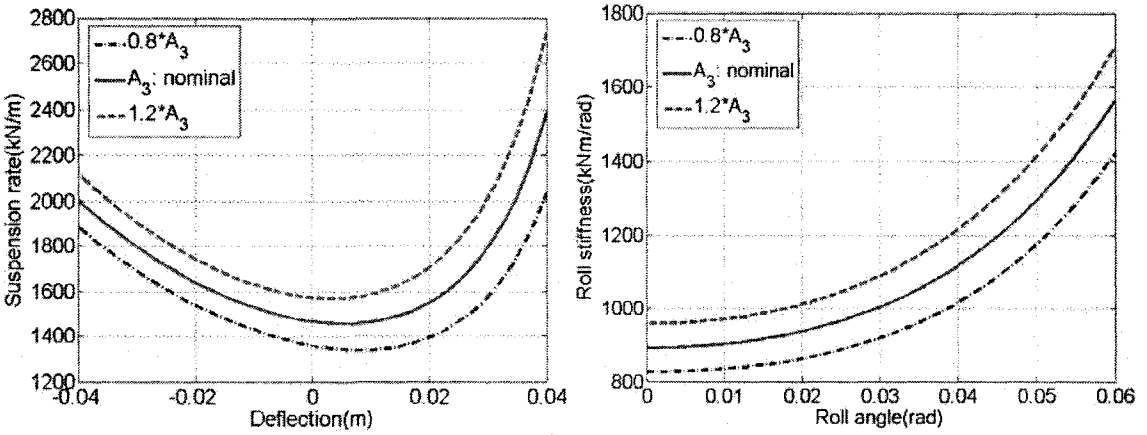

Figure 5.5: Effects of variations in the annular area of chamber 3 on the stiffness properties of the twin-gas-chamber strut suspension A_{UR}: (a) suspension rate; and (b) roll stiffness.

5.2.3 Dynamic Responses in the Roll Plane

The relative dynamic response characteristics of the three suspension configurations (A_{UR}, B_{UR} and B_{URb}) are further evaluated in terms of vertical and roll dynamic responses of the vehicle model presented in Figure 2.2. The vehicle responses are evaluated in terms of the ride height drift, suspension topping, dynamic tire deflection, sprung mass roll deflection and vertical and roll ride qualities, which are closely related to ride, handling, roadholding and roll stability performance characteristics. While the stiffness properties of all the three suspensions have been presented in Figure 5.1, the symmetric

vertical mode damping properties are assumed. The damping orifices and transition velocities are selected to achieve nearly identical force-velocity properties of all the three suspension configurations.

RIDE HEIGHT DRIFT

A few studies have investigated the effects of asymmetric damping and stiffness properties on the ride height drift [16, 161]. These studies concluded that the progressively hardening force-deflection properties tend to introduce an upward ride height drift (packing up), while the asymmetric damping with higher damping in rebound would cause a downward ride height drift (packing down). The ride height drift affects various design and performance measures of a vehicle, such as suspension stroke, ground clearance, vehicle aerodynamics, vehicle attitude, roll stability limit, headlight dip angle, and crashworthiness. It is thus desirable to reduce the variations in the ride height to an acceptable range, which may be realized by reducing the degree of asymmetry in the suspension force-deflection and force-velocity properties. In the present analysis, the assumption of symmetric damping does not permit for assessment of ride height drift due to asymmetric damping, while the effects of stiffness symmetry/asymmetry could be assessed.

The ride height drift of the suspension system can be conveniently evaluated under an in-phase harmonic excitation at the tire-road interface in the vicinity of the sprung mass resonance. The ride height drift properties of the suspension configurations are evaluated in terms of the mean vertical displacement response of the sprung mass under a 1.5 Hz harmonic excitation. The influence of excitation magnitude on the ride height shift

is also evaluated by considering three different displacement amplitudes (5, 10 and 15 mm). Figure 5.6 illustrates the normalized ride height drift (NRHD) responses of the three suspension configurations with respect to the excitation amplitude. The results clearly show that the asymmetric force-deflection properties of the single-gas-chamber strut suspensions (B_{UR} and B_{URb}) yield considerable ride height drift of the sprung mass, which increases with excitation amplitude in a nonlinear manner and exceeds over 20% under the 15 mm excitation. The ride height drift is associated with asymmetric vertical deflection of the sprung mass and thus the suspension travel, which also cause asymmetric damping forces in compression and rebound, although a symmetric damping is assumed. The twin-gas-chamber strut suspension A_{UR} with its more symmetric spring rate yields significantly lower shift in the normalized ride height, in the order of 3-4%, suggesting nearly linear changes in the drift with excitations amplitude.

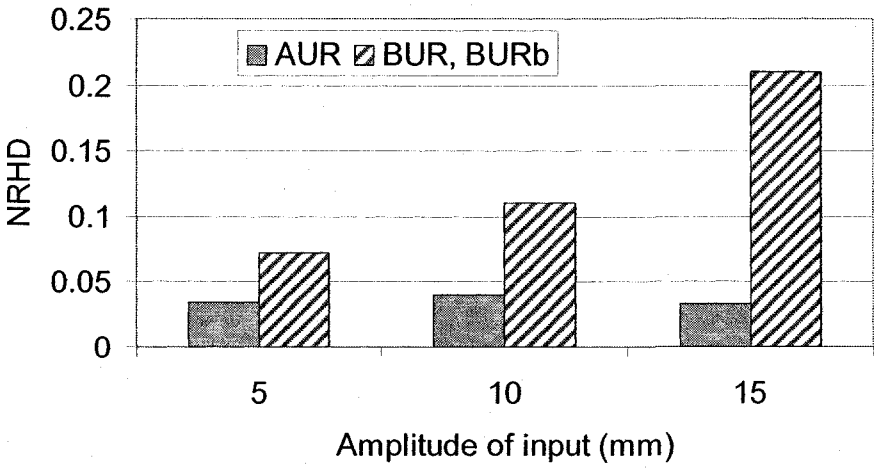

Figure 5.6: NRHD responses of different suspension configurations.

SUSPENSION TOPPING AND TIRE DEFLECTION

Both the suspension and tire deflections strongly influence various performance measures of a road vehicle, namely the ride vibration, roadholding and handling. The

suspension deflections may also cause impacts due to topping, while the dynamic tire forces transmitted to the pavement, known to contribute to pavement fatigue, are closely related to the dynamic tire deflection due to the very light damping offered by the tires. The relative suspension and tire deflection responses of the vehicle models with the selected suspension configurations are thus evaluated. The deflection responses can be evaluated under deterministic road bump excitations, which can be characterized by a versed sine pulse. The suspension travel response is assessed under a 0.3 s versed sine pulse applied to both wheels (peak amplitude = 0.08 m), which yields an excitation in the vicinity of the resonance of the sprung mass. The tire deflection responses, however, are evaluated at a relatively higher frequency pulse by applying 0.1 s in-phase versed sine pulse with an amplitude of 0.07 m.

Figure 5.7(a) presents the variations in the suspension travel responses of the vehicle model with different suspension configurations. Both the B_{UR} and B_{URb} configurations yield identical but considerably higher peak deflection in rebound than the twin-gas-chamber strut suspension A_{UR}. This is mostly attributed to lower suspension rate of configuration B_{UR} in the rebound stroke. The results suggest that suspension B_{UR} could cause impacts against the rebound bump leading to poor ride quality and handling, considering that the typical suspension travel of most road vehicles is in the order of ±0.09 m [162]. The variations in the dynamic tire deflection responses of the vehicle involving different suspensions are shown in Figure 5.7(b). The suspensions B_{UR} and B_{URb} exhibit identical but larger tire deflections than the suspension A_{UR}. The results suggest that the proposed twin-gas chambers strut could reduce the frequency and

severity of suspension topping, dynamic tire forces transmitted to the road surface and the rattle space requirement.

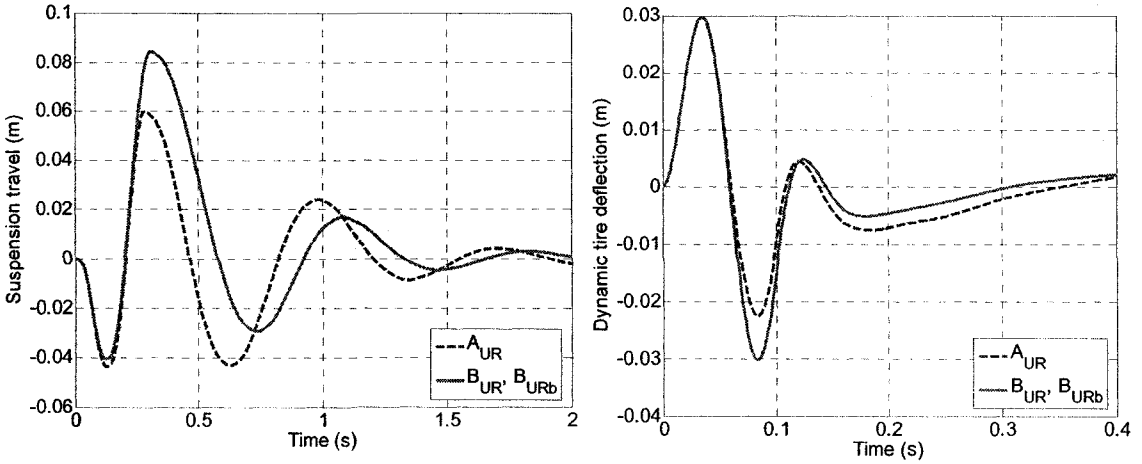

(a) (b)

Figure 5.7: Comparisons of responses of different suspension configurations: (a) suspension topping; and (b) dynamic tire deflections.

ROLL DYANMIC RESPONSES

The relative roll dynamic responses of different suspension configurations are assessed under a centrifugal force excitation arising from a steady turning maneuver or crosswind, which can be characterized by a rounded-step lateral acceleration, as described in Equation (3.1) and shown in Figure 5.8(a), where the magnitude of acceleration is selected as 3.5 m/s^2. Figure 5.8(b) illustrates the sprung mass roll angle responses of the vehicle with different suspension configurations, subjected to the defined round-step lateral acceleration excitation. The results show that the suspension B_{UR} yields significantly larger sprung mass roll angle, although the static roll stiffness of suspension configurations A_{UR} and B_{UR} are identical (Figure 5.1(b)). The proposed twin-gas chamber strut yields hardening roll stiffness with increasing deflection, while the suspension B_{UR}

exhibits opposite softening effect, which causes considerably higher roll deflection response.

The addition of the anti-roll bar helps to reduce the peak roll angle response, as shown in Figure 5.8(b). The peak roll angle response of configuration B_{URb} is nearly identical to that of suspension A_{UR}, although the static roll stiffness of suspension A_{UR} is lower than that of suspension B_{URb}. The results presented in Figure 5.1 clearly show that the roll stiffness of suspension A_{UR} is significantly higher than that of B_{URb} under roll deflections greater than 0.04 rad. The steady-state roll deflection response of the vehicle with suspension A_{UR} is thus slightly lower, while the corresponding oscillation frequency is higher.

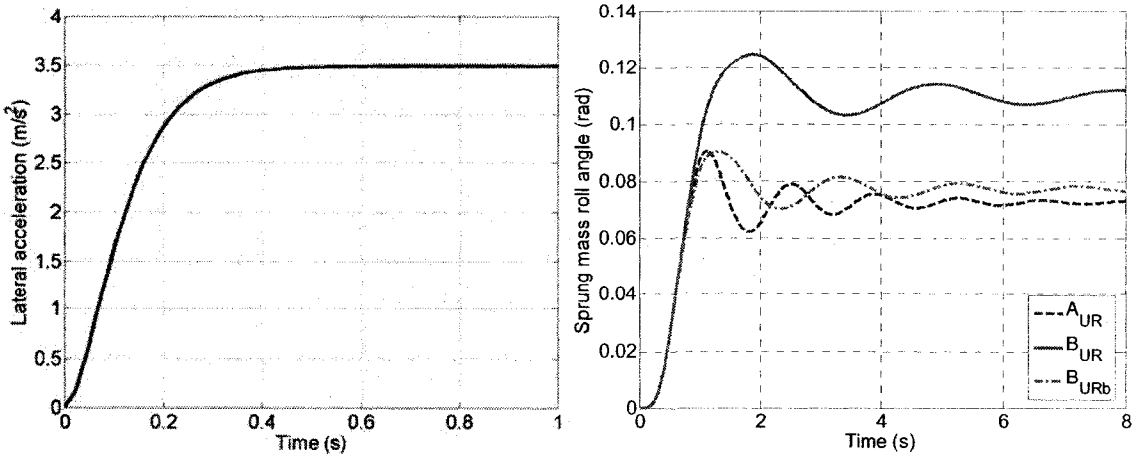

(a) (b)

Figure 5.8: (a) Rounded-step lateral acceleration excitation; and (b) sprung mass roll angle responses due to different suspension configurations.

RIDE CHARACTERISTICS UNDER RANDOM ROAD INPUTS

The relative ride vibration responses of the vehicle model with three suspension configurations are further evaluated under a range of random road inputs and vehicle speeds, in terms of rms sprung mass bounce and roll accelerations. The analyses are

performed under excitations arising from three different road profiles presented in Section 3.2.1, and two different constant vehicle speeds (70 and 100 km/h). Figures 5.9(a) and (b) illustrate the rms sprung mass bounce and roll acceleration responses of different suspension configurations, respectively. All the three suspensions yield nearly identical values of the rms bounce acceleration under the ranges of road roughness and speed considered, except that the suspensions B_{UR} and B_{URb} yield slightly lower values under *medium-rough* and *rough* road excitations. This is most likely attributed to the higher upward drift of suspension B_{UR} under relatively rough road excitations, which leads to lower effective suspension rate.

The suspensions A_{UR} and B_{UR} also exhibit very similar rms values of the sprung mass roll acceleration due to their identical static roll stiffness. The addition of an anti-roll bar, however, yields about 3~14% higher roll acceleration depending upon the vehicle speed and the road roughness due to its higher roll stiffness. The results indicate that the use of twin-gas-chamber struts affects the vertical and roll ride only slightly, while it significantly enhances the roll dynamics performance. The use of an anti-roll bar tends to deteriorate the roll ride quality, while its effect on the vertical ride is negligible.

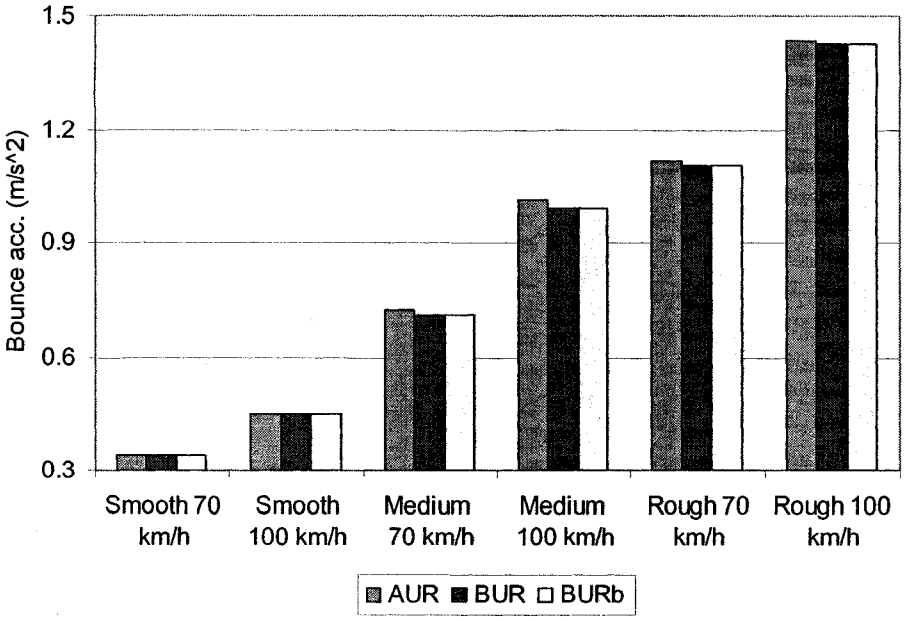

(a)

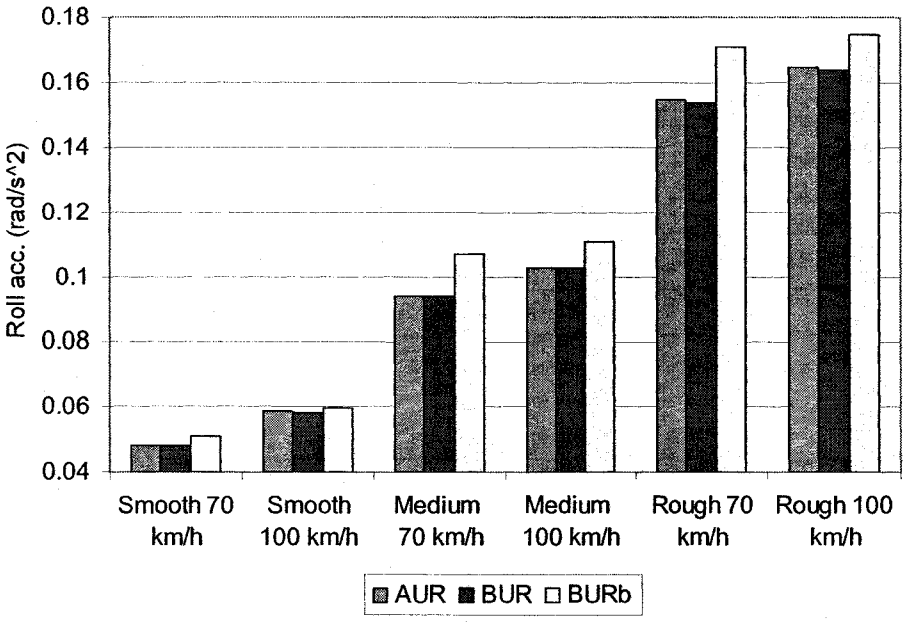

(b)

Figure 5.9: Comparisons of the sprung mass dynamic responses with different suspension configurations: (a) rms vertical acceleration; and (b) rms roll acceleration.

5.3 Pitch Plane Analysis of Twin-Gas-Chamber Strut Suspension

Compared to the roll plane analysis, pitch plane analysis of vehicle suspension systems may be more complex due to generally asymmetric and varying load

distributions, and wheelbase filtering effect. The load distribution in the roll plane is generally assumed to be symmetric about the vertical centerline, while the load distributions between the front and rear axles generally differ. In commercial freight and passenger transport vehicles, rear axles generally support considerably larger loads than the front axle.

In the previous chapter, the vehicle model was formulated for a load distribution of $l_f/(l_f+l_r)=0.653$, based on the measured and estimated data of a heavy vehicle [152]. The pitch stiffness properties of the unconnected (B_{UP}) and the interconnected (A_{IP34}, B_{IP13} and $H_{IP1\text{-}4}$) suspension configurations revealed softening tendency in the pitch stiffness with peak values at negative pitch-deflections, respectively, as seen in Figures 4.2(a) and 4.9(b). The results further showed that the peak stiffness occurs in the vicinity of zero pitch-deflection under an even load distribution. The results from this dissertation research have demonstrated this phenomenon for both the unconnected or interconnected suspension configuration [163]. This is also consistent with those observed in the roll stiffness property (Figure 3.7 and Figure 5.1). The results also revealed that a higher load distributed on the front axle would yield a peak pitch stiffness occurring under a positive pitch deflection.

However, the unconnected and interconnected suspension configurations invariably exhibit a softening effect in the roll and pitch stiffness properties in both directions. Since heavy vehicles experience negative pitch deflection under braking, a higher pitch stiffness corresponding to negative pitch deflections would help inhibit pitch attitude to some extent. The larger deflection caused by a severe braking maneuver, however, may

not correspond to peak pitch stiffness. This can also be seen from Figures 4.2(a) and 4.7(b), where the peak sprung mass pitch angle is about -0.017 rad for the unconnected configuration B_{UP}, while the pitch stiffness peaks near -0.009 rad. The softening effect in pitch stiffness would thus be undesirable for heavy vehicles under severe braking.

The roll properties and responses of twin-gas-chamber strut suspension, presented in Section 5.2, revealed hardening effect in roll stiffness with increasing roll deflection, which is opposite to the trends in roll properties of the single-gas-chamber strut suspension. It is hypothesized that the twin-gas-chamber struts could also yield similar hardening effect in the pitch stiffness. This property can be more easily realized for vehicles with greater proportion of the load on the front axle. The pitch plane analysis of twin-gas-chamber strut suspension A_{UP} (Figure 2.8) is performed based on a sport utility vehicle (SUV), with more load distributed on the front side. The simulation parameters of the vehicle model are summarized in Table 5.2 [140].

The mathematical formulations derived for the strut forces and pitch moments in Sections 2.6 and 2.7 are used to evaluate the vertical and pitch stiffness properties of the proposed suspension configurations, single-gas-chamber (A_{UP}) and twin-gas-chamber (B_{UP}). The design parameters of both the configurations are selected upon consideration of identical load carrying capacity for the SUV with a load distribution of $l_f/(l_f+l_r)=0.45$, which are also summarized in Table 5.2.

The selected design parameters for the A_{UP} and B_{UP} configurations resulted in identical bounce mode natural frequencies of the front and rear suspensions at the design ride height, in the order of 1.3 Hz. This is relatively lower than those of heavy vehicles,

due to the fact that heavy vehicles generally employ stiffer suspensions to achieve higher stability and safety limits [21, 110]. The sizes of the bleed and damping valves flow areas of the front suspension struts were chosen to achieve identical front-axle bounce mode damping properties of both the suspensions (A_{UP} and B_{UP}), which were realized by obtaining identical relationships between the damping-force and the strut-velocity. The identical rear-axle bounce mode damping properties of both the suspensions (A_{UP} and B_{UP}) were also achieved in a similar manner.

Table 5.2: Simulation parameters for the SUV model and the suspension struts.

Parameter	Value	Parameter	Value
	SUV		
m_s	1773 kg	k_t	216000 N/m
m_{uf}	98.5 kg	c_t	400 Ns/m
m_{uf}	98.5 kg	l_f	1.305 m
I_{yys}	3679 kgm^2	l_r	1.595 m
r_f	0.32 m	r_r	0.32 m
	Twin-gas-chamber struts		
A_{2f}	0.00252 m^2	A_{2r}	0.00206 m^2
A_{3f}	0.00063 m^2	A_{3r}	0.0005015 m^2
P_0	2000000 Pa		
	Single-gas-chamber struts		
A_{2f}	0.00252 m^2	A_{2r}	0.0206 m^2
A_{3f}	0.00126 m^2	A_{3r}	0.00103 m^2
P_0	2000000 Pa		

An additional configuration of each of the strut suspension is also conceived to achieve relatively lower natural frequency of the front-axle suspension but identical values of total static suspension stiffness (k_{vf0}+k_{vr0}). These configurations, employing twin- and single-gas-chamber struts, are referred to as A_{UPT} and B_{UPT}, respectively. Table

5.3 summarizes the static stiffness properties of the four suspension configurations. The results show that the effective pitch stiffnesses of configurations A_{UPT} and B_{UPT} are slightly larger than those of nominal suspensions A_{UP} and B_{UP}.

Table 5.3: Static suspension stiffness properties at the design right height.

Suspension configuration	A_{UP}, B_{UP}	A_{UPT}, B_{UPT}
Front suspension rate, k_{vf0} (kN/m)	695.52	625.52
Rear suspension rate, k_{vr0} (kN/m)	569.56	638.56
Pitch stiffness, k_{p0} (kNm/rad)	263.09	265.75

5.3.1 Pitch Plane Property Analysis

Figures 5.10(a) and (b) present the suspension rates of the front and rear struts, respectively, employed in the four configurations. The results suggest that the single-gas-chamber struts employed in configurations B_{UP} and B_{UPT} yield greater softening and hardening effects in extension and compression, respectively, compared to the twin-gas-chamber struts. The hardening/softening behaviors of the twin-gas-chamber struts in suspension configurations A_{UP} and A_{UPT} are considerably less aggressive. These are attributed to the effect of the gas in the uncoupled chamber 3 of the twin-gas-chamber strut. The suspension rates of front struts of configurations A_{UPT} and B_{UPT} remain smaller than those of the struts in suspensions A_{UP} and B_{UP} throughout the deflection range considered, while the rear strut suspension rates exhibit opposite trends, as it would be expected.

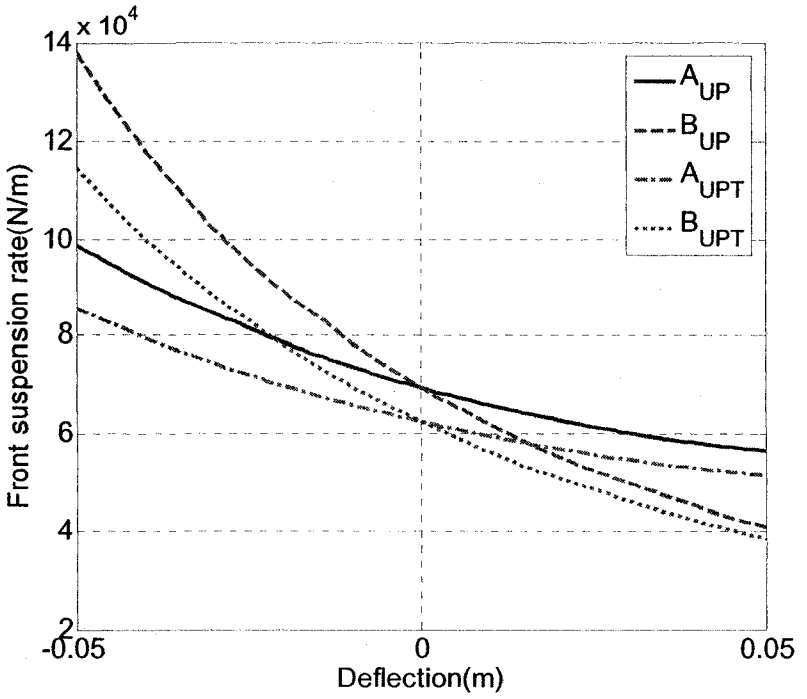
x 10^4
14
12
10
8
6
4
2
Front suspension rate(N/m)
-0.05
0
0.05
Deflection(m)
A_UP
B_UP
A_UPT
B_UPT

(a)

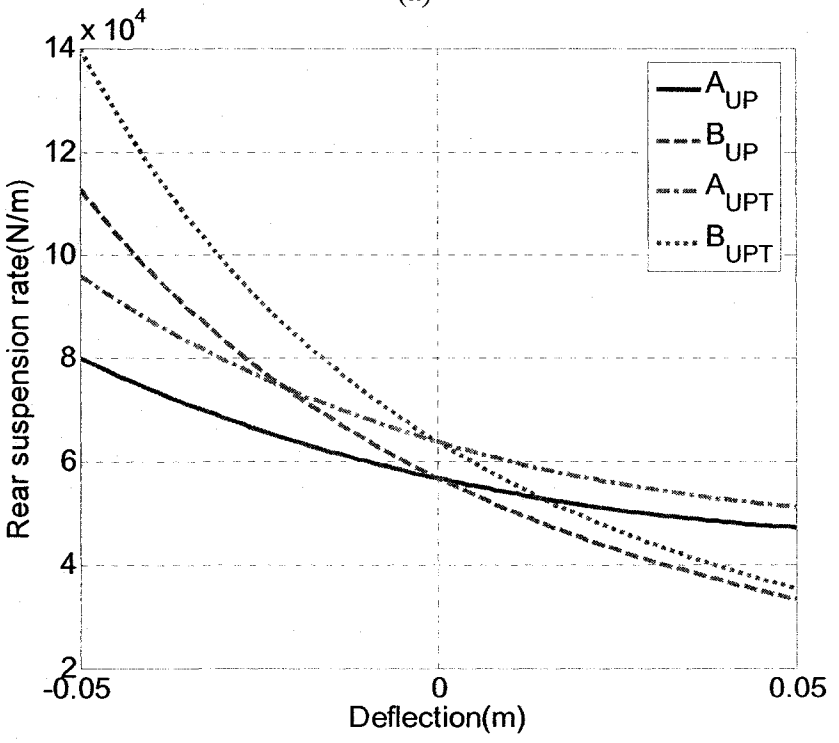
x 10^4
14
12
10
8
6
4
2
Rear suspension rate(N/m)
-0.05
0
0.05
Deflection(m)
A_UP
B_UP
A_UPT
B_UPT

(b)

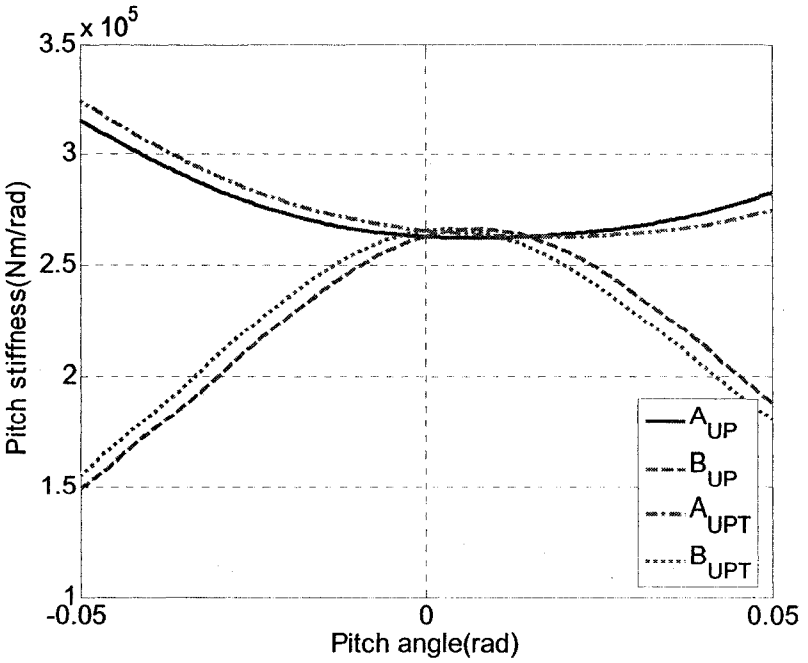

(c)

Figure 5.10: Comparisons of pitch-plane stiffness characteristics of different strut and suspension configurations: (a) front strut suspension rate; (b) rear strut suspension rate; and (c) pitch stiffness.

Figure 5.10(c) illustrates comparisons of pitch stiffness characteristics of different suspension configurations. The results clearly show considerably different properties of the twin-gas-chamber strut suspensions (A_{UP} and A_{UPT}) compared to those of the single-gas-chamber strut suspensions (B_{UP} and B_{UPT}). All the suspension configurations exhibit comparable values of pitch stiffness near the static ride height, with the static pitch stiffness of A_{UPT} and B_{UPT} configurations being slightly higher, as evident in Table 5.3. The pitch stiffnesses of the single-gas-chamber strut configurations, B_{UP} and B_{UPT}, decrease rapidly with increasing magnitude of pitch deflection, while those of the twin-chamber configurations, A_{UP} and A_{UPT}, increase. The configurations B_{UP} and B_{UPT}, however, exhibit only slightly higher pitch stiffness corresponding to deflections of +0.01 and +0.005 rad, respectively. The softening tendency in the pitch stiffnesses of configurations B_{UP} and B_{UPT} is attributed to the longitudinal load transfers and

considerable variations in the front and rear suspension rates. Such softening property in the pitch stiffness would be highly undesirable for pitch attitude control during braking/traction maneuvers, where relatively large pitch deflections are generally encountered. Compared to configurations B_{UP} and B_{UPT}, the twin-gas-chamber strut suspensions A_{UP} and A_{UPT} yield slightly lower pitch stiffness near the design ride height, but hardening effects in both the pitch deflection directions. This indicates a larger pitch stiffness corresponding to a larger pitch deflection, which is a desirable feature for inhibiting the pitch attitude variations under braking and acceleration inputs. Under positive pitch deflections, the configurations A_{UPT} and B_{UPT} with relatively soft front suspension design yield slightly lower values of pitch stiffness than those of the suspensions A_{UP} and B_{UP}, respectively. The opposite effects can be seen under negative pitch deflections.

5.3.2 Design Flexibility of Twin-Gas-Chamber Strut Suspension

The pitch plane stiffness property of a twin-gas-chamber strut suspension is closely related to the strut design parameters, especially the static gas pressure (P_0) and sizes of chambers 3 and 4, as seen in Equations (2.118) and (2.133). The design flexibility of the twin-gas-chamber strut suspension A_{UP} is thus explored through parametric analyses including variations in static gas pressure (P_0), the annular piston areas (A_{3i}; $i=f,r$) and the initial lengths (x_{30i} and x_{40i}) of gas chambers 3 and 4, respectively, while areas (A_{4i}) of chambers 4 are assumed to be constant. The variations in P_0 would directly influence the load carrying capacity, while the variations in the chambers parameters A_{3i}, x_{30i} and x_{40i} do not affect the suspension load carrying capacity.

Figure 5.11 presents the effects of variations in the static gas pressure (P_0) on the bounce and pitch stiffness properties of the twin-gas-chamber strut suspension A_{UP}, which are obtained by varying P_0 by $\pm 20\%$ about its nominal value. An increase in P_0, as expected, yields higher suspension rates of each strut with significant increase in pitch stiffness. The influence of variations in the annular piston areas (A_{3i}) on the bounce and pitch stiffness characteristics of the twin-gas-chamber strut suspension A_{UP} is illustrated in Figure 5.12.

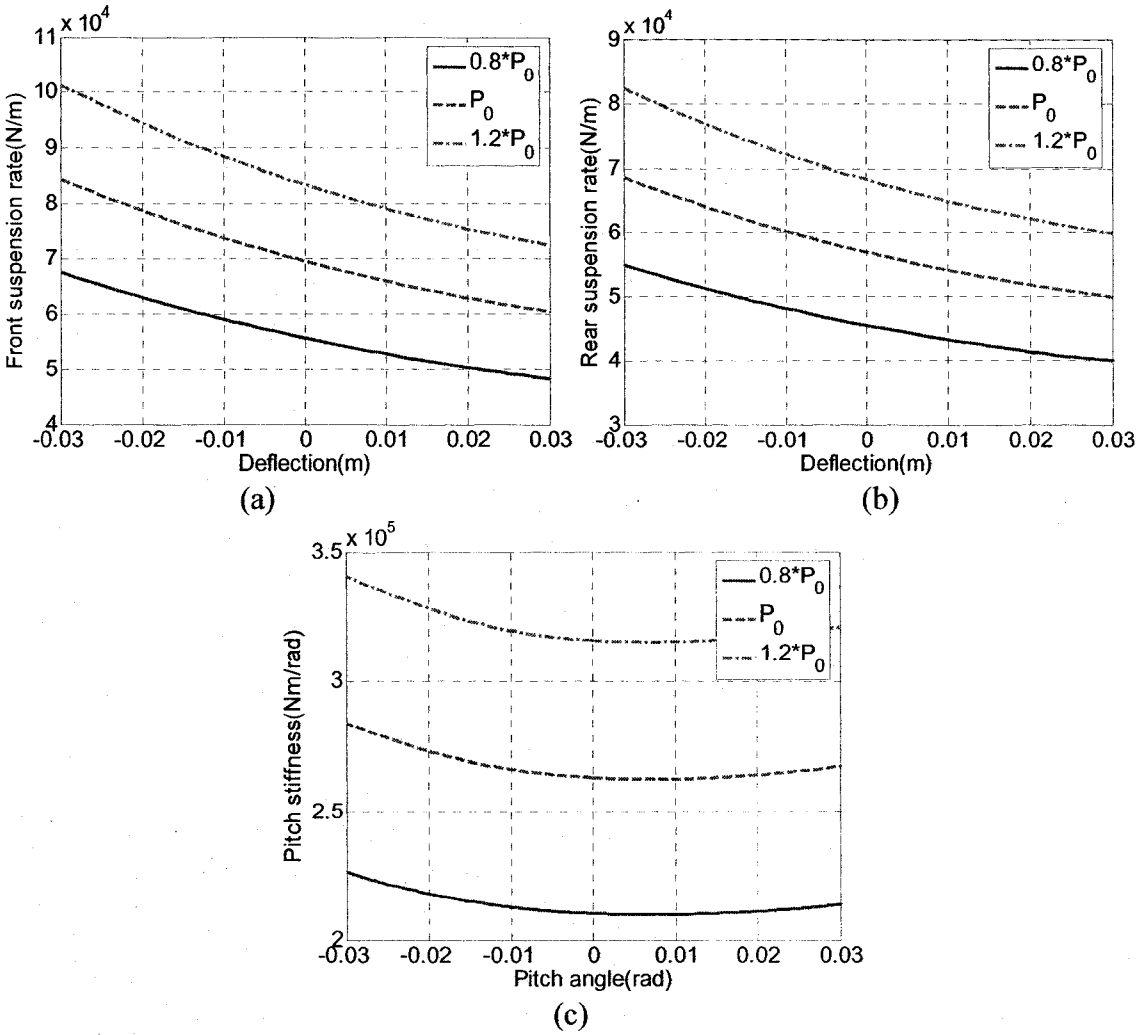

Figure 5.11: Influence of variations in static gas pressure P_0 on pitch-plane properties of the twin-gas-chamber strut suspension A_{UP}: (a) front strut suspension rate; (b) rear strut suspension rate; and (c) pitch stiffness.

The results are attained by varying A_{3i} by ± 20% about its nominal value, respectively. The results suggest that an increase in the gas volume in chamber 3, realized by increasing the annular piston areas (A_{3i}), causes higher suspension rates of the struts, and higher pitch stiffness. However, unlike the variations in P_0, the variations in A_{3i} do not influence the load carrying capacity. This suggests that for a particular load condition, the suspension bounce and pitch stiffness properties can be conveniently tuned through selection of an appropriate A_{3i}.

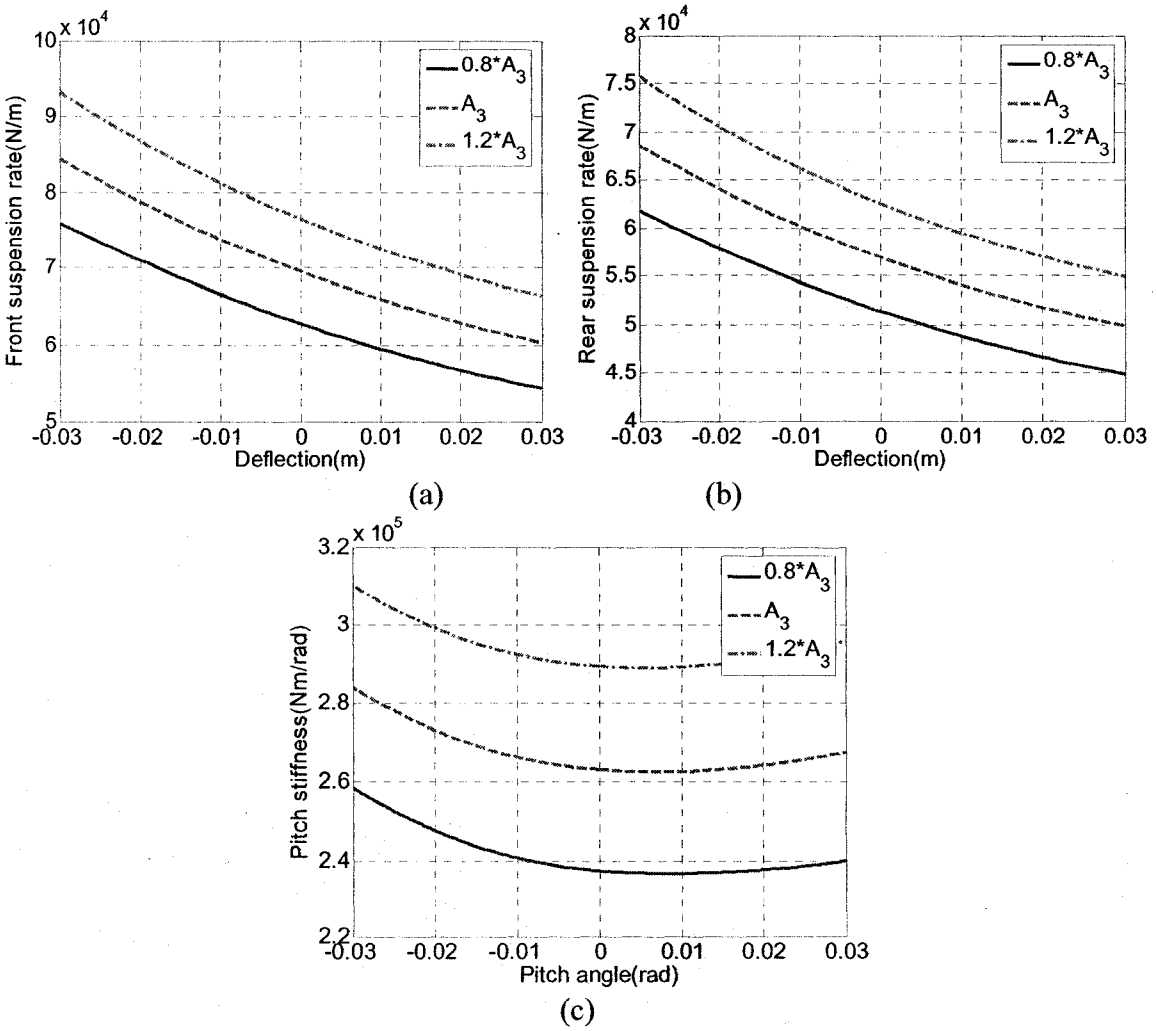

Figure 5.12: Influence of variations in annular piston areas A_{3i} (i=f,r) on pitch-plane properties of the twin-gas-chamber strut suspension A_{UP}: (a) front strut suspension rate; (b) rear strut suspension rate; and (c) pitch stiffness.

Figures 5.13 and 5.14 further illustrate the effects of variations in gas volumes in chambers 3 and 4, respectively, realized by varying the chamber lengths, on the stiffness properties of the twin-gas-chamber strut suspension A_{UP}. The results show that a decrease in initial length of either chamber 3 or 4 would yield higher suspension rates and thus pitch stiffness, which can be easily evaluated from Equation (2.118) by assuming zero strut-deflection (or at static design ride height).

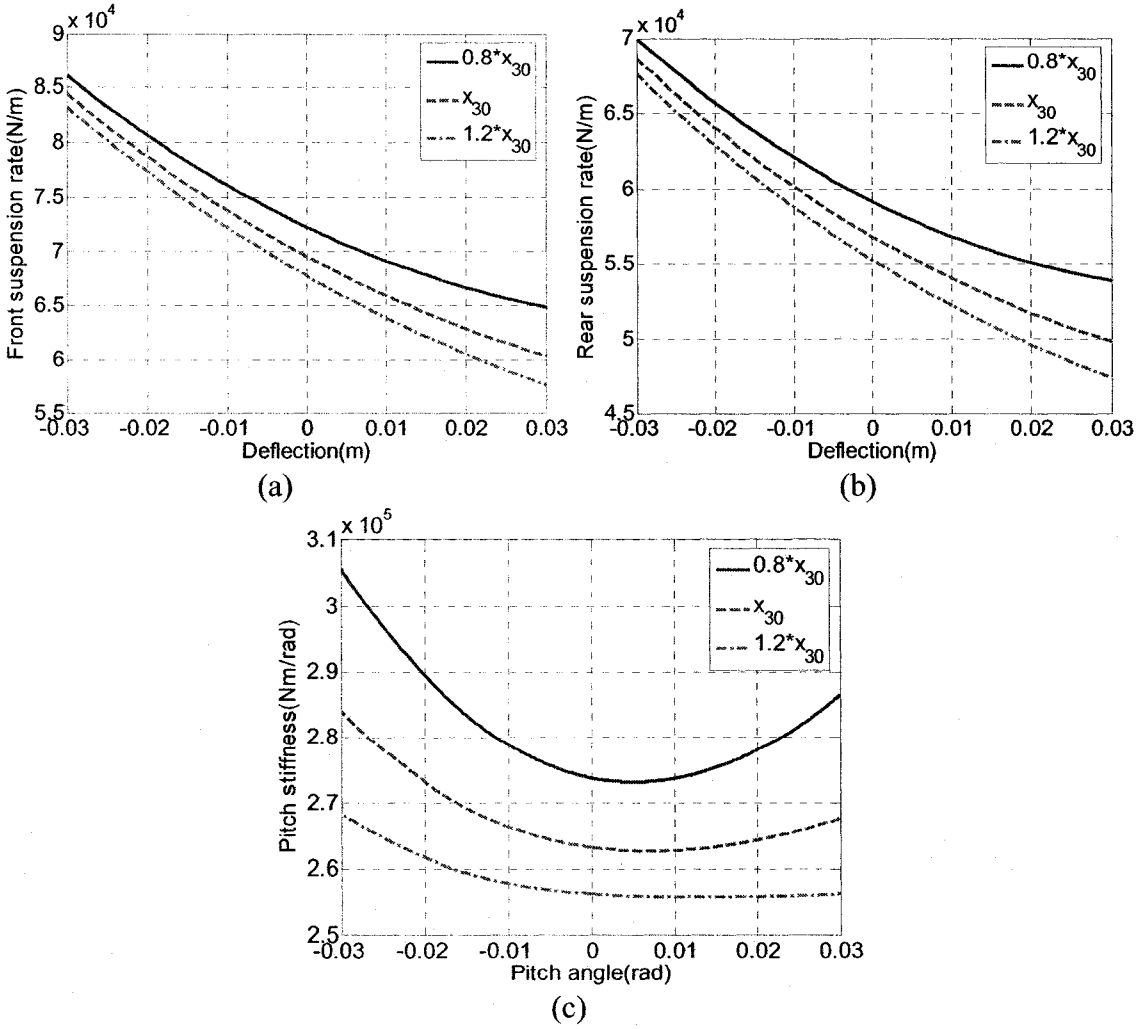

Figure 5.13: Influence of variations in initial lengths of gas chambers 3 on pitch-plane properties of the twin-gas-chamber strut suspension A_{UP}: (a) front strut suspension rate; (b) rear strut suspension rate; and (c) pitch stiffness.

The variations in the length of gas chamber 3, however, show more pronounced effect on the suspension rate in rebound than in compression, while the variations in length of chamber 4 exhibit an opposite effect. This is attributed to the fact that chambers 3 and 4 dominant the suspension rates in rebound and compression motions, respectively. The results presented in Figures 5.10 to 5.14 demonstrate that the twin-gas-chamber strut suspension offers considerable tuning flexibility and potential to realize desirable suspension properties in the bounce and pitch modes.

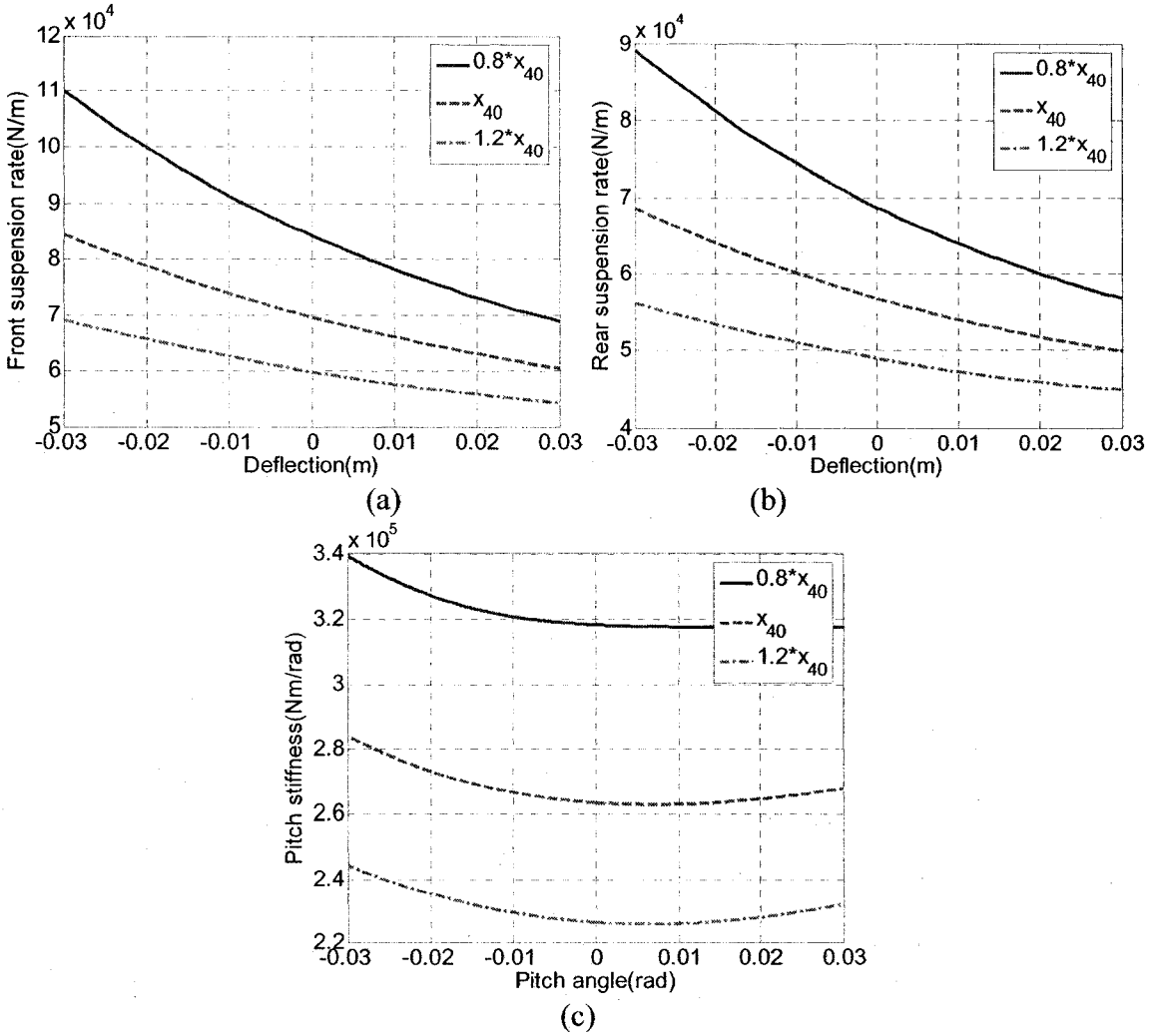

Figure 5.14: Influence of variations in initial lengths of gas chambers 4 on pitch-plane properties of the twin-gas-chamber strut suspension A_{UP}: (a) front strut suspension rate; (b) rear strut suspension rate; and (c) pitch stiffness.

5.3.3 Dynamic Responses

The relative dynamic response characteristics of the four suspension configurations (A_{UP}, B_{UP}, A_{UPT} and B_{UPT}) are further evaluated in terms of vertical and pitch responses, subject to excitations arising from random road roughness and braking maneuvers. The stiffness properties of all the four suspensions have been shown in Figure 5.10.

RESPONSES UNDER RANDOM ROAD ROUGHNESS EXCITATIONS

The relative ride dynamic responses of the vehicle model with different suspension configurations are evaluated under excitations arising from the three random road inputs, described in Section 3.2.1. The equations of motion for the vehicle model (Equation (2.91)) integrating different suspension configurations are analyzed together with formulations of the dynamic strut forces described in Equations (2.110) and (2.111). Considering the wheelbase filtering effect, the analyses are performed over a wide range of driving speeds: 30, 50, 70, 90 and 110 km/h. The relative performance characteristics of different suspension systems are evaluated in terms of: (a) rms pitch and bounce accelerations, considered as simplified measures of the vibration ride comfort [45]; (b) rms pitch angle of the sprung mass, a measure of the vehicle attitude; (c) rms front and rear suspension travels, which can provide the rattlespace design requirements; and (d) rms front and rear dynamic tire deflections (DTD), which could serve as measures of the vehicle roadholding quality [6].

Figure 5.15 illustrates the rms sprung mass bounce acceleration responses of the vehicle model with four different suspension configurations to excitations arising from three road roughness profiles at different speeds. The results show that the sprung mass

bounce acceleration response increases with an increase in road roughness and vehicle speed, irrespective of the suspension configuration. All the four suspension configurations (A_{UP}, B_{UP}, A_{UPT} and B_{UPT}) yield very similar bounce acceleration response of the sprung mass, irrespective of the road roughness and forward speed. Both the A_{UPT} and B_{UPT} configurations with softer front-axle struts generally yield only slightly higher rms accelerations than the suspensions A_{UP} and B_{UP}.

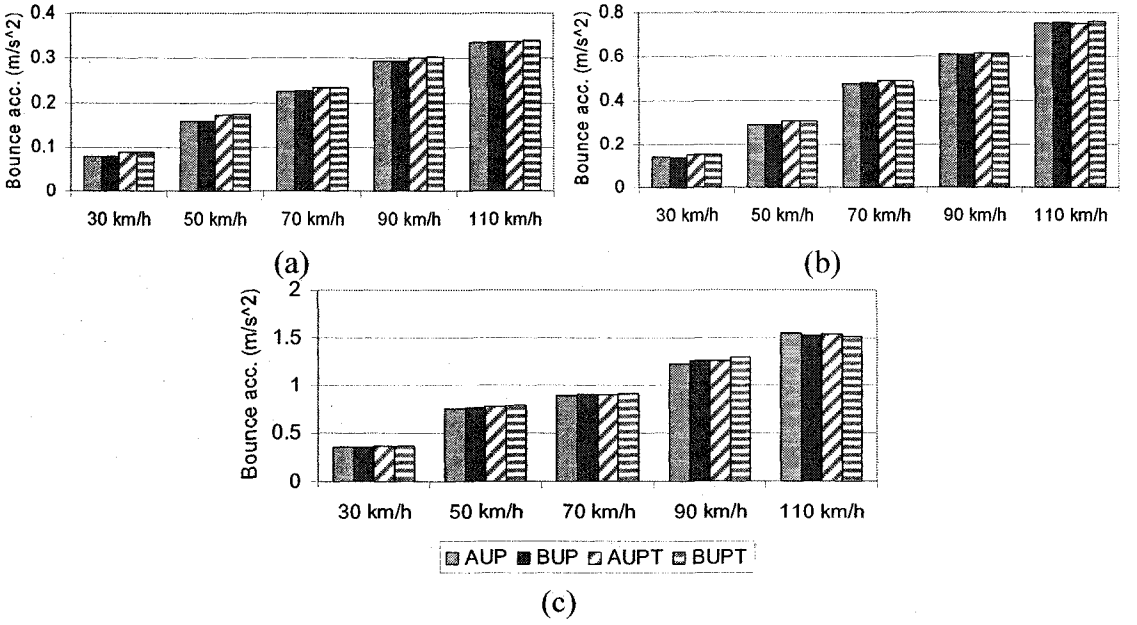

Figure 5.15: Comparisons of rms sprung mass bounce acceleration responses of the vehicle model with different suspension configurations under different road excitations: (a) smooth; (b) medium-rough; and (c) rough.

The rms pitch acceleration and displacement responses of the sprung mass of the vehicle model with the four suspension configurations are presented in Figure 5.16, subject to the selected road excitations. The rms pitch acceleration and deflection responses also increase with increasing road roughness. Unlike the bounce acceleration response, the pitch responses show inconsistent trend with variations in the forward speed. The pitch deflection responses of the A_{UPT} and B_{UPT} configurations tend to decrease with increasing vehicle speed when the vehicle operates at speeds above 50

km/h, irrespective of road roughness. This trend is also observed for A_{UP} and B_{UP} suspensions for *smooth* and *medium-rough* roads. The pitch deflection responses to *rough* road excitations do not show a definite pattern with vehicle speed, most likely attributed to the wheelbase filtering effect. The A_{UP} and B_{UP} suspensions yield comparable rms values of pitch acceleration and deflection responses, which is due to their comparable pitch stiffness properties near the static right height. Configurations A_{UPT} and B_{UPT} with relatively soft front suspension struts tend to yield lower acceleration and deflection responses. The average reductions in rms acceleration and deflection are obtained as 7% and 20%, respectively, compared to those of configurations A_{UP} and B_{UP}.

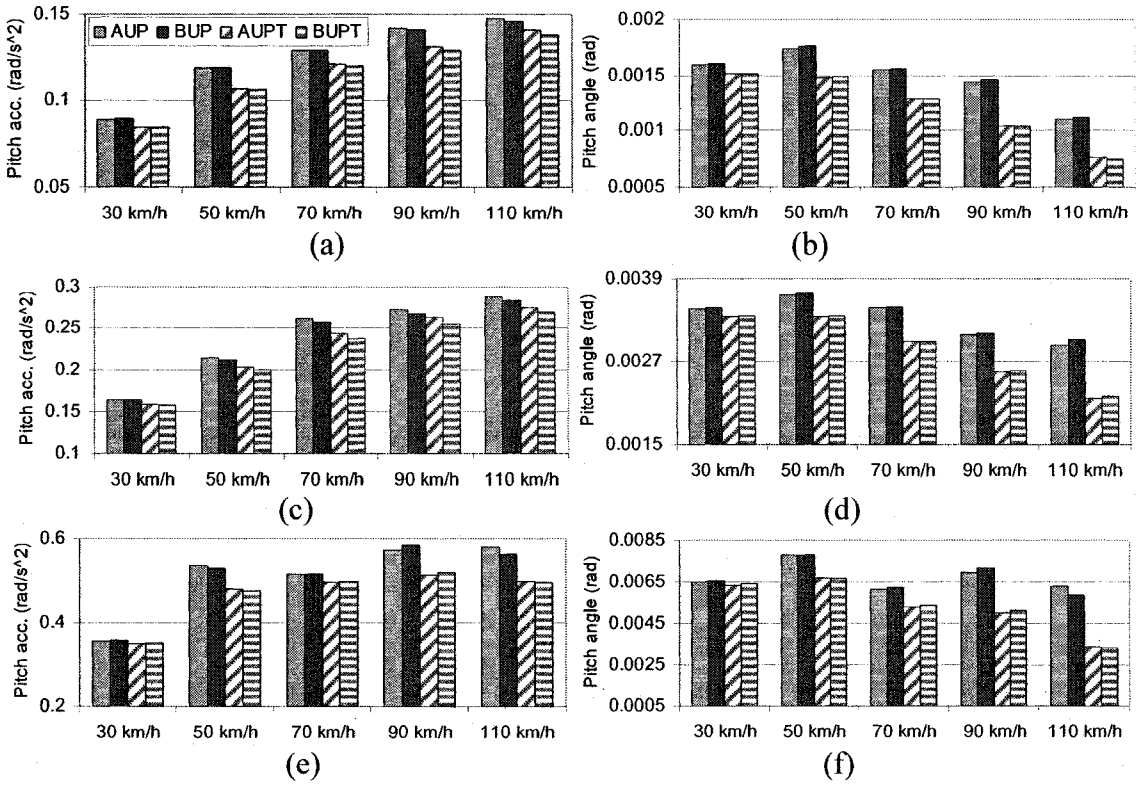

Figure 5.16: Comparisons of rms sprung mass pitch responses of the vehicle model with different suspension configurations under different road excitations: (a) pitch acceleration-smooth road; (b) pitch deflection-smooth road; (c) pitch acceleration-medium-rough road; (d) pitch deflection-medium-rough road; (e) pitch acceleration-rough road; and (f) pitch deflection-rough road.

The results from Figures 5.15 and 5.16 suggest that the two suspension configurations (A_{UP} and B_{UP}) yield very similar vertical ride vibration comfort, while the configurations A_{UPT} and B_{UPT} with relatively soft front suspension could provide improved pitch ride and pitch deflection responses without influencing the vertical ride.

The rms values of front and rear suspension travels of different suspension configurations are illustrated in Figure 5.17 under excitations arising from the three road profiles and different speeds. The results show that both the front and rear suspension travel responses increase with increasing road roughness or vehicle velocity, with only one exception (*rough* road at 70 km/h). All the four suspension configurations yield quite comparable rms values of the suspension travels. The configurations A_{UP} and A_{UPT}, however, yield slightly lower rms values of the front suspension travel, compared to the configurations B_{UP} and B_{UPT}, respectively. The rms DTD responses of the vehicle model with different suspension configurations are presented in Figure 5.18. Similar to the suspension travel responses, the rms DTD responses also increase with an increase in road roughness or vehicle speed. Configurations A_{UP} and B_{UP} yield nearly identical front as well as rear DTD responses, while similar results are also observed for the suspensions A_{UPT} and B_{UPT}. The front DTD responses of the vehicle model with the configurations A_{UP} and B_{UP}, however, are slightly larger than those of the model with A_{UPT} and B_{UPT} suspensions. The rear DTD responses, however, exhibit opposite trends. The results in Figures 5.17 and 5.18 suggest that the twin-gas-chamber strut suspension could provide a slight gain in the suspension travel responses with only minimal effect on the dynamic tire deflections. The relatively soft front suspension designs in configurations A_{UPT} and

B_{UPT} yield only slight influence on the suspension travel and overall tire deflection responses.

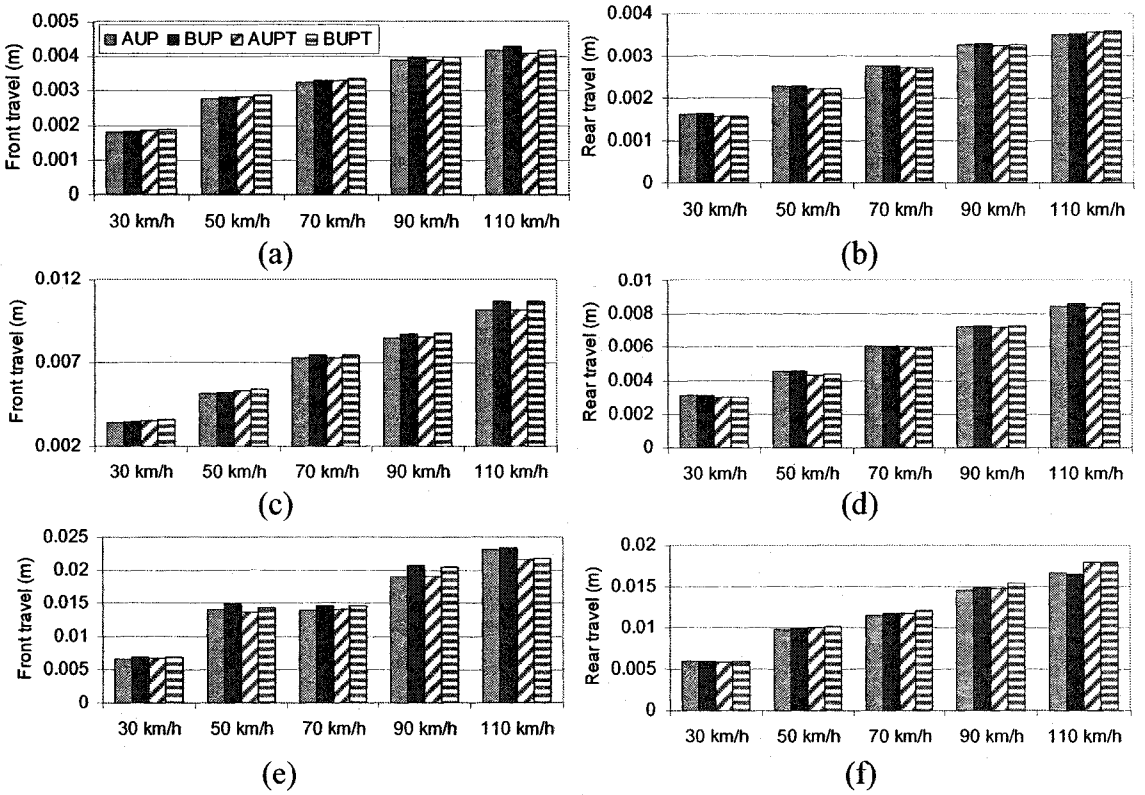

Figure 5.17: Comparisons of rms suspension travel responses of the vehicle model with different suspension configurations under different road excitations: (a) front travel-smooth road; (b) rear travel-smooth road; (c) front travel-medium-rough road; (d) rear travel-medium-rough road; (e) front travel-rough road; and (f) rear travel-rough road.

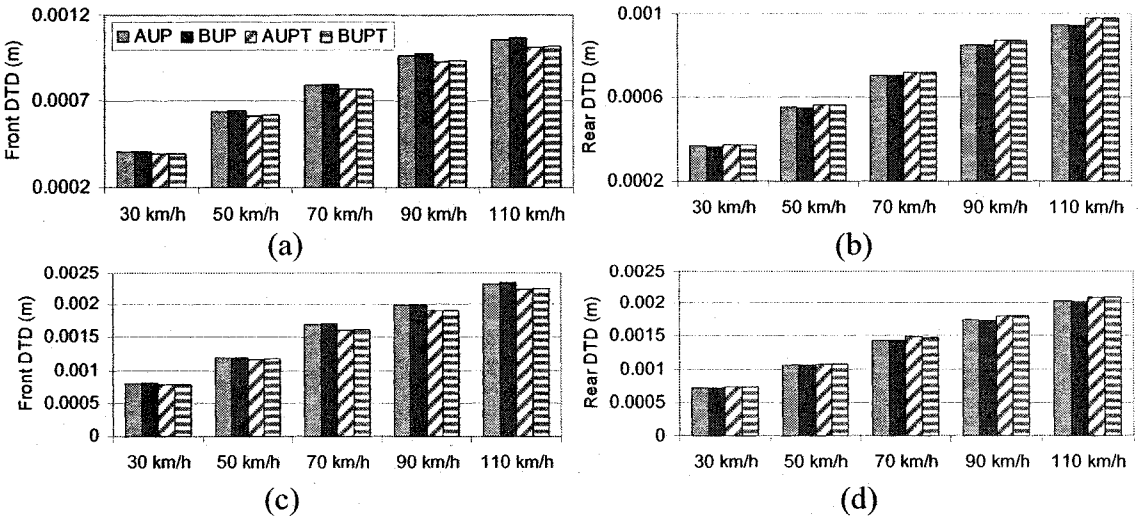

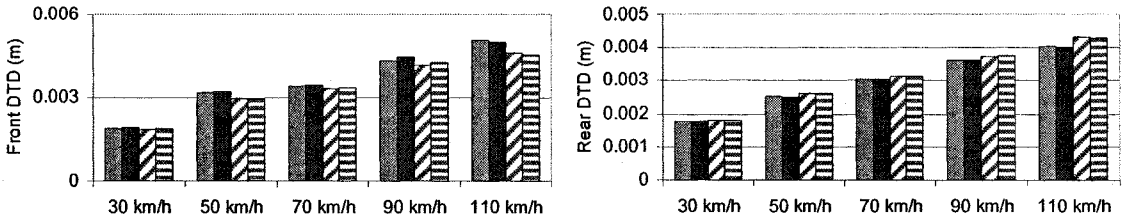

(e) (f)

Figure 5.18: Comparisons of rms DTD responses of the vehicle model with different suspension configurations under different road excitations: (a) front DTD-smooth road; (b) rear DTD-smooth road; (c) front DTD-medium-rough road; (d) rear DTD-medium-rough road; (e) front DTD-rough road; and (f) rear DTD-rough road.

STRAIGHT-LINE BRAKING RESPONSES

The relative performance characteristics of the proposed suspension configurations are also evaluated in terms of dynamic responses of the vehicle under straight-line braking inputs applied for speed correction. The responses to such inputs can be effectively evaluated in terms of sprung mass pitch angle and suspension travel. The initial vehicle speed is set as 90 km/h, while the braking torque distribution is selected proportional to the static load distribution, using the braking torque model presented in Equation (4.1). The model parameters used in the analyses are summarized in Table 5.4, while the corresponding braking torques applied to the front and rear wheels are illustrated in Figure 5.19. Two road surfaces with different friction characteristics are considered for the analyses: (*a*) a dry road with friction coefficient of 0.9, referred to as '*dry surface*'; and (*b*) a wet road with friction coefficient of 0.5, referred to as '*wet surface*'.

Table 5.4: Braking torque model parameters.

Parameters	b_1	b_2	b_3	b_4	b_5	b_6	b_7	b_8
Front	1610	0.1	16	4	1	1.4	5	5
Rear	1345	0.1	16	4	1	1.4	5	5

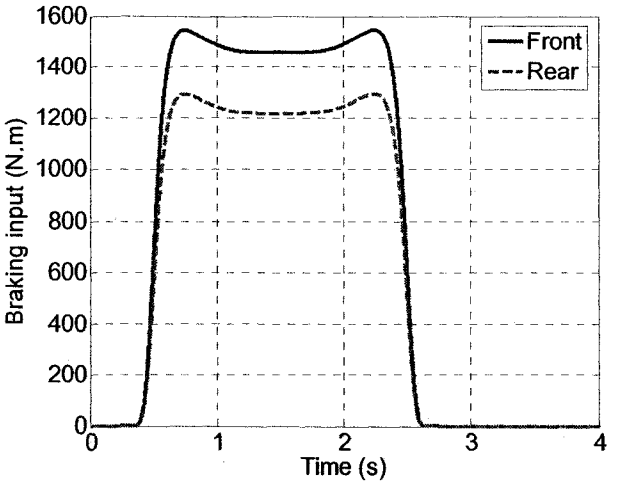

Figure 5.19: Variations in the front and rear braking torque inputs derived from the proposed model.

Figure 5.20 illustrates the sprung mass bounce and pitch acceleration responses of the vehicle model with different suspension configurations subject to braking inputs on the *dry surface*. The results clearly show that the suspension configurations B_{UP} and B_{UPT} yield significantly larger peak bounce acceleration responses compared to the twin-gas-chamber strut suspension configurations A_{UP} and A_{UPT}. Configurations A_{UPT} and B_{UPT} with relatively soft front struts yield slightly lower peak bounce accelerations, compared to configurations A_{UP} and B_{UP}, respectively. Configurations A_{UP} and A_{UPT} yield 60% and 87% lower peak bounce accelerations, respectively, compared to B_{UP} suspension, as evident in Figure 5.20(a). The configuration B_{UPT} with softer front strut also yields a reduction of 14% in the peak acceleration, compared to the B_{UP} suspension. Configurations A_{UPT} and B_{UPT} with relatively soft front struts yield pitch acceleration responses similar to those of configurations A_{UP} and B_{UP}, respectively.

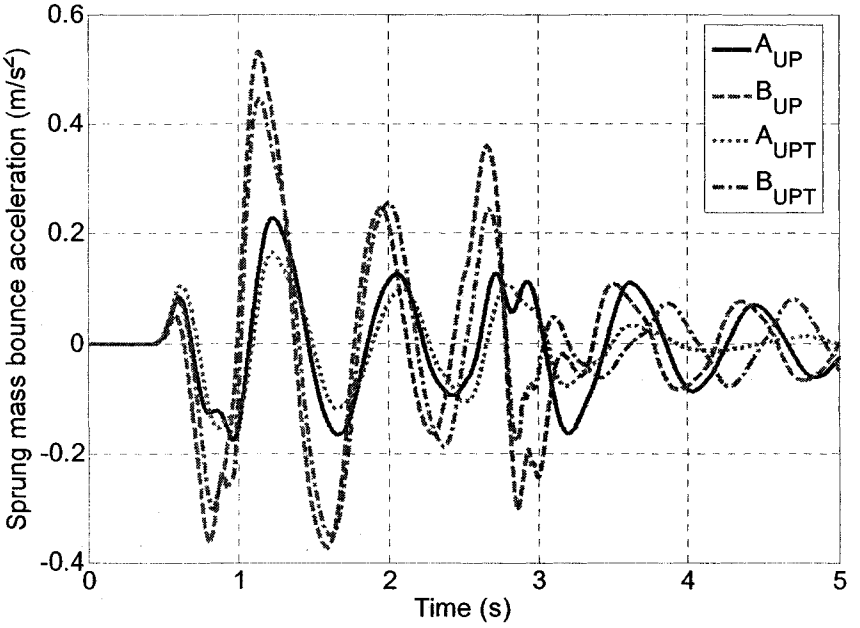

(a)

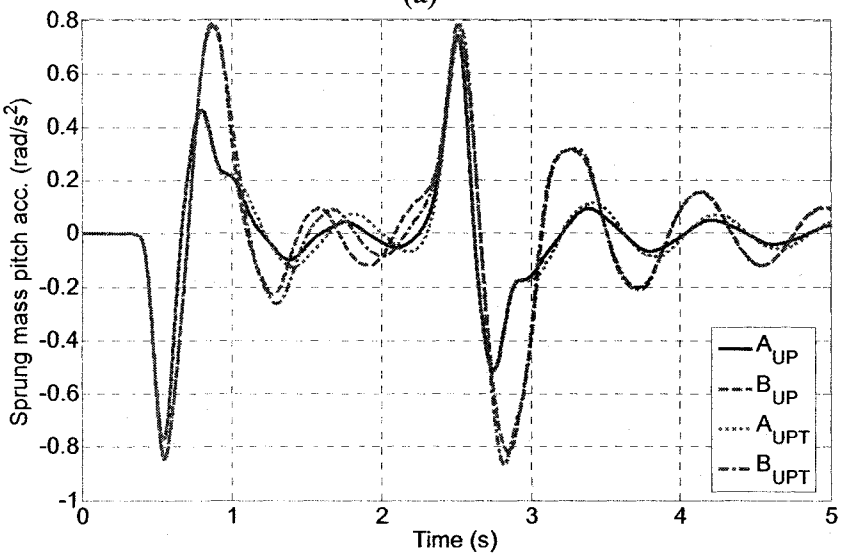

(b)

Figure 5.20: Comparisons of sprung mass bounce and pitch acceleration responses of the vehicle model with different suspension configurations under braking inputs on the dry surface: (a) bounce acceleration; and (b) pitch acceleration.

The twin-gas-chamber strut suspension, however, tends to reduce the magnitude of the pitch accelerations by approximately 40%, corresponding to some of the peaks, as seen in Figure 5.20(b). Furthermore, the pitch acceleration responses due to configurations A_{UP} and A_{UPT} decay more quickly than those of configurations B_{UP} and

B_{UPT}. Similar trends were also observed for responses to braking on the *wet surface* (results are not presented). The results suggest that the twin-gas-chamber strut suspension could enhance the bounce and pitch ride comfort during braking maneuvers, while the relatively soft front suspension design could further improve bounce ride under braking inputs.

Figure 5.21 presents pitch attitude and suspension travel responses of different suspension configurations under braking inputs on the *dry surface*. The results show that the suspensions A_{UPT} and B_{UPT} with relatively soft front struts yield sprung mass pitch angle responses similar to those of configurations A_{UP} and B_{UP}, respectively. The twin-gas-chamber strut suspension configurations A_{UP} and A_{UPT}, however, yield nearly 25% reduction in the peak pitch angle responses, compared to suspensions B_{UP} and B_{UPT}. Moreover, the pitch angle responses due to configurations A_{UP} and A_{UPT} decay more quickly. Furthermore, the configurations A_{UP} and A_{UPT} yield considerably lower peak suspension travels, compared to B_{UP} and B_{UPT}, respectively. The peak front suspension travels of configurations A_{UP} and A_{UPT} are approximately 10% and 14% lower than those of suspensions B_{UP} and B_{UPT}, respectively. Such reductions in peak rear suspension travel are far more significant, in the order of 30%. The more rapid decay in suspension travel due to the twin-gas-chamber strut suspensions can also be observed. The relatively soft front suspensions (A_{UPT} and B_{UPT}) yield relatively larger front suspension travels, but lower peak travels of the rear struts compared to configurations A_{UP} and B_{UP}, respectively. Similar trends were also observed in responses to braking on the *wet surface*. The results presented in Figures 5.20 and 5.21 suggest that the twin-gas-chamber strut suspension could considerably enhance the bounce and pitch ride vibration comfort,

pitch attitude control and suspension travel responses during braking maneuvers. The results also suggest that a relatively soft front suspension design could further improve the bounce ride during barking.

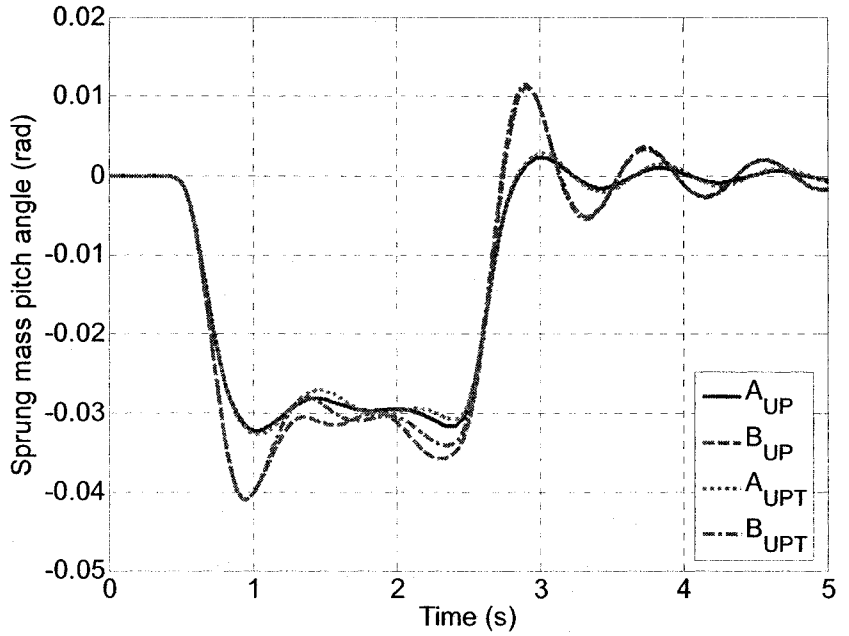

(a)

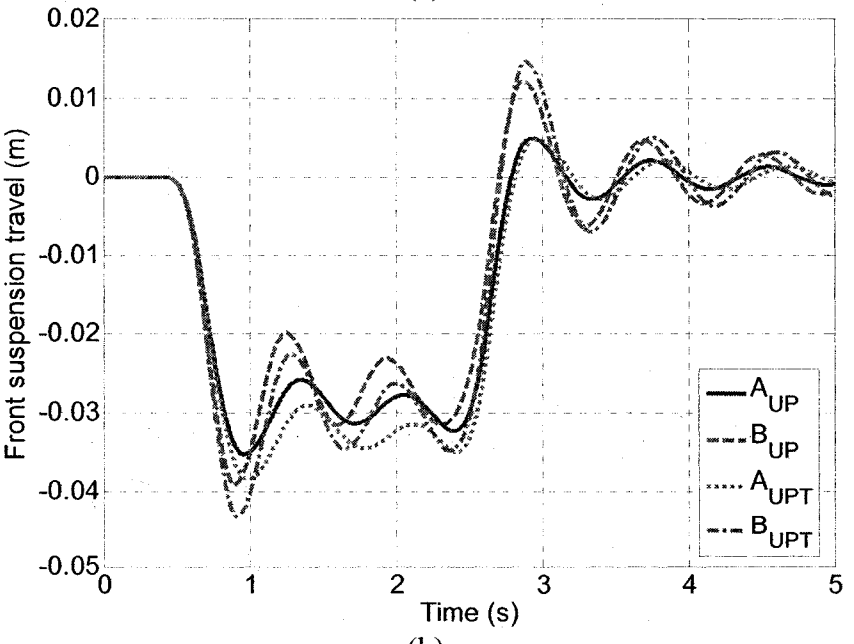

(b)

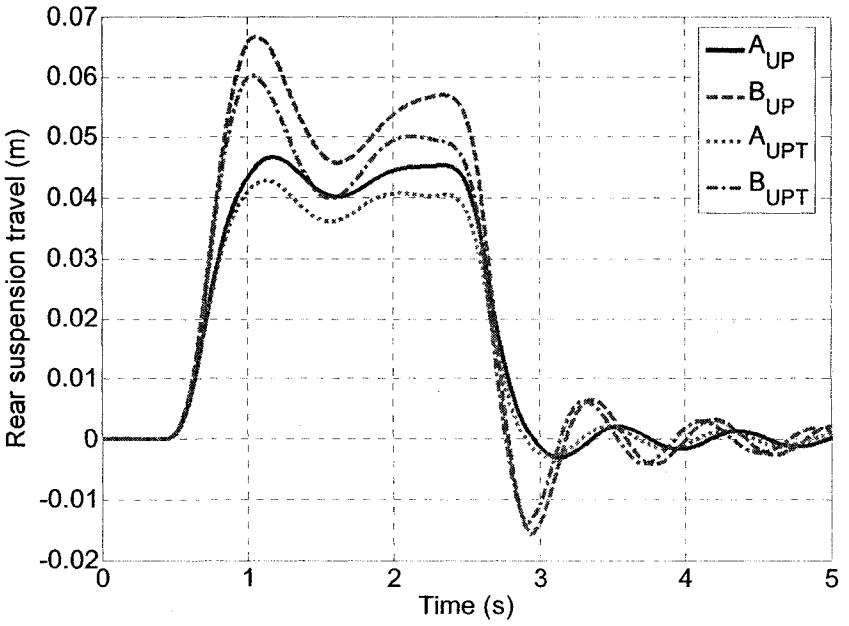

(c)

Figure 5.21: Comparisons of pitch attitude and suspension travel responses of the vehicle model with different suspension configurations under braking inputs on the dry surface: (a) sprung mass pitch angle; (b) front suspension travel; and (c) rear suspension travel.

5.4 Fundamental Pitch Dynamics and Suspension Tuning of Heavy Vehicles

From the comprehensive literature review, it was concluded that the fundamental aspects of vehicle pitch dynamics have received far less attention, particularly the theoretical foundations and the design rules. Such efforts are mostly non-existent for the heavy vehicles, although the pitch motions are known to strongly influence the vehicle ride quality, passenger/driver perception of comfort or annoyance, attitude control, and braking and handling performance characteristics, particularly when the tire-road adhesion limits are approached. In the course of this dissertation research, fundamental pitch dynamics and suspension tuning of heavy vehicles are explored through analytical and simulation studies. The formulations and the results have been accepted for publication in the journal *Vehicle System Dynamics*, and presented in Appendix A. The theoretical formulations are presented for three fundamental dimensionless measures of

the pitch-plane suspension properties proposed on the basis of a generalized pitch plane model of a two-axle vehicle model. The relationships among the three fundamental measures are further presented in order to develop essential design rules. Fundamental relationships between the vehicle responses and the proposed three dimensionless measures are further explored to establish a set of suspension tuning rules in the pitch plane, which does not yet exist for heavy vehicles.

5.5 Summary

The analyses of the proposed twin-gas-chamber strut suspension were performed in terms of roll- as well as pitch-plane suspension properties and dynamic responses of the vehicle. The responses are compared with those of an unconnected single-gas-chamber strut suspension. The simulation results on the properties showed that the proposed twin-gas-chamber struts yield nearly symmetric but progressively hardening suspension rates in both the compression and extension, as opposed to the conventional air suspensions and single-gas-chamber strut suspension that generally cause softening in rebound. Unlike conventional suspensions, the roll or pitch stiffness of the proposed twin-gas-chamber struts also revealed progressively hardening effect with increasing roll or pitch deflections, respectively, attributed to the novel twin-gas-chamber design. The dynamic responses of the road vehicles with different suspensions were also evaluated under various excitations. From the simulation results, it is concluded that the proposed twin-gas-chamber strut design offers considerable potential for enhancing vehicle attitude control, roll stability, braking performance, handling and ride characteristics of road vehicles, due to its nearly symmetric vertical stiffness in compression and rebound, and progressively hardening roll/pitch stiffness property. Moreover, the proposed design

offers superior design flexibility and a light weight alternative to anti-roll bar. The fundamental pitch dynamics and suspension tuning of heavy vehicles were further explored, and a set of suspension tuning rules were established based on the analytical and simulation analyses (Appendix A).

CHAPTER 6

ANALYSIS OF FULL-VEHICLE INTERCONNECTED SUSPENSION SYSTEM

6.1 Introduction

The potential benefits of in-plane interconnected hydro-pneumatic suspensions have been demonstrated in the previous chapters, based on either roll- or pitch-plane vehicle model. In these analyses, some of performance measures derived from the in-plane vehicle models could be treated as indirect indicators for vehicle handling quality and directional stability. A more effective evaluation of handling dynamics and directional stability of road vehicles, however, generally necessitates a relatively more comprehensive vehicle model, such as full-vehicle model with yaw and lateral DOF that strongly affect the handling [4, 6, 14, 15, 32, 53, 81]. Furthermore, a 3-D full-vehicle model is essential for investigating the effects of different suspension systems on the coupled vehicle roll, pitch, and directional responses.

This chapter focuses on exploring interconnected hydro-pneumatic suspension systems in a full-vehicle arrangement that involves four suspension-strut units. A 14-DOF full-vehicle model is analytically developed and validated using the measured data. The different suspension systems, either interconnected or unconnected, are subsequently evaluated using the validated model. The feasibilities of various full-vehicle interconnected suspensions involving the two previously-proposed hydro-pneumatic struts are analyzed based on a simplified measure for heavy vehicles. The fundamental suspension properties and vehicle dynamic responses of a hydraulically X-coupled suspension system are investigated and compared with an unconnected suspension

system. The suspension stiffness and damping properties are evaluated in terms of four fundamental modes, namely bounce, roll, pitch and warp. The analytical formulations of strut forces and suspension properties due to both suspension systems connected and unconnected are derived and compared. The dynamic responses of the vehicle model with both suspensions are further evaluated under braking-in-a-turn and split-μ straight-line braking inputs.

6.2 Development of a Generalized 3-D Full-Vehicle Model

A generalized 14-DOF two-axle full-vehicle model is developed to investigate vehicle dynamic responses due to different interconnected or unconnected suspension systems under steering and braking inputs, as well as excitations arising from road roughness and crosswinds. The vehicle model, shown in Figure 6.1, includes six DOFs of the sprung mass, two DOFs (bounce and roll) of each unsprung mass, and one rotational DOF of each of the tire-wheel assembly, as summarized in Table 6.1. The sprung mass is assumed to rotate about its roll axis [1, 4, 21]. The vehicle attitude and position with respect to the inertial system *XYZ* are derived through successive coordinate-transformations through Euler angles (roll θ, pitch φ, and yaw ψ) [53, 81]. The identical front-wheel steering input (δ_f) is assumed for both the front wheels, while the rear-wheel steering input (δ_r) can also be conveniently included in the vehicle model, which permits the analyses of vehicles with four-wheel-steering [53, 81]. For analyses of front-wheel-steering vehicles, the rear-wheel steering input is simply assumed to be zero. The excitations arising from crosswinds can be effectively modeled by an equivalent force (f_{wind}) directly applied to the vehicle c.g. together with a yaw moment (M_{wind}) [164].

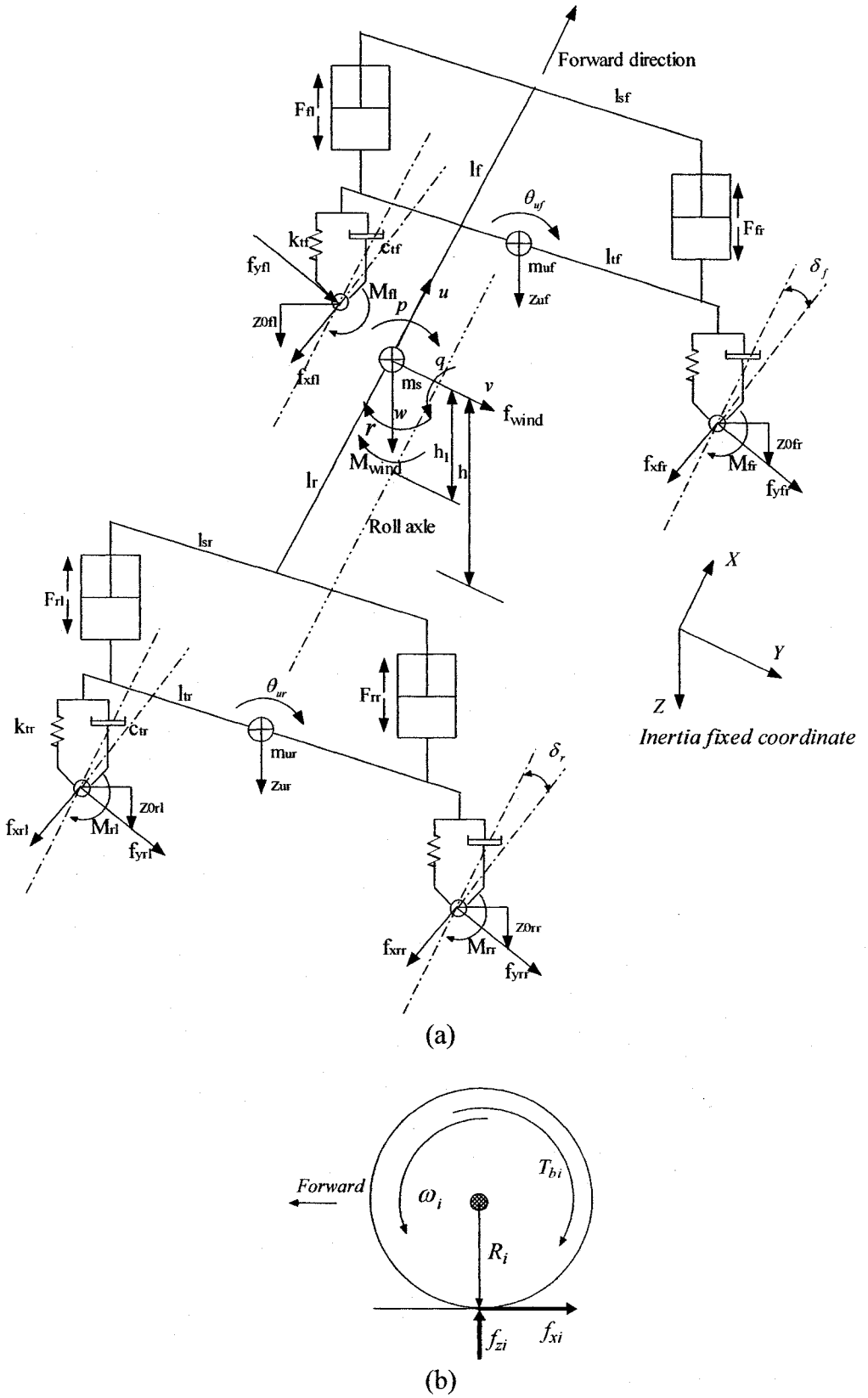

Figure 6.1: (a) Representation of a 14-DOF two-axle vehicle model; and (b) forces and moments acting on a wheel and tire assembly under braking.

Table 6.1: The motions of the generalized two-axle vehicle model.

Motion	Description
u	Longitudinal velocity of the sprung mass
v	Lateral velocity of the sprung mass
w	Bounce velocity of the sprung mass
p	Roll velocity of the sprung mass
q	Pitch velocity of the sprung mass
r	Yaw velocity of the sprung mass
z_{uf}, z_{ur}	Bounce displacements of the front and rear unsprung masses, respectively
θ_{uf}, θ_{ur}	Roll angles of the front and rear unsprung masses, respectively
ω_{fl}, ω_{fr}, ω_{rl}, ω_{rr}	Angular velocities of the front-left, front-right, rear-left and rear-right wheels, respectively

The full vehicle model includes total forces developed by suspension struts, comprising the static as well as dynamic components of the front-left (f_{fl}), front-rear (f_{fr}), rear-left (f_{rl}) and rear-right (f_{rr}) struts. The vertical properties of tires are represented by linear stiffness and damping elements, assuming point-contact with the road surface. Assuming small motions, the equations of motion are developed using Lagrangian dynamics, which are summarized as:

$$m_s(\dot{u} + wq - vr + \dot{w}\varphi - vq\theta) = -(f_{yfl} + f_{yfr})\sin\delta_f - (f_{xfl} + f_{xfr})\cos\delta_f$$
$$-(f_{yrl} + f_{yrr})\sin\delta_r - (f_{xrl} + f_{xrr})\cos\delta_r$$

$$m_s(\dot{v} + ur - wp - \dot{w}\theta + uq\theta) = (f_{yfl} + f_{yfr})\cos\delta_f - (f_{xfl} + f_{xfr})\sin\delta_f$$
$$+(f_{yrl} + f_{yrr})\cos\delta_r - (f_{xrl} + f_{xrr})\sin\delta_r + (F_{fl} + F_{fr})\theta_{uf} + (F_{rl} + F_{rr})\theta_{ur} + f_{wind}$$

$$m_s(\dot{w} + vp - uq) = m_s g - (F_{fl} + F_{fr} + F_{rl} + F_{rr}) - m_s(-\dot{u}\varphi + ur\theta + \dot{v}\theta + vr\varphi)$$

$$
\begin{aligned}
&I_x\dot{p}-\left(I_{yy}-I_z\right)qr = F_{fl}l_{sf}-F_{fr}l_{sf}+F_{rl}l_{sr}-F_{rr}l_{sr}-k_{fbar}\left(\theta-\theta_{uf}\right)-k_{rbar}\left(\theta-\theta_{ur}\right)\\
&+I_{xz}\left(\dot{r}+pq\right)+\left(I_{yy}q^2\theta+I_zr^2\theta-I_{xz}pr\theta\right)+h_1\left[m_sg\theta+f_{wind}\right]\\
&+h_1\left[-\left(f_{yfl}+f_{yfr}\right)\cos\delta_f+\left(f_{xfl}+f_{xfr}\right)\sin\delta_f-\left(f_{yrl}+f_{yrr}\right)\cos\delta_r+\left(f_{xrl}+f_{xrr}\right)\sin\delta_r\right]\\
&I_{yy}\dot{q}-\left(I_z-I_x\right)pr = F_{fl}l_f+F_{fr}l_f-F_{rl}l_r-F_{rr}l_r+I_z\left(\dot{r}\theta+r^2\phi\right)\\
&+I_{xz}\left(r^2-p^2+rq\theta-\dot{p}\theta-rp\phi\right)-I_xpq\theta\\
&+h\left[-\left(f_{yfl}+f_{yfr}\right)\sin\delta_f-\left(f_{xfl}+f_{xfr}\right)\cos\delta_f-\left(f_{yrl}+f_{yrr}\right)\sin\delta_r-\left(f_{xrl}+f_{xrr}\right)\cos\delta_r\right]\\
&I_z\dot{r}-\left(I_x-I_{yy}\right)pq = \left(f_{yfl}+f_{yfr}\right)l_f\cos\delta_f-\left(f_{xfl}+f_{xfr}\right)l_f\sin\delta_f-\left(f_{yrl}+f_{yrr}\right)l_r\cos\delta_r\\
&+\left(f_{xrl}+f_{xrr}\right)l_r\sin\delta_r-\left(f_{yfl}-f_{yfr}\right)l_{tf}\sin\delta_f-\left(f_{xfl}-f_{xfr}\right)l_{tf}\cos\delta_f\\
&-\left(f_{yrl}-f_{yrr}\right)l_{tr}\sin\delta_r-\left(f_{xrl}-f_{xrr}\right)l_{tr}\cos\delta_r+M_{fl}+M_{fr}+M_{rl}+M_{rr}\\
&-I_x\left(pr\theta-\dot{p}\phi\right)-I_{yy}\dot{q}\theta-I_{yy}qr\phi-I_{xz}\left(rq-\dot{p}+\dot{r}\phi-r^2\theta\right)+M_{wind}\\
&m_{uf}\ddot{z}_{uf} = m_{uf}g+F_{fl}+F_{fr}+k_{tf}\left(z_{0fl}+z_{0fr}-2z_{uf}\right)+c_{tf}\left(\dot{z}_{0fl}+\dot{z}_{0fr}-2\dot{z}_{uf}\right)\\
&m_{ur}\ddot{z}_{ur} = m_{ur}g+F_{rl}+F_{rr}+k_{tr}\left(z_{0rl}+z_{0rr}-2z_{ur}\right)+c_{tr}\left(\dot{z}_{0rl}+\dot{z}_{0rr}-2\dot{z}_{ur}\right)\\
&I_{uf}\ddot{\theta}_{uf} = -F_{fl}l_{sf}+F_{fr}l_{sf}+k_{fbar}\left(\theta-\theta_{uf}\right)-k_{tf}l_{tf}\left(z_{0fl}-z_{0fr}+2l_{tf}\theta_{uf}\right)\\
&-c_{tf}l_{tf}\left(\dot{z}_{0fl}-\dot{z}_{0fr}+2l_{tf}\dot{\theta}_{uf}\right)\\
&I_{ur}\ddot{\theta}_{ur} = -F_{rl}l_{sr}+F_{rr}l_{sr}+k_{rbar}\left(\theta-\theta_{ur}\right)-k_{tr}l_{tr}\left(z_{0rl}-z_{0rr}+2l_{tr}\theta_{ur}\right)\\
&-c_{tf}l_{tf}\left(\dot{z}_{0fl}-\dot{z}_{0fr}+2l_{tf}\dot{\theta}_{uf}\right)\\
&I_{wi}\dot{\omega}_i = f_{xi}R_i-T_{bi}\quad(i=fl,fr,rl,rr)\\
&\begin{bmatrix}\dot{\theta}\\ \dot{\varphi}\\ \dot{\psi}\end{bmatrix} = \begin{bmatrix}p+r\varphi\\ q-r\theta\\ r+q\theta\end{bmatrix}
\end{aligned}
\tag{6.1}
$$

where, f_{yi} and M_i are cornering force and aligning moment developed by tire i (i=*fl*, *fr*, *rl*, *rr*), respectively. I_z is yaw mass moment of inertia of the vehicle, and I_{xz} is pitch-plane cross moment. l_{sf} and l_{sr} are half lateral-spacings of the front and rear suspensions, respectively, and l_{tf} and l_{tr} are half tire track-widths of the front and rear axles, respectively.

The Magic Formula tire model is used to derive braking and cornering forces and aligning moment developed by a tire, as a function of the longitudinal-slip ratio and/or slip angle, as well as normal tire load [147, 148]. The longitudinal slip ratio (ss_i) and slip angle (α_i) used in the tire model can be expressed as:

$$ss_{fl} = \left(1 - \frac{R_{fl}\omega_{fl}}{u + w\phi + l_{tf}\dot{\psi}}\right) \times 100\%;\ ss_{fr} = \left(1 - \frac{R_{fr}\omega_{fr}}{u + w\phi - l_{tf}\dot{\psi}}\right) \times 100\%$$

$$ss_{rl} = \left(1 - \frac{R_{rl}\omega_{rl}}{u + w\phi + l_{tr}\dot{\psi}}\right) \times 100\%;\ ss_{rr} = \left(1 - \frac{R_{rr}\omega_{rr}}{u + w\phi - l_{tr}\dot{\psi}}\right) \times 100\%$$

$$\alpha_{fl} = \delta_f - \frac{v - w\theta + l_f\dot{\psi}}{u + w\varphi + l_{tf}\dot{\psi}};\ \alpha_{fr} = \delta_f - \frac{v - w\theta + l_f\dot{\psi}}{u + w\varphi - l_{tf}\dot{\psi}}$$

$$\alpha_{rl} = \delta_r - \frac{v - w\theta - l_r\dot{\psi}}{u + w\varphi + l_{tr}\dot{\psi}};\ \alpha_{rr} = \delta_r - \frac{v - w\theta - l_r\dot{\psi}}{u + w\varphi - l_{tr}\dot{\psi}} \tag{6.2}$$

6.2.1 Model Validation

The validatity of the formulated 14-DOF full-vehicle model was examined using the measured data reported in [20, 53] for a straight truck with wheelbase of 4.83 m. The model simulation results were obtained under steady-state turning and braking-in-a-turn maneuvers on a dry road surface with friction coefficient of 0.85, and compared with the field measured data.

The reported field tests under steady turning maneuvers were performed under constant vehicle speed that was maintained until steady-state responses were achieved, while the drive torque was applied whenever it was necessary to maintain the constant vehicle speed [53]. However, the application of a drive torque was not considered for the model simulation. The vehicle speed in the simulation thus decreased slowly during the steady-state steering, which was partially attributed to dissipation of some of the kinetic

energy through the damping properties of the suspension and the tires. The initial vehicle speed in the simulation was thus selected to be slightly higher than that used in the field tests. The vehicle model would reach a steady-state turn status where the vehicle speed gradually decreased. The lateral acceleration and yaw rate responses of the model were considered when the vehicle speed approached the desired field-test speed. Moreover, an average steer angle was assumed in the simulation.

Figures 6.2 and 6.3 illustrate comparisons of model results with the measured data under steady-state turning with two different vehicle speeds (12 m/s and 14.3 m/s), respectively. The simulation results in lateral acceleration and yaw rate show reasonably good agreements with the measured data for both the vehicle speeds, as a function of the steer angle. Under relatively high steer angle inputs, the results attained from simulation tend to be higher than the measured data, which may be attributed to the assumption of parallel steering and the differences in the assumed tire properties and the actual tire data, although the tire model parameters were identified from measured tire data.

The braking-in-a-turn field tests were performed under an initial constant vehicle speed until the vehicle approached its steady-state, in terms of a steady lateral acceleration response. A quasi-step braking maneuver was subsequently applied, while the steer angle was held constant until the vehicle approached a full stop [53]. The braking input was applied at time t=2 s after the vehicle entered a steady turn, and the magnitude of braking pressure was held constant until the vehicle approached full stop. The measured steer angles were 7 and 8.5 degrees for the left- and right-wheels [53].

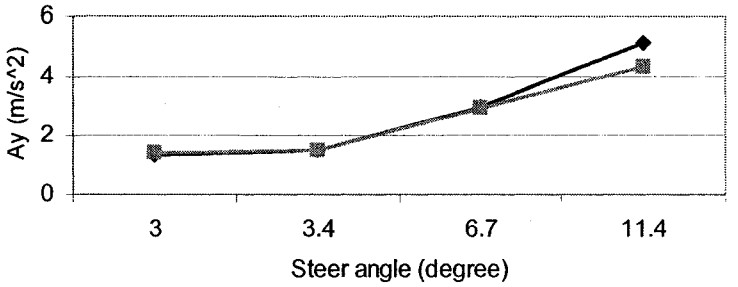

(a)

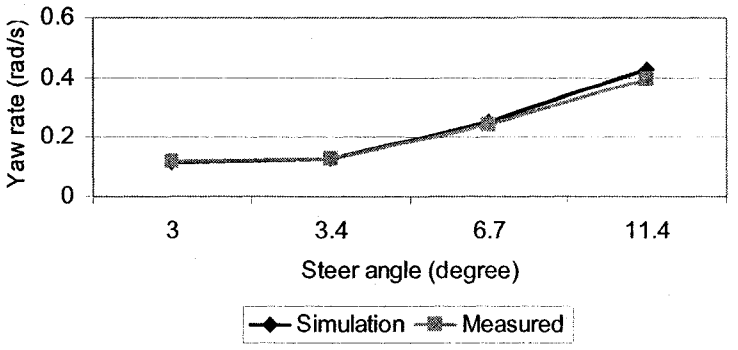

(b)

Figure 6.2: Comparison of full-vehicle model responses with the measured data under steady-state turning maneuver with vehicle speed of 12 m/s: (a) lateral acceleration; and (b) yaw rate.

The simulations were performed under an average steer angle of 7.7 degree, as shown in Figure 6.4(a). The simulated and measured speeds were identical (11.1 m/s) when applying braking. Figures 6.4(b), (c) and (d) present the comparisons of simulation responses of lateral acceleration, longitudinal acceleration and yaw rate with the measured data during the braking-in-a-turn maneuver, respectively. The comparisons revealed reasonably good agreements between the simulation results and the measured data. The observed differences between the two are partially attributed to assumption of parallel steering. On the basis of the comparisons (presented in Figures 6.2~6.4), it is concluded that the proposed model can predict the turning and braking-in-a-turn responses reasonably well.

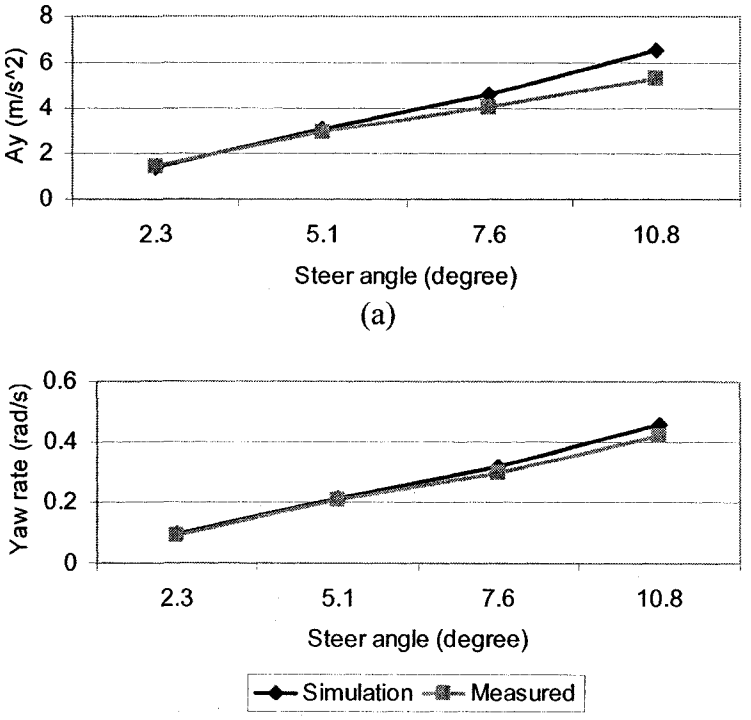

Figure 6.3: Comparison of full-vehicle model responses with the measured data during steady-state turning maneuver with vehicle speed of 14.3 m/s: (a) lateral acceleration; and (b) yaw rate.

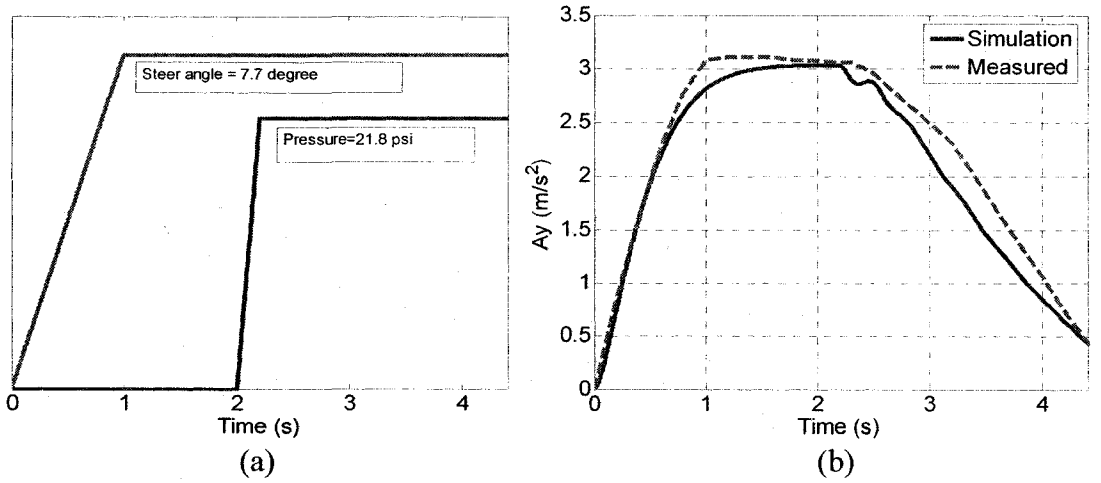

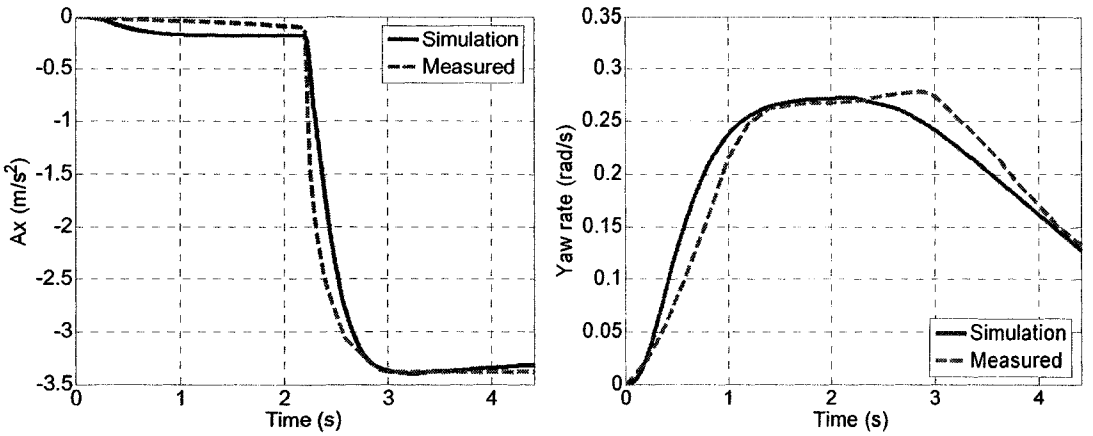

(c) (d)

Figure 6.4: Comparison of full-vehicle model responses with the measured data during braking-in-a-turn maneuver: (a) braking-in-a-turn input; (b) lateral acceleration; (c) longitudinal acceleration; and (d) yaw rate.

6.3 Feasibility Analysis of Full-Vehicle Interconnected Suspension Configurations

Unlike the roll and pitch planes, the full-vehicle suspensions offer greater numbers of possible interconnections among the four wheels suspension struts. From the analyses of pitch- and roll-plane interconnections, it is evident that different interconnection configurations yield considerably different suspension stiffness and damping properties. The strong influence of the type of interconnection and the large number of possible interconnections necessitate classification of various full-vehicle interconnected suspension systems so as to identify feasible and desirable interconnection configurations. Figure 6.5 illustrates a full-vehicle interconnected suspension configuration, as an example, which involves eight interconnecting pipes among the four suspension struts in the roll- and pitch-planes. Such interconnected configuration, however, yields only two independent pressures, as evident in Figure 6.5, and could be infeasible when load variations are considered.

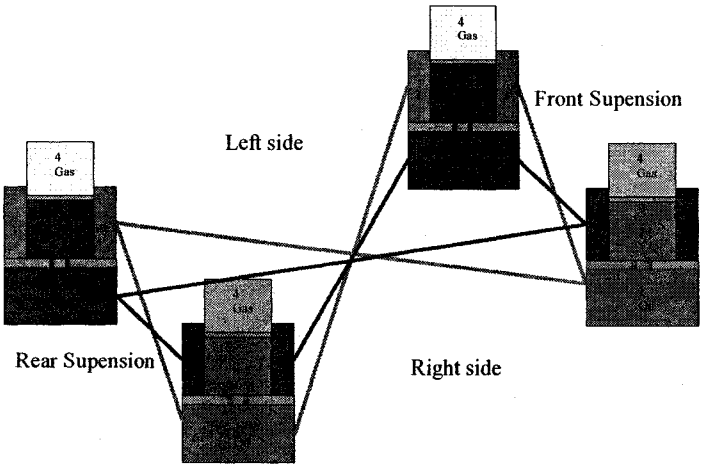

Figure 6.5: Representation of an interconnection configuration in the roll- and pitch-plane arrangement.

Although many interconnection configurations could be conceived for the roll- and pitch-plane arrangement, only a small number of configurations could be considered feasible for applications to vehicles, particularly when significant variations in the payload may be encountered. In this dissertation research, a number of possible configurations were conceived and their feasibility was examined in view of the static equilibrium. The feasibility analysis was conducted based on the following proposed measures:

Equivalent Static Interconnected Suspension (ESIS):

For a given or conceived interconnected struts configuration, an alternative interconnected suspension could be obtained by adding/removing one or several interconnecting pipes. If the resulting configuration contributes to provide the same static equilibrium under varying load conditions, the configuration is called an Equivalent Static Interconnected Suspension (ESIS) of the original configuration. An interconnected suspension may have many ESIS configurations. Considerable differences, however,

might be expected between the properties and dynamic responses of the ESIS and the original configuration.

Minimum Equivalent Static Interconnected Suspension (MESIS):

Of all the equivalent static configurations of an interconnected suspension, those with minimum number of interconnections are referred to as Minimum Equivalent Static Interconnected Suspension (MESIS) of the original interconnected suspension configuration. An interconnected suspension configuration may have a number of MESIS configurations.

Order of Minimum Equivalent Static Interconnected Suspension (OMESIS):

The order of a MESIS is defined by the number of its interconnections.

Degrees-of-Freedom (DOF) of Interconnected Suspension:

The number of independent fluid pressures required to define the static equilibrium of an interconnected suspension is referred to as its DOF. For a full-vehicle suspension configuration involving the suspension struts proposed in Chapter 2, the maximum DOF of the interconnected suspension would be eight.

The loads applied to the four suspension struts of an interconnected suspension in the roll- and pitch-plane arrangement could vary considerably, particularly for applications involving freight vehicles. In order to maximize the advantage of an interconnected suspension, the load should be fully supported by the interconnected suspension system [29]. At least four independent fluid-pressures are thus required to obtain the static equilibrium over a wide range of loading conditions, which defines the necessary

condition for a feasible full-vehicle interconnected suspension. The examples of feasible full-vehicle interconnected suspension configurations are presented below.

Two different configurations of feasible 4-DOF interconnected suspensions with four single-gas-chamber struts, involving hydraulic couplings, are shown in Figure 6.6. Figure 6.7 illustrates two examples of feasible 4-DOF interconnected suspensions with four twin-gas-chamber struts, involving pneumatic couplings. The examples of feasible 4-DOF interconnected suspensions using both types of struts are shown in Figure 6.8, which involve hybrid fluidic couplings. Figure 6.9 illustrates a feasible 6-DOF full-vehicle interconnected suspension involving pneumatic couplings. It can be seen that a number of feasible full-vehicle interconnected suspensions can be realized on the basis of the two previously proposed hydro-pneumatic struts.

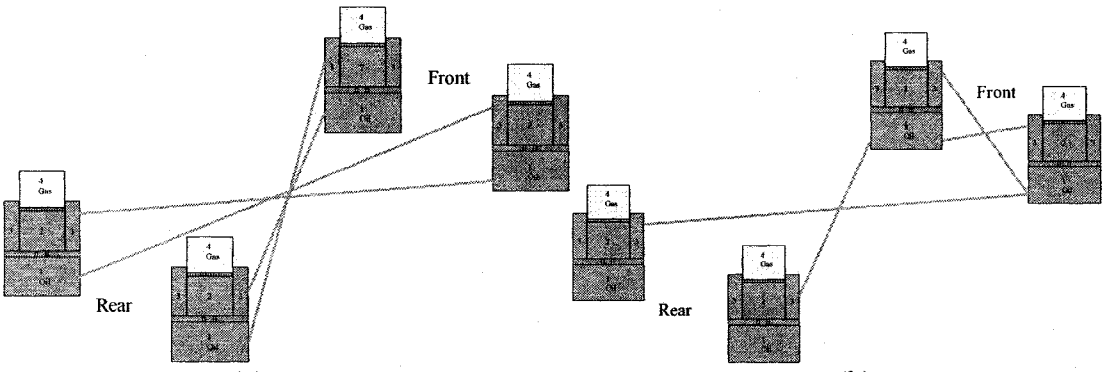

Figure 6.6: Two feasible 4-DOF full-vehicle interconnected suspensions involving single-gas-chamber struts.

Considering a large number of possible feasible configurations, a preliminary analysis was performed to select a few for comprehensive analyses of the suspension properties. It can also be observed that some of the full-vehicle interconnected suspension configurations are simply a combination of the in-plane interconnections, analyzed in Chapters 2~4. The knowledge and understanding obtained from the properties of in-plane

connected suspension is used to identify potentially beneficial and feasible configurations.

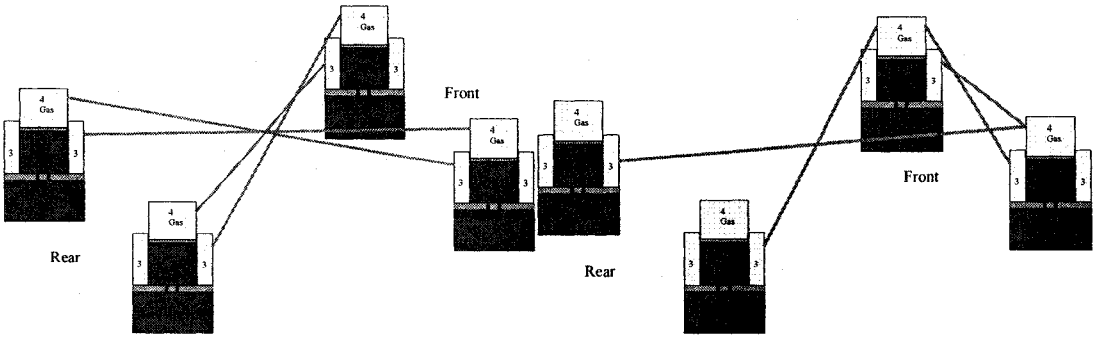

(a) (b)

Figure 6.7: Two feasible 4-DOF interconnected suspensions involving twin-gas-chamber struts.

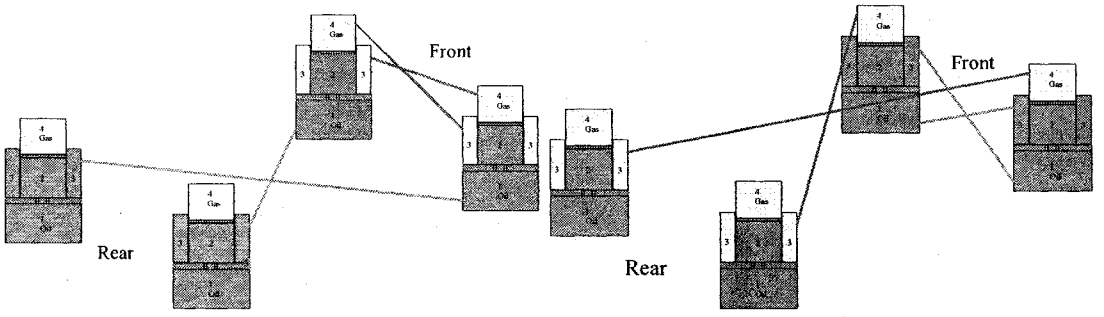

(a) (b)

Figure 6.8: Two feasible 4-DOF interconnected suspensions involving both the struts.

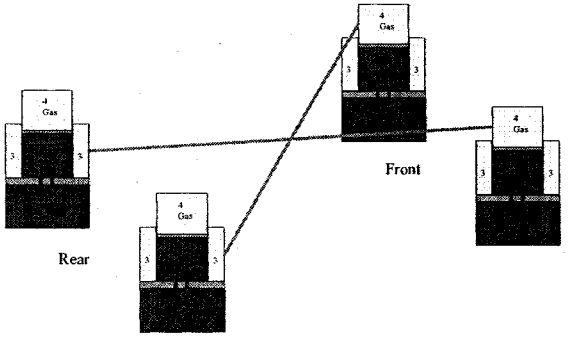

Figure 6.9: A 6-DOF interconnected suspension system using only twin-gas-chamber struts.

6.3.1 Identification of Feasible Full-Vehicle Interconnected Suspension Systems

In this dissertation, a total of twenty-two full-vehicle suspension configurations, including four unconnected (U1~U4) and eighteen interconnected (C1~C18), are selected for the comparison of relative suspension properties. Figure 6.10 illustrates the four unconnected suspension configurations. Configuration U1 consists of four single-gas-chamber struts, while configuration U2 includes four two-gas-chamber struts. Both the configurations U3 and U4 comprise two single-gas-chamber struts as well as two twin-gas-chamber struts, respectively.

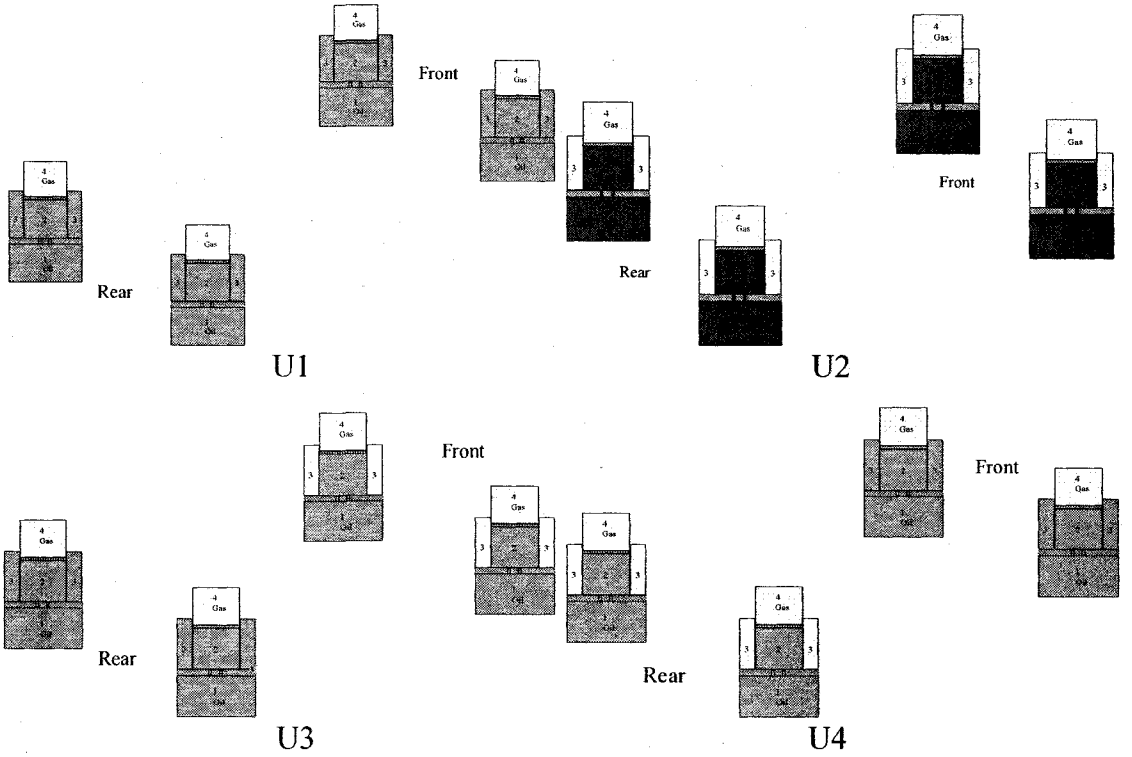

Figure 6.10: Four full-vehicle unconnected suspension systems.

Figure 6.11 presents the four 4-DOF full-vehicle interconnected suspension configurations that involve diagonal fluidic couplings (or X-couplings) among the different strut units. Configuration C1 involves diagonal hydraulic-interconnections among the four single-gas-chamber struts, while configuration C2 includes diagonal

pneumatic-interconnections among the twin-gas-chamber strut units. Configurations C3 and C4 involve hybrid fluidic-interconnections among the four struts.

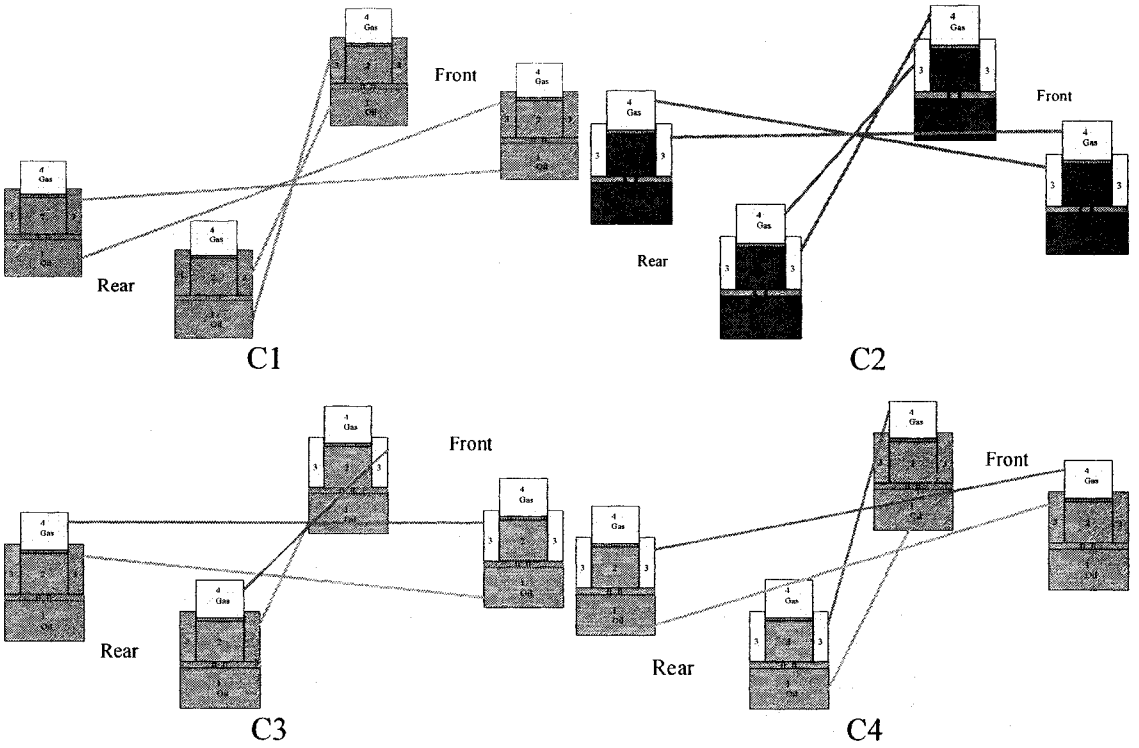

Figure 6.11: Four 4-DOF full-vehicle interconnected suspension systems involving X-couplings.

Figure 6.12 presents the four 4-DOF full-vehicle interconnected suspension configurations that involve roll-plane fluidic couplings. Configuration C5 that consists of four single-gas-chamber struts includes the roll-plane hydraulic interconnections between the left- and right-struts of the front and rear suspensions, respectively. In a similar manner, configuration C6 involves roll-plane pneumatic interconnections. Configurations C7 and C8 are conceived through roll-plane hybrid fluidic couplings.

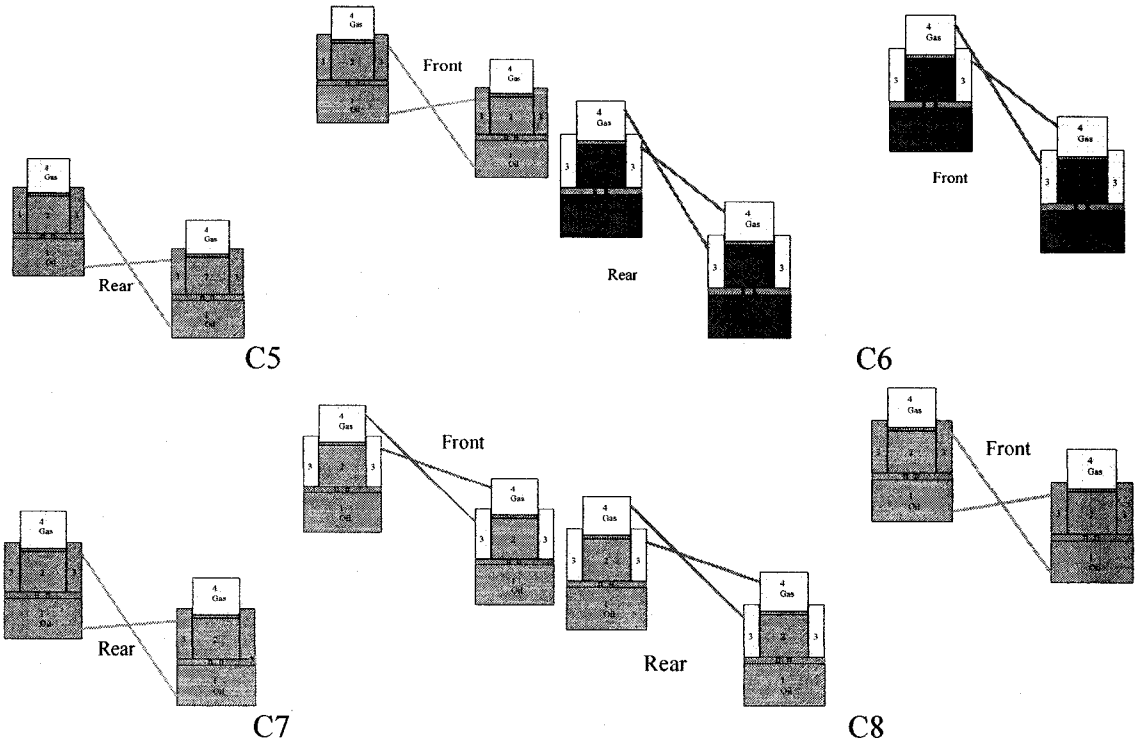

Figure 6.12: Four 4-DOF full-vehicle interconnected suspension systems involving roll-plane couplings.

Figure 6.13 illustrates four full-vehicle interconnected suspension configurations that involve pitch-plane pneumatic couplings. Configurations C9 and C10 are realized by two pitch-plane pneumatic interconnections between the chambers 4 and 3 of front- and rear-struts, respectively. Configuration C11 includes two twin-gas-chamber struts in the front and two single-gas-chamber struts in the rear, while the pitch-plane pneumatic interconnections are realized between the chambers 4 of the front- and rear-struts. Configuration C12 includes two single-gas-chamber struts in the front and two twin-gas-chamber struts in the rear, while the pitch-plane pneumatic interconnections are also realized between the chambers 4 of the front- and rear-struts.

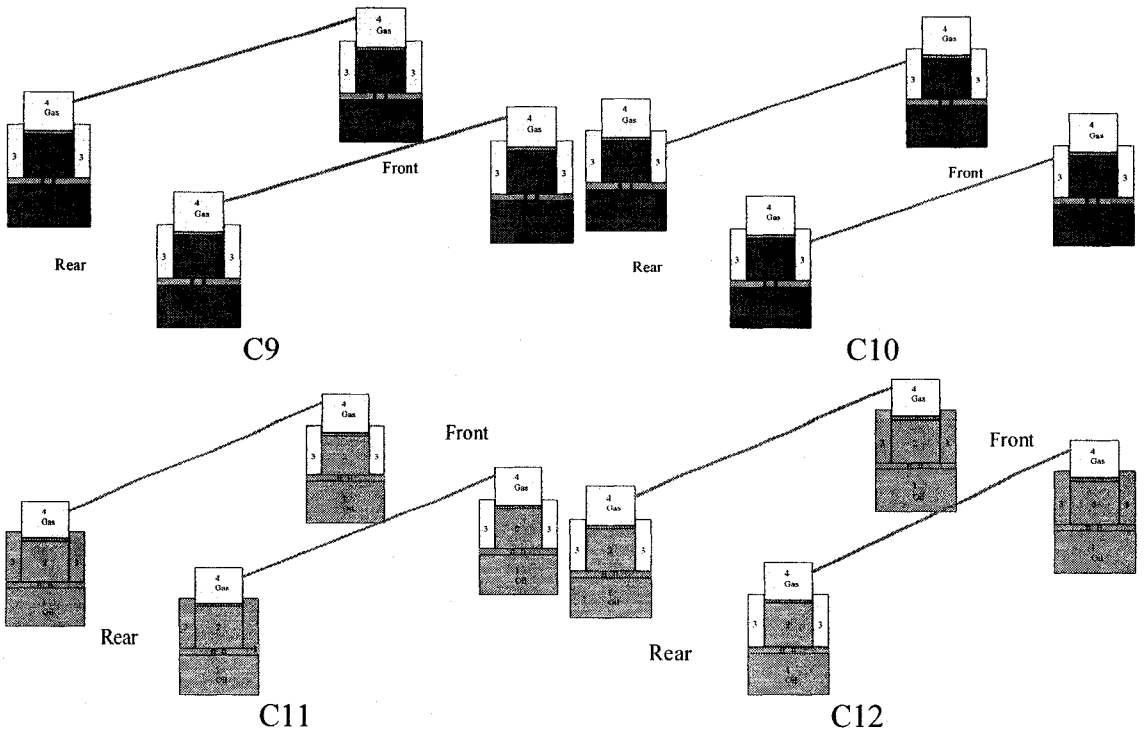

Figure 6.13: Four full-vehicle interconnected suspension systems involving pitch-plane pneumatic couplings.

Figure 6.14 illustrates two 6-DOF full-vehicle interconnected suspension configurations that involve pneumatic X-couplings. Figure 6.15 illustrates two 4-DOF full-vehicle interconnected suspension configurations that involve relatively more complex couplings among the four suspension struts. Figure 6.16 illustrates two 4-DOF full-vehicle interconnected suspension configurations that involve pitch-plane couplings. Configuration C17 consists of pitch-plane hydraulic interconnections between the front and rear single-gas-chamber struts, while configuration C18 involves pitch-plane pneumatic interconnections between the front and rear twin-gas-chamber struts.

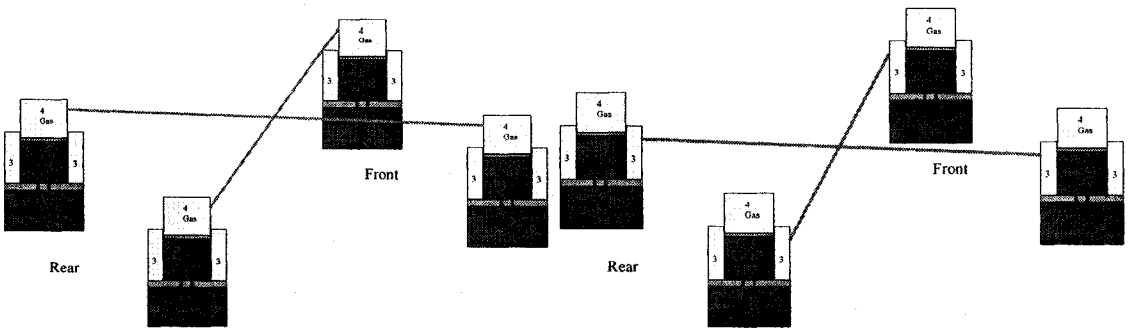

Figure 6.14: Two 6-DOF interconnected full-vehicle suspension systems involving X-couplings.

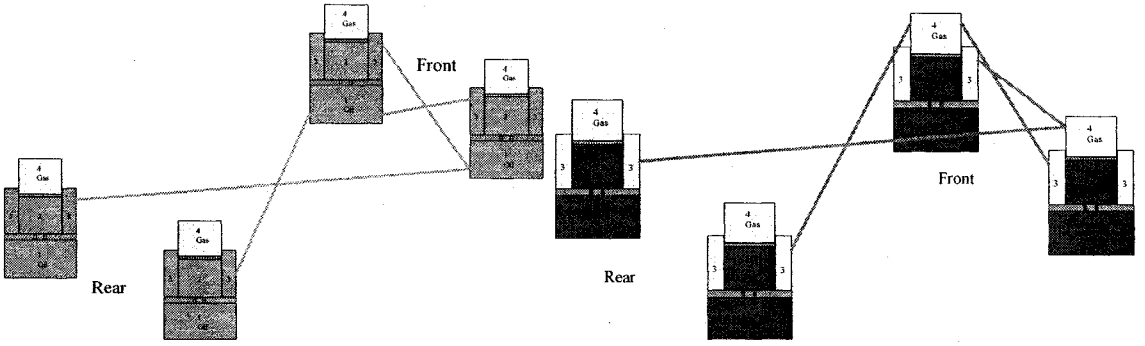

Figure 6.15: Two 4-DOF interconnected full-vehicle suspension systems involving roll- and pitch-plane couplings.

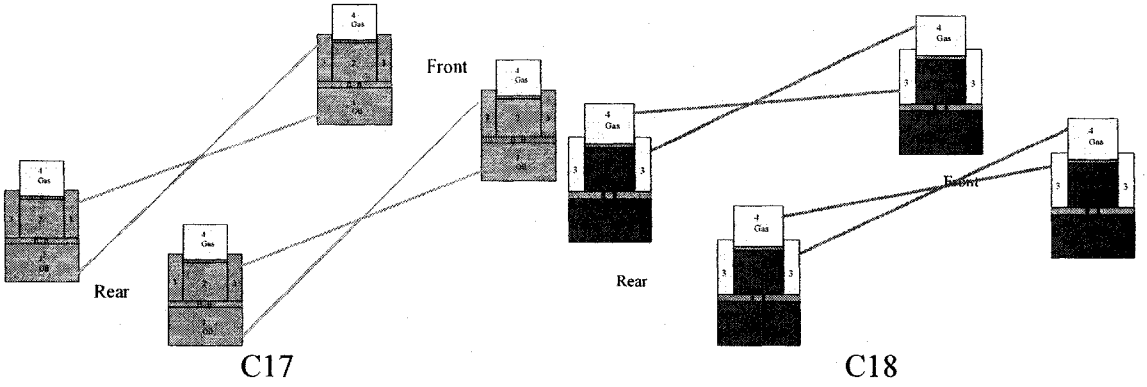

Figure 6.16: Two 4-DOF interconnected full-vehicle suspension systems involving pitch-plane couplings.

The design and tuning of a full-vehicle suspension system concerns four fundamental vibration modes, namely bounce, roll, pitch and warp [31, 32, 121-125]. The vertical ride quality generally necessitates soft bounce-mode, while the relatively stiff roll and pitch

modes would be beneficial for controlling vehicle attitude during steering and braking/traction maneuvers, and thus improved ride and handling qualities [5, 50, 165]. It is also generally accepted that the warp mode should be as soft as possible in order to improve the roadholding property and thus the handling quality [31, 32, 121-125]. In this dissertation, a simplified measure, vehicle property index (VPI), is defined as a weighted stiffness measure to facilitate the comparison of properties of the above selected full-vehicle suspension configurations, such that:

$$VPI = \alpha_v |K_v - K_{vo}| + \alpha_R |K_R - K_{Ro}| + \alpha_P |K_P - K_{Po}| + \alpha_\psi |K_\psi - K_{\psi o}| \tag{6.3}$$

where K_{vo}, K_{Ro}, K_{Po} and $K_{\psi o}$ represent desirable suspension bounce-, roll-, pitch- and warp-mode stiffness properties for a road vehicle, respectively. K_v, K_R, K_P and K_ψ represent actual suspension bounce-, roll-, pitch- and warp-mode stiffness properties, respectively, and α_v, α_R, α_P and α_ψ are the corresponding weighting coefficients for the four modes. In order to simplify the comparison of different suspension systems, the suspension stiffness values are scaled from 1(low) to 5(high). For a typical heavy road vehicle, K_{vo}, K_{Ro}, K_{Po} and $K_{\psi o}$ could be 3, 5, 5 and 1, respectively, while weighting coefficients α_b, α_r, α_p and α_w are selected as 0.3, 0.5, 0.1 and 0.1, respectively. This set of desirable properties suggests a relatively soft vertical ride and enhanced roadholding and axle-articulation qualities, as well as improved anti-roll and anti-pitch properties. The selected weighting coefficients suggest a considerable weighting on roll stability of heavy vehicles. From Eq. (6.3), it can be seen that a lower VPI value would suggest a more desirable suspension configuration.

Table 6.2 summarizes the vehicle property indices (VPI) of the selected full-vehicle suspension configurations, either interconnected or unconnected, based on the knowledge

and understanding obtained from the analyses of various in-plane interconnected suspensions in the previous chapters. The results clearly show that different suspension configurations could yield considerably different stiffness properties. Furthermore, the configurations C1~C4 involving fluidic X-couplings yield the lowest VPI and could be considered potentially beneficial for heavy vehicles.

Table 6.2: Comparison of vehicle property index (VPI) of different suspension configurations for a heavy vehicle.

Suspension	**Static Stiffness Properties**				**VPI**
	Bounce	**Roll**	**Pitch**	**Warp**	
U1	3	3	3	3	1.4
U2	3	3	3	3	1.4
U3	3	3	3	3	1.4
U4	3	3	3	3	1.4
U1bar*	3	5	3	4	0.5
U2bar	3	5	3	4	0.5
U3bar	3	5	3	4	0.5
U4bar	3	5	3	4	0.5
C1	3	5	5	3	**0.2**
C2	3	5	5	3	**0.2**
C3	3	5	5	3	**0.2**
C4	3	5	5	3	**0.2**
C5	3	5	3	4	0.5
C6	3	5	3	4	0.5
C7	3	5	3	4	0.5
C8	3	5	3	4	0.5
C9	3	3	1	2	1.5
C10	3	3	1	2	1.5
C11	3	3	1	2	1.5
C12	3	3	1	2	1.5
C13	3	1	1	1	2.4
C14	3	1	1	1	2.4
C15	3	5	4	4.5	0.45
C16	3	5	4	4.5	0.45
C17	3	3	5	4	1.3
C18	3	3	5	4	1.3

*: U1bar means that configuration U1 together with anti-roll bars.

It has been shown that the hydraulic interconnections yield enhanced roll- or pitch-mode damping for roll- or pitch-interconnected suspension, respectively. The

configuration C1 is thus expected to provide improved roll- and pitch-mode properties. In the following sections, the properties of the X-coupled suspension configuration C1 (Figure 6.10) will be analyzed and compared with those of the unconnected suspension configuration U1 (Figure 6.11), in terms of suspension stiffness and damping properties, as well as vehicle dynamic responses during steering and braking inputs. The analyses in the following sections are also used to validate the effectiveness of the proposed simplified measure VPI used for preliminarily evaluations of the full-vehicle suspension designs.

6.4 Analytical Formulations of Selected Full-Vehicle Suspension Configurations

In order to be consistent with the previous chapters, the hydraulically X-coupled suspension configuration C1 is referred to as B_X, while the unconnected suspension configuration U1 is referred to as B_U. The mathematical formulations of strut forces and suspension properties of both the suspension configurations are derived, based on which the stiffness and damping properties, and vehicle dynamic responses are analyzed and compared.

6.4.1 Strut Forces

Although the X-coupled suspension B_X involves complex fluid flows across front and rear as well as left and right suspension struts, the forces developed by each strut can be conveniently derived using the generalized model presented in Section 2.6, which permits the evaluation of restoring and dissipative suspension forces due to hydro-pneumatic struts in an in-plane arrangement, irrespective of unconnected or interconnected. In a similar manner to the pitch-interconnected suspension configuration B_{IP} (Section 2.6), the

forces developed by the front-left (*fl*) and -right (*fr*) struts of the hydraulically X-coupled suspension B_X are derived as:

$$F_f = P_0 A_{1f}\left[\left(\frac{V_{40f}}{V_{40f}+A_{1f}x_f - A_{3r}x_r}\right)^n - 1\right] - P_0 A_{3f}\left[\left(\frac{V_{40r}}{V_{40r}+A_{1r}x_r - A_{3f}x_f}\right)^n - 1\right] - \frac{128\mu L A_{3f}^2 \dot{x}_f}{\pi D^4} \\ - \frac{\rho A_{1f}\left|A_{1f}\dot{x}_f - A_{3r}\dot{x}_r\right|(A_{1f}\dot{x}_f - A_{3r}\dot{x}_r)}{2C_d^2 a_{12f}^2} + \frac{\rho A_{3f}\left|A_{1r}\dot{x}_r - A_{3f}\dot{x}_f\right|(A_{1r}\dot{x}_r - A_{3f}\dot{x}_f)}{2C_d^2 a_{12r}^2} \tag{6.4a}$$

where *r*=*rr* for the front-left strut (*f*=*fl*), and *r*=*rl* for the front-right strut (*f*=*fr*). The forces developed by the rear struts are also expressed in a similar manner, as:

$$F_r = P_0 A_{1r}\left[\left(\frac{V_{40r}}{V_{40r}+A_{1r}x_r - A_{3f}x_f}\right)^n - 1\right] - P_0 A_{3r}\left[\left(\frac{V_{40f}}{V_{40f}+A_{1f}x_f - A_{3r}x_r}\right)^n - 1\right] - \frac{128\mu L A_{3r}^2 \dot{x}_r}{\pi D^4} \\ - \frac{\rho A_{1r}\left|A_{1r}\dot{x}_r - A_{3f}\dot{x}_f\right|(A_{1r}\dot{x}_r - A_{3f}\dot{x}_f)}{2C_d^2 a_{12r}^2} + \frac{\rho A_{3r}\left|A_{1f}\dot{x}_f - A_{3r}\dot{x}_r\right|(A_{1f}\dot{x}_f - A_{3r}\dot{x}_r)}{2C_d^2 a_{12f}^2} \tag{6.4b}$$

where *f*=*fl* for the rear-right strut (*r*=*rr*), and *f*=*fr* for the rear-left strut (*r*=*rl*).

In the above formulations, F_i is the dynamic force developed by strut *i* (*i*=*fl*, *fr*, *rl*, *rr*), x_i and $\dot{x}_i$ are the relative displacement and velocity across the strut *i*, respectively, assuming small motions with positive direction being upward.

The dynamic strut forces due to the unconnected single-gas-chamber strut suspension B_U are also developed in a similar manner, such that:

$$F_i = P_0 A_{2i}\left[\left(\frac{V_{40i}}{V_{40i}+A_{2i}x_i}\right)^n - 1\right] - \frac{\rho A_{2i}^3 \left|\dot{x}_i\right|\dot{x}_i}{2C_d^2 a_{12i}^2} - \frac{\rho A_{3i}^3 \left|\dot{x}_i\right|\dot{x}_i}{2C_d^2 a_{13i}^2} \qquad (i = fl, fr, rl, rr) \tag{6.5}$$

6.4.2 Suspension Properties – Method of Analysis

The fundamental properties of vehicle suspension systems can be effectively evaluated using two different approaches [8, 166, 167]. An analytical approach based upon coupled vibration-modes of a vehicle, e.g. coupled roll and bounce modes, in an

ideal manner that neglects the influence of structural-deflection modes and suspension kinematics, has been used to determine the stiffness and damping characteristics of the suspension [166]. This approach considers the entire vehicle motions and is quite sensitive to variations in vehicle inertial and geometry parameters. An alternative approach assumes a fixed vehicle body (sprung mass) to appropriately reduce the contributions of couplings among various vibrations-modes of the vehicle body and thus facilitate the characterization of stiffness properties of suspension system in individual modes [8, 167]. This method can be considered to be more suspension-oriented, and less sensitive to variations in vehicle inertial parameters. Moreover, this approach is far simpler than the former method, due to the absence or reduction in coupling of the vehicle vibration-modes.

The first evaluation method based upon the coupled vehicle dynamics and modes may be more theoretically accurate, considering the fact that the strong coupling effects of vibration-modes of a vehicle with nonlinear suspension system [92]. Such method has been used to develop and analyze properties of either the roll- or pitch-plane interconnected suspension arrangement, also as evident from the formulations in Chapter 2. However, this method may not be efficient for evaluating a full-vehicle suspension system, which involves very complex couplings among the bounce-, roll-, pitch- and warp-modes. Therefore, the second method that assumes a fixed sprung mass is used in this chapter to evaluate the properties of the unconnected and X-coupled suspension configurations.

Figure 6.17 illustrates the simplified model for evaluating the properties of full-vehicle suspension configurations, where the sprung mass is held fixed. Four independent

excitations (X_{fl}, X_{fr}, X_{rl}, X_{rr}) are applied to the bottoms of the four suspension units as shown, respectively, which represent the compression/extension motions of the suspension units.

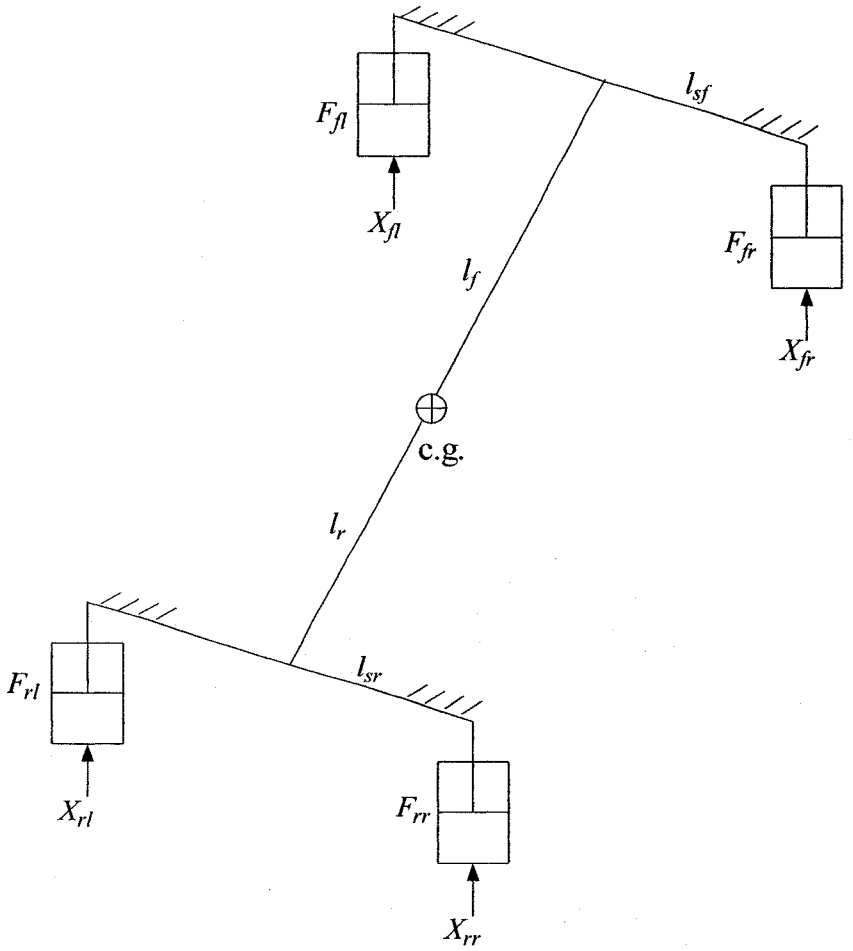

Figure 6.17: Simplified model representation for evaluating the properties of unconnected as well as coupled full-vehicle suspension systems.

The bounce-mode stiffness properties (suspension rate) of the unconnected and interconnected suspensions are evaluated by letting $X_{fl} = X_{fr} = X_{rl} = X_{rr} = x$. The suspension rates ($k_{vf}$ and k_{vr}) of front and rear suspensions are expressed as:

$$k_{vf} = -\frac{d\left(F_{fl} + F_{fr}\right)}{dx};\ k_{vr} = -\frac{d\left(F_{rl} + F_{rr}\right)}{dx} \tag{6.6}$$

The bounce-mode stiffness of a vehicle is simply the sum of the suspension rates of its front and rear suspensions.

The roll-mode stiffness properties of a full-vehicle suspension, whether unconnected or interconnected, are evaluated by letting $X_{fl} = -X_{fr} = X_{rl} = -X_{rr} = x$. The roll-mode stiffness properties (k_{Rf} and k_{Rr}) of the front and rear suspensions are expressed as:

$$k_{Rf} = -\frac{dM_f}{d\theta_f} = -\frac{d\left(F_{fl} - F_{fr}\right)}{dx} l_{sf}^2 \; ; \; k_{Rr} = -\frac{dM_r}{d\theta_r} = -\frac{d\left(F_{rl} - F_{rr}\right)}{dx} l_{sr}^2 \tag{6.7}$$

The roll stiffness of a vehicle is the sum of the roll stiffnesses of the front and rear suspensions.

The pitch-mode stiffness property (k_p) of a full-vehicle suspension, whether unconnected or interconnected, is evaluated by letting $X_{fl} = X_{fr} = -X_{rl} = -X_{rr} = x$, such that:

$$k_p = -\frac{dM_p}{d\varphi} = -\frac{d\left(\left(F_{fl} + F_{fr}\right) l_f - \left(F_{rl} + F_{rr}\right) l_r\right)}{dx} \frac{\left(l_f + l_r\right)}{2} \tag{6.8}$$

The warp-mode stiffness property (k_w) of a full-vehicle suspension are assessed by letting $X_{fl} = -X_{fr} = -X_{rl} = X_{rr} = x$. The warp-mode stiffness can be simply expressed as the front and rear suspension stiffness in series, such that [168]:

$$k_{\psi f} = -\frac{dM_f}{d\psi_f} = -\frac{d\left(F_{fl} - F_{fr}\right)}{dx} l_{sf}^2 \; ; \; k_{\psi r} = -\frac{dM_r}{d\psi_r} = -\frac{d\left(F_{rl} - F_{rr}\right)}{dx} l_{sr}^2 \; ; \; k_w = \frac{k_{\psi f} k_{\psi r}}{k_{\psi f} + k_{\psi r}} \tag{6.9}$$

Suspension stiffness properties:

The above generalized formulations are applied to derive the properties of both the suspension configurations (B_X and B_U) in different modes. The formulations of the bounce-mode stiffness properties of the X-coupled suspension B_X are derived from Eqs. (6.4) and (6.6), such that:

$$k_{vf} = 2nP_0V_{40f}^n \frac{A_{1f}^2 - A_{1f}A_{3r}}{\left[V_{40f} + A_{1f}x - A_{3r}x\right]^{n+1}} + 2nP_0V_{40r}^n \frac{A_{3f}^2 - A_{1r}A_{3f}}{\left[V_{40r} + A_{1r}x - A_{3f}x\right]^{n+1}}$$

$$k_{vr} = 2nP_0V_{40r}^n \frac{A_{1r}^2 - A_{1r}A_{3f}}{\left[V_{40r} + A_{1r}x - A_{3f}x\right]^{n+1}} + 2nP_0V_{40f}^n \frac{A_{3r}^2 - A_{1f}A_{3r}}{\left[V_{40f} + A_{1f}x - A_{3r}x\right]^{n+1}} \tag{6.10}$$

The formulations of the bounce-mode stiffness properties of the suspension B_U are derived in a similar manner, such that:

$$k_{vi} = 2nP_0V_{40i}^n \frac{A_{2i}^2}{\left[V_{40i} + A_{2i}x\right]^{n+1}} \qquad (i = f,r) \tag{6.11}$$

The roll-mode stiffness properties of the X-coupled suspension B_X are derived from Eqs. (6.4) and (6.7), such that:

$$\begin{aligned} k_{Rf} = {} & nP_0V_{40f}^n l_{sf}^2 \frac{A_{1f}^2 + A_{1f}A_{3r}}{\left[V_{40f} + A_{1f}x + A_{3r}x\right]^{n+1}} + nP_0V_{40r}^n l_{sf}^2 \frac{A_{3f}^2 + A_{1r}A_{3f}}{\left[V_{40r} - A_{1r}x - A_{3f}x\right]^{n+1}} \\ & + nP_0V_{40f}^n l_{sf}^2 \frac{A_{1f}^2 + A_{1f}A_{3r}}{\left[V_{40f} - A_{1f}x - A_{3r}x\right]^{n+1}} + nP_0V_{40r}^n l_{sf}^2 \frac{A_{3f}^2 + A_{1r}A_{3f}}{\left[V_{40r} + A_{1r}x + A_{3f}x\right]^{n+1}} \\ k_{Rr} = {} & nP_0V_{40r}^n l_{sr}^2 \frac{A_{1r}^2 + A_{1r}A_{3f}}{\left[V_{40r} + A_{1r}x + A_{3f}x\right]^{n+1}} + nP_0V_{40f}^n l_{sr}^2 \frac{A_{3r}^2 + A_{1f}A_{3r}}{\left[V_{40f} - A_{1f}x - A_{3r}x\right]^{n+1}} \\ & + nP_0V_{40r}^n l_{sr}^2 \frac{A_{1r}^2 + A_{1r}A_{3f}}{\left[V_{40r} - A_{1r}x - A_{3f}x\right]^{n+1}} + nP_0V_{40f}^n l_{sr}^2 \frac{A_{3r}^2 + A_{1f}A_{3r}}{\left[V_{40f} + A_{1f}x + A_{3r}x\right]^{n+1}} \end{aligned} \tag{6.12}$$

The roll-mode stiffness properties of the suspension B_U are also derived as:

$$k_{Ri} = nP_0V_{40i}^n l_{si}^2 \frac{A_{2i}^2}{\left[V_{40i} + A_{2i}x\right]^{n+1}} + nP_0V_{40i}^n l_{si}^2 \frac{A_{2i}^2}{\left[V_{40i} - A_{2i}x\right]^{n+1}} \qquad (i = f,r) \tag{6.13}$$

The formulation of the pitch-mode stiffness property of the X-coupled suspension B_X is derived from Eqs. (6.4) and (6.8), such that:

$$k_P = nP_0 l_f \left(l_f + l_r\right)\left\{V_{40f}^n \frac{A_{1f}^2 + A_{1f}A_{3r}}{\left[V_{40f} + A_{1f}x + A_{3r}x\right]^{n+1}} + V_{40r}^n \frac{A_{3f}^2 + A_{1r}A_{3f}}{\left[V_{40r} - A_{1r}x - A_{3f}x\right]^{n+1}}\right\}$$
$$+nP_0 l_r \left(l_f + l_r\right)\left\{V_{40r}^n \frac{A_{1r}^2 + A_{1r}A_{3f}}{\left[V_{40r} - A_{1r}x - A_{3f}x\right]^{n+1}} + V_{40f}^n \frac{A_{3r}^2 + A_{1f}A_{3r}}{\left[V_{40f} + A_{1f}x + A_{3r}x\right]^{n+1}}\right\} \quad (6.14)$$

The formulation of the pitch-mode stiffness property of the suspension B_U is derived in a similar manner, such that:

$$k_P = nP_0 V_{40f}^n l_f \left(l_f + l_r\right)\frac{A_{2f}^2}{\left[V_{40f} + A_{2f}x\right]^{n+1}} + nP_0 V_{40r}^n l_r \left(l_f + l_r\right)\frac{A_{2r}^2}{\left[V_{40r} - A_{2r}x\right]^{n+1}} \quad (6.15)$$

The formulations of the warp-mode stiffness properties of the X-coupled suspension B_X are derived in a similar manner from Eqs. (6.4) and (6.9), such that:

$$k_{\psi f} = nP_0 V_{40f}^n l_{sf}^2 \frac{A_{1f}^2 - A_{1f}A_{3r}}{\left[V_{40f} + A_{1f}x - A_{3r}x\right]^{n+1}} + nP_0 V_{40r}^n l_{sf}^2 \frac{A_{3f}^2 - A_{1r}A_{3f}}{\left[V_{40r} + A_{1r}x - A_{3f}x\right]^{n+1}}$$
$$+nP_0 V_{40f}^n l_{sf}^2 \frac{A_{1f}^2 - A_{1f}A_{3r}}{\left[V_{40f} - A_{1f}x + A_{3r}x\right]^{n+1}} + nP_0 V_{40r}^n l_{sf}^2 \frac{A_{3f}^2 - A_{1r}A_{3f}}{\left[V_{40r} - A_{1r}x + A_{3f}x\right]^{n+1}}$$

$$k_{\psi r} = nP_0 V_{40r}^n l_{sr}^2 \frac{A_{1r}^2 - A_{1r}A_{3f}}{\left[V_{40r} + A_{1r}x - A_{3f}x\right]^{n+1}} + nP_0 V_{40f}^n l_{sr}^2 \frac{A_{3r}^2 - A_{1f}A_{3r}}{\left[V_{40f} + A_{1f}x - A_{3r}x\right]^{n+1}}$$
$$+nP_0 V_{40r}^n l_{sr}^2 \frac{A_{1r}^2 - A_{1r}A_{3f}}{\left[V_{40r} - A_{1r}x + A_{3f}x\right]^{n+1}} + nP_0 V_{40f}^n l_{sr}^2 \frac{A_{3r}^2 - A_{1f}A_{3r}}{\left[V_{40f} - A_{1f}x + A_{3r}x\right]^{n+1}}$$

$$k_w = \frac{k_{\psi f}k_{\psi r}}{k_{\psi f} + k_{\psi r}} \quad (6.16)$$

The formulations of the warp-mode stiffness properties of the suspension B_U are derived in a similar manner, such that:

$$k_{\psi i} = nP_0 V_{40i}^n l_{si}^2 \frac{A_{2i}^2}{\left[V_{40i} + A_{2i}x\right]^{n+1}} + nP_0 V_{40i}^n l_{si}^2 \frac{A_{2i}^2}{\left[V_{40i} - A_{2i}x\right]^{n+1}} \qquad (i = f, r)$$

$$k_w = \frac{k_{\psi f} k_{\psi r}}{k_{\psi f} + k_{\psi r}} \tag{6.17}$$

Suspension damping properties:

The damping properties of the two full-vehicle suspension configurations (B_X and B_U) are determined using the method employed for evaluating the stiffness properties, where the displacement inputs are replaced by the velocity inputs. Unlike the stiffness properties, the damping properties are expressed in a relatively simpler manner. The damping properties of the two selected full-vehicle suspension systems are expressed by the dissipative components of the strut forces in each mode, as evident in Eqs. (6.4 and 6.5).

The bounce mode damping forces, developed by the struts in the X-coupled arrangement are directly extracted from Eq. (6.4) by letting $\dot{X}_{fl} = \dot{X}_{fr} = \dot{X}_{rl} = \dot{X}_{rr} = \dot{x}$, such that:

$$F_{dvf} \approx \frac{\rho A_{1f} \left|A_{1f}\dot{x} - A_{3r}\dot{x}\right| (A_{1f}\dot{x} - A_{3r}\dot{x})}{2C_d^2 a_{12f}^2} - \frac{\rho A_{3f} \left|A_{1r}\dot{x} - A_{3f}\dot{x}\right| (A_{1r}\dot{x} - A_{3f}\dot{x})}{2C_d^2 a_{12r}^2} \tag{6.18a}$$

where *r=rr* for the front-left strut (*f=fl*), and *r=rl* for the front-right strut (*f=fr*).

$$F_{dvr} \approx \frac{\rho A_{1r} \left|A_{1r}\dot{x} - A_{3f}\dot{x}\right| (A_{1r}\dot{x} - A_{3f}\dot{x})}{2C_d^2 a_{12r}^2} - \frac{\rho A_{3r} \left|A_{1f}\dot{x} - A_{3r}\dot{x}\right| (A_{1f}\dot{x} - A_{3r}\dot{x})}{2C_d^2 a_{12f}^2} \tag{6.18b}$$

where *f=fl* for the rear-right strut (*r=rr*), and *f=fr* for the rear-left strut (*r=rl*). The formulations of warp-mode damping property of the suspension B_X are identical to those of bounce-mode damping, as presented in Eq. (6.18).

The roll mode damping forces, developed by the struts in the X-coupled arrangement are also deducted from Eq. (6.4)by letting $\dot{X}_{fl} = -\dot{X}_{fr} = \dot{X}_{rl} = -\dot{X}_{rr} = \dot{x}$, such that:

$$F_{dRf} \approx \frac{\rho A_{1f}\left|A_{1f}\dot{x}+A_{3r}\dot{x}\right|(A_{1f}\dot{x}+A_{3r}\dot{x})}{2C_d^2 a_{12f}^2}+\frac{\rho A_{3f}\left|A_{1r}\dot{x}+A_{3f}\dot{x}\right|(A_{1r}\dot{x}+A_{3f}\dot{x})}{2C_d^2 a_{12r}^2} \tag{6.19a}$$

where r=*rr* for the front-left strut (f=*fl*), and r=*rl* for the front-right strut (f=*fr*).

$$F_{dRr} \approx \frac{\rho A_{1r}\left|A_{1r}\dot{x}+A_{3f}\dot{x}\right|(A_{1r}\dot{x}+A_{3f}\dot{x})}{2C_d^2 a_{12r}^2}+\frac{\rho A_{3r}\left|A_{1f}\dot{x}+A_{3r}\dot{x}\right|(A_{1f}\dot{x}+A_{3r}\dot{x})}{2C_d^2 a_{12f}^2} \tag{6.19b}$$

where f=*fl* for the rear-right strut (r=*rr*), and f=*fr* for the rear-left strut (r=*rl*). The formulations of pitch-mode damping property of the suspension B_X are identical to those of roll-mode damping, as presented in Eq. (6.19).

The formulations of bounce-mode damping property of the unconnected suspension B_U are derived, such that:

$$F_{dvi} \approx \frac{\rho A_{2i}^3\left|\dot{x}\right|(\dot{x})}{2C_d^2 a_{12i}^2} \quad (i = fl, fr, rl, rr) \tag{6.20}$$

The formulations of other mode damping properties (roll, pitch and warp) of the unconnected suspension B_U are identical to those of bounce-mode damping, as presented in Eq. (6.20), due to the fact that there is no coupling among different suspension struts.

6.5 Properties of the Full-Vehicle Suspension Configurations

The design parameters of both the configurations are selected, upon consideration of identical load carrying capacity for the heavy vehicle model presented in Section 3.2 with parameters described in (Tables 3.1 and 4.1). The selected design parameters for the X-coupled (B_X) and unconnected (B_U) configurations resulted in identical bounce mode natural frequencies of the front and rear suspensions at the static design ride height, in the order of 1.5 Hz. The bleed and damping valves flow areas, and interconnecting pipe sizes are further chosen to achieve nearly identical bounce mode damping properties of the

front and rear struts of both the suspensions (B_U and B_X). The simulation results describing the properties of both the configurations are presented and discussed below.

6.5.1 Bounce Mode Properties

Figures 6.18(a) and (b) present the bounce mode stiffness and damping properties of the two suspension configurations B_U and B_X, respectively. Under the in-phase bounce-mode excitations, both the suspensions yield identical front and rear suspension rates throughout the deflection range considered. The front suspension rate of both the configurations is lower than that of the rear suspension due to the larger load supported by the rear axle. Both the front and rear suspensions exhibit progressively hardening property in bump, but softening effect in rebound, as evident in Figure 6.18(a), which is attributed to the force-deflection property of the gas.

Both the suspension configurations also reveal identical bounce mode damping property of the front- and rear-axle suspensions, as shown in Figure 6.18 (b), expressed in terms of force-velocity relationships. It should be noted that both configurations are evaluated assuming the symmetric damping in compression and rebound, although the asymmetric damping properties can also be easily realized in a similar manner. The flows through the valves are initiated, when the strut velocity approaches or exceeds 0.08 m/s, and the valves become fully open at 1.5 m/s. The results in Figures 6.18(a) and (b) show that the uncoupled and X-coupled suspensions possess identical suspension rate and damping properties in the bounce mode, and the X-coupled suspension (B_X) would thus be expected to retain the same vertical ride quality as the unconnected suspension B_U.

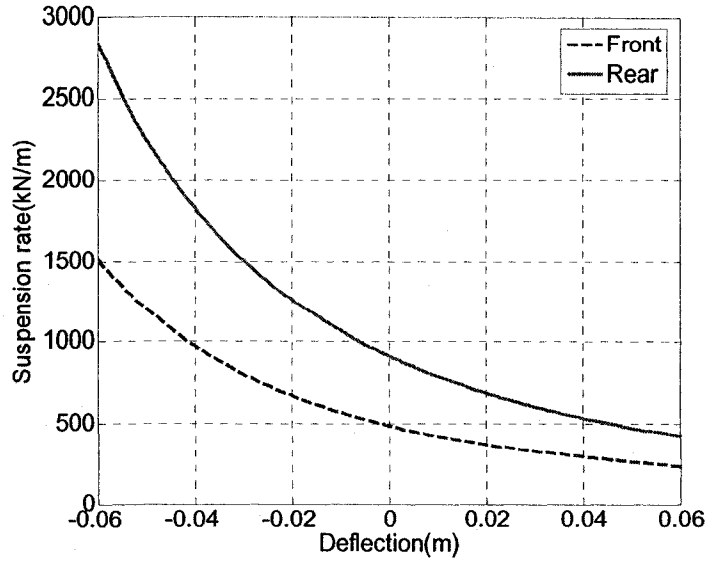

(a)

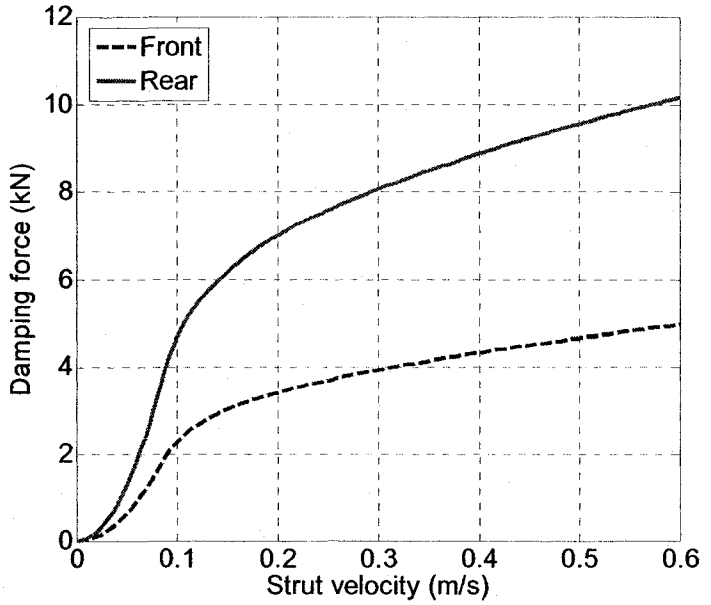

(b)

Figure 6.18: Bounce-mode properties of the full-vehicle suspension configurations (B_U and B_X): (a) suspension rate; and (b) bounce-mode damping.

6.5.2 Roll Mode Properties

Figures 6.19(a) and (b) illustrate the roll-mode properties of both the suspension configurations B_U and B_X in terms of roll stiffness and roll-mode damping, respectively. Unlike the bounce-mode properties, the X-coupled suspension B_X exhibits significantly

different roll mode properties, when compared to the uncoupled suspension configuration B_U, as it was realized for the roll-plane interconnection. The X-coupled configuration B_X yields considerably higher roll stiffness than the unconnected suspension B_U. The use of passive anti-roll bars generally yields an upward parallel shift of the effective roll stiffness of the unconnected suspension, as it was shown in Figure 3.5, while it cannot augment the roll mode damping. An X-coupled suspension configuration yields considerably enhanced roll-mode damping, as evident in Figure 6.19(b), which would be very beneficial for controlling the transient roll motions during steering maneuvers.

Roll stiffness property of a suspension system strongly affects not only the roll stability of vehicles, but also the vehicle handling quality and directional stability [3, 6]. Roll stiffness distribution is known to influence the handling balance (understeer/oversteer behavior). A vehicle with greater roll stiffness distributed over the front axle would exhibit greater understeer tendency. The static roll stiffnesses of the front and rear suspensions can thus be tuned to help achieve a desirable understeer characteristic.

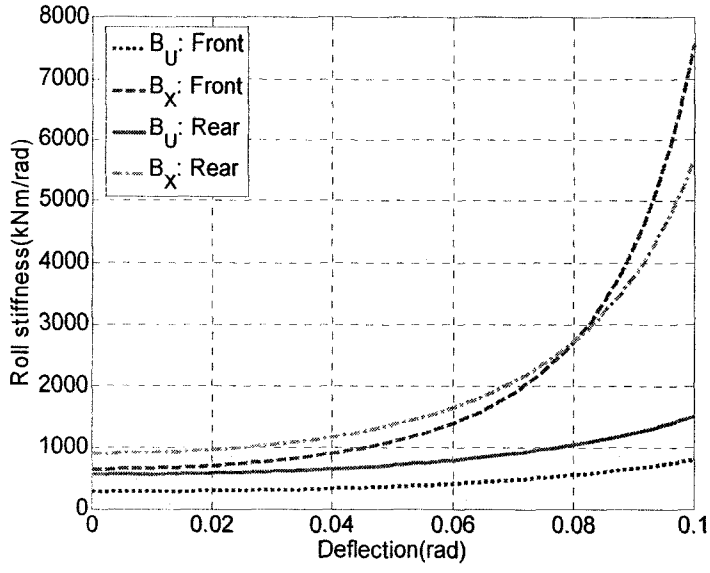

(a)

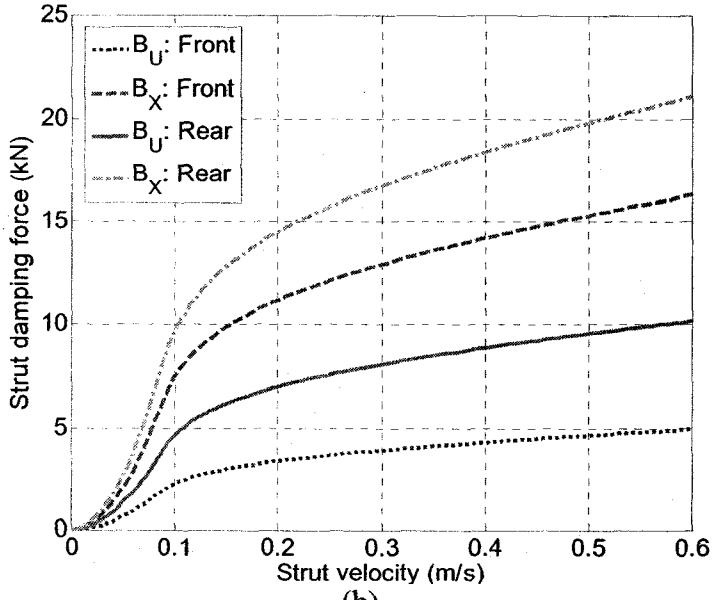

(b)

Figure 6.19: Roll-mode properties of the full-vehicle suspension configurations (B_U and B_X): (a) roll stiffness; and (b) roll-mode damping.

A conventional nonlinear suspension system may induce considerable variations in the roll stiffness distribution over the range of vehicle roll deflections during steering, which may contribute to variations in the understeer coefficient. It is therefore highly desirable to investigate the dynamic roll stiffness distribution characteristics of a suspension with varying roll deflections. The relative roll stiffness distribution ratio

(RSDR), defined as the ratio of front suspension roll stiffness per unit sprung mass supported by the front suspension to that of the rear suspenion $\left(k_{Rf}/m_{sf}\right)/\left(k_{Rr}/m_{sr}\right)$, is used as a measure of the dynamic roll stiffness distribution property, which may be applied to study the variations in understeer behavior under a directional maneuver. Figure 6.20 illustrates variations in the RSDR characteristics of both the suspension configurations (B_U and B_X) as a function of the roll deflection. The results show constant roll stiffness distribution for the unconnected suspension configuration B_U over the entire range of roll deflection considered, while the RSDR of the X-coupled suspension B_X increases progressively with an increase in roll deflection. Such progressive increase in RSDR with increasing roll deflection would indicate a greater understeer tendency during relatively high lateral-acceleration steering maneuvers.

Some studies have stated the understeer coefficient increasing with an increase in lateral acceleration (or during the nonlinear operating range of the tires) would be desirable for improving vehicle yaw or directional stability during tight or emergency steering maneuvers [3, 6, 58, 73]. These indicate that the proposed X-coupled suspension configuration would have considerable potential in enhancing both the roll as well as directional stabilities of the heavy vehicles.

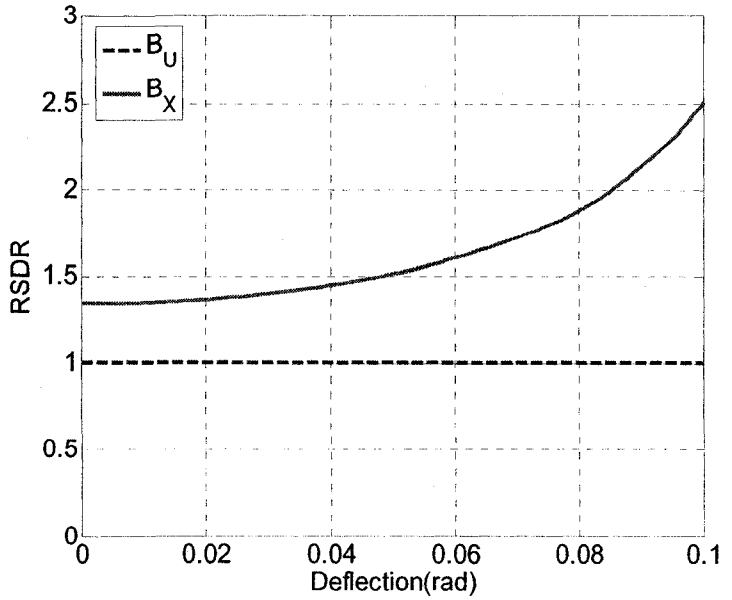

Figure 6.20: A comparison of the RSDR characteristics of the full-vehicle suspension configurations (B_U and B_X).

6.5.3 Pitch Mode Properties

Figure 6.21 illustrates the pitch stiffness properties of the two suspension configurations (B_U and B_X). Similar to the roll stiffness property, the X-coupled configuration B_X yields considerably higher pitch stiffness than the uncoupled suspension B_U. The suspension damping in the pitch mode varies identical to that in the roll mode, as observed in Figure 6.19(b), for each of the configurations. The X-coupled suspension B_X thus yields considerably enhanced pitch-mode damping characteristics due to additional flows through the connecting pipes. The significantly higher pitch stiffness and pitch-mode damping of the X-coupled suspension would help reduce the vehicle pitch motion and thus the longitudinal load transfer during maneuvers involving braking or acceleration, and therefore improved braking and handling performance.

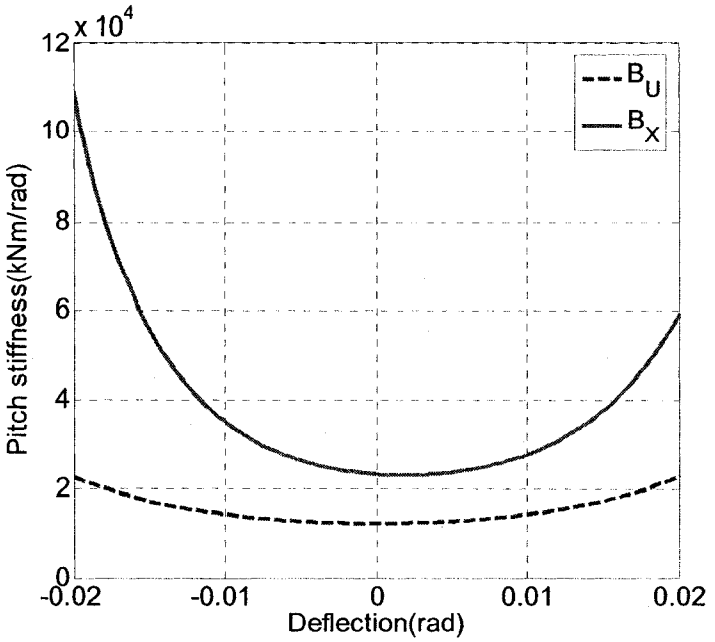

Figure 6.21: Variations in pitch stiffness of the full-vehicle uncoupled (B_U) and X-coupled (B_X) suspension configurations.

6.5.4 Warp Mode Properties

The road-holding and traction performances of a vehicle are greatly influenced by the warp stiffness of the suspension. A relatively low suspension warp stiffness is desirable for improved road-holding and traction performance. The use of anti-roll bars, however, tends to increase the effective suspension warp stiffness, due to the corresponding greater coupling between the roll and warp modes. Figure 6.22 illustrates comparison of the warp stiffness of both the suspension configurations B_U and B_X, while the warp-mode damping was found to be identical to that of bounce-mode for each configuration, shown in Figure 6.18(b). Both the configurations yield identical warp stiffness over the entire range of warp deflection considered, as in the case of bounce mode stiffness. This suggests that the fluidic X-coupling does not alter the warp property of the suspension, while it yields significant gains in the roll as well as pitch mode stiffness and damping properties. This is also consistent with the VPI measure described in Table 6.2.

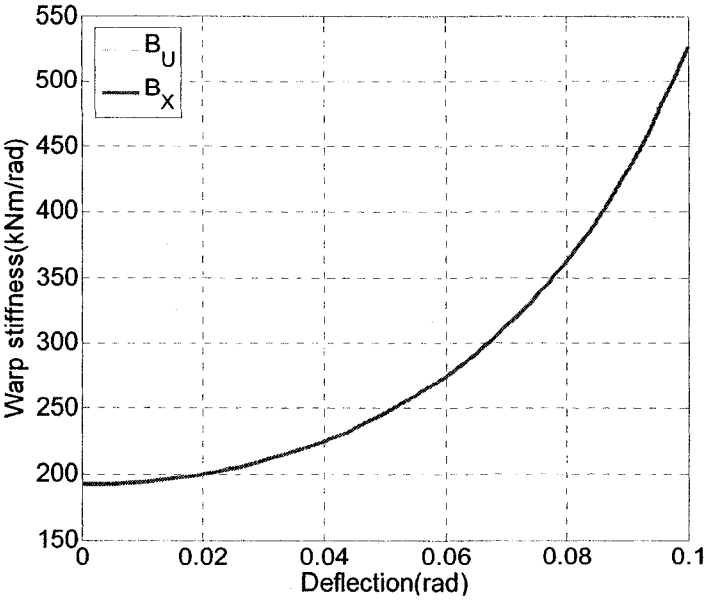

Figure 6.22: Variations in warp stiffness of the full-vehicle uncoupled (B_U) and X-coupled (B_X) suspension configurations.

6.5.5 Design Flexibility and Tuning of the X-Coupled Suspension

The properties of the X-coupled suspension configuration presented in Figures 6.18 to 6.22, clearly show that X-coupling of the individual wheel struts could considerably increase the roll- and pitch-mode stiffness and damping, while maintaining relatively low bounce- and warp-mode properties compared to those of an unconnected suspension. This suggests that the proposed X-coupled suspension configuration could help realize greater decoupling between the roll/pitch and bounce/warp modes, so as to achieve an enhanced design compromise among the four vehicle vibration-modes. Such improved decoupling characteristics of the X-coupled suspension can help achieve improved roll and directional stabilities, pitch attitude control and handling performance, without affecting the primary vertical ride and roadholding qualities. The higher roll and pitch mode stiffnesses were reflected in the VPI values presented in Table 6.2. The Table further anticipated minimal changes in the bounce and warp stiffness properties

compared to those of the unconnected configuration. This confirms the effectiveness of the simplified VPI measure for preliminary assessments and feasibility analyses of alternative suspension interconnections.

Apart from the desirable stiffness and damping properties, the X-coupled hydro-pneumatic suspension offers greater design flexibility. The suspension properties could be conveniently varied through variations in the strut geometry. The design flexibility through variations in the annular piston areas (A_3) of the struts, connected either in the roll-plane or pitch-plane, was demonstrated in Sections 3.3.4 and 4.4. The results reveal that variations in A_3 affect the suspension properties most significantly, without influencing the load carrying capacity and the operating pressure requirements. The influence of variations in the annular piston area (A_{3f}) of the front suspension struts on the resulting stiffness properties of the X-coupled suspension configuration B_X is thus investigated through variations of $\pm 20\%$ about the nominal value, while maintaining identical load carrying capacity and static gas pressure.

Figures 6.23(a) and (b) present the influence of variations in the annular piston area of the front struts on the front and rear suspension rates, respectively. The results show that the variations in A_{3f} cause only minimal changes in the front and rear suspension rates in the rebound mode, which the effect is relatively large on both the suspension rates in the compression mode. It is further observed that an increase in A_{3f} yields a higher front suspension rate, but a lower rear suspension rate, which is attributed to the coupling effect between the front and rear suspension struts. The influence of variations in A_{3f} on the front and rear suspension roll stiffness properties is presented in Figure 6.24, while the influence on the roll stiffness distribution ratio (RSDR) is presented in Figure

6.25. An increase in A_{3f} not only yields higher roll mode stiffness of both the front and rear suspensions, but also a higher RSDR of the full-vehicle X-coupled suspension system. An increase in A_{3f} would thus yield a more understeer tendency with increasing roll deflection of the suspension.

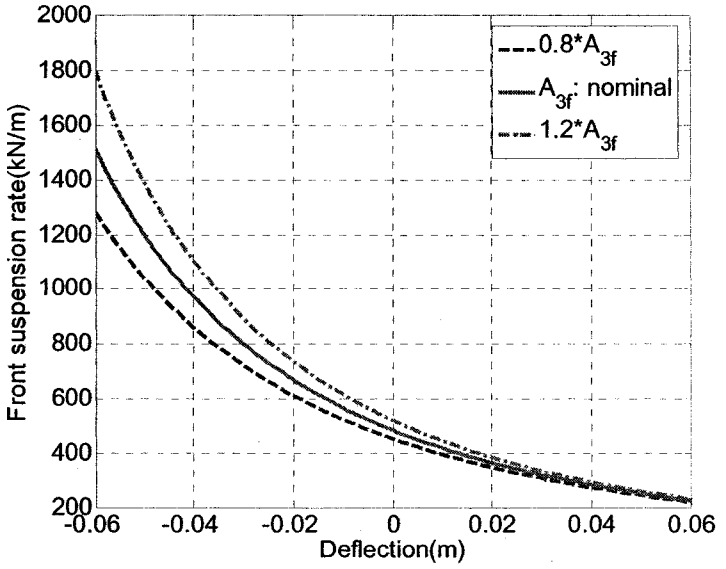

(a)

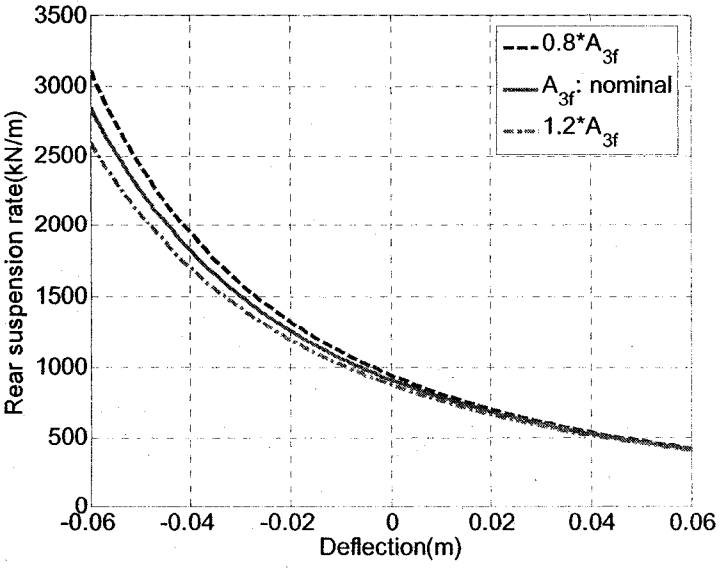

(b)

Figure 6.23: Influence of variations in front-strut annular area A_{3f} on bounce mode stiffness properties of the X-coupled suspension: (a) front suspension rate; and (b) rear suspension rate.

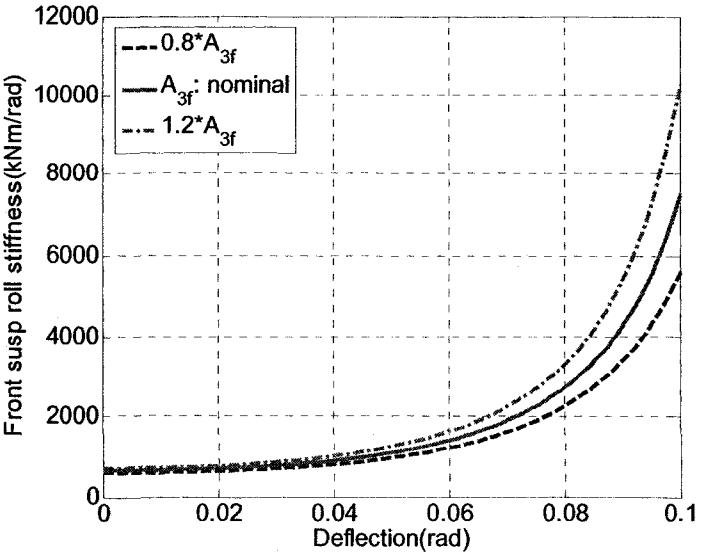

(a)

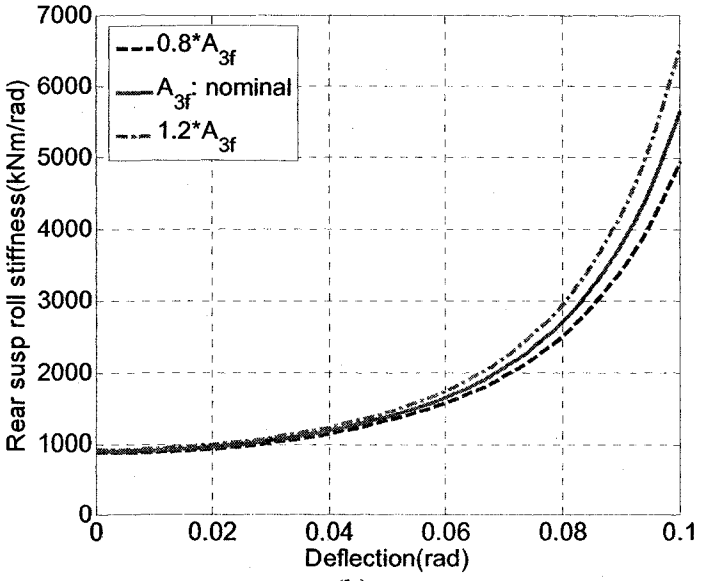

(b)

Figure 6.24: Influence of variations in front-strut annular area A_{3f} on the roll mode stiffness properties of the X-coupled suspension: (a) front suspension roll stiffness; and (b) rear suspension roll stiffness.

Figure 6.26 presents the influence of variations in A_{3f} on the pitch stiffness of the X-coupled suspension B_X. The results show that an increase in A_{3f} yields higher suspension pitch stiffness, suggesting a stronger coupling between the front and rear suspensions. The influence of variations in A_{3f} on the suspension warp stiffness is illustrated in Figure

6.27. The results suggest that a decrease in A_{3f} would reduce the warp stiffness of the X-coupled suspension.

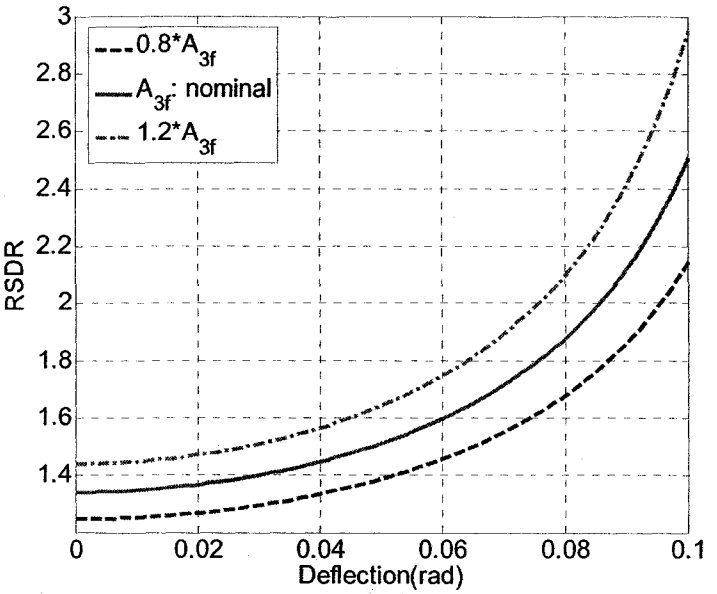

Figure 6.25: Influence of variations in A_{3f} on the RSDR of the X-coupled suspension.

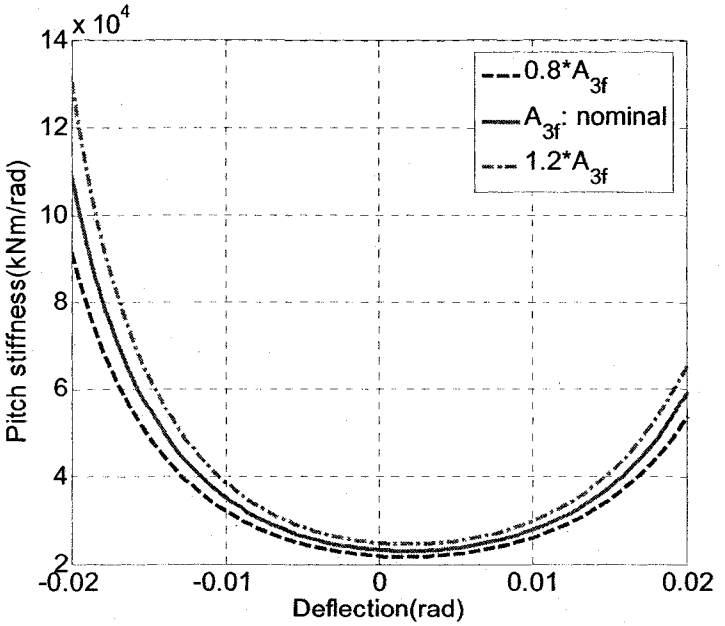

Figure 6.26: Influence of variations in A_{3f} on pitch stiffness of the X-coupled suspension.

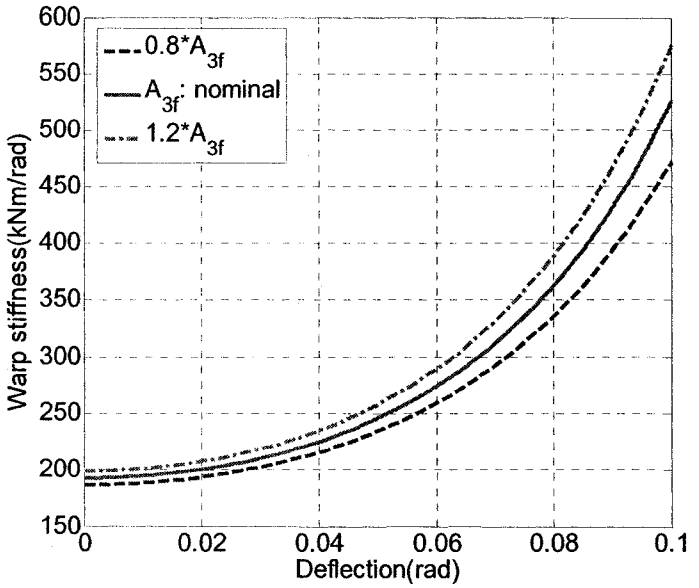

Figure 6.27: Influence of variations in front-strut annular area A_{3f} on warp stiffness of the X-coupled suspension.

6.6 Dynamics Responses of the Vehicle

The performance potentials of the proposed X-coupled suspension configuration B_X are further evaluated in terms of dynamic responses of the vehicle, subject to braking and steering inputs, compared to the unconnected configuration B_U. The equations of motion for the full-vehicle model (Figure 6.1) equipped with different suspension configurations are analyzed through simultaneous solutions of Eqs. (6.1) and (6.2), combined with dynamic strut forces presented in Eqs. (6.4) and (6.5).

The nonlinear roll- and pitch-plane vehicle models formulated in Chapter 2, served as effective means in evaluating the ride, and roll or pitch performance characteristics of road vehicles with different suspension designs. These models, however, are not adequate in evaluating the handling and directional performance of road vehicles, particularly under combined steering and braking inputs. The 14-DOF full-vehicle model developed and validated in this chapter can be applied to evaluate the coupled roll, pitch and

directional dynamic responses of the vehicle with the two suspension configurations (B_X and B_U).

Two critical handling maneuvers, braking-in-a-turn and split-μ straight-line braking, are used for the relative analyses of handling dynamic response and directional stability of the vehicle [4, 5, 53, 61, 169, 170]. Two road surfaces with different friction characteristics are considered for the dynamic analyses: (i) a dry road with friction coefficient of 0.9, referred to as '*dry surface*'; and (ii) a wet road with friction coefficient of 0.5, referred to as '*wet surface*' [158]. The initial vehicle speed for the analyses is set as 28 m/s, while the braking torque distribution is selected to be proportional to the static weight distribution between the two axles of the vehicle [4, 100]. The braking model (Eq. (4.1)) developed in Chapter 4 is used in the analysis. The braking torque and steer angle inputs applied during a braking-in-a-turn maneuver are presented in Figure 6.28. Figure 6.29 illustrates the front and rear braking-torque inputs for the split-μ straight-line braking maneuver, where the left- and right-vehicle tracks are assumed to have road friction coefficients of 0.9 and 0.5, respectively.

Vehicle dynamic performance during braking-in-a-turn can be effectively evaluated in terms of: (a) roll performance measures: sprung mass roll angle and rate; (b) pitch performance measures: sprung mass pitch angle and rate; and (c) handling or directional performance measures: yaw rate, lateral acceleration and vehicle path [1-6, 15, 40, 53]. Vehicle dynamic performance during the split-μ straight-line braking is further evaluated in terms of the above roll and pitch performance measures.

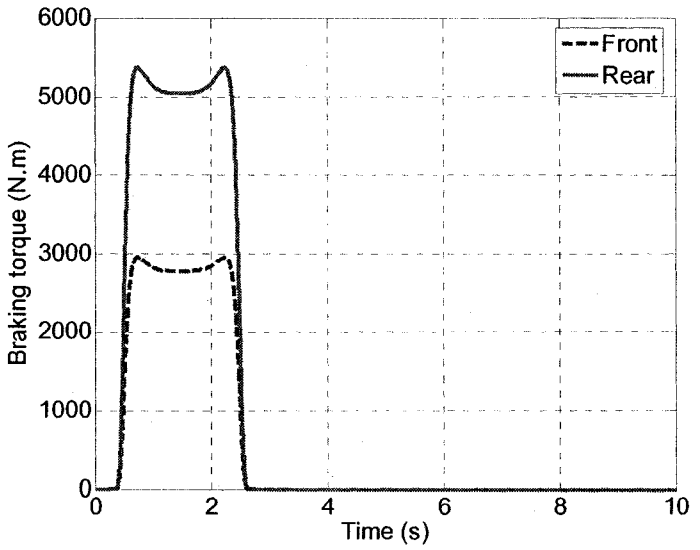

(a)

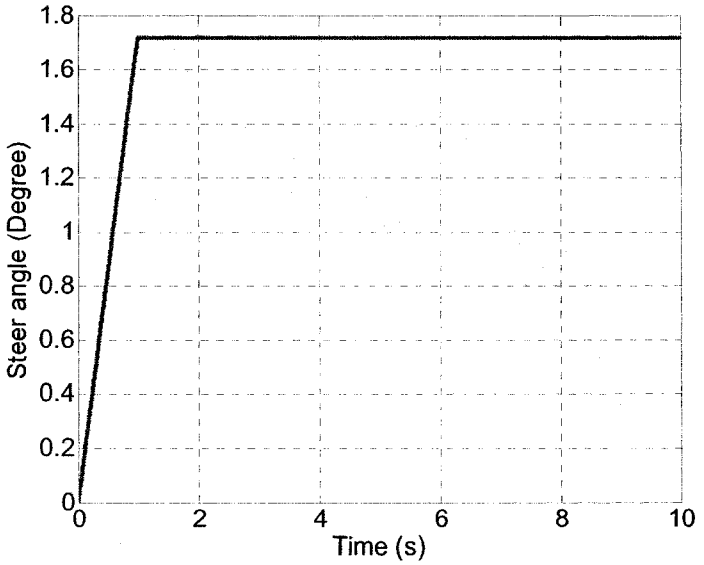

(b)

Figure 6.28: Representations of the braking-in-a-turn inputs: (a) braking torques; and (b) steer angle.

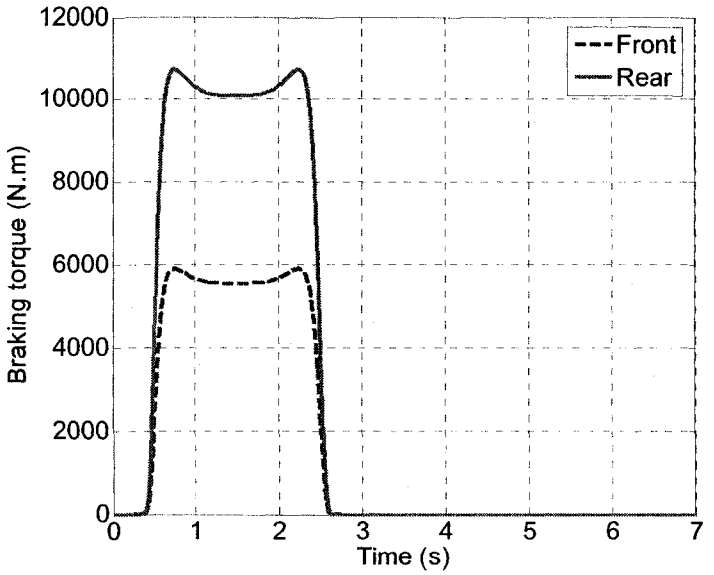

Figure 6.29: Representations of the split-μ straight-line braking inputs.

6.6.1 Responses to a Braking-in-a-Turn Maneuver

Figure 6.30 presents the sprung mass roll dynamic responses (roll angle and rate) of the vehicle with the two different suspension configurations (B_X and B_U) under the defined braking-in-a-turn inputs on the *dry surface*. The results show that the X-coupled suspension configuration B_X yields considerably lower sprung mass roll angle as well as velocity compared to the unconnected suspension B_U. Furthermore, the roll responses due to configuration B_X decay more rapidly, as seen in Figures 6.30(a) and (b). These are attributed to the enhanced roll stiffness and roll-mode damping properties of the X-coupled suspension, as evident in Figures 6.19(a) and (b). The responses on the *wet surface* exhibit similar trends and are thus not presented.

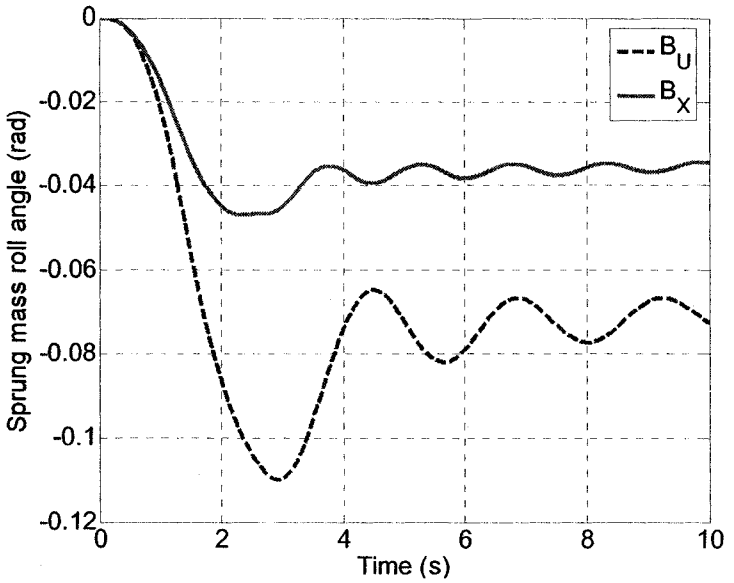

(a)

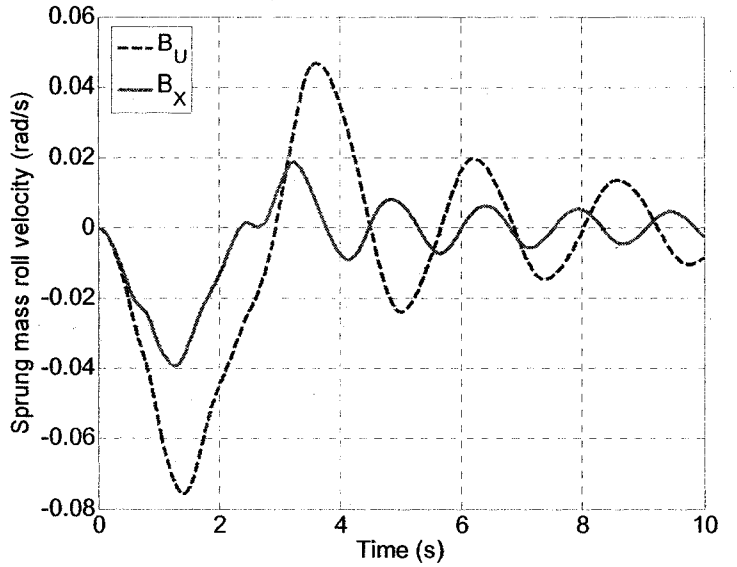

(b)

Figure 6.30: Dynamic roll responses of the heavy vehicle with two different suspension configurations (B_U and B_X) during a braking-in-a-turn maneuver on the dry surface: (a) sprung mass roll angle; and (b) sprung mass roll velocity.

Figure 6.31 presents the sprung mass pitch angle and velocity responses of the vehicle with the two suspension configurations under the defined braking-in-a-turn inputs on the *dry surface*. Similar to the roll responses, the X-coupled suspension B_X yields significantly lower pitch angle and velocity when compared to those of the vehicle with

suspension configuration B_U, which is attributed to the enhanced pitch stiffness and pitch-mode damping of the X-coupled suspension. The results in Figures 6.30 and 6.31 suggest the considerably enhanced anti-roll and anti-pitch properties of the vehicle comprising X-couplings among different suspension strut units.

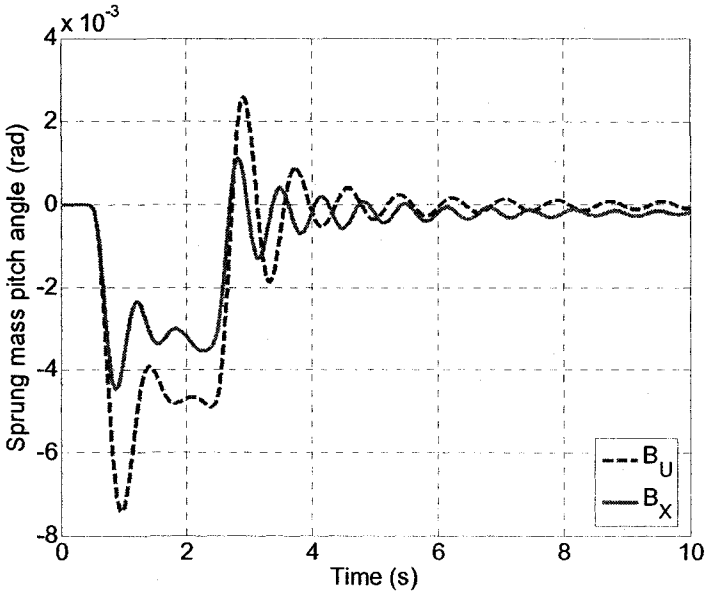

(a)

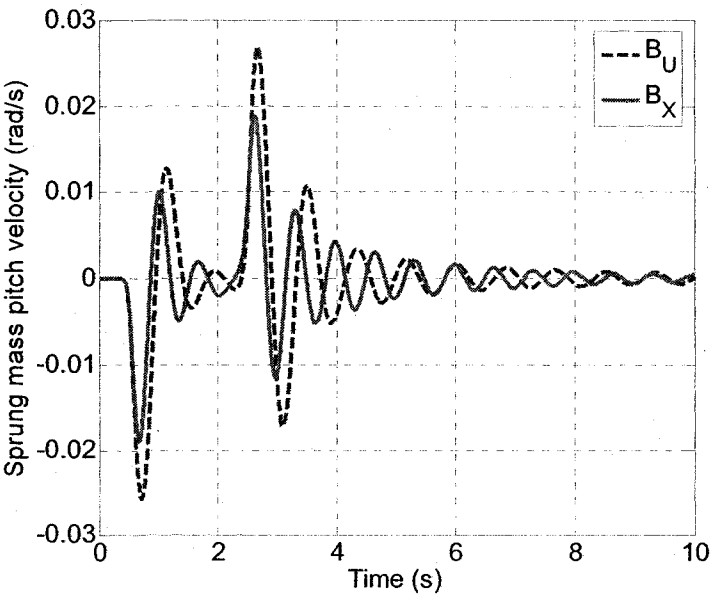

(b)

Figure 6.31: Dynamic pitch responses of the heavy vehicle with two different suspension configurations (B_U and B_X) during a braking-in-a-turn maneuver on the dry surface: (a) sprung mass pitch angle; and (b) sprung mass pitch velocity.

Figures 6.32(a), (b) and (c) present the relative handling and directional responses of the vehicle with two suspensions in terms of yaw rate, lateral acceleration and vehicle path during the defined braking-in-a-turn maneuver on the *dry surface*, respectively. The results show that the X-coupled suspension B_X yields slightly lower yaw rate and lateral acceleration, which leads to a slightly larger turning radius, compared to the unconnected suspension B_U. These are mostly attributed to the relatively higher RSDR and roll-mode damping of the X-coupled suspension B_X, as evident in Figure 6.20. The results suggest a slightly improved understeer tendency, which is beneficial for enhancing vehicle yaw or directional stability during tight or emergent steering maneuvers [3, 6, 58, 73].

Owing to the identical bounce-mode stiffness and damping properties, The X-coupled suspension (B_X) and unconnected suspension (B_X) are expected to yield comparable vertical ride performance, as observed from the responses of roll- and pitch-connected suspensions. It can thus be deduce that the proposed X-coupled hydro-pneumatic suspension configuration offers considerable potential benefits in realizing enhanced anti-roll and anti-pitch properties, handling performance, and roll and directional stabilities, without deteriorating the vertical ride and roadholding qualities of the vehicle.

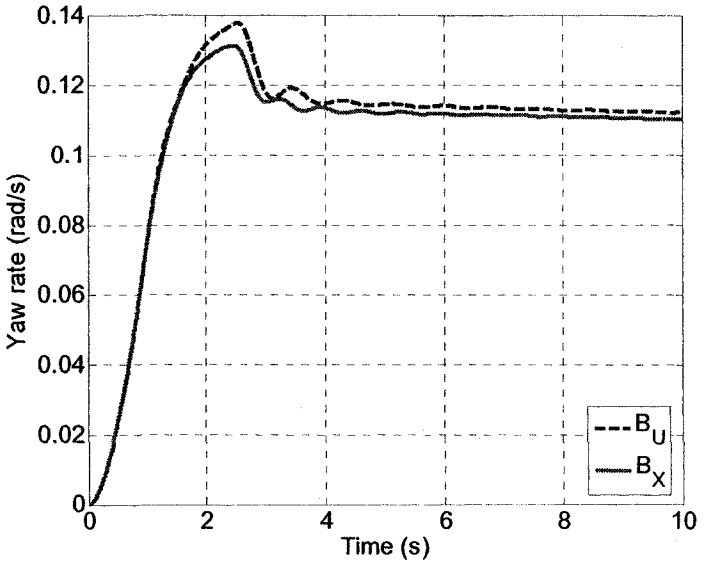
0.14
0.12
0.1
0.08
0.06
0.04
0.02
0
Yaw rate (rad/s)
0
2
4
6
8
10
Time (s)
B_U
B_X

(a)

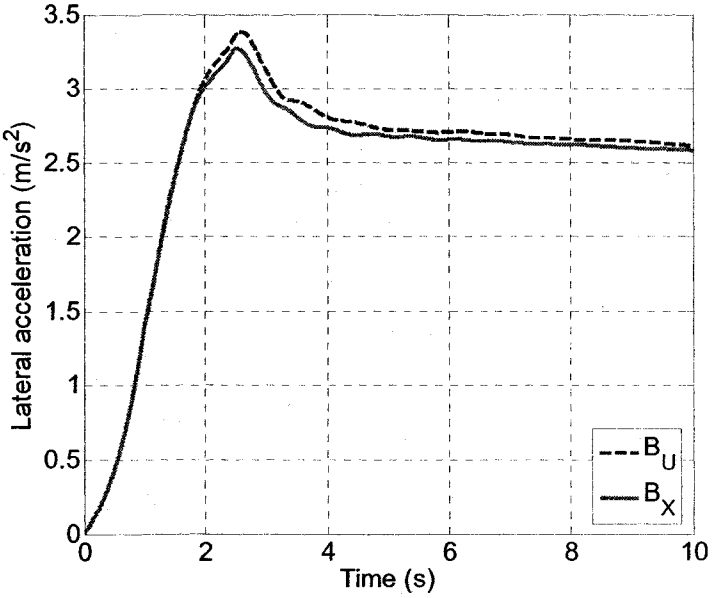
3.5
3
2.5
2
1.5
1
0.5
0
Lateral acceleration (m/s^2)
0
2
4
6
8
10
Time (s)
B_U
B_X

(b)

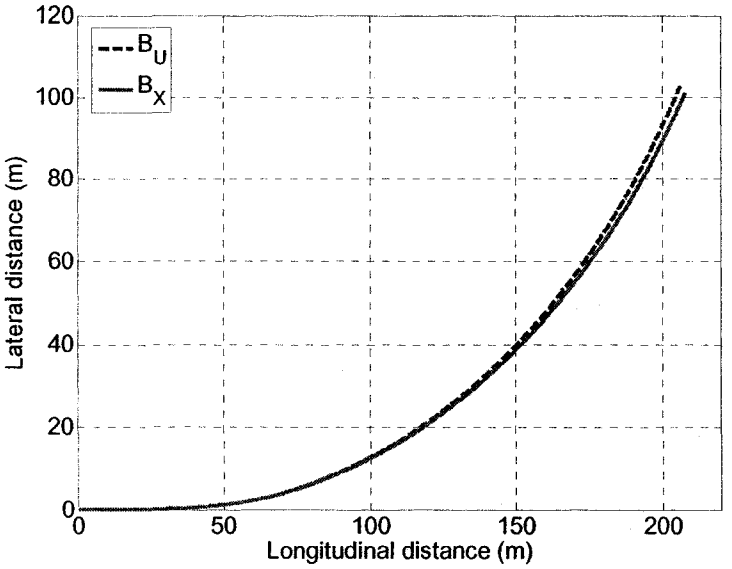

(c)

Figure 6.32: Directional responses of the heavy vehicle with two different suspension configurations (B_U and B_X) during a braking-in-a-turn maneuver on the dry surface: (a) yaw rate; (b) lateral acceleration; and (c) vehicle path.

6.6.2 Responses under a Split-μ Straight-Line Braking

Figures 6.33 and 6.34 present the sprung mass roll and pitch responses of the vehicle during the defined split-μ straight-line braking inputs (Figure 6.29), respectively. The results show that the X-coupled suspension B_X yields lower magnitudes of roll and pitch deflections and velocities of the sprung mass, as those were observed under the braking-in-a-turn maneuver. The results thus further confirm the improved anti-roll and anti-pitch properties of the X-coupled suspension, and thereby enhanced directional stability and control performance [50].

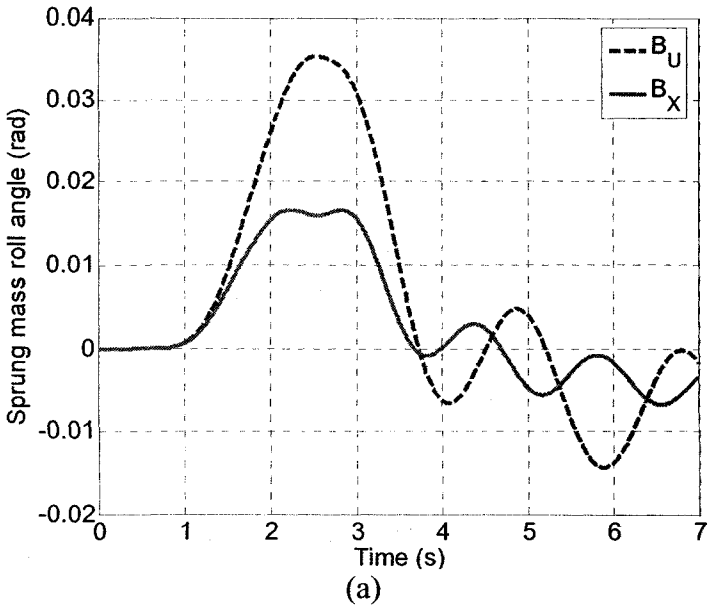

(a)

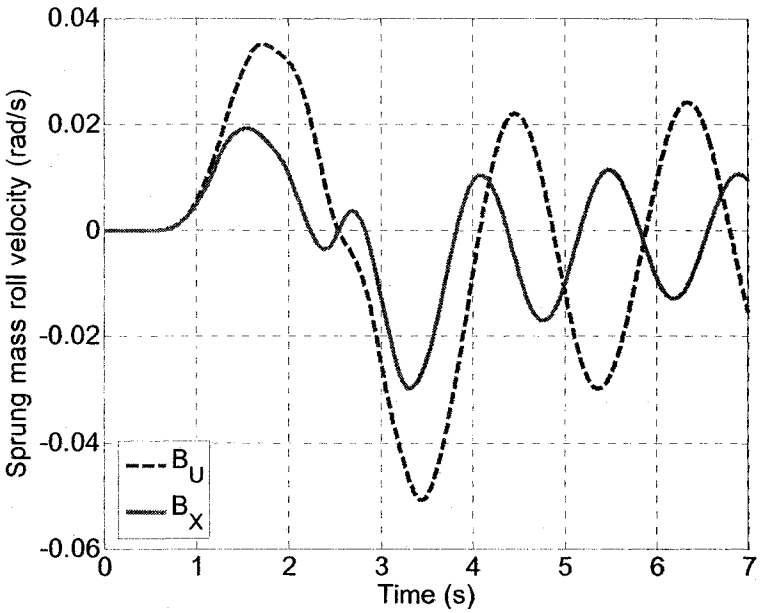

(b)

Figure 6.33: Dynamic roll responses of the heavy vehicle with two different suspension configurations (B_U and B_X) during split-μ straight-line braking: (a) sprung mass roll angle; and (b) sprung mass roll velocity.

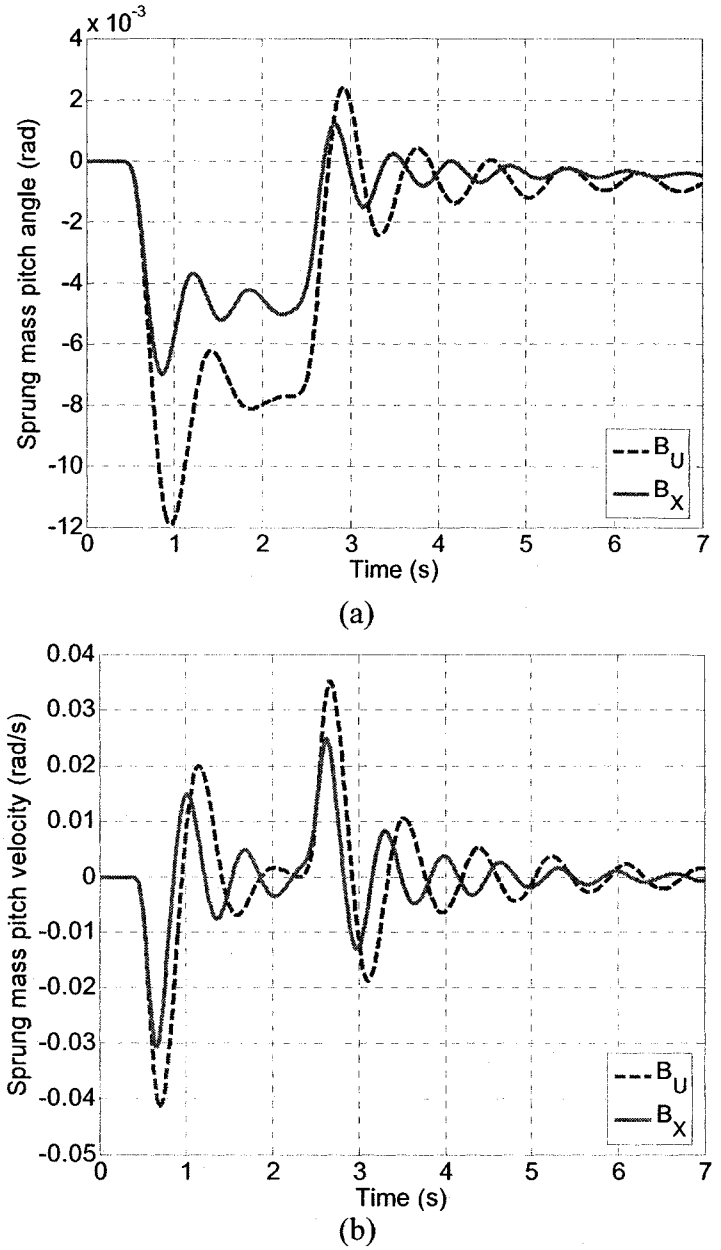

Figure 6.34: Dynamic pitch responses of the heavy vehicle with two different suspension configurations (B_U and B_X) during split-μ straight-line braking: (a) sprung mass pitch angle; and (b) sprung mass pitch velocity.

6.7 Summary

In this chapter, a number of feasible configurations of full-vehicle interconnected suspensions were conceived and investigated, in terms of their feasibility and anticipated suspension property. The relative properties of the selected X-coupled configuration are

evaluated and compared to those of the unconnected suspension. The design flexibility and vehicle dynamic responses are further evaluated under split-μ straight-line braking and braking-in-a-turn maneuvers. A 14-DOF nonlinear two-axle vehicle model was developed to study the directional dynamic responses, and was validated using the available measured data. A number of feasible full-vehicle interconnected suspensions were identified and preliminarily evaluated based on a proposed simplified measure, vehicle property index (VPI), which demonstrated that different interconnected suspension configurations could yield quite different properties. A full-vehicle X-coupled suspension configuration that involves diagonal hydraulic-interconnections among the suspension strut units was selected for further investigation compared to an unconnected hydro-pneumatic suspension.

The analytical formulations of strut forces and suspension properties of the selected full-vehicle X-coupled suspension configuration were derived based on the previously formulated generalized model. The suspension stiffness and damping properties were evaluated and compared with those of an unconnected full-vehicle suspension configuration in the bounce-, roll-, pitch- and warp-modes. The suspension design flexibility of the X-coupled suspension was also investigated using parametric studies. Vehicle dynamic responses, in terms of roll, pitch and directional performance measures, were further assessed under two critical handling maneuvers: braking-in-a-turn and split-μ straight-line braking. The results demonstrated that the proposed X-coupled suspension could yield considerably enhanced anti-roll and anti-pitch properties, handling performance, and roll and directional stabilities, without deteriorating the vertical ride and roadholding qualities of road vehicles.

CHAPTER 7

CONCLUSIONS AND RECOMMENDATIONS

7.1 Highlights of the Dissertation Research

This dissertation research has systematically explored two advanced passive vehicle suspension design concepts, interconnected hydro-pneumatic suspension and twin-gas-chamber strut suspension, which have considerable potential applications to heavy vehicles, SUVs, military vehicles, and racing cars. Both the suspension concepts offer substantial flexibility for realizing variable stiffness and damping properties. The proposed struts designs, including single- and twin-gas-chamber struts, also offer larger working area and thus lower pressure requirements, and integrated damping components. The studies of the these advanced passive suspension design concepts have been performed through comprehensive analytical formulations of the compressible and incompressible hydraulic fluids and analyses under various excitations arising from vehicle-road interactions, steering and braking maneuvers, and crosswinds. The analytical models and the methodologies were validated on the basis of the available experimental data. Apart from these advanced suspension design concepts, fundamental pitch dynamics of heavy vehicles have also been explored so as to establish a set of suspension tuning rules in the vehicle pitch plane.

The major highlights of the dissertation work are described below:

- Two hydro-pneumatic strut design concepts, single- and twin-gas-chamber struts, were proposed to obtain a compact deign with considerably larger effective operating area. These struts designs integrate gas chamber(s) and damping valves within the same units, based on which various fluidic interconnections can be conveniently conceived. The novel twin-gas-chamber strut design further provides potential benefits in realizing nearly symmetric suspension rates in

compression and rebound, and considerably improved roll- and pitch-mode stiffnesses.

- The nonlinear in-plane (roll- and pitch-plane) vehicle models have been developed for facilitating the investigation of fundamental properties of different unconnected and interconnected suspension configurations, as well as vehicle dynamic responses under a variety of excitations arising from road roughness profiles, steering and braking maneuvers, and crosswinds. A number of roll- or pitch-interconnected and unconnected suspension configurations, based on the two proposed strut designs, were analyzed to develop the strut forces and suspension properties, which incorporate hydraulic fluid compressibility, floating piston dynamics, and variable symmetric and asymmetric damping valves.

- A generalized model of strut forces of various interconnected and unconnected suspension configurations was formulated to unify different suspension configurations in an integrated frame, which may further provide a foundation for exploring common characteristics of various suspension configurations in a theoretical manner.

- The roll plane suspension properties and dynamic responses of a vehicle were analyzed and compared for five different suspension configurations, based on the formulated nonlinear roll-plane vehicle model. These included four configurations with symmetric damping: unconnected with and without an anti-roll bar, hydraulically interconnected, and pneumatically interconnected. An additional hydraulically interconnected configuration with asymmetric damping and increased roll stiffness is also considered. The relative vertical and roll responses of the vehicle model with different suspension configurations were evaluated under excitations arising from tire interactions with random road profiles and discrete road bumps, and centrifugal accelerations corresponding to steady turning and lane-change maneuvers, as well as crosswinds.

- The pitch-plane suspension properties and dynamic responses of the nonlinear pitch-plane vehicle model with different pitch-interconnected suspensions configurations were investigated, under the braking inputs and random road roughness excitations. These interconnected suspension configurations involved pneumatic, hydraulic and hybrid fluidic interconnections between the front and rear struts. The essential properties of the pitch-connected configurations were evaluated in terms of front and rear suspension rates, pitch stiffness, and bounce and pitch mode damping characteristics, and compared with those of the unconnected suspension. The pitch-plane dynamic responses of a heavy vehicle with proposed suspension configurations were also evaluated under braking inputs and random road roughness excitations. A novel braking torque model was proposed to characterize the brake-fade effects. The ride height control ability of pitch-interconnected suspensions was also analytically proven. The effects of load variations on the performance of the vehicle with different suspensions as well as ride height leveling system were further investigated.

- In a similar manner to the study of interconnected suspensions, the analyses of the proposed twin-gas-chamber strut suspension were also performed in terms of roll- as well as pitch-plane suspension properties and dynamic responses of the vehicle, based on the two formulated in-plane vehicle models. The responses are compared with those of an unconnected single-gas-chamber strut suspension.

- The full-vehicle interconnected suspensions were investigated, in terms of the feasibility, suspension property, design flexibility and vehicle dynamic responses. A 14-DOF nonlinear two-axle vehicle model was developed and validated using the available measured data. A number of feasible full-vehicle interconnected suspensions were identified and preliminarily evaluated based on a simplified measure, vehicle property index (VPI), which demonstrated that different interconnected suspension configurations could yield quite different suspension properties.

- A full-vehicle X-coupled suspension configuration that involves diagonal hydraulic-interconnections among the suspension strut units was selected for further investigation compared to an unconnected hydro-pneumatic suspension. The suspension stiffness and damping properties were evaluated and compared, in terms of bounce-, roll-, pitch- and warp-modes. The design flexibility of the X-coupled suspension was also investigated using parametric studies. Vehicle dynamic responses, in terms of roll, pitch and directional performance measures, were further assessed under two critical handling maneuvers: braking-in-a-turn and split-μ straight-line braking.

- The front/rear suspension stiffness tunings of two-axle heavy vehicles with unconnected suspensions were systematically explored, under a wide range of random road inputs and driving speeds, as well as braking inputs. Upon considerations of the mathematical formulations of two pitch plane models of a two-axle heavy vehicle with unconnected and coupled suspensions, three dimensionless measures of suspension properties, namely the pitch margin (PM), pitch stiffness ratio (PSR) and coupled pitch stiffness ratio (CPSR), were proposed and analyzed for different unconnected suspension tunings and load conditions. The simulation results were explored in an attempt to derive influences of suspension tunings and measures on the responses, and for establishing some basic suspension tuning rules of heavy vehicles with conventional unconnected suspensions.

7.2 Conclusions

Based upon the studies carried out in the dissertation, the following major conclusions are drawn:

- The analytical formulations of strut forces and stiffness and damping properties of the various in-plane (roll- or pitch-plane) interconnected suspension

configurations clearly demonstrated the coupling effects of springing forces between the different suspension struts. These formulations further showed that the hydraulically and hybrid-fluidically interconnected suspension configurations involve the coupled damping forces.

- The generalized model of strut forces of various in-plane interconnected and unconnected suspension configurations provides an integrated frame for different suspension configurations, as well as a theoretical foundation for exploring fundamental characteristics of various coupled suspension configurations.

- Comparisons of roll-plane properties of different suspension configurations demonstrated that both hydraulically and pneumatically interconnected suspensions yield enhanced roll stiffness while maintaining soft vertical ride. The hydraulic interconnections further offer improved roll-mode damping attributed to the hydraulic-coupling effect. The results attained from the parametric studies showed the superior design flexibility of the fluidic-interconnections. The roll stiffness of the connected struts could be conveniently improved by varying the design parameters of the struts, which is unlike the use of anti-roll bar that would add weight and also pose a challenge in view of the chassis design space.

- The results of the roll dynamic responses showed that fluidic interconnections yield improved roll response, with only negligible influence on the vertical ride performance, irrespective of driving speed and road roughness. For the centrifugal acceleration excitations, the roll responses of the vehicle evaluated in terms of the sprung mass roll angle and LTR are nearly identical with pneumatic interconnection and unconnected suspension with anti-roll bar. The hydraulic interconnections yield much lower roll angle responses, which tend to decay more rapidly and can be attributed to its enhanced roll-mode damping and stiffness properties. The asymmetric damping coupled with hydraulic interconnections also yields improved shock and roll motion isolation performance under the deterministic road inputs considered.

- The analyses of the pitch-plane suspension properties suggested that the pitch-interconnections, either hydraulic or pneumatic, can yield significantly higher pitch stiffness without affecting the vertical suspension rates and bounce damping, which could thus achieve improved vehicle anti-dive performance and reduce dynamic longitudinal load transfers under braking maneuvers. The hydraulic interconnections further permit considerably higher pitch-mode damping compared to the unconnected suspension, pneumatically and hybrid-fluidically interconnected configurations. The most significant benefits of pitch-connected suspension arise from its design flexibility. The results attained from parametric analyses revealed that the proposed struts and interconnections can be easily tuned to achieve desired pitch properties with negligible influence on the bounce properties. The improved anti-dive performance could thus be realized with soft vertical ride.

- The results of the vehicle dynamic responses of the pitch-plane interconnected

suspensions demonstrated that the proposed pitch-interconnected suspensions could considerably inhibit vehicle attitude and suspension travels during straight-line braking maneuvers. The interconnected suspensions also revealed reduced suspension travel without greatly affecting the vertical ride under excitations arising from random roads of varying surface roughness. The braking and ride responses showed only little sensitivity to load variations. The results suggested that pitch-connected suspension offers significant potential for enhancing the vehicle pitch performance, irrespective of various operating and load conditions considered. Moreover, these offer greater design flexibility for realizing desired pitch-mode stiffness and damping without affecting the bounce properties.

- The property analyses of the twin-gas-chamber strut suspension showed that the proposed twin-gas-chamber struts yield nearly symmetric but progressively hardening suspension rates in both the compression and extension, as opposed to the conventional air suspensions and single-gas-chamber strut suspension that generally cause softening in rebound. Unlike conventional suspensions, the roll or pitch stiffness of the proposed twin-gas-chamber struts also revealed progressively hardening effect with increasing roll or pitch deflections, respectively, attributed to the novel twin-gas-chamber design.

- The results of the vehicle dynamic responses demonstrated that the proposed twin-gas-chamber strut design offers considerable potential for enhancing vehicle attitude control, roll stability, braking performance, handling and ride characteristics of road vehicles, due to its nearly symmetric vertical stiffness in compression and rebound, and progressively hardening roll/pitch stiffness property. Moreover, the proposed design offers superior design flexibility and a light weight alternative to anti-roll bar.

- A set of terms was defined, based on which the feasibility analysis of various full-vehicle interconnected suspension systems could be conveniently performed, and feasible interconnected suspension configurations could be easily identified. A simplified measure, vehicle property index (VPI), was further proposed to preliminarily evaluate different feasible full-vehicle interconnected suspension systems. The effectiveness of the proposed measure was also validated using the analyses of the property and vehicle dynamic responses of the selected X-coupled and unconnected suspensions.

- The full-vehicle model analyses showed that the proposed hydraulically X-coupled suspension could yield considerably enhanced anti-roll and anti-pitch properties, handling performance, and roll and directional stabilities, without deteriorating vertical ride and roadholding qualities of road vehicles. Moreover, the parametric studies also suggested the superior design flexibility of the proposed X-coupled suspension in suspension property tuning.

- Maintaining a constant value of sum of the front and rear suspension spring rates would still induce variations in vertical acceleration responses, irrespective of the load distribution, which is attributed to the coupling effect between the bounce

and pitch modes of the sprung mass. For a vehicle with a particular load distribution, the use of an unconnected suspension yields a definite relationship between the dimensionless suspension property measures, namely the pitch margin (PM) and pitch stiffness ratio (PSR).

- A positive value of PM could considerably improve pitch ride, irrespective of the load distribution. It, however, generally deteriorates vertical ride, particularly for vehicles with even load distribution or greater load on the front axle. The PM and PSR show coupled effects on both vertical and pitch ride. A lower value of PSR together with a positive PM value could yield considerable improvement in the pitch ride.
- The peak pitch angle and peak suspension travel responses during braking are directly related to PSR. A higher PSR would be desirable for reducing both the peak pitch angle and peak suspension travel responses during braking maneuvers.
- For typical heavy vehicles with greater load on the rear axle, a positive PM tuning that yields a relatively lower PSR could considerably enhance the pitch ride with only negligible influence on vertical ride response. Such suspension tuning, however, would significantly deteriorate the pitch attitude control and suspension travel responses of the vehicles during braking maneuvers.
- A positive PM tuning also represents a relatively lower front suspension natural frequency, which indicates a lower roll stiffness of the front suspension. The use of anti-roll bar or roll plane coupled suspension would thus be helpful for increasing the roll stiffness without affecting vertical stiffness property.
- For vehicles with even load distribution or greater load on the front axle, an appropriate negative PM tuning could considerably improve vertical ride with only slight increase in pitch acceleration response.
- The suspension tuning could help reduce DLC due to forces developed by tires at one of the axles with an increase in DLC due to the other axle tire forces. A negative PM tuning tends to deteriorate the DLC responses of vehicles, irrespective of the load distribution and road roughness. A positive tuning, however, could generally yield slightly lower DLC.
- The suspension tuning could improve the rms travel response of suspension at one of the axles, while that of the suspension at the other axle would generally deteriorate. Suspension tuning with a positive PM tends to slightly deteriorate suspension travel responses of the vehicles with even or more load on the rear axle. A negative PM tuning, however, could slightly improve suspension travel responses of the vehicles with even or more load on the rear axle.
- Unlike unconnected suspension, pitch plane coupled suspension, could permit independent tunings of the vertical and pitch stiffness rates, and thus the PM and PSR. A pitch-connected suspension could thus offer significant potential for improving both the ride and handling qualities of vehicles.

7.3 Recommendations for Future Studies

The fluidically-coupled vehicle suspension systems offer significant potentials as the future suspensions for their passive principles and enhanced tuning flexibility. Moreover, the twin-gas-chamber strut suspension can also provide extensive tuning flexibility for heavy vehicle applications. It would be desirable to translate the fundamental and conceptual design studies of these suspension designs into analyses for specific vehicles as well as laboratory prototype developments. It would also be desirable to explore the semi-active fluidically-coupled suspension and alternative compressible fluids to attain variable stiffness suspension. These research efforts would attract interests from the commercial vehicle, military vehicle and motorsport sectors, which have either employed or are planning to employ such design concepts. Particular topics of future work may include the following:

- Semi-active and active interconnected hydro-pneumatic suspensions;
- Suspension designs with road- and bridge-friendliness, and driver-friendliness;
- Further extensive studies on the applications to SUVs, military vehicles, heavy vehicles and racing cars;
- Experimental study and field test of various interconnected suspensions;
- Experimental study and field test of twin-gas-chamber strut suspension;

REFERENCES

1. Ervin, R.D., 1986, 'The dependence of truck roll stability on size and weight variables', International Journal of Vehicle Design, 7, p.192-208.
2. Winkler, C., 2000, 'Rollover of heavy commercial vehicles', UMTRI Research Review, 31, The University of Michigan, USA.
3. Cole, D.J., 2001, 'Fundamental issues in suspension design for heavy road vehicles', Vehicle System Dynamics, 35, p.319-360.
4. Kang, X.D., 2001, 'Optimal tank design and directional dynamic analysis of liquid cargo vehicles under steering and braking', PhD thesis, Concordia University, Canada.
5. Dahlberg, E., 1999, 'Yaw instability due to longitudinal load transfer during braking in a curve', SAE paper 1999-01-2952.
6. Wong, J.Y., 2001, 'Theory of ground vehicles', 3rd Edition, John Wiley & Sons, Inc., USA.
7. Holen, P. and Thorvald, B., 2004, 'Possibilities and limitations with distributed damping in heavy vehicles', Vehicle System Dynamics Supplement, 41, p. 172-181.
8. Sutton, T., Pope, R., Brandewie, K. and Henry, J., 2001, 'International truck and engine high performance vehicle driveability – ride and handling', SAE paper 2001-01-2787.
9. Holen, P. and Thorvald, B., 2002, 'Aspects on roll and bounce damping for heavy vehicles', SAE paper 2002-01-3060.

10. Ledesma, R., 2002, 'Ride performance comparison of trailer suspension systems using computational methods', SAE paper 2002-01-3103.

11. Palkovics, L. and Fries, A., 2001, 'Intelligent electronic systems in commercial vehicles for enhanced traffic safety', Vehicle System Dynamics, 35, p. 227-289.

12. Abe, M., 1999, 'Vehicle dynamics and control for improving handling and active safety: from four-wheel steering to direct yaw moment control', Journal of Multi-Body Dynamics, 213, p. 87-101.

13. Pintado, P. and Castell, M.-A., 1999, 'Independent suspension, self steered axle, and 4ws for buses', Vehicle System Dynamics, 31, p. 137-155.

14. Crolla, D.A., 1996, 'Vehicle dynamics - theory into practice', Journal of Automobile Engineering, 210, p. 83-94.

15. Gillespie, T.D., 1992, 'Fundamentals of vehicle dynamics', SAE Inc., PA, USA.

16. Joarder, M.N., 2003, 'Influence of nonlinear asymmetric suspension properties on the ride characteristics of road vehicle', Master thesis, Concordia University, Canada.

17. Dixon, J.C., 1996, 'Tires, suspension and handling', 2nd Edition, SAE Inc., PA, USA.

18. Norman, I.A., Scharff, R. and Corinchoc, J.A., 1995, 'Heavy-duty truck systems', 2nd Edition, Delmar Publishers, USA.

19. Matschinsky, W., 1998, 'Road vehicle suspensions', Springer-Verlag Berlin Heideberg, Germany.

20. Murphy, R.W., Bernard, J.E. and Winkler, C.B., 1972, 'A computer based mathematical method for predicting the braking performance of trucks and

tractor-trailers', UMTRI Report UM-HSRI-PF-72-1, The University of Michigan, USA.

21. Cebon, D., 1999, 'Handbook of vehicle-road interaction', Swets & Zeitlinger, the Netherlands.

22. Feury, M., Halle, N., Simon, G. and Stinson, M., 2001, 'Future heavy tactical truck', SAE paper 2001-01-0889.

23. Giliomee, C.L., 2003, 'Analysis of a Four State Switchable Hydro-Pneumatic Spring and Damper System', Master thesis, University of Pretoria, South Africa.

24. Gunter, D., Bylsma, W., Letherwood, M., Dennis, S., Argeropoulos, K., Teschendorf, D. and Gorsich, D., 2005, 'Using 3D multi-body simulation to evaluate future truck technologies', SAE paper 2005-01-0934.

25. Felez, J. and Vera, C., 1987, 'Bond graph assisted models for hydro-pneumatic suspensions in crane vehicles', Vehicle System Dynamics, 16, p.313-332.

26. Crolla, D.A., Pitcher, R.H. and Lines, J.A., 1987, 'Active suspension control for an off-road vehicle', Journal of Automobile Engineering, 201, p.1-10.

27. Su, H., 1990, 'An investigation of vibration isolation systems using active, semi-active and tunable passive mechanisms with applications to vehicle suspensions', PhD thesis, Concordia University, Canada.

28. Liu, P., 1994, 'An analytical study of ride and handling performance of an interconnected vehicle suspension', Master thesis, Concordia University, Canada.

29. Chaudhary, S., 1998, 'Ride and roll performance analysis of a vehicle with spring loaded interconnected hydro-pneumatic suspension', Master thesis, Concordia University, Canada.

30. Wu, L., 2003, 'Analysis of hydro-pneumatic interconnected suspension struts in the roll plane vehicle model', Master thesis, Concordia University, Canada.

31. Wilde, J.R., Heydinger G.J., Guenther, D.A., Mallin, T. and Devenish, A.M., 2005, 'Experimental evaluation of fishhook maneuver performance of a kinetic suspension system', SAE paper 2005-01-0392.

32. Wilde, J.R., Heydinger, G.J. and Guenther, D.A., 2006, 'ADAMS simulation of ride and handling performance of kinetic™ suspension system', SAE paper 2006-01-1972.

33. Ledesma, R. and Shih, S., 1999, 'Heavy and medium duty vehicle suspension-related performance issues and effective analytical models for system design guide', SAE paper 1999-01-3781.

34. Dudding, A.T. and Wilson, W., 2000, 'Development of a new front air suspension and steer axle system for on highway commercial vehicles', SAE paper 2000-01-3449.

35. Siqueira, L.P., Nogueira, F., Ramos, C.C., Herrmann, J.G., Sartori, S., Villiger, C., Paula, G.R., Fuhrken, F. and Araujo, V., 2002, 'Tractor air suspension design and tuning', SAE paper 2002-01-3041.

36. Ledesma, R., 2004, 'An analytical target setting procedure for the design of the suspension system of a tractor-trailer combination', SAE paper 2004-01-2692.

37. Goldman, R.W., El-Gindy M. and Kulakowski, B.T., 2001, 'Rollover dynamics of road vehicles: literature survey', International Journal of Heavy Vehicle Systems, 8, p. 103-141.

38. White, D.L., 2000, 'Parametric study of leveling system characteristics on roll stability of trailing arm air suspension for heavy trucks', SAE paper 2000-01-3480.

39. Kar, S., Rakheja, S. and Ahmed, A.K.W., 2006, 'A normalized measure of relative roll instability for open-loop rollover warning', International Journal of Heavy Vehicle Systems, 13, p. 74-97.

40. El-Gindy, M., 1995, 'An overview of performance measures for heavy commercial vehicles in North America', International Journal of Vehicle Design, 16, p. 441-463.

41. Rakheja, S, Piche, A. and Sankar, T.S., 1991, 'On the development of an early warning safety monitor for articulated freight vehicles', International Journal of Vehicle Design, 12, p. 420-449.

42. Liu, P., Rakheja, S. and Ahmed, A.K.W., 1998, 'Dynamic rollover threshold of articulated freight vehicles', International Journal of Heavy Vehicle Systems, 5, p. 300-322.

43. Cooperrider, N., Thomas, T. and Hammound, S., 1990, 'Testing and analysis of vehicle rollover behavior', SAE paper 900366.

44. Bastow, B., 1987, 'Car suspension and handling', Pentech Press Limited, London, UK.

45. ISO 2631-1, 1997, 'Mechanical vibration and shock-Evaluation of human exposure to whole-body vibration-Part 1: General requirements', International Organization of Standardization.

46. Muijderman, J.H.E.A., Kok, J.J., Huisman, R.G.M., Veldpaus, F.E. and Van heck, J.G.A.M., 1999, 'Preview-based control of suspension systems for commercial vehicles', Vehicle System Dynamics, 32, p. 237-247.

47. Sharp, R.S., 2002, 'Wheelbase filtering and automobile suspension tuning for minimizing motions in pitch', Journal of Automobile Engineering, 216, p. 933-946.

48. Crolla, D.A and King, R.P., 1999, 'Olley's "flat ride" revisited', Vehicle System Dynamics Supplement, 33, p. 762-774.

49. Sharp, R.S., 1999, 'Influences of suspension kinematics on pitching dynamics of cars in longitudinal maneuvering', Vehicle System Dynamics Supplement, 33, p. 23-36.

50. Sharp, R.S., 1999, 'Vehicle dynamics and the judgment of quality', Vehicle Performance, Edited by Pauwelussen, J.P., Swets & Zeitlinger Publishers, Lisse, the Netherlands, p. 87-96.

51. Holdmann, O. and Holle, M., 1999, 'Possibilities to improve the ride and handling performance of delivery trucks by modern mechatronic systems', JSAE Review, 20, p. 505-510.

52. Hecker, F., Hummel, S., Jundt, O., Leimbach, K.-D., Faye, I. and Schramm, H., 1997, 'Vehicle dynamics control for commercial vehicles', SAE paper 973284.

53. Bernard, J.E. Winkler, C.B. and Fancher, P.S., 1973, 'A computer based mathematical method for predicting the directional response of trucks and tractor-trailers', UMTRI Technical Report UM-HSRI-PF-73-1, The University of Michigan, USA.

54. Savkoor, A.R., Happel, H. and Horkay, F., 1999, 'Vehicle handling and sensitivity in transient maneuvers', Vehicle Performance, Edited by Pauwelussen, J.P., Swets & Zeitlinger Publishers, Lisse, the Netherlands, p. 121-147.

55. Pauwelussen. J.P., 1999, 'Effect of tire handling characteristics on driver judgement of vehicle directional stability', Vehicle Performance, Edited by Pauwelussen, J.P., Swets & Zeitlinger Publishers, Lisse, the Netherlands, p. 151-176.

56. Stephens P. and Kohn, H.J., 1999, 'Influence of the tire on subjective handling at the limit', Vehicle Performance, Edited by Pauwelussen, J.P., Swets & Zeitlinger Publishers, Lisse, the Netherlands, p. 177-195.

57. Chen, D.C. and Crolla, D.A., 1998, 'Subjective and objective measures of vehicle handling: drivers & experiments', Vehicle System Dynamics Supplement, 28, p. 576-597.

58. Sampson, D.J.M. and Cebon, D., 2003, 'Achievable roll stability of heavy road vehicles', Journal of Automobile Engineering, 217, p. 269-297.

59. Furukawa, Y., Yuhara, N., Sano, S., Takeda, H. and Matsushita, Y., 1989, 'A review of four-wheel steering studies from the viewpoint of vehicle dynamics and control', Vehicle System Dynamics, 18, p. 151-186.

60. Pascali, L., Gabrielli, P. and Caviasso, G., 2003, 'Improving vehicle handling and comfort performance using 4WS', SAE paper 2003-01-0961.

61. Data, S. and Frigerio, F., 2002, 'Objective evaluation of handling quality', Journal of Automobile Engineering, 216, p. 297-305.

62. Fancher, P.S. and Gillespie, T.D., 1997, 'Truck operating characteristics', Report for Transportation Research Board, National Research Council, National Academy Press, DC, USA.

63. Macadam, C.C., 2003, 'Understanding and modeling the human driver', Vehicle System Dynamics, 40, p. 101-134.

64. Blundell, M.V., 1999, 'The modelling and simulation of vehicle handling. Part 1: analysis methods', Journal of Multi-Body Dynamics, 213, p. 103-118.

65. Sharp, R.S., 1991, 'Computer codes for road vehicle dynamic models', Proceedings of Autotech '91, Birmingham, UK.

66. Blundell, M.V., 2000, 'The modelling and simulation of vehicle handling. Part 3: tyre modelling', Journal of Multi-Body Dynamics, 214, p. 1-32.

67. Blundell, M.V., 2000, 'The modelling and simulation of vehicle handling. Part 4: handling simulation', Journal of Multi-Body Dynamics, 214, p. 71-94.

68. Hegazy, S., Rahnejat, H. and Hussain, K., 2000, 'Multi-body dynamics in full-vehicle handling analysis under transient manoeuver', Vehicle System Dynamics, 34, p. 1-34.

69. Giangiulio, E., 2006, '14 d.o.f. VERTEC vehicle model VDSIM – Vehicle Dynamic SIMulator Implementation and validation', 3rd International Colloquium on Vehicle-Tyre-Road Interaction, Stuttgart, Germany.

70. Uys, P.E., Els, P.S. and Thoresson, M.J., 2006, 'Criteria for handling measurement', Journal of Terramechanics, 43, p. 43-67.

71. Louca, L.S., Rideout, D.G., Stein, J.L. and Hulbert, G.M, 2004, 'Generating proper dynamic models for truck mobility and handling', International Journal of Heavy Vehicle Systems, 11, p. 209-236.

72. Hac, A. and Bodie, M.O., 2002, 'Improvements in vehicle handling through integrated control of chassis systems', International Journal of Vehicle Design, 29, p. 23-50.

73. Metz, L.D., 2004, 'What constitutes good handling?', SAE paper 2004-01-3532.

74. He, J., Crolla, D.A., Levesley, M.C. and Manning, W.J., 2006, 'Coordination of active steering, driveline, and braking for integrated vehicle dynamics control', Journal of Automobile Engineering, 220, p. 1401-1421.

75. Mashadi, b. and Crolla, D.A., 2005, 'Influence of ride motions on the handling behavior of a passenger vehicle', Journal of Automobile Engineering, 219, p. 1047-1058.

76. Cossalter, V., Da Lio, M., Lot, R. and Fabbri, L., 1999, 'A general method for the evaluation of vehicle maneuverability with special emphasis on motorcycles', Vehicle System Dynamics, 31, p. 113-135.

77. Yuhara, N. and Tajima, J. 2001, 'Advanced steering system adaptable to lateral control task and driver's intention', Vehicle System Dynamics, 36, p. 119-158.

78. Ungoren, A.Y. and Peng, H., 2005, 'An adaptive lateral preview driver model', Vehicle System Dynamics, 43, p. 245-259.

79. Gobbi, M., Mastinu, G. and Doniselli, C., 1999, 'Optimising a car chassis', Vehicle System Dynamics, 32, p. 149-170.

80. Lin, M., Popov, A.A. and Mcwilliam, S., 2004, 'Stability and performance studies of driver-vehicle systems with electric chassis control', Vehicle System Dynamics Supplement, 41, p. 477-486.

81. Shim, T. and Ghike, C., 2007, 'Understanding the limitations of different vehicle models for roll dynamics studies', Vehicle System Dynamics, 45, p. 191-216.

82. Ma, W.-H. and Peng, H., 1999, 'Worst-case vehicle evaluation methodology – examples on truck rollover/jackknifing and active yaw control systems', Vehicle System Dynamics, 32, p. 389-408.

83. Allen, R.W., Rosenthal, T.J., Klyde, D.H. and Hogue, J.R., 1999, 'Computer simulation analysis of light vehicle lateral/directional dynamic stability', SAE paper 1999-01-0124.

84. Shimizu, Y., Kawai, T. and Yuzuriha, J., 1999, 'Improvement in driver-vehicle system performance by varying steering gain with vehicle speed and steering angle: VGS (variable gear-ratio steering system)', SAE paper 1999-01-0395.

85. Gillespie, T.D. and Sayers, M.W., 1999, 'A multibody approach with graphical user interface for simulating truck dynamics', SAE paper 1999-01-3705.

86. Bodie, M.O. and Hac, A., 2000, 'Closed loop yaw control of vehicles using magneto-rheological dampers', SAE paper 2000-01-0107.

87. Letherwood, M.D. and Gunter, D.D., 2000, 'Virtual modeling and simulation of military ground vehicles' SAE paper 2000-01-1580.

88. Everett, N.R., Brown, M.D. and Crolla, D.A., 2000, 'Investigation of a roll control system for an off-road vehicle', SAE paper 2000-01-1646.

89. Sherman, M. and Myers, G., 2000, 'Vehicle dynamics simulation for handling optimization of heavy trucks', SAE paper 2000-01-3437.

90. Higuchi, A. and Sakai, H., 2001, 'Objective evaluation method of on-center handling characteristics', SAE paper 2001-01-0481.

91. Ledesma, R. and Shih, S., 2001, 'The effect of kingpin inclination angle and wheel offset on medium-duty truck handling', SAE paper 2001-01-2732.

92. Hac, A., 2002, 'Influence of active chassis systems on vehicle propensity to maneuver-induced rollovers', SAE paper 2002-01-0967.

93. Ledesma, R., 2002, 'Ride performance comparison of trailer suspension systems using computational methods', SAE paper 2002-01-3103.

94. Salaani, M.K., Heydinger, G.J. and Grygier, P.A., 2003, 'Heavy tractor-trailer vehicle dynamics modeling for the national advanced driving simulator', SAE paper 2003-01-0965.

95. Heathershaw, A., 2004, 'Matching of chassis and variable ratio steering characteristics to improve high speed stability', SAE paper 2004-01-1103.

96. Pacejka, H.B., 2002, 'Tire and vehicle dynamics ', SAE Inc., PA, USA.

97. Hac, A., 2005, 'Influence of chassis characteristics on sustained roll, heave and yaw oscillations in dynamic rollover testing', SAE paper 2005-01-0398.

98. Cooper, N., Crolla, D., Levesley, M. and Manning, W., 2005, 'Integration of active suspension and active driveline to ensure stability while improving vehicle dynamics', SAE paper 2005-01-0414.

99. Crolla, D.A., Chen, D.C., Whitehead, J.P. and Alstead, C.J., 1998, 'Vehicle handling assessment using a combined subjective-objective approach', SAE paper 980226.

100. Fancher, P.S., Ervin, R.D., Winkler, C.B. and Gillespie, T.D., 1986, 'A factbook of the mechanical properties of the components for single-unit and articulated heavy trucks', UMTRI Report UMTRI-86-12, The University of Michigan, USA.

101. Fancher, P.S. and Mathew, A., 1987, 'A vehicle dynamics handbook for single-unit and articulated heavy trucks', UMTRI Report UMTRI-86-37, The University of Michigan, USA.

102. Nalecz, A.G. and Genin, J., 1984, 'Dynamic stability of heavy articulated vehicles', International Journal of Vehicle Design, 5, p. 417-426.

103. Vlk, F., 1982, 'Lateral dynamics of commercial vehicle combinations – a literature survey', Vehicle System Dynamics, 11, p. 305–324.

104. Vlk, F., 1985, 'Handling performance of truck-trailer vehicles: A state-of-the-art survey', International Journal of Vehicle Design, 6, p. 323–361.

105. Cole, D.J., 2000, 'Evaluation of design alternatives for roll-control of road vehicles', Proceedings of AVEC 2000, Ann Arbor, USA.

106. ISO 15073-1, 2006, 'Road vehicles – vehicle dynamics test procedures – Part 1: general conditions for passenger cars', International Organization of Standardization.

107. ISO 4138, 2004, 'Passenger cars steady-state circular driving behaviour open-loop test methods', International Organization of Standardization.

108. ISO 7401, 2003, 'Road vehicles – lateral transient response test methods – open-loop test methods', International Organization of Standardization.

109. ISO 3888-1, 1999, 'Passenger cars – test track for a severe lane-change manoeuvre – part 1: double lane-change', International Organization of Standardization.

110. Gillespie, T.D., 1985, 'Heavy truck ride', SAE paper 850001.

111. Jiang, Z., Streit, D.A. and El-Gindy, M., 2001, 'Heavy vehicle ride comfort: Literature survey', International Journal of Heavy Vehicle Systems, 8, p. 258-284.

112. Gillespie, T.D., 2004, 'Foreword: Road profiles: measurement, analysis, and applications', International Journal of Vehicle Design, 36, p. 101-102.

113. Ferris, J.B., 2004, 'Characterising road profiles as Markov Chains', International Journal of Vehicle Design, 36, p.103-115.

114. Hrovat, D., 1997, 'Survey of advanced suspension developments and related optimal control applications', Automatica, 33, p. 1781-1817.

115. Alleyne, A., 1997, 'Improved vehicle performance using combined suspension and braking forces', Vehicle System Dynamics, 27, p. 235-265.

116. Rakheja, S. and Woodrooffe, J., 1996, 'Role of suspension damping in enhancement of road friendliness of heavy vehicles', International Journal of Heavy Vehicle Systems, 3, p. 363-381.

117. Chalasani, R.M., 1986, 'Ride performance potential of active suspension systems. Part I: simplified analysis based on quarter-car models', ASME Symposium on Simulation of Ground vehicles and transport Systems, Anaheim, USA.

118. Rakheja, S., Ahmed, A.K.W., Yang, X. and Guerette, C., 1999, 'Optimal suspension damping for improved driver- and road-friendliness of urban buses', SAE paper 1999-01-3728.

119. Kitching, K.J., Cole, D.J. and Cebon, D., 2000, 'Theoretical investigation into the use of controllable suspensions to minimize road damage', Journal of Automobile Engineering, 214, p. 13-31.

120. Cebon, D., 1989, 'Vehicle-generated road damage: a review', Vehicle System Dynamics, 18, p. 107-150.

121. Woods, D.E. and Jawad, B.A., 1999, 'Numerical design of racecar suspension parameters', SAE paper 1999-01-2257.

122. Zapletal, E., 2000, 'Balanced suspension', SAE paper 2000-01-3572.

123. Buj, J.F., 2002, 'Integral suspension system for motor vehicles based on passive components', SAE paper 2002-01-3105.

124. Smith, M.C. and Walker, G.W., 2005, 'Interconnected vehicle suspension', Journal of Automobile Engineering, 219, p. 295-307.

125. Mavroudakis, B. and Eberhard, P., 2006, 'Mode decoupling in vehicle suspensions applied to race cars', III European Conference on Computational Mechanics Solids, Structures and Coupled Problems in Engineering, Lisbon, Portugal.

126. Newton, K., Steeds, W. and Garrett, T.K., 2001, 'The motor vehicle', 13th edition, SAE Inc., PA, USA.

127. Sharp, R.S. and Dodu, M., 2004, 'Kinematic cross-linking in automotive suspension systems', Vehicle System Dynamics Supplement, 41, p. 63–72.

128. Moulton, A.E. and Best, A., 1979, 'From hydrolastic to hydragas suspension', Proc Instn Mech Engrs, 193, p. 15-34.

129. Moulton, A.E. and Best, A., 1970, 'Rubber springs and inter-connected suspension systems', Engineering Design Show Conference, Paper No. 15a.

130. Moulton, A.E. and Best, A., 1979, 'Hydragas suspension', SAE paper 790374.

131. Bhave, S.Y., 1992, 'Effect of connecting the front and rear air suspensions of a vehicle on the transmissibility of road undulation inputs', Vehicle System Dynamics, 21, p. 225-245.

132. Kusahara, Y., Li, X.S., Hata, N. and Watanabe, Y., 1994, 'Feasibility study of active roll stabilizer for reducing roll angle of an experimental medium-duty truck', Proceedings of AVEC'94, 9438501.

133. Rosam, N. and Darling, J., 1997, 'Development and simulation of a novel roll control system for the interconnected hydragas suspension', Vehicle System Dynamics, 27, p. 1-18.

134. Schumann, A.R. and Anderson, R.J., 2002, 'Optimal control of an active anti roll suspension for an off-road utility vehicle using interconnected hydragas suspension units', Vehicle System Dynamics Supplement, 37, p. 145–156.

135. Lovins, A.B. and Cramer, D.R., 2004, 'Hypercars, hydrogen, and the automotive transition', International Journal of Vehicle Design, 35, p. 50-85.

136. Horton, D.N.L. and Crolla, D.A., 1986, 'Theoretical analysis of a semi-active suspension fitted to an off-road vehicle', Vehicle System Dynamics, 15, p. 351-372.

137. Fukuda, T., Zhang, X., Hasegawa, Y., Matsuno, T. and Hoshino, H., 2004, 'Preview posture control and impact load control of rough terrain vehicle with interconnected suspension', Proceedings of 2004 IEEE/RSJ, Japan, p. 761-766.

138. Yang, X., Rakheja, S. and Stiharu, I., 2002, 'Structure of the driver model for articulated vehicles', International Journal of Heavy Vehicle Systems, 9, p. 27-51.

139. Sampson, D.J.M. and Cebon, D., 2003, 'Active roll control of single unit heavy road vehicles', Vehicle System Dynamics, 40, p. 229-270.

140. Barak, P., Panakanti, N. and Desai, T., 2004, 'Effect of chassis design factors (CDF) on the ride quality using a seven degree of freedom vehicle model', SAE paper 2004-01-1555.

141. Halfmann, C., Nelles, O. and Holzmann, H., 1999, 'Semi-physical modeling of the vertical vehicle dynamics', Proceedings of the American Control Conference, San Diego, USA.

142. http://www.carbibles.com/suspension_bible.html.

143. Cole, D.J. and Cebon, D., 1996, 'Truck suspension design to minimize road damage', Journal of Automobile Engineering, 210, p. 95-107.

144. Dixon, J.C., 1999, 'The shock absorber handbook', SAE Inc., PA, USA.

145. Quaglia, G. and Sorli, M., 2001, 'Air suspension dimensionless analysis and design procedure', Vehicle System Dynamics, 35, p. 443-475.

146. Cavanaugh, R.D., 1994, 'Air suspension and servo-controlled isolation systems', Shock and vibration handbook, 2nd Edition, Chapter 33, (Editors: Harris, C.M. and Crede, C.E.), McGraw-Hill, NY, USA.

147. Bakker, E., Byborg, L. and Pacejka, H.B., 1987, 'Tyre modeling for use in vehicle dynamic studies', SAE paper 870421.

148. Pacejka, H.B. and Bakker, E., 1991, 'The magic formula tyre model', Proc. of 1st Tyre Colloquium, Delft, The Netherland.

149. Cao, D., Rakheja, S. and Su, C.-Y., 2005, 'Comparison of roll properties of hydraulically and pneumatically interconnected suspensions for heavy vehicles', SAE paper 2005-01-3593.

150. Cao, D., Rakheja, S. and Su, C.-Y., 2005, 'Roll plane analysis of interconnected hydro-pneumatic suspension struts', Proc. of ASME Int. Mech. Engineering Congress and Exposition, IMECE2005-80484, Orlando, USA.

151. Todd, K.B. and Kulakowski, B.T., 1990, 'Handling performance of road vehicles with different active suspensions', Transportation Systems, AMD, 108, ASME, p. 19-26.

152. Rakheja, S., Wang Z. and Ahmed A.K.W., 2001, 'Urban bus optimal passive suspension study. Phase II: Enhancement of road- and driver-friendliness of urban buses through optimal suspension damping', Transportation Canada Report T-8200-4-4556, Canada.

153. Hetrick, S., 1997, 'Examination of driver lane change behavior and the potential effectiveness of warning onset rules for lane change or "side" crash avoidance systems', Master thesis, Virginia Polytechnic Institute & State University, USA.

154. Warner, B., 1996, 'An analytical and experimental investigation of high performance suspension dampers', PhD thesis, Concordia University, Canada.

155. Winkler, C.B., Bernard, J.E., Fancher, P.S., Macadam, C.C. and Post T.M., 1976, 'Predicting the braking performance of trucks and tractor-trailers', UMTRI Report UM-HSRI-76-26-1, The University of Michigan, USA.

156. Suh, M.-W., Park, Y.-K., Kwon, S.-J., Yang, S.-H. and Park, B.-C., 2000, 'A simulation program for the braking characteristics of tractor-semitrailer vehicle', SAE paper 2000-01-3415.

157. Kaneko, T., Kageyama, I. and Tsunashima, H., 2002, 'Braking stability of articulated vehicles on highway', Vehicle System Dynamics Supplement 37, p. 1-11.

158. Fancher, P.S., 1995, 'Generic data for representing truck tire characteristics in simulations of braking and braking-in-a-turn maneuvers', UMTRI Report 95-34, The University of Michigan, USA.

159. Williams, R.A., 1997, 'Automotive active suspensions. Part 2: practical considerations', Journal of Automobile Engineering, 211, p. 427-444.

160. Liu, H., Zhuang, D., Lin, Y., Wang, W., Zhang, F., Zhang, W. and Liu, F., 2002, 'A study on nonlinear stiffness characteristic of air spring for a bus', SAE paper 2002-01-3092.

161. Rajalingham, C. and Rakheja, S., 2003, 'Influence of suspension damper asymmetry on vehicle vibration responses to ground excitation', Journal of Sound and Vibration, 266, p. 1117-1129.

162. Williams, R.A., 1997, 'Automotive active suspensions Part 1: basic principles', Journal of Automobile Engineering, 211, p. 415-426.

163. Cao, D., Rakheja, S. and Su, C.-Y., 2006, 'A generalized model of a class of interconnected hydro-pneumatic suspensions and analysis of pitch properties', Proc. of ASME Int. Mech. Engineering Congress, IMECE2006-13961, Chicago, USA.

164. Klasson, J., 2002, 'A generalized crosswind model for vehicle simulation purposes, Vehicle System Dynamics Supplement, 37, p. 350-359.

165. El-Demerdash, S.M., Selim, A.M. and Crolla, D.A., 1999, 'Vehicle body attitude control using an electronically controlled active suspension', SAE paper 1999-01-0724.

166. Rakheja, S., Liu, P., Ahmed, A.K.W. and Su, H., 1993, 'Analysis of an interlinked hydro-pneumatic suspension', Proc. of ASME Winter Annual Meeting, New Orleans, USA.

167. Ahmadian, M. and Ahn, Y.K., 2003, 'On-vehicle evaluation of heavy truck suspension kinematics', SAE paper 2003-01-3394.

168. Milliken, W.F. and Milliken, D.L., 2002, 'Chassis design: principles and analysis', SAE Inc., USA.

169. Hebden, R.G., Edwards, C. and Spurgeon, S.K., 2004, 'Automotive steering control in a split-μ maneuver using an observer-based sliding mode controller', Vehicle System Dynamics, 41, p. 181-202.

170. Ledesma, R., 2000, 'The effect of tire stiffness parameters on medium-duty truck handling', SAE paper 2000-01-1645.

171. Cao, D., Rakheja, S. and Su, C.-Y., 'Heavy vehicle pitch dynamics and suspension tuning. Part I: Unconnected suspension', Vehicle System Dynamics. (In press)

172. Cao, D., Rakheja, S. and Su, C.-Y., 'Dynamic analyses of heavy vehicle with pitch-interconnected suspensions', International Journal of Heavy Vehicle Systems. (In press)

173. Cao, D., Rakheja, S. and Su, C.-Y., 2008, 'Pitch attitude control and braking performance analysis of heavy vehicles with interconnected suspensions', SAE Transactions, Journal of Passenger Cars: Mechanical Systems, V116-6. (In press)

174. Cao, D., Rakheja, S. and Su, C.-Y., 'Dynamic analyses of roll plane interconnected hydro-pneumatic suspension systems', International Journal of Vehicle Design. (In press)

175. Cao, D., Rakheja, S. and Su, C.-Y., 2007, 'Roll plane analysis of a hydro-pneumatic suspension with twin-gas-chamber struts', International Journal of Heavy Vehicle Systems, 14, p. 355-375.

176. Cao, D., Rakheja, S. and Su, C.-Y., 'Pitch plane analysis of a twin-gas-chamber strut suspension', Journal of Automobile Engineering. (In press)

177. Cao, D., Rakheja, S. and Su, C.-Y., 2008, 'Property analysis of an X-coupled suspension for sport utility vehicles', SAE paper 2008-01-1149.

178. Cao, D., Rakheja, S. and Su, C.-Y., 2007, 'Optimal damping design of heavy vehicle with interconnected hydro-pneumatic suspension', SAE paper 2007-01-0584.

179. Cao, D., Rakheja, S. and Su, C.-Y., 2007, 'Pitch attitude control and braking performance analysis of heavy vehicles with interconnected suspensions', SAE paper 2007-01-1347.

180. Cao, D., Rakheja, S. and Su, C.-Y. and Ahmed, A.K.W., 2006, 'Analysis of a twin-gas-chamber hydro-pneumatic vehicle suspension', Proc. of Int. Conf. on Dynamics, Instrumentation and Control, Queretaro, Mexico.

181. Cao, D., Rakheja, S. and Su, C.-Y., 2006, 'Roll and bounce dynamic responses of heavy vehicles with interconnected suspensions', Proc. of CSME Forum, Symposium on Intelligent Vehicles and Transportation Systems, Calgary, Canada.

APPENDIX A

FUNDAMENTAL PITCH DYNAMICS AND SUSPENSION TUNING OF HEAVY VHEICLES

A.1 Introduction

The performance characteristics of a heavy vehicle are strongly related to its pitch motion, which include the ride, handling, suspension stroke and dynamic tire loads. This is partially attributed to the relatively large wheelbase and coupling between the vertical and pitch motions of heavy vehicles. Moreover, heavy vehicles are generally characterized by highly variable gross vehicle weight (GVW) and load distributions, compared with passenger cars. Passenger cars are generally designed to achieve front/rear load distribution ratio and dynamic index (k^2/ab) close to unity [1, 2], where k is the radius of gyration of the sprung mass in pitch, and a and b are the longitudinal distances from the center of gravity (c.g.) to the front and rear wheel centers, respectively. These ratios are significantly different for heavy vehicles, where the dynamic index may assume a value greater than 1 for two-axle vehicles, leading to pitch mode natural frequency lower than the bounce mode frequency [3]. The dynamic characteristics of heavy vehicle systems are therefore considerably different from those of the passenger cars [2].

Suspension design of road vehicles necessities a complex compromise among different performance measures related to ride and handling qualities. Unlike automobiles, the transport productivity and efficiency are generally prioritized for heavy vehicles, particularly the directional and roll dynamic performance [4-6]. The ride properties of heavy vehicles concern the preservation of health, safety and comfort of the drivers and/or passengers, and protection of the cargoes, while the suspension design is

subject to the constraints imposed by requirements on productivity and functional efficiency [4]. Considering the long exposure duration of professional drivers of commercial vehicles, the driver fatigue arising from ride vibration environment may also affect the safety and efficiency of vehicle operations in an adverse manner [7]. The ride comfort performance of heavy vehicles are generally dominated by the pitch plane motions, while the lateral and roll vibrations have been considered to be relatively less important [4]. The heave vibration arises from combined bounce and pitch motions, while the longitudinal vibration at the driver location is predominated only by pitch motions. Furthermore, the pitch motions are generally considered 'objectionable' and annoying, as they encourage pitch oscillation of the seat backrest and thus 'head nod' [1, 8]. The suppression of pitch vibration is therefore very important for enhancement of ride comfort of heavy vehicles.

The vehicle braking or acceleration maneuvers induce pitch motions and longitudinal load transfers among different axles, and thus variations in normal tire load [9, 10]. Considerably larger load transfers may be anticipated in heavy vehicles with floating cargoes, such as partly-filled tank trucks [11]. Such variations in normal load can influence the longitudinal, and cornering forces, and self-aligning torque developed by a tire. The directional and braking control performance of heavy vehicles can therefore be influenced by the pitch-induced normal load variations.

The road-friendliness of heavy vehicles has been one of the important design and regulation objectives. The variations in dynamic tire load have been known to accelerate road-damage [12]. The road damaging potential of an articulated vehicle combination is

influenced by interactions between the vehicle units, which are strongly coupled by their respective pitch motions [13].

Studies on coupled bounce and pitch motions of automobiles have resulted in some guidelines on suspension design in order to achieve pitch ride control. A few studies have investigated the effects of suspension tuning for passenger cars on ride performance enhancement. The simulation results obtained for a 4-DOF pitch plane model suggested that the front/rear suspension stiffness ratio significantly affects pitch displacement responses [14], while the well-known 'Olley's tuning' is beneficial at higher speeds [15, 16]. Odhams and Cebon [17] developed a pitch plane vehicle model with coupling between the front and rear suspensions, where the conventional unconnected suspension was shown to be a special case of coupled suspension. The study presented that pitch plane formulations leaded to a relation between the bump and pitch response of an automobile, which was similar to the concept of Static Margin used in vehicle handling analysis. The study concluded that for the unconnected suspensions, the 'Olley's tuning' provided a nearly optimal solution for minimizing horizontal acceleration at the chest. The resulting vertical chest acceleration, however, could not be considered optimal. The study also demonstrated that an interconnected suspension with lower pitch stiffness, opposed to the conventional unconnected suspension, could offer benefits for improving dynamic tire force and body acceleration responses of a passenger car.

The tuning methodologies and design guidance provided in above-mentioned studies are applicable for passenger car suspensions, and may not be valid for heavy vehicle suspensions. Similar design rules for heavy vehicles have not yet been established, which may in part be attributed to vast variations in loading conditions. Furthermore, the

validity of the recommended design rules has not been investigated in view of responses under braking and acceleration inputs. Cole [2] also pointed out that optimal suspension tunings achieved under certain driving velocities may not work well for other speeds, since heavy vehicles operate in a wide range of speeds. This assertion would also be applicable for passenger cars. Odhams and Cebon [17] showed that minimizing the front and rear tire force responses of a passenger car yields different suspension design parameters, which would necessitate a design compromise. Moreover, control of suspension travel that influences both the ride and handling qualities of vehicles is another important design task. The minimization of suspension travel could also improve the productivity of heavy vehicles, considering the regulations on the heavy vehicle dimensions [2]. The study also suggested that the power dissipations due to alternative suspension designs should be assessed in future studies. Carruthers [18] stated that for a particular passenger car, the power dissipation of the suspension system is approximately 80 W and 100 W at 50 km/h and 100 km/h, respectively.

Heavy vehicle pitch-coupled suspension systems have been investigated in a few studies [19, 20]. A generalized model for a class of interconnected hydro-pneumatic suspensions was developed and analyzed under braking and road roughness inputs. The results of the studies demonstrated that the pitch-connected suspension configurations could help realize tuning of suspension pitch stiffness and damping properties independent of the front and rear vertical suspension rates. The heavy vehicle integrating pitch-connected suspensions with enhanced pitch stiffness and/or damping could inhibit braking dive and improve straight-line braking performance.

Pitch dynamics and suspension tuning of a two-axle heavy vehicle with unconnected suspension are explored in this Appendix, in an attempt to establish a relationship between the performance characteristics of the vehicle and suspension properties. The analysis provides valuable information for heavy vehicle suspension tuning and design. The effects of coupling between the front and rear suspensions on the resulting pitch properties are further investigated using a generalized pitch plane model of a two-axle heavy vehicle. Three performance measures are proposed to describe suspension properties in a dimensionless manner, namely the pitch margin (PM), pitch stiffness ratio (PSR) and coupled pitch stiffness ratio (CPSR). These measures are defined and analyzed for different suspension tuning and load conditions. The effects of suspension tuning on the dynamic responses of the vehicle are evaluated under braking inputs, and excitations arising from different road roughness conditions and driving speeds. Some basic suspension tuning rules of heavy vehicles with unconnected suspensions are proposed on the basis of analytical and simulation results.

A.2 Pitch Plane Modeling and Formulations

A simplified linear pitch plane model of a two-axle heavy vehicle, involving either unconnected or coupled suspension, is formulated in order to investigate the effect of suspension tuning on the dynamic responses of heavy vehicles. Figure 1 presents the pitch plane vehicle model involving unconnected or coupled suspension. The vehicle model with unconnected suspension, shown in Fig. 1(a), has been widely used in a number of studies for analysis of vehicle ride [14, 17]. The vehicle model with coupled suspension has also been proposed in a recent study [17], where the front and rear unsprung masses are assumed to be coupled through a massless beam. A generalized

pitch-plane vehicle model was formulated comprising an equivalent bump stiffness (k_b) and damping (c_b) with coordinates a_k and a_c, respectively, as shown in Fig. 1(b). The effective pitch stiffness and damping due to the coupled suspension are represented by rotational spring k_p and damping constant c_p. Each tire is represented by a linear spring assuming point-contact with the road and negligible damping.

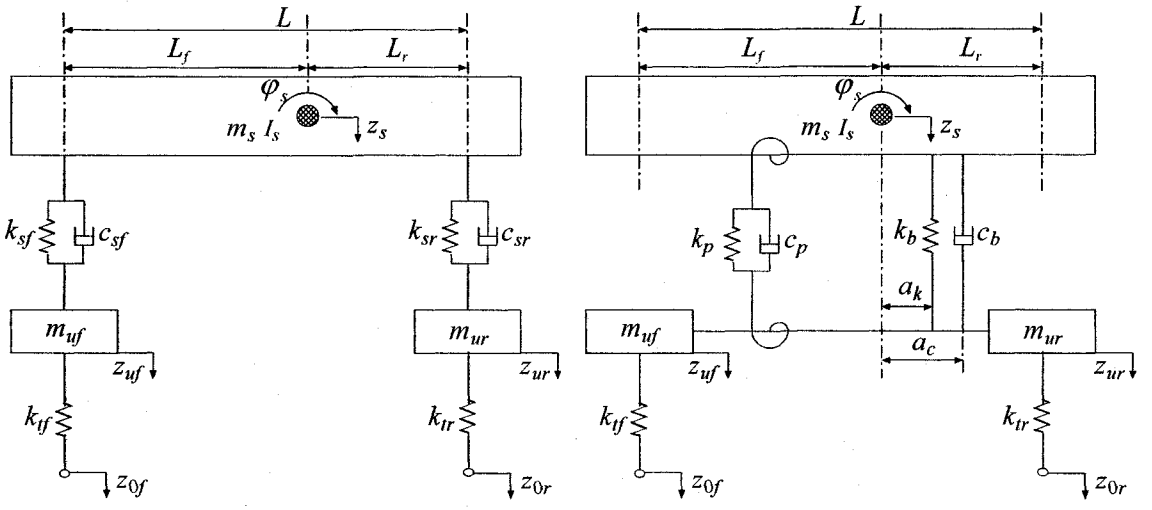

Figure 1: Pitch plane model of a two-axle heavy vehicle: (a) unconnected suspension; and (b) coupled suspension.

Assuming linear suspension properties, the equations of motion for the model with uncoupled suspension are derived as:

$$
\begin{aligned}
&m_s\ddot{z}_s - c_{sf}\left(\dot{z}_{uf} - \dot{z}_s + L_f\dot{\varphi}_s\right) - c_{sr}\left(\dot{z}_{ur} - \dot{z}_s - L_r\dot{\varphi}_s\right) - k_{sf}\left(z_{uf} - z_s + L_f\varphi_s\right) - k_{sr}\left(z_{ur} - z_s - L_r\varphi_s\right) = 0 \\
&I_s\ddot{\varphi}_s + c_{sf}L_f\left(\dot{z}_{uf} - \dot{z}_s + L_f\dot{\varphi}_s\right) - c_{sr}L_r\left(\dot{z}_{ur} - \dot{z}_s - L_r\dot{\varphi}_s\right) \\
&+ k_{sf}L_f\left(z_{uf} - z_s + L_f\varphi_s\right) - k_{sr}L_r\left(z_{ur} - z_s - L_r\varphi_s\right) = 0 \\
&m_{uf}\ddot{z}_{uf} + c_{sf}\left(\dot{z}_{uf} - \dot{z}_s + L_f\dot{\varphi}_s\right) + k_{tf}z_{uf} + k_{sf}\left(z_{uf} - z_s + L_f\varphi_s\right) = k_{tf}z_{0f} \\
&m_{ur}\ddot{z}_{ur} + c_{sr}\left(\dot{z}_{ur} - \dot{z}_s - L_r\dot{\varphi}_s\right) + k_{tr}z_{ur} + k_{sr}\left(z_{ur} - z_s - L_r\varphi_s\right) = k_{tr}z_{0r}
\end{aligned}
\qquad (1)
$$

where m_s and I_s are mass and pitch mass moment of inertia of the sprung mass, m_{uf} and m_{ur} are the front and rear unsprung masses, respectively. z_{uf} and z_{ur} are vertical motions of the front and rear unsprung masses, respectively, and z_s and φ_s are vertical and pitch

motions of the sprung mass, respectively. L_f and L_r define the longitudinal distances between the sprung mass c.g. and the front and rear axles, respectively, and L is the wheelbase. k_{ti} is vertical stiffness of tires on axle i (i=f,r), and k_{si} and c_{si} (i=f,r) are the vertical stiffness and damping coefficients of suspension at axle i, respectively. z_{0f} and z_{0r} represent the road inputs in the vicinity of the front and rear tire-road contacts, respectively.

The equations of motion for the vehicle model with coupled suspension are derived in a similar manner and expressed as:

$$
\begin{aligned}
& m_s\ddot{z}_s - F_{cb} - F_{kb} = 0 \\
& I_s\ddot{\varphi}_s + T_{cp} - F_{cb}a_c + T_{kp} - F_{kb}a_k = 0 \\
& m_{uf}\ddot{z}_{uf} + \frac{(L_r - a_c)}{L}F_{cb} + \frac{1}{L}(T_{cp} + T_{kp}) + \frac{(L_r - a_k)}{L}F_{kb} = k_{tf}(z_{0f} - z_{uf}) \\
& m_{ur}\ddot{z}_{ur} + \frac{(L_f + a_c)}{L}F_{cb} - \frac{1}{L}(T_{cp} + T_{kp}) + \frac{(L_f + a_k)}{L}F_{kb} = k_{tr}(z_{0r} - z_{ur})
\end{aligned}
\tag{2}
$$

where $F_{cb} = c_b\left[\dot{z}_{uf} + (\dot{z}_{ur} - \dot{z}_{uf})\frac{(L_f + a_c)}{L} - \dot{z}_s - a_c\dot{\varphi}_s\right]$, $T_{cp} = c_p\left[\dot{\varphi}_s - \frac{(\dot{z}_{ur} - \dot{z}_{uf})}{L}\right]$,

$F_{kb} = k_b\left[z_{uf} + (z_{ur} - z_{uf})\frac{(L_f + a_k)}{L} - z_s - a_k\varphi_s\right]$, and $T_{kp} = k_p\left[\varphi_s - \frac{(z_{ur} - z_{uf})}{L}\right]$. The equations of motions of the two models can be analyzed to develop relationships between the parameters of coupled and unconnected suspensions. The stiffness matrices for the unconnected (K_U) and coupled (K_C) suspension models can be expressed as:

$$
K_U = \begin{bmatrix}
-k_{sf} - k_{sr} & k_{sf}L_f - k_{sr}L_r & k_{sf} & k_{sr} \\
 & -k_{sf}L_f^2 - k_{sr}L_r^2 & -k_{sf}L_f & k_{sr}L_r \\
 & & -k_{sf} - k_{tf} & 0 \\
\textit{symmetric} & & & -k_{sr} - k_{tr}
\end{bmatrix}
\tag{3}
$$

$$K_C = \begin{bmatrix} -k_b & -k_b a_k & k_b \dfrac{L_r - a_k}{L} & k_b \dfrac{L_f + a_k}{L} \\ & -k_b a_k^2 - k_p & -\dfrac{k_p}{L} + k_b a_k \dfrac{L_r - a_k}{L} & \dfrac{k_p}{L} + k_b a_k \dfrac{L_f + a_k}{L} \\ & & -\dfrac{k_p}{L^2} - k_{sf} - k_b \dfrac{(L_r - a_k)^2}{L^2} & \dfrac{k_p}{L^2} - k_b \dfrac{(L_r - a_k)(L_f + a_k)}{L^2} \\ \textit{symmetric} & & & -\dfrac{k_p}{L^2} - k_{sr} - k_b \dfrac{(L_f + a_k)^2}{L^2} \end{bmatrix} \quad (4)$$

Odhams and Cebon [17] established a number of important relations for the two suspension models by comparing the stiffness matrices in Eqs. (3) and (4). From Eq. (4), it is apparent that $a_k = 0$ yields uncoupled bounce and pitch modes of the sprung mass. The position coordinate a_k is thus termed as the stiffness coupling factor between the bounce and pitch modes. Furthermore, both stiffness matrices are identical under uncoupled bounce and pitch modes, when

$$k_{sf} L_f - k_{sr} L_r = 0;\ k_b = k_{sf} + k_{sr};\ k_p = k_{sf} L_f^2 + k_{sr} L_r^2;\ \text{and}\ \frac{k_p}{k_b} = L_f L_r \quad (5)$$

The matrices K_U and K_C are generally identical under all conditions, when

$$k_b = k_{sf} + k_{sr};\ \frac{1}{k_p} = \frac{1}{k_{sf} L^2} + \frac{1}{k_{sr} L^2};\ \frac{k_p}{k_b} = (L_f + a_k)(L_r - a_k);\ \text{and}\ a_k = \frac{k_{sr} L_r - k_{sf} L_f}{k_{sf} + k_{sr}} \quad (6)$$

The above suggests that the vehicle model with unconnected suspension can be considered as a special case of the model with coupled suspension. Moreover, it was shown that the relation $a_k = \dfrac{k_{sr} L_r - k_{sf} L_f}{k_{sf} + k_{sr}}$ is similar to the static margin (SM) defined in vehicle handling analysis, which may be expressed as $SM = \dfrac{S}{L}$, where $S = \dfrac{c_{\alpha r} L_r - c_{\alpha f} L_f}{c_{\alpha f} + c_{\alpha r}}$, $c_{\alpha f}$ and $c_{\alpha r}$ are cornering stiffnesses of the front and rear tires, respectively.

For the above relations, it can be further deduced that pitch stiffness of the coupled suspension k_p is equal to two equivalent rotational springs ($k_{sf}L_f^2$ and $k_{sr}L_r^2$) connected in parallel, when bounce and pitch modes are uncoupled. In all the other situations, k_p is equal to the two rotational springs in series. In all conditions, the bump stiffness k_b is invariably equal to the sum of the front and rear spring rates ($k_{sf}+k_{sr}$).

A.2.1 Dimensionless Measures of Suspension Properties

The above relations and discussions can provide a basic understanding of vehicle suspension properties in pitch plane, including uncoupled and coupled. In order to more clearly understand and investigate relationships between suspension tunings of unconnected suspensions and dynamic responses of the heavy vehicles, three dimensionless measures of suspension properties are defined and analyzed in this study, namely pitch margin (PM), pitch stiffness ratio (PSR) and coupled pitch stiffness ratio (CPSR).

PITCH MARGIN (PM)

From the above analysis, it is shown that the bounce spring stiffness is equal to the sum of front and rear suspension spring rates ($k_b = k_{sf}+k_{sr}$), when the two stiffness matrices K_U and K_C are identical. The relations $k_{sf} = k_b \sin^2\theta$ and $k_{sr} = k_b \cos^2\theta$ can therefore be obtained by introducing a variable θ, based on which $a_k = \dfrac{k_{sr}L_r - k_{sf}L_f}{k_{sf}+k_{sr}}$ in Eq. (6) can be rewritten as:

$$a_k = L_r \cos^2\theta - L_f \sin^2\theta \tag{7}$$

By setting $L_f = L\cos^2\gamma$ and $L_r = L\sin^2\gamma$, the pitch margin (PM) can be defined from Eq. (7):

$$PM = \frac{a_k}{L} = \frac{\cos 2\theta - \cos 2\gamma}{2} \tag{8}$$

where $0 < \theta < \pi/2$ and $0 < \gamma < \pi/2$, and γ is a constant for a given load distribution. Equation (8) would yield a positive value of pitch margin (PM) for $\theta < \gamma$. The pitch margin (PM) of a vehicle suspension can also be described from the dimensionless pitch margin diagram, shown in Fig. 2, where the positive direction of PM is considered to be pointing right. In this diagram, the upper semi-circle of diameter equal to unity scribing ΔACB represents the load distribution, while the lower-semi-circle scribing ΔADB describes the suspension spring rate tuning.

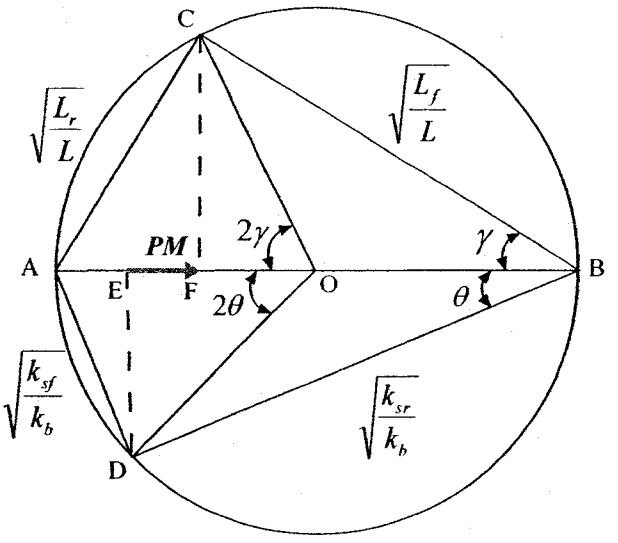

Figure 2: Dimensionless pitch margin diagram.

For a particular load distribution, Equation (8) can be simplified as:

$$PM = \frac{\cos 2\theta - D}{2} \tag{9}$$

where $D = \cos 2\gamma$ is a constant. The above equation suggests that the PM of a vehicle with a particular load distribution is only a function of θ alone, which itself is related to front/rear suspension stiffness ratio. From the dimensionless pitch margin diagram, it is evident that $PM = \dfrac{(OE - OF)}{2R} = EF$, where R is the radius. Considering $0 < \theta < \pi/2$, the bounds of PM can be derived as:

$$-\frac{1+D}{2} < PM < \frac{1-D}{2} \tag{10}$$

The above formulation indicates the range of PM corresponding to a given load distribution, which can be varied through tuning of front and rear suspension spring rates.

PITCH STIFFNESS RATIO (PSR)

The pitch stiffness ratio (PSR) is defined as the maximum ratio of pitch to bump rate (k_p / k_b) of a suspension system in a dimensionless manner. From Eq. (6), it can be shown that peak k_p / k_b ratio is obtained for $a_k = \dfrac{L_r - L_f}{2}$, which yields:

$$PSR = \frac{k_p}{k_b (L/2)^2} \tag{11}$$

Using $k_{sf} = k_b \sin^2\theta$ and $k_{sr} = k_b \cos^2\theta$, and the relationship between k_p and k_{sf} and k_{sr} in Eq. (6), the PSR can be obtained as:

$$PSR = \frac{k_b L^2 \sin^2\theta \cos^2\theta}{k_b (L/2)^2} = \sin^2 2\theta \tag{12}$$

The above formulation indicates that pitch stiffness ratio (PSR) is only related to the front/rear suspension stiffness ratio or θ, irrespective of load distribution. A relation between PM and PSR can also be derived from Eqs. (9) and (12) as:

$$PSR = 1 - (2PM + D)^2 \tag{13}$$

The above equation suggests that for a vehicle involving unconnected suspension with a particular load distribution, a definite relation exists between the pitch margin (PM) and pitch stiffness ratio (PSR). Equations (12) and (13) further show that for an unconnected suspension, $0 < PSR \leq 1$ and $0 < k_p \leq 0.25 k_b L^2$.

COUPLED PITCH STIFFNESS RATIO (CPSR)

Alternatively, coupled pitch stiffness ratio (CPSR) of an unconnected suspension is also defined upon consideration of the coupling factor a_k between the pitch and bounce modes, such that:

$$CPSR = \frac{k_p + k_b a_k^2}{k_b (L/2)^2} \tag{14}$$

The above can be simplified using Eqs. (6) and (7), such that:

$$CPSR = 1 - 2\cos 2\theta \cos 2\gamma + \cos^2 2\gamma \tag{15}$$

The above relation suggests that unlike PSR, CPSR is also dependent upon the load distribution. Eqs. (8), (12) and (15) further yield a relation among PM, PSR and CPSR:

$$CPSR = PSR + 4PM^2 \tag{16}$$

The above indicates that for $PM = 0$, which implies $a_k = 0$, the pitch and bounce modes are decoupled ($PSR = CPSR$), as observed from the two stiffness matrices K_U and K_C.

For a vehicle with a particular load distribution, γ is a constant, Equation (15) reduces to:

$$CPSR = 1 - 2D\cos 2\theta + D^2 \tag{17}$$

where $D = \cos 2\gamma$. The CPSR reduces to a function of the front/rear suspension stiffness ratio, as in the case of PSR. Considering the limits of suspension stiffness ratio $0 < \theta < \pi/2$, and those of load distribution $0 < \gamma < \pi/2$, Equation (17) can be solved to yield following limiting values of CPSR for different load distributions.

$$\begin{cases} (1-D)^2 < CPSR < (1+D)^2 & D \geq 0 \\ (1+D)^2 < CPSR < (1-D)^2 & D < 0 \end{cases} \tag{18}$$

Equations (9) and (17) further yield a relationship between PM and CPSR for an unconnected suspension, under a particular load condition:

$$CPSR = 1 - 4D * PM - D^2 \tag{19}$$

The above equation indicates that for $D > 0$, when a relatively lower load is supported by the front axle, an increase in the pitch margin (PM) would yield lower CPSR, and vice versa. For $D = 0$, $CPSR = 1$.

A.2.2 Analysis of the Three Measures of Suspension Properties

From Eqs. (8), (12) and (15), it is evident that PM and CPSR are functions of both γ and θ, while PSR is a function of θ alone, where $\gamma = \arctan\sqrt{L_r/L_f}$, and $\theta = \arctan\sqrt{k_{sf}/k_{sr}}$. Figures 3(a) and (c) illustrate variations in PM and CPSR as functions of γ and θ, while variations in PSR are presented in Fig. 3(b), as a function of θ. The variations in these measures are presented over a wide range of γ and θ

($0 < \gamma < \pi/2$ and $0 < \theta < \pi/2$). The results indicate that an increase in ratio L_r/L_f increases the pitch margin (PM), while an increase in ratio k_{sf}/k_{sr} causes a decrease in the PM, for a particular load distribution. The PSR achieves a maximum value of 1, for $k_{sf}/k_{sr} = 1$, where increasing or decreasing the ratio k_{sf}/k_{sr} would decrease the PSR, irrespective of the load distribution condition. For the coupled pitch stiffness ratio (CPSR), an increase in the ratio k_{sf}/k_{sr} yields an increase in CPSR for $L_r/L_f < 1$ ($0 < \gamma < \pi/4$). The CPSR assumes a constant unity value, irrespective of the ratio k_{sf}/k_{sr}, when $L_f = L_r$ ($\gamma = \pi/4$). The condition of $L_r/L_f > 1$ ($\pi/4 < \gamma < \pi/2$) yields an opposite trend in CPSR, where an increase in ratio k_{sf}/k_{sr} causes a decrease in the CPSR.

The results suggest that the load distribution and front/rear suspension stiffness ratio strongly affect the proposed dimensionless measures of suspension properties. The load condition and front/rear suspension tuning are also known to significantly influence vehicle dynamic responses. Some relations may therefore exist between the proposed dimensionless measures of suspension pitch properties and vehicle performance characteristics. The following sections will explore the performance characteristics of heavy vehicles under random road excitations as well as braking inputs, for different load conditions and suspension stiffness tunings, in an attempt to establish such relations.

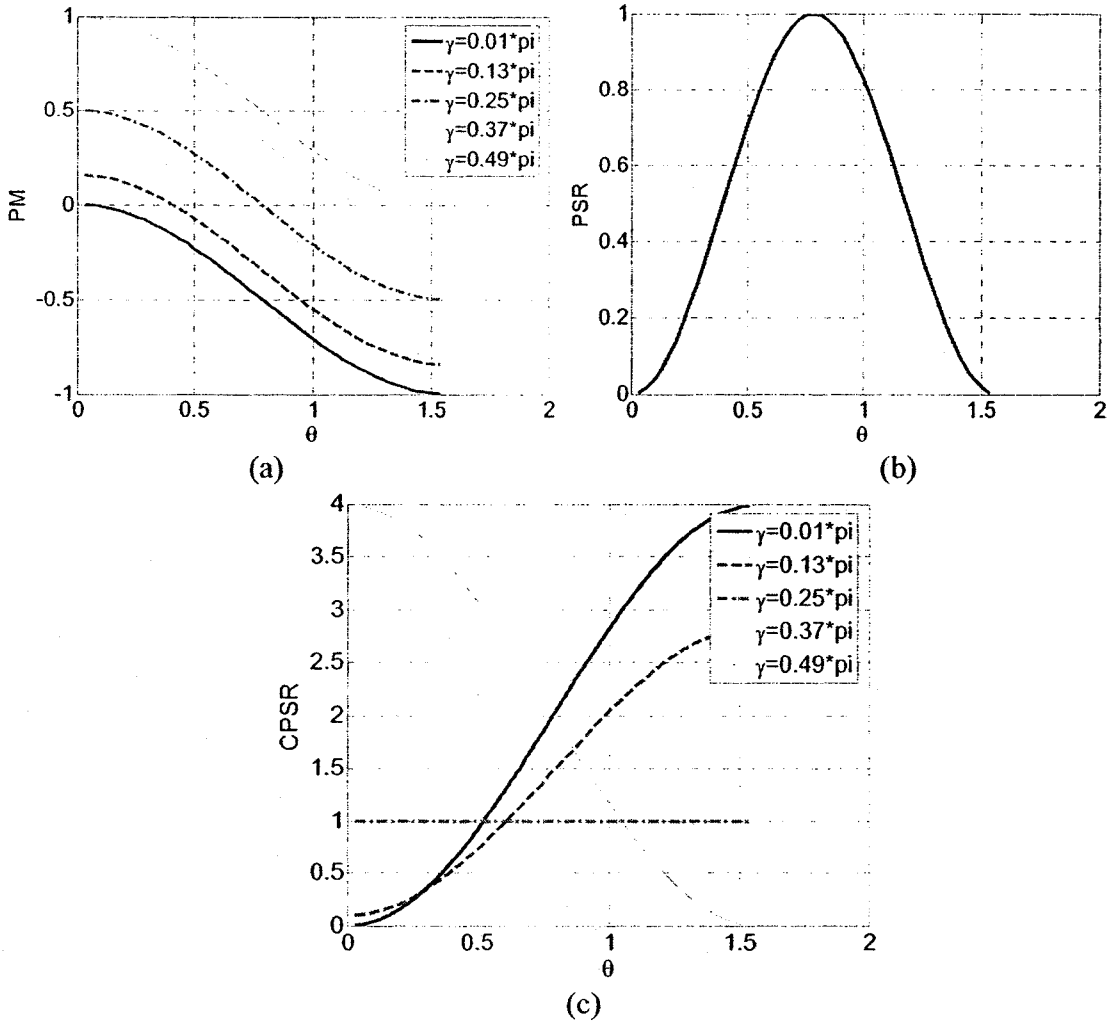

Figure 3: Variations in measures of suspension properties as functions of γ and θ: (a) PM; (b) PSR; and (c) CPSR.

A.3 Vertical and Pitch Ride under Random Road Excitations

Random road roughness is known to be the major excitation for evaluating vehicle ride performance characteristics of alternative suspension designs, which are generally measured in terms of acceleration responses of the vehicles [2, 4, 21]. The vertical and pitch ride performance of heavy vehicles with different suspension configurations can be conveniently assessed using the pitch plane ride model of road vehicles (Fig. 1), subject to excitations arising from random road elevations. The ride performance is evaluated in terms of: (a) rms vertical acceleration of the sprung mass, measured at five different

positions that are evenly distributed along the wheelbase, including the front and rear suspension mountings; and (b) rms pitch acceleration of the sprung mass. The former measure accounts for coupling between the vertical and pitch modes of vibration. The ride analysis are performed under different road roughness inputs, which have been designated as 'smooth', 'medium' and 'rough' on the basis of their relative spatial power spectral densities (PSD) of vertical displacement [22, 23]. Figure 4 illustrates the displacement PSD of the three road profiles considered in the study. A relatively wide range of vehicle speeds are also chosen for the analysis (30, 50, 70, 90 and 110 km/h), considering the wheelbase filtering.

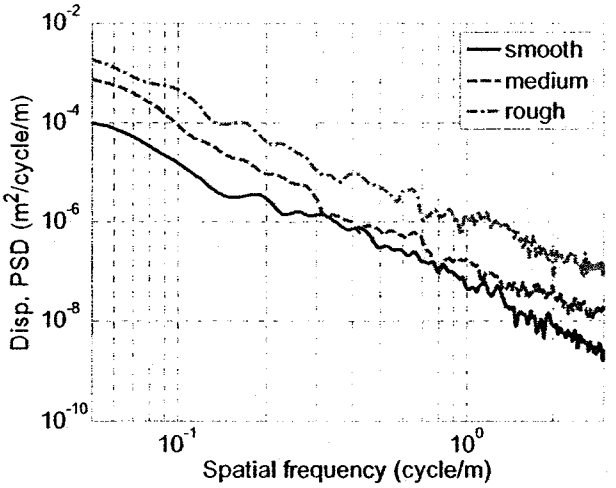

Figure 4: Displacement PSD of the three road profiles.

Three heavy vehicle configurations that represent different load distributions are considered for the analysis. The inertial and bounce stiffness parameters are chosen to yield identical bounce mode frequency in the order of 1.2 Hz. The selected model parameters for the three configurations are: (I) $m_s = 15753$ kg, $I_s = 175034$ kgm^2, $k_b = 900$ kN/m, and $L_f / L_r = 1.88$; (II) $m_s = 10932.6$ kg, $I_s = 116689$ kgm^2,

$k_b = 624.6$ kN/m, and $L_f/L_r = 1$; and (III) $m_s = 10932.6$ kg, $I_s = 116689$ kgm^2, $k_b = 624.6$ kN/m, and $L_f/L_r = 0.67$. The chosen load distributions yield $D_I = 0.306$, $D_{II} = 0$ and $D_{III} = -0.2$, respectively. The analyses are performed to derive the suspension property measures and dynamic responses of the selected vehicle configurations.

VEHICLE CONFIGURATION I

The heavy vehicle configuration I involves greater load distributed on the rear axle, which yields $\gamma = 0.63$ rad. The variations in PM of the suspension are evaluated as a function of θ, ranging from 0 to $\pi/2$, and shown in Fig. 5(a). The pitch stiffness ratio (PSR) and coupled pitch stiffness ratio (CPSR) are evaluated as a function of the pitch margin (PM), as illustrated in Figs. 5(b) and (c), respectively. The results show that an increase in θ (or ratio k_{sf}/k_{sr}) reduces the PM, while the CPSR decreases with an increase in PM in a linear manner. The PSR increases with increasing PM, and achieves the maximum value of 1, when $PM = -D/2$. A further increase in PM yields a reduction in PSR, as evident in Fig. 5(b).

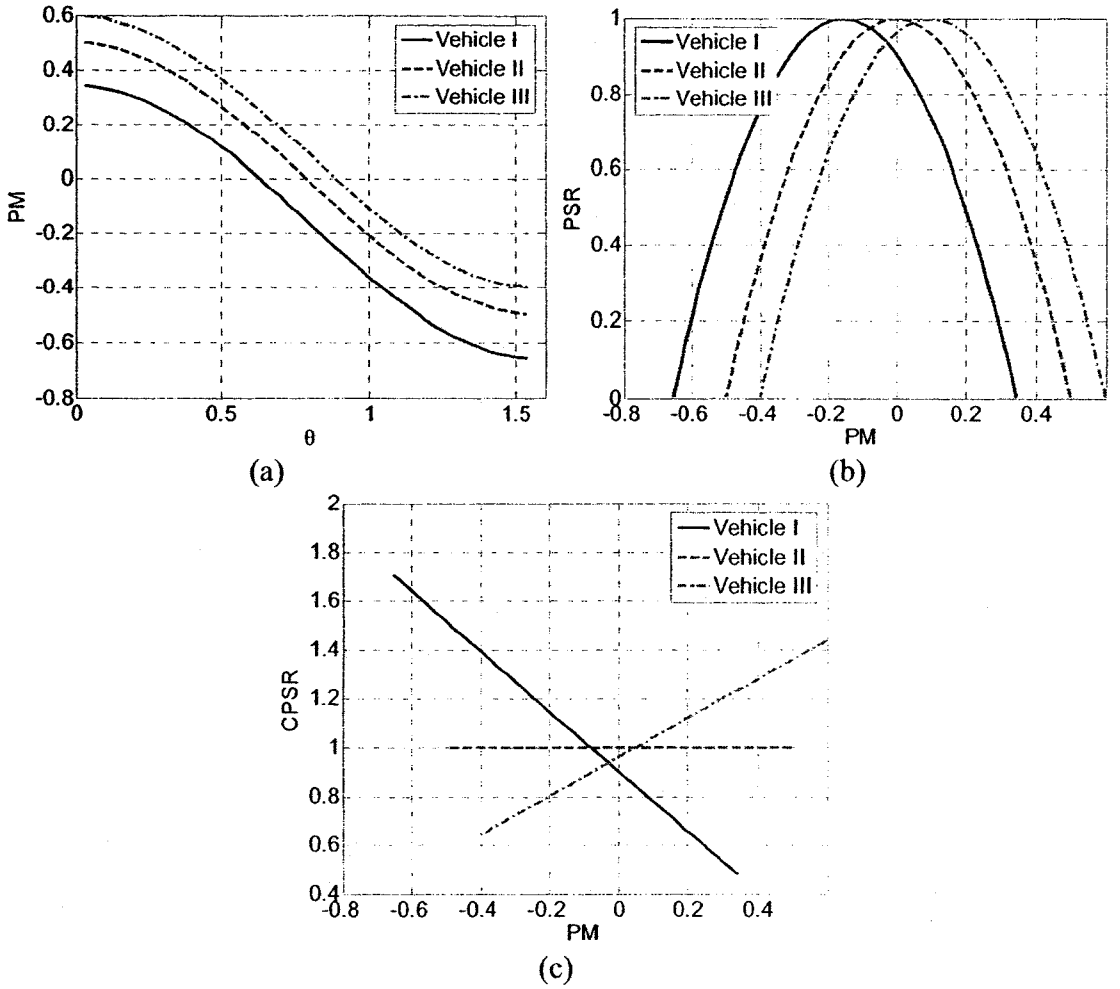

Figure 5: Variations in suspension property measures of different vehicle configurations: (a) PM vs θ; (b) PSR as a function of PM; and (c) CPSR as a function of PM.

The above results show that the proposed pitch measures are strongly dependent upon the front to rear suspension spring rate ratio. The influence of front and rear suspension rates on the resulting properties are evaluated for five different stiffness tunings of the linear unconnected suspension, which are summarized in Table 1. The sum of the front and rear suspension spring rates is held constant ($k_b = 900$ kN/m) for all the five stiffness tunings considered, so as to maintain the total bounce stiffness of the vehicle unaffected [14]. For the selected distributions, tuning S1 results in nearly identical natural frequencies for both the front and rear suspensions, while S3 and S5

cause lowest and highest front suspension natural frequencies, respectively. The tuning S1 provides identical values of PSR and CPSR, while S3 and S5 cause lowest and highest values of PSR and CPSR, respectively, as illustrated in Table 1. The tuning S1 that yields $PM = 0$ suggests decoupled front and rear suspensions, often considered as theoretically ideal suspension tuning for ride comfort [10]. A relatively lower value of front suspension rate (S2 and S3) yields $PM > 0$, while higher front suspension rate (S4 and S5) results in $PM < 0$.

Table 1: Influence of front and rear suspension spring rate ratio on the suspension property measures of vehicle configuration I.

Tuning	k_{sf} (kN/m)	k_{sr} (kN/m)	θ (rad)	PM	PSR	CPSR
S1	312.3	587.7	0.63	0	0.906	0.906
S2	222.3	677.7	0.52	0.1	0.744	0.784
S3	132.3	767.7	0.39	0.2	0.502	0.661
S4	402.3	497.7	0.73	-0.1	0.989	1.029
S5	492.3	407.7	0.83	-0.2	0.991	1.151

The vertical and pitch acceleration responses to random road excitations are evaluated for different suspension tunings and vehicle speeds. The damping ratios of the front and rear suspensions are tuned to achieve a value of 0.2 for all the suspension tunings considered in the analysis. The vertical responses assessed at five selected locations, and pitch responses are expressed in terms of rms accelerations. The vertical ride is then expressed as the root mean value of the rms accelerations evaluated at the five positions ($\sqrt{\sum_{n=1}^{5} \ddot{z}_{rmsn}^2 / 5}$). Figure 6 presents comparisons of rms vertical and pitch acceleration responses of different tunings, under the three random road inputs and a range of vehicle speeds. The results generally show comparable vertical responses of different suspension tunings under given road roughness and vehicle speed conditions,

although slight variations are also evident, which may be partly attributed to wheelbase filtering effect. The rms vertical acceleration generally tends to increase with increasing speed and road roughness. Unlike the vertical acceleration response, the pitch acceleration response is strongly influenced by the suspension stiffness tunings, except at the low speed of 30 km/h. The suspension tunings S2 and S3 with positive PM and relatively lower PSR and CPSR yield considerably lower pitch acceleration, irrespective of the road roughness and vehicle speed above 30 km/h, as seen in Fig. 6. The S4 and S5 tunings with negative PM and higher PSR and CPSR, on the other hand, result in considerably larger pitch acceleration responses, compared to S2 and S3 at the speeds above 30 km/h.

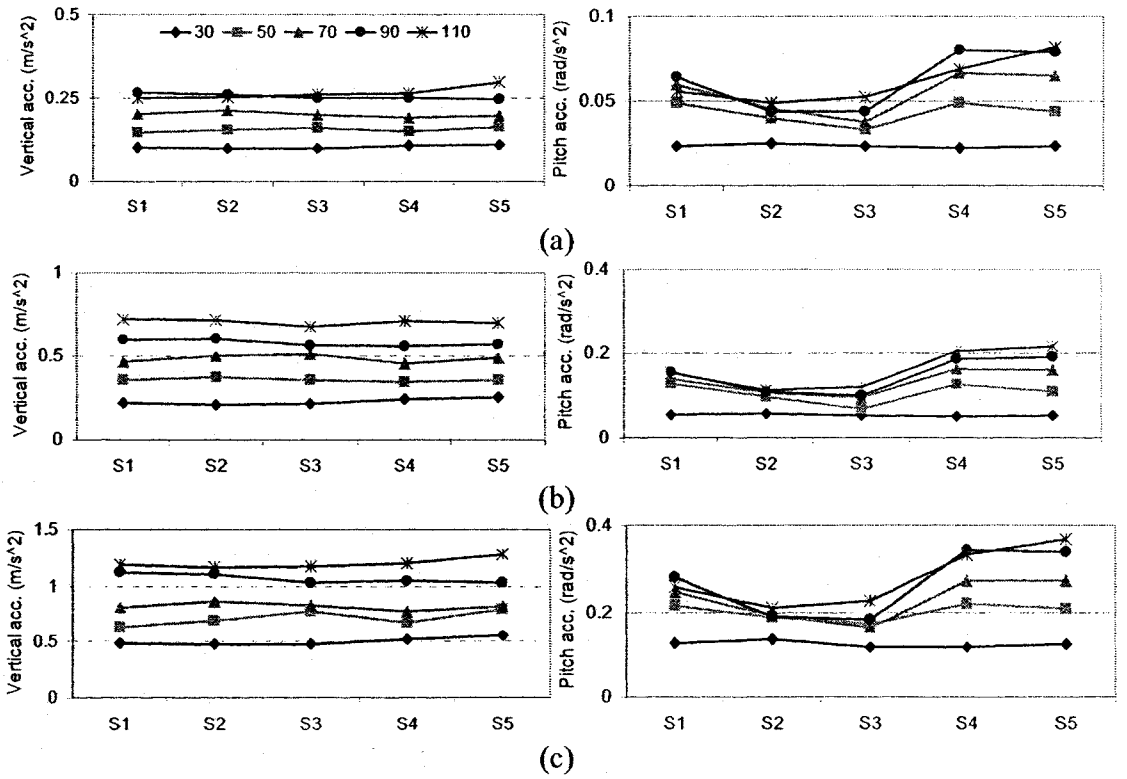

Figure 6: Comparisons of rms vertical and pitch acceleration responses of vehicle configuration I with different suspension tunings under random road inputs: (a) smooth; (b) medium; and (c) rough.

VEHICLE CONFIGURATION II

Unlike the vehicle configuration I, the vehicle configuration II exhibits an identical load distribution on each axle, which yields $\gamma = \pi/4$ rad. The variations in PM with θ ($0 < \theta < \pi/2$) is presented in Fig. 5(a). The corresponding variations in PSR and CPSR as a function of PM are illustrated in Figs. 5(b) and (c), respectively. The results indicate that the PM decreases with an increase in θ, as observed for vehicle configuration I. The CPSR maintains a constant value of 1, irrespective of the PM. The PSR, however, achieves the maximum value of 1 for PM=0, and decreases with increasing PM in both directions in a symmetric manner, as evident in Fig. 5(b).

Table 2 summarizes the influence of various suspension stiffness tunings (S1 to S5) of the linear unconnected suspension on the suspension property measures of the vehicle configuration. In this case, the front and rear suspension rates are varied to attain total suspension spring rate ($k_b = k_{sf} + k_{sr}$) of 624.6 kN/m for all the five tunings. For the even load condition, tuning S1 yields identical natural frequencies of the front and rear suspensions, while S3 and S5 tunings would yield lowest and highest front suspension natural frequencies, respectively. The tuning S1 yields a PM of 0, indicating decoupled bounce and pitch vibration modes. The tunings S2 and S3 with relatively lower front suspension rates have positive PMs of 0.144 and 0.288, respectively. The S4 and S5 tunings with relatively higher front suspension rates, on the other hand, yield negative PM. Owing to the symmetric variations in PSR, the tunings S2 and S4 yield identical values of PSR, which are lower than that of S1 tuning, while tunings S3 and S5 yield lowest PSR. Unlike the PSR, the value of CPSR remains 1 for all the tunings.

Table 2: Influence of front and rear suspension spring rate ratio on the suspension property measures of vehicle configuration II.

Tuning	k_{sf} (kN/m)	k_{sr} (kN/m)	θ (rad)	PM	PSR	CPSR
S1	312.3	312.3	0.79	0	1	1
S2	222.3	402.3	0.64	0.144	0.917	1
S3	132.3	492.3	0.48	0.288	0.668	1
S4	402.3	222.3	0.93	-0.144	0.917	1
S5	492.3	132.3	1.09	-0.288	0.668	1

The relative ride responses of the vehicle configuration II with different suspension tunings are also evaluated under the three random road excitations and different vehicle speeds. The damping ratios of the front and rear suspension are tuned to realize identical value of 0.2 for all the suspension tunings. Figure 7 presents comparisons of rms vertical and pitch acceleration responses of the vehicle involving different suspension tunings and operating conditions (speed and road roughness). Unlike the configuration I, the suspension tunings seem to have a strong effect on the vertical rms acceleration response of the vehicle configuration II, particularly at higher speeds and rougher road. Reducing the front suspension spring rate (S2 and S3) yields higher vertical acceleration responses. The rms pitch acceleration responses of the sprung mass are significantly different due to different tunings, as observed for configuration I. Compared to S1 tuning, the tunings S2 and S3 with positive PM and relatively lower PSR and k_{sf}, could significantly reduce pitch acceleration responses of the vehicle at speeds above 30 km/h, irrespective of the road roughness. These two tunings, however, tend to slightly increase the pitch acceleration responses at the low speed of 30 km/h, which has also been observed in the reported studies [15, 16]. Tunings S4 and S5 with negative PM, relatively lower PSR and higher k_{sf}, however, exhibit considerably higher pitch acceleration responses, compared to those of S2 and S3 at speeds above 30 km/h.

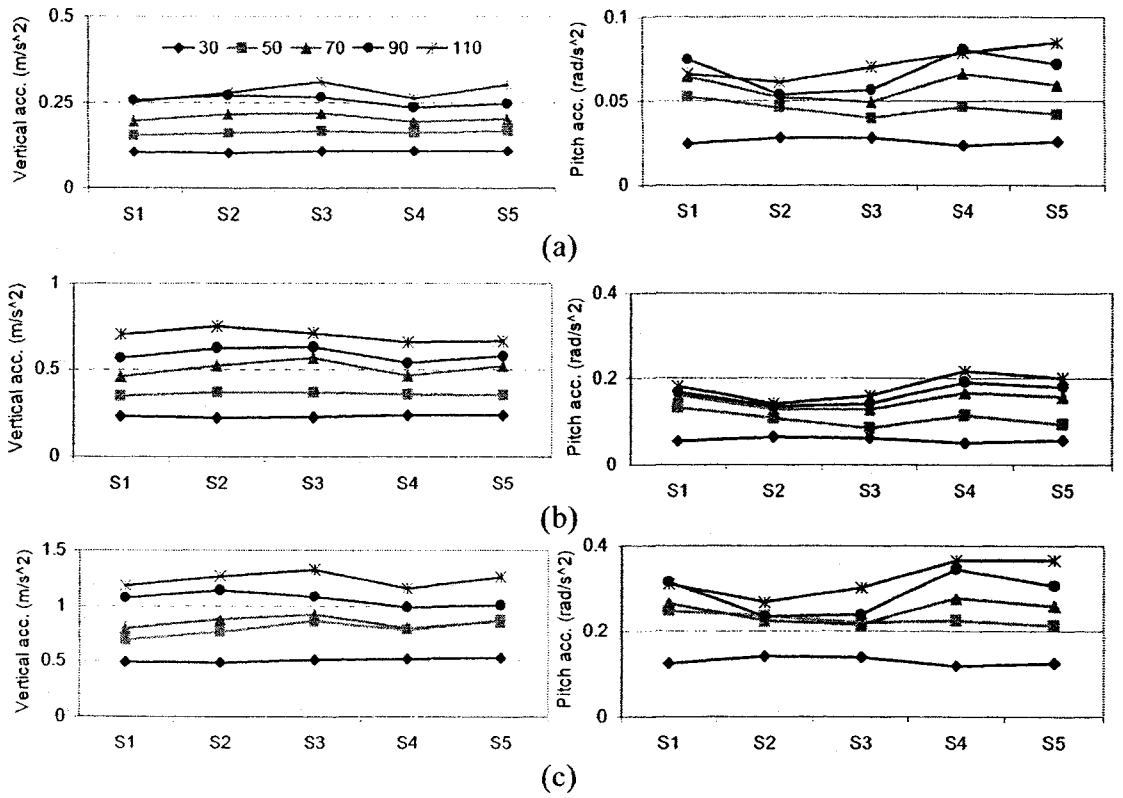

Figure 7: Comparisons of rms vertical and pitch acceleration responses of vehicle configuration II with different suspension tunings under random road inputs: (a) smooth; (b) medium; and (c) rough.

VEHICLE CONFIGURATION III

The vehicle configuration III involves relatively larger load on the front axle ($L_f/L_r = 0.67$) with $\gamma = 0.89$ rad. Figure 5(a) presents the variations in PM as a function of θ, while the variations in PSR and CPSR are illustrated in Figs. 5(b) and (c), as a function of PM. The results show that the PM decreases with increasing θ (or ratio k_{sf}/k_{sr}), as in case of configurations I and II. While the CPSR increases linearly with an increase in PM, the PSR achieves its peak value of 1 for PM=0.1, where PSR decreases with increasing PM in both directions.

The dimensionless measures of suspension properties of configuration III are evaluated for the five different spring rate tunings, in a similar manner, where the total

spring rate k_b is held as 624.6 kN/m, as summarized in Table 3. Tuning S1 yields nearly identical natural frequencies for both front and rear suspensions, while S3 and S5 tunings would yield lowest and highest front suspension natural frequencies, respectively. Tuning S1 that yields a PM of 0, suggests decoupling between the bounce and pitch vibration modes of the sprung mass, while tunings S2 and S3 yield positive values of PM. The tunings S4 and S5, on the other hand, exhibit negative PM values. The tuning S2 with identical front and rear suspension rates yields higher PSR than S1 and S3 tunings, which show identical PSR. Tunings S4 and S5 with relatively lower rear suspension rates exhibit relatively lower PSR. Unlike the PSR, the CPSR of S3 tuning is highest among the five tunings considered.

Table 3: Influence of front and rear suspension spring rate ratio on the suspension property measures of vehicle configuration III.

Tuning	k_{sf} (kN/m)	k_{sr} (kN/m)	θ (rad)	PM	PSR	CPSR
S1	374.76	249.84	0.89	0	0.96	0.96
S2	312.3	312.3	0.79	0.1	1	1.04
S3	249.84	374.76	0.67	0.2	0.96	1.12
S4	437.22	187.38	0.99	-0.1	0.84	0.88
S5	499.68	124.92	1.11	-0.2	0.64	0.8

The rms vertical and pitch acceleration responses of the vehicle configuration III involving different suspension tunings are also evaluated under different random road inputs and vehicle speeds, while the damping ratios of the front and rear suspension for each tuning are selected as 0.2. Figure 8 illustrates comparisons of rms vertical and pitch acceleration responses of different tunings for different road roughness and speed inputs. The results show that the vehicle with all the five different suspension tunings exhibits similar vertical acceleration responses for the low speed of 30 km/h, as it was observed for configurations I and II. A relatively softer front suspension (S2 and S3), however,

yields higher rms vertical acceleration at speeds above 30 km/h. This trend is similar to that observed for configuration II. The pitch acceleration responses of S4 and S5 tunings with negative PM, and relatively higher k_{sf} and lower PSR, are comparable with those of S1, but considerably larger than those of S2 and S3 tunings with positive PM, for vehicle speeds above 30 km/h. For the low speed of 30 km/h, the rms pitch acceleration responses of S2 and S3, however, are higher than those of S1, S4 and S5 tunings.

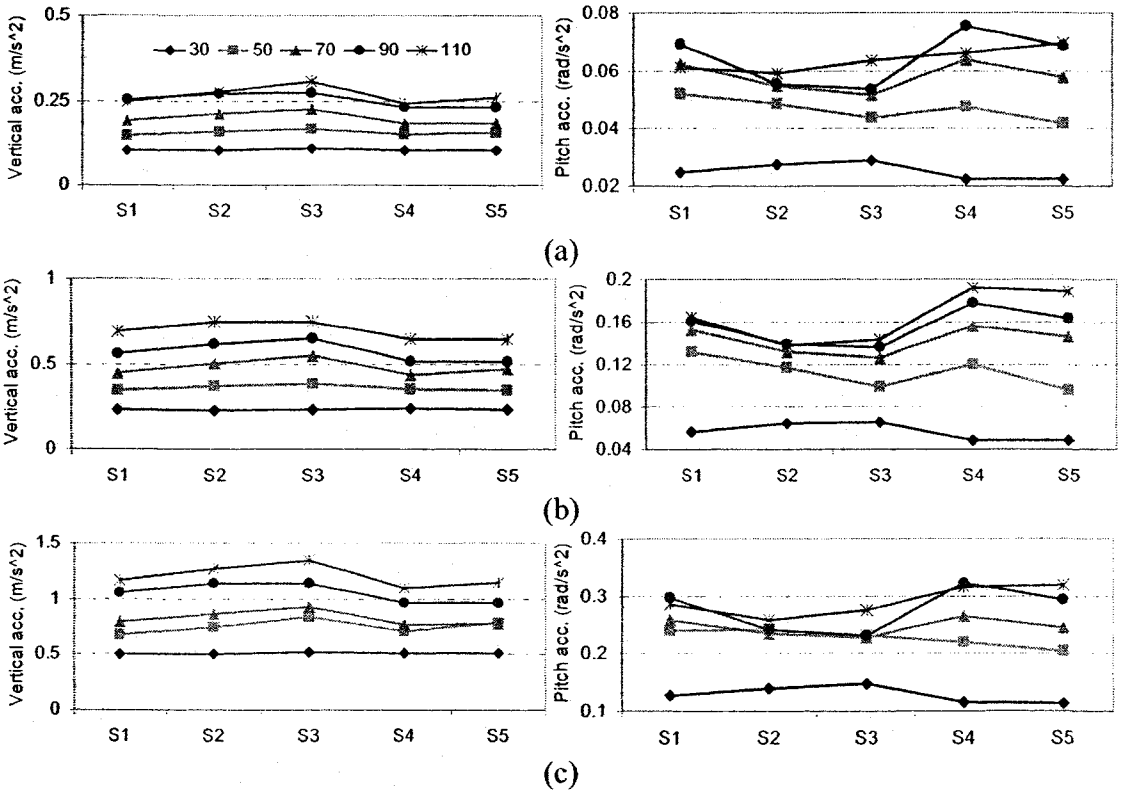

Figure 8: Comparisons of rms vertical and pitch acceleration responses of vehicle configuration III with different suspension tunings under random road inputs: (a) smooth; (b) medium; and (c) rough.

A.3.1 Discussions

From the above results attained under a wide range of random road roughness inputs and vehicle speeds, it is evident that the suspension stiffness tunings could strongly affect the pitch acceleration responses, while their influence on vertical acceleration responses

is strongly dependent upon road roughness characteristics. The above analyses, however, do not reveal clear relationships between the vertical and pitch ride responses and the proposed dimensionless measures (PM, PSR and CPSR). This is mainly due to different wheelbase filtering effects under various speeds and variations in load distributions considered in the study. An alternative simplified quantitative measure, based on the sum of acceleration responses of a particular suspension tuning under different speeds and road roughness inputs normalized with respect to that of tuning S1, is explored in an attempt to establish a more definite relationship. This measure is referred to as normalized cumulative acceleration (NCA), which is expected to reduce the contribution due to wheelbase filtering, while it imposes equal weighting for various road roughness inputs. The effect of load variations may thus be observed more clearly from the proposed alternative measure.

Table 4 summarizes the NCA measures of vertical and pitch acceleration responses of the three vehicle configurations with different suspension tunings (S1 to S5) together with the corresponding values of PM, PSR and CPSR. An NCA value of a particular tuning below 1 implies lower cumulative acceleration response than the baseline tuning S1 that yields identical front and rear suspension frequencies. The NCA>1 would imply larger cumulative acceleration response than that of the S1 tuning. The variations in VCA measures do not show a clear trend with CPSR. From the results, following relations of the vertical and pitch mode NCA with the dimensionless measures of the suspension could be obtained:

- Maintaining a constant value of sum of the front and rear suspension spring rates would still induce variations in vertical acceleration responses, irrespective of the load distribution, which is attributed to coupling between the bounce and pitch modes of the sprung mass.

- A positive value of PM generally yields a higher value of vertical NCA, suggesting deterioration of vertical ride, particularly when $L_f/L_r = 1$ (configuration II) and $L_f/L_r < 1$ (configuration III).
- A positive value of PM, however, generally yields considerably lower values of pitch NCA, irrespective of the load distribution.
- The PM and PSR show coupled effects on both vertical and pitch NCA. A lower value of PSR coupled with a positive PM yields a considerable reduction in pitch NCA.
- For typical heavy vehicles ($L_f/L_r > 1$), a positive PM tuning would yield a lower value of PSR and thus significant improvement in the pitch ride performance. The corresponding change in vertical ride is very small.
- For vehicles with either even or greater load on the front axle, a positive PM tuning is beneficial for pitch ride performance. An appropriate negative PM tuning, on the other hand, could yield considerable vertical ride improvement with only slight increase in pitch NCA.

Table 4: Comparisons of NCA of vehicle configurations with different suspension tunings.

Tuning	PM	PSR	CPSR	Vertical NCA	Pitch NCA
			Configuration I		
S1	0	0.906	0.906	1	1
S2	0.1	0.744	0.784	1.016	0.794
S3	0.2	0.502	0.661	0.983	0.735
S4	-0.1	0.989	1.029	0.989	1.142
S5	-0.2	0.991	1.151	1.048	1.156
			Configuration II		
S1	0	1	1	1	1
S2	0.144	0.917	1	1.072	0.846
S3	0.288	0.668	1	1.027	0.853
S4	-0.144	0.917	1	0.901	1.05
S5	-0.288	0.668	1	1.061	0.993
			Configuration III		
S1	0	0.96	0.96	1	1
S2	0.1	1	1.04	1.079	0.906
S3	0.2	0.96	1.12	1.053	0.891
S4	-0.1	0.84	0.88	0.849	1.03
S5	-0.2	0.64	0.8	1.024	0.967

A.4 Dynamic Tire Load Responses

Dynamic tire loads of road vehicles, especially heavy vehicles, are known to accelerate road damages. The relative dynamic tire load responses of different vehicle configurations involving different suspension tunings are therefore assessed under different random road inputs and vehicle speeds, as a measure of road-friendliness characteristics of the vehicles. For a given speed, the dynamic tire load responses of the vehicle with a particular tuning revealed similar trends under excitations arising from different road roughness. As an example, Figure 10 illustrates the dynamic load coefficients (DLC) due to front and rear wheels of the three vehicle configurations with different suspension tunings (described in Tables 1 to 3), subject to the excitations from medium road. The DLC due to tire force is evaluated as the ratio of rms dynamic tire force to the static tire force [12]. The front or rear tire force DLC responses exhibit very similar trends, for the three vehicle configurations considered. The results show that the influence of suspension tuning on the DLC is relatively insignificant at the low speed of 30 km/h, irrespective of the load distribution. The suspension tuning, however, strongly influence the DLC responses at higher speeds. The S2 and S3 tunings with relatively lower front suspension rate and thus positive PM yield lower magnitudes of DLC at the front wheel, but higher magnitudes of DLC at the rear. As expected, the tunings S4 and S5 with relatively higher front suspension stiffness exhibit opposite trends, as seen in Fig. 9. The results also suggest that a relatively soft suspension is helpful for improving dynamic tire load performance of a heavy vehicle, which is consistent with the results reported in many studies [12, 24].

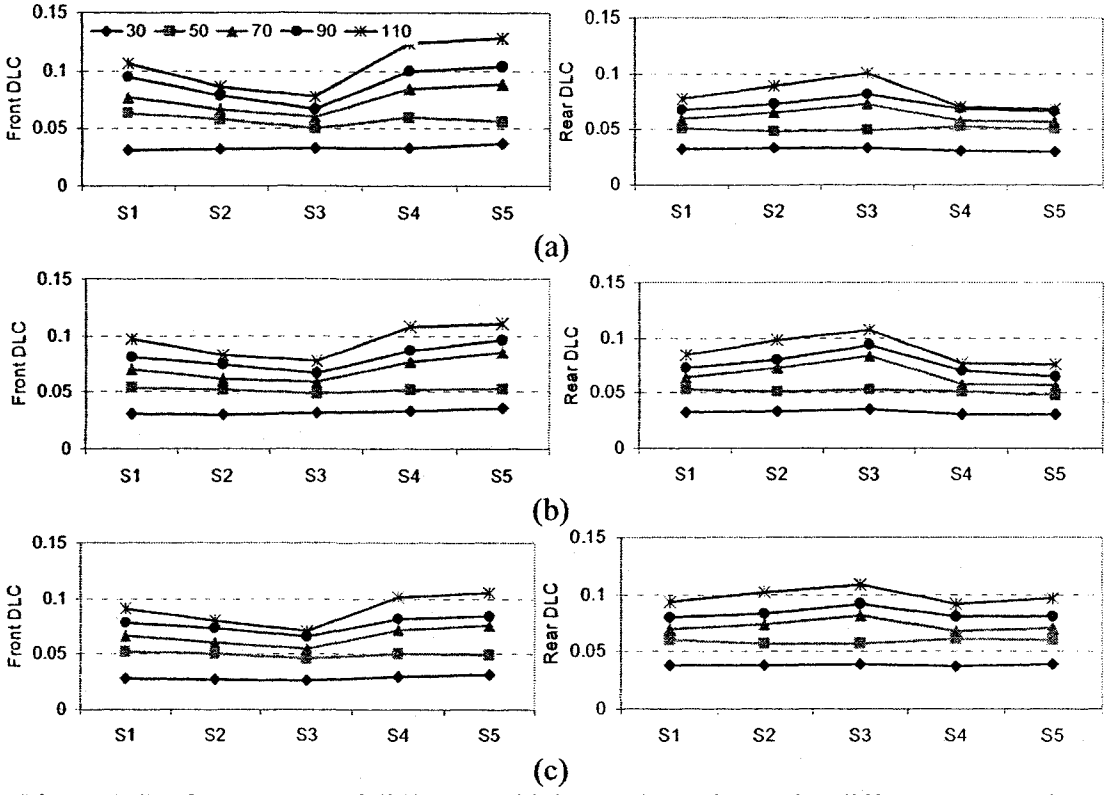

Figure 9: DLC responses of different vehicle configurations with different suspension tunings under medium road inputs: (a) configuration I; (b) configuration II; and (c) configuration III.

In order to further compare the effects of different suspension tunings on the overall dynamic tire load characteristics of the vehicles, a simplified quantitative measure is formulated on the basis of normalized cumulative DLC (NCD). This measure of a vehicle with a particular suspension tuning is derived upon summing the DLC values due to the front and rear tire forces attained for different road roughness and speed conditions considered in this study. The resulting cumulative DLC is normalized with respect to that of the vehicle with tuning S1.

Table 5 summarizes the NCD responses of the three vehicle configurations with five different suspension tunings, together with the corresponding PM values. The results suggest that suspension tuning with a negative value of PM tends to deteriorate the cumulative DLC of vehicle, irrespective of the load distribution and road roughness. A

positive tuning, however, could yield slightly lower values of cumulative DLC, except when $L_f/L_r = 1$. The results indicate that positive PM tuning is desirable for improved pitch ride and dynamic tire load performance.

Table 5: Comparisons of normalized cumulative DLC (NCD) responses of vehicle configurations with different suspension tunings.

Tuning	Configuration I		Configuration II		Configuration III	
	PM	NCD	PM	NCD	PM	NCD
S1	0	1	0	1	0	1
S2	0.1	0.972	0.144	0.995	0.1	0.982
S3	0.2	0.992	0.288	1.056	0.2	0.98
S4	-0.1	1.03	-0.144	1.016	-0.1	1.032
S5	-0.2	1.062	-0.288	1.064	-0.2	1.086

A.5 Suspension Travel Responses

Suspension designs and tunings of road vehicles are subjected to the constraints posed by rattle space. Although a very soft suspension is known to be beneficial for ride comfort and road friendliness of vehicles, it could induce significantly larger suspension travel. The suspension travel responses of the three vehicle configurations with different suspension tunings are assessed under different random road excitations and speeds. The rms travel responses of a suspension with a particular tuning were observed to depend upon the road roughness in a manner similar to that observed for dynamic tire loads. The influences of the suspension tuning on the rms suspension travel, however, are relatively smaller when compared to those on DLC. Figure 10, as an example, presents the front and rear suspension travel responses of the three vehicle configurations involving different suspension tunings under the medium-rough road input at various speeds. Suspension tunings with PM<0 (S4 and S5) yield lower front suspension travel but higher rear suspension travel, which is attributed to relatively stiffer and softer front and rear suspensions, respectively. The responses under the higher speed of 100 km/h, however,

form an exception, which may be partly due to greater contribution of wheelbase filtering. With the exception of responses at 110 km/h, the tunings S2 and S3 with PM>0 yield only minimal influences on the travel responses. The rms magnitudes tend to be slightly larger at the front and lower at the rear, when compared to those of tuning S1.

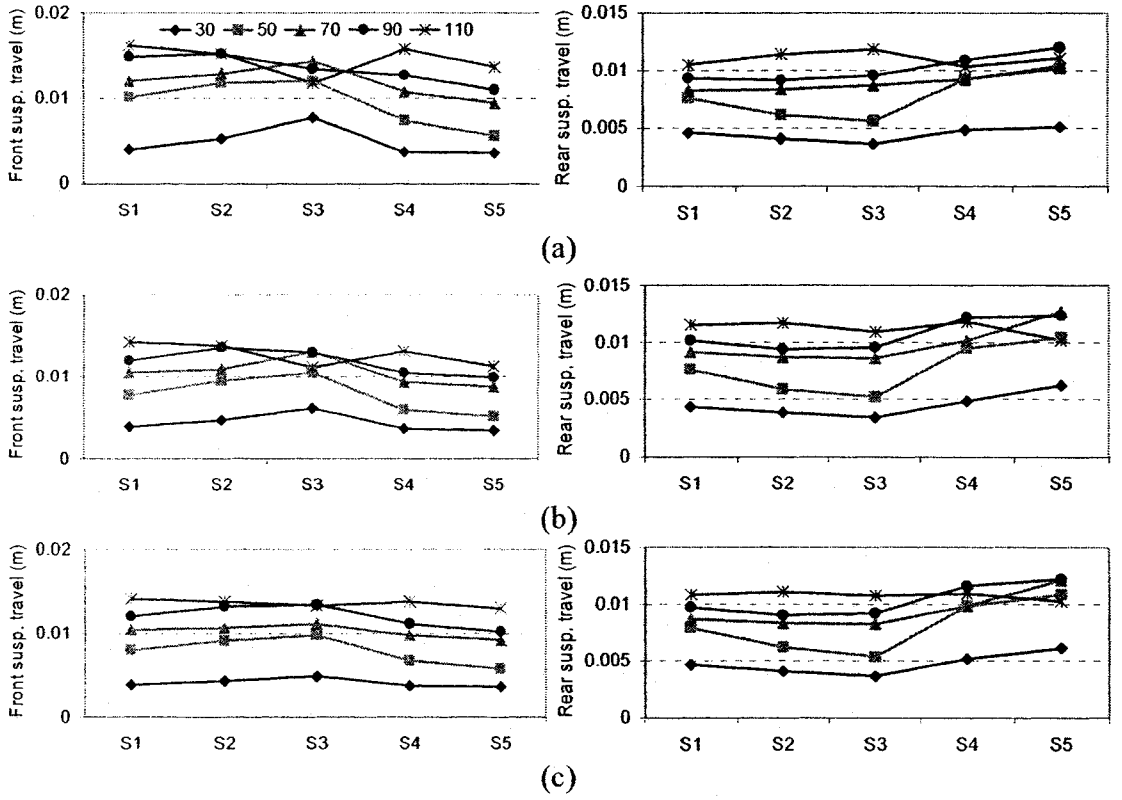

Figure 10: Suspension travel responses of vehicle configurations with different suspension tunings under medium road inputs: (a) configuration I; (b) configuration II; and (c) configuration III.

The effect of suspension tuning on the overall suspension travel performance of the vehicles is further evaluated, on the basis of a simplified quantitative measure, namely normalized cumulative suspension travel (NCST). For a vehicle configuration with a particular suspension tuning, NCST is formulated as the sum of the front and rear suspension travels for different speeds and road inputs normalized with respect to that of the S1. Table 6 summarizes the NCST responses of the three vehicle configurations with different suspension tunings, as well as the PM values. From the results, it is apparent

that influences on the NCST are very small for the range of tunings considered. The results shown in Fig. 10 and Table 6 suggest that a particular tuning may yield slightly lower travel of suspension at one of the axles, while the response at the other axle may be slightly higher. Suspension tuning with PM>0 tends to slightly deteriorate the cumulative suspension travel response of the vehicles, when $L_f/L_r \geq 1$. A negative PM tuning, however, could slightly improve the cumulative suspension travel response, when $L_f/L_r \geq 1$.

Table 6: Comparisons of normalized cumulative suspension travel (NCST) responses of vehicle configurations with different suspension tunings.

Tuning	Configuration I		Configuration II		Configuration III	
	PM	NCST	PM	NCST	PM	NCST
S1	0	1	0	1	0	1
S2	0.1	1.022	0.144	1.007	0.1	0.998
S3	0.2	1.019	0.288	1.006	0.2	0.997
S4	-0.1	0.972	-0.144	0.997	-0.1	1.013
S5	-0.2	0.949	-0.288	0.996	-0.2	1.027

A.6 Pitch Attitude Responses under Braking Inputs

The variations in vehicle pitch attitude induced by braking maneuvers could induce the variations in normal tire loads and thus affect the handling quality of vehicles [9-11]. The influence of suspension tuning on the vehicle response to braking inputs are further investigated using a pitch and vertical dynamics model of the vehicle. A pitch plane braking model of a heavy vehicle, shown in Fig. 11 [20], is used to investigate the braking responses of the three vehicle configuration coupled with different suspension tunings in terms of peak pitch angle and suspension travel. The model is sufficiently generalized for investigating coupled as well as unconnected suspension systems, and it

incorporates: longitudinal motion (x) of the vehicle, vertical motions of the front and rear unsprung masses (z_{uf}, z_{ur}), vertical (z_s) and pitch (φ_s) motions of the sprung mass, and angular velocities of the front and rear wheels (ω_f, ω_r). The vertical properties of tires are represented by linear stiffness and damping elements, assuming point-contact with the road surface. Figure 11(b) illustrates the forces and moments considered to act on a wheel and tire assembly under braking. The equations of motion for the pitch plane vehicle model are formulated under excitations arising from the vehicle-road interactions and the braking torque. The formulations include total suspension forces, comprising the static and dynamic forces developed by the front (f_f) and rear (f_r) suspensions. Assuming small pitch motions, the equations of motion are summarized below:

$$
\begin{aligned}
&m_s\ddot{z}_s = -f_f - f_r + m_s g \\
&I_s\ddot{\varphi}_s = f_f L_f - f_r L_r - f_{xf}(h + z_{0f} - z_s) - f_{xr}(h + z_{0r} - z_s) \\
&m_{uf}\ddot{z}_{uf} = f_f + k_{tf}(z_{0f} - z_{uf}) + c_{tf}(\dot{z}_{0f} - \dot{z}_{uf}) + m_{uf} g \\
&m_{ur}\ddot{z}_{ur} = f_r + k_{tr}(z_{0r} - z_{ur}) + c_{tr}(\dot{z}_{0r} - \dot{z}_{ur}) + m_{ur} g \\
&(m_s + m_{uf} + m_{ur})\ddot{x} = -(f_{xf} + f_{xr}) - m_s g \varphi_s \\
&I_{wi}\dot{\omega}_i = f_{xi} \cdot r_i - T_{bi} \quad (i = f, r)
\end{aligned}
\tag{20}
$$

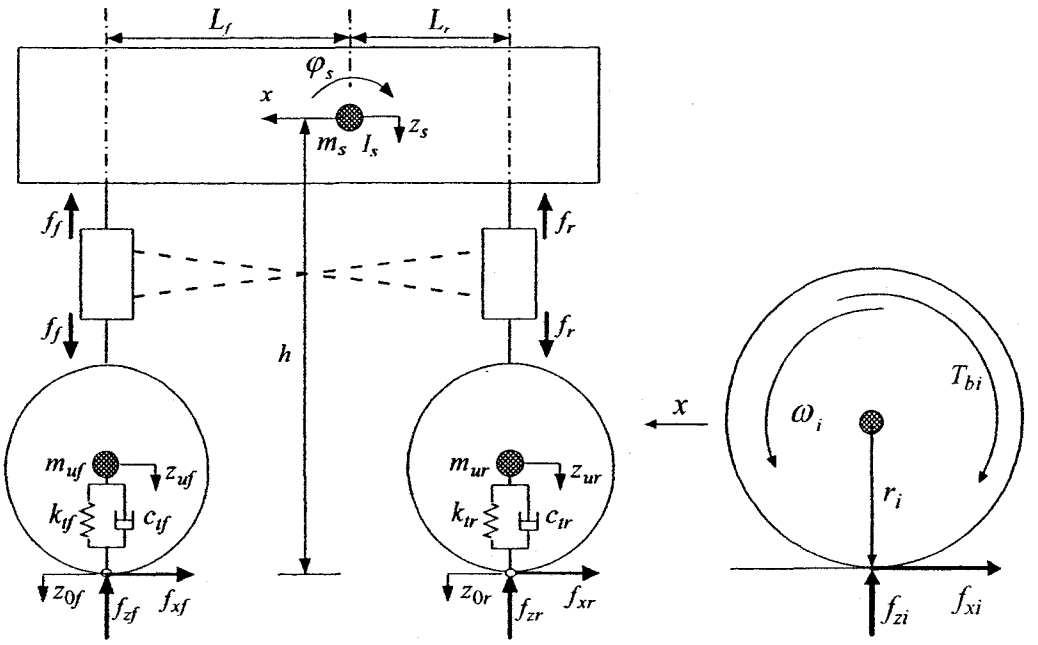

Figure 11: (a) Pitch plane braking model of a two-axle heavy vehicle; and (b) forces and moments acting on a wheel and tire assembly under braking.

where c_{ti} (i=f,r) is vertical damping coefficient of tire, f_{xf} and f_{xr} are braking efforts developed by the front- and rear-axle tires, respectively, and f_{zf} and f_{zr} are the respective normal forces applied to the road surface, h is vehicle c.g. height from the ground, T_{bi} is applied braking torque, r_i is effective radius of tire i, and I_{wi} is polar mass moment of inertia of wheel i. The Magic Formula tire model was utilized to derive the braking forces developed by the tires, as a function of slip and normal load [25, 26]. The validation of the vehicle model was investigated in view of the measured data reported by Murphy et al. [27], under different load conditions and braking inputs. Comparisons of results attained from the model with the reported measured data showed reasonably good agreement between them.

The vehicle model is analyzed for the three configurations and five suspension tunings under a braking input. The total braking gain was chosen as 98.2 Nm/kPa for all the three configurations [20, 28]. The sum of the driver's reaction time and the braking

system time lag was set as 0.75 s, while the rise time of the braking system was set as 0.25 s [28, 29]. The initial vehicle speed for the analyses was set as 100 km/h, while the braking input was selected as 172 kPa for all the three vehicle configurations considered. Figure 12 presents the peak pitch angle and peak suspension travel responses of the three vehicle configurations with different suspension tunings under the selected braking input. The results show that both the peak pitch angle and suspension travel responses are strongly influenced by suspension tuning, and exhibit similar trends for a particular load distribution. The peak pitch angle and peak suspension travel responses during braking are directly related to the suspension PSR, defined in Eq. (11). An examination of the PSR values of different suspension tunings, presented in Table 4, and the peak responses suggests that an increase in suspension PSR would yield considerably lower peak pitch angle and suspension travel responses under braking inputs.

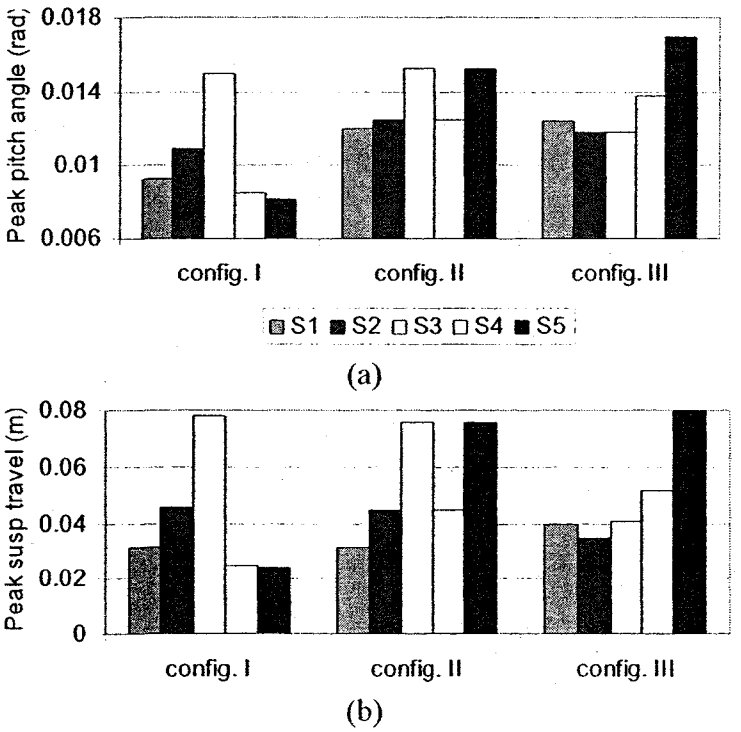

Fig. 12: Dynamic responses of different vehicle configurations with different suspension tunings under braking inputs: (a) peak pitch angle responses; and (b) peak suspension travel responses.

The results attained from Section 3 and Fig. 12 indicate that for typical heavy vehicles with greater load on the rear axle, a positive PM tuning that yields a relatively lower PSR could considerably enhance pitch ride with insignificant influence on vertical ride. Such suspension tuning, however, would significantly deteriorate the pitch attitude control and suspension travel performance during braking maneuvers. This is attributed to the definite relationship between PM and PSR of an unconnected suspension for a given load distribution. Pitch plane coupled suspensions, however, could offer considerable potential for independent tuning of PM and PSR, to achieve improved ride and handling performance of heavy vehicles.

A.7 Conclusions

The front/rear suspension stiffness tunings of two-axle heavy vehicles with unconnected suspensions were systematically explored in this study, under a wide range of random road inputs and driving speeds, as well as braking inputs. Upon considerations of the mathematical formulations of two pitch plane models of a two-axle heavy vehicle with unconnected and coupled suspensions, three dimensionless measures of suspension properties, namely the pitch margin (PM), pitch stiffness ratio (PSR) and coupled pitch stiffness ratio (CPSR), were proposed and analyzed for different unconnected suspension tunings and load conditions. The simulation results were explored in an attempt to derive influences of suspension tunings and measures on the responses, and for establishing some basic suspension tuning rules of heavy vehicles with conventional unconnected suspensions. The major findings of the study are summarized below.

- Maintaining a constant value of sum of the front and rear suspension spring rates would still induce variations in vertical acceleration responses, irrespective of the load distribution, which is attributed to the coupling effect between the bounce and

- For a vehicle with a particular load distribution, the use of an unconnected suspension yields a definite relationship between the dimensionless suspension property measures, namely the pitch margin (PM) and pitch stiffness ratio (PSR).
- A positive value of PM could considerably improve pitch ride, irrespective of the load distribution. It, however, generally deteriorates vertical ride, particularly for vehicles with even load distribution or greater load on the front axle.
- The PM and PSR show coupled effects on both vertical and pitch ride. A lower value of PSR together with a positive PM value could yield considerable improvement in the pitch ride.
- The peak pitch angle and peak suspension travel responses during braking are directly related to PSR. A higher PSR would be desirable for reducing both the peak pitch angle and peak suspension travel responses during braking maneuvers.
- For typical heavy vehicles with greater load on the rear axle, a positive PM tuning that yields a relatively lower PSR could considerably enhance the pitch ride with only negligible influence on vertical ride response. Such suspension tuning, however, would significantly deteriorate the pitch attitude control and suspension travel responses of the vehicles during braking maneuvers.
- A positive PM tuning also represents a relatively lower front suspension natural frequency, which indicates a lower roll stiffness of the front suspension. The use of anti-roll bar or roll plane coupled suspension would thus be helpful for increasing the roll stiffness without affecting vertical stiffness property.
- For vehicles with even load distribution or greater load on the front axle, an appropriate negative PM tuning could considerably improve vertical ride with only slight increase in pitch acceleration response.
- The suspension tuning could help reduce DLC due to forces developed by tires at one of the axles with an increase in DLC due to the other axle tire forces. A negative PM tuning tends to deteriorate the DLC responses of vehicles, irrespective of the load distribution and road roughness. A positive tuning, however, could generally yield slightly lower DLC.
- The suspension tuning could improve the rms travel response of suspension at one of the axles, while that of the suspension at the other axle would generally deteriorate. Suspension tuning with a positive PM tends to slightly deteriorate suspension travel responses of the vehicles with even or more load on the rear axle. A negative PM tuning, however, could slightly improve suspension travel responses of the vehicles with even or more load on the rear axle.
- Unlike unconnected suspension, pitch plane coupled suspension, could permit independent tunings of the vertical and pitch stiffness rates, and thus the PM and PSR. A pitch-connected suspension could thus offer significant potential for improving both the ride and handling qualities of vehicles.

References:

[1] Gillespie, T.D., 1992, 'Fundamentals of vehicle dynamics'. SAE Inc., PA, USA.

[2] Cole, D.J., 2001, 'Fundamental issues in suspension design for heavy road vehicles'. Vehicle System Dynamics, 35, 319-360.

[3] Bastow, B., 1987, 'Car suspension and handling'. Pentech Press Limited, London, UK.

[4] Gillespie, T.D., 1985, 'Heavy truck ride'. SAE paper 850001.

[5] Fancher, P. and Balderas, L., 1987, 'Development of microcomputer models of truck braking and handling'. UMTRI Report UMTRI-87-37, The University of Michigan, USA.

[6] Lewis, A.S. and El-Gindy, M., 2003, 'Sliding mode control for rollover prevention of heavy vehicle based on lateral acceleration'. International Journal of Heavy Vehicle Systems, 10, 9-34.

[7] Jiang, Z., Streit, D.A. and El-Grindy, M., 2001, 'Heavy vehicle ride comfort: literature survey'. International Journal of Heavy Vehicle Systems, 8, 258-284.

[8] Qiu Y. and Griffin, M.J., 2005, 'Transmission of roll, pitch and yaw vibration to the backrest of a seat supported on a non-rigid car floor'. Journal of Sound and Vibration, 288, 1197-1222.

[9] Dahlberg, E., 1999, 'Yaw instability due to longitudinal load transfer during braking in a curve'. SAE paper 1999-01-2952.

[10] Wong, J.Y., 2001, 'Theory of ground vehicles'. 3rd Edition, John Wiley & Sons, Inc., USA.

[11] Kang, X., Rakheja, S. and Stiharu, I., 2002, 'Cargo load shift and its influence on tank vehicle dynamics under braking and turning'. International Journal of Heavy Vehicle Systems, 9, 173-203.

[12] Cebon, D., 1999, 'Handbook of vehicle-road interactions'. Swets & Zeitlinger, Lisse, Netherlands.

[13] Cole, D.J. and Cebon, D., 1998, 'Front-rear interaction of a pitch-plane truck model'. Vehicle System Dynamics, 30, 117-141.

[14] Crolla, D.A. and King, R.P., 1999, 'Olley's 'flat ride' revisited'. Vehicle System Dynamics Supplement, 33, 762-774.

[15] Sharp, R.S. and Pilbeam, C., 1993,' Achievability and value of passive suspension designs for minimum pitch response'. Proc. IMechE Conference on Vehicle Ride and Handling, London, UK, 243-259.

[16] Sharp, R.S., 2002, 'Wheelbase filtering and automobile suspension tuning for minimizing motions in pitch'. Journal of Automobile Engineering, 216, 933-946.

[17] Odhams, A.M.C. and Cebon, D., 2006, 'An analysis of ride coupling in automobile suspensions'. Journal of Automobile Engineering, 220, 1041-1061.

[18] Carruthers, I.D.B., 2005, 'Simulation and testing of energy dissipation in passenger vehicle dampers'. Master thesis, Queen's University, Canada.

[19] Cao, D., Rakheja, S. and Su, C.-Y., 2006, 'A generalized model of a class of interconnected hydro-pneumatic suspensions and analysis of pitch properties'. Proc. of ASME Int. Mech. Engineering Congress, IMECE 2006-13961, Chicago, USA.

[20] Cao, D., Rakheja, S. and Su, C.-Y., 2007, 'Pitch attitude control and braking performance analysis of heavy vehicles with interconnected suspensions'. SAE paper 2007-01-1347.

[21] ISO 2631-1, 1997, 'Mechanical vibration and shock-Evaluation of human exposure to whole-body vibration-Part 1: General requirements'. International Standard Organization.

[22] Rakheja, S., Wang Z. and Ahmed A.K.W., 2001, 'Urban bus optimal passive suspension study. Phase II: Enhancement of road- and driver-friendliness of urban buses through optimal suspension damping'. Transportation Canada Report T-8200-4-4556, Canada.

[23] Cao, D., Rakheja, S. and Su, C.-Y., 2006, 'Roll and bounce dynamic responses of heavy vehicles with interconnected suspensions'. Proc. of CSME Symposium on Intelligent Vehicles and Transportation Systems, Calgary, Canada.

[24] Rakheja, S. and Woodrooffe, 1996, 'Roll of suspension damping in enhancement of road friendliness of heavy duty vehicles'. International Journal of Heavy Vehicle Systems, 3, 363-381.

[25] Bakker, E., Byborg, L. and Pacejka, H.B., 1987, 'Tyre modeling for use in vehicle dynamic studies'. SAE paper 870421.

[26] Pacejka, H.B. and Bakker, E., 1991, 'The magic formula tyre model'. Proc. of 1st Tyre Colloquium, Delft, The Netherland.

[27] Murphy, R.W., Bernard, J.E. and Winkler, C.B., 1972, 'A computer based mathematical method for predicting the braking performance of trucks and tractor-trailers'. UMTRI Report UM-HSRI-PF-72-1, The University of Michigan, USA.

[28] Fancher, P.S., Ervin, R.D., Winkler, C.B. and Gillespie, T.D., 1986, 'A factbook of the mechanical properties of the components for single-unit and articulated heavy trucks'. UMTRI Report UMTRI-86-12, The University of Michigan, USA.

[29] Delaigue, P. and Eskandarian, A., 2004, 'A comprehensive vehicle braking model for predictions of stopping distance'. Journal of Automobile Engineering, 218, 1409-1417.